SYNTHESIS AND CHARACTERIZATION OF SILVER NANOPARTICLE ELECROCATALYST EMBEDDED ONTO INDIUM TIN OXIDE ELECTRODES FOR DEGRADATION OF AZO DYES

MARTIN OUMA OSEMBA

A THESIS SUBMITTED FOR THE FULFILMENT OF THE REQUIREMENTS FOR

THE AWARD OF DOCTOR OF PHILOSOPHY IN CHEMISTRY OF

MOUNT KENYA UNIVERSITY

AUGUST 2025

DECLARATION AND APPROVAL

Student's Declaration

The thesis is my own work and has not been presented in other institution for any other award whatsoever in its present form. Therefore, no part of this work should in any way undergo reproduction without my consent as the principal author or/ and that of Mount Kenya University.

Signature _____ Date 5/11/2025

Martin Ouma Osemba

PHDAC/2021/76363

Approvals of the Supervisors

We hereby, confirm that the work in this thesis has been undertaken by the candidate under our supervision as per the guidelines put in place.

Signature _____ Date 4/11/2025

Prof. Mary Muriuki-Hutchins

College of Science, Technology, Engineering and Mathematics

Harris Stowe State University

Saint Louis, MO 63103, USA

Signature _____ Date 05/11/2025

Dr. Samuel Karenga

School of Pure & Applied Sciences

Mount Kenya University

Signature _____ Date 4/11/2025

Dr. Godfrey Keru

Department of Chemistry, Whitworth University,

SPOKANE, WA, USA.

DEDICATION

This thesis is dedicated to the almighty God for his constant love. Secondly, my late mother

Mary, my wife Mwakisha and children.

ACKNOWLEDGEMENT

I am very grateful to all the people who contributed directly or indirectly to this work. I take this auspicious opportunity to sincerely appreciate my supervisors: - Prof. Mary Muriuki Hutchins, Dr. Samuel Karenga and Dr. Godfrey Keru for their great effort and work towards completion of the thesis. My dear wife Jediliah Mwakisha for her prayers and encouragement and my children Genius, Condoleezza, Angla Markel and Natalia Martins for being my motivation in everything pertaining my career. I would also wish to thank the laboratory technicians, chemistry department of the Pwani University for the relentless participation towards the project.

To God be the glory.

ABSTRACT

The research was conducted to establish the effectiveness of silver nanoparticles embedded on indium tin oxide (ITO) thin film conducting material in causing the textile azo dyes effluent degradation. The Overall Objective was to synthesize and characterize silver nanoparticles electrocatalyst embedded on indium tin oxide for the degradation of azo dye in the textile effluent. The 40.0 g of powdered crab shells resulted in 23.0g of chitin after demineralization and 7.2 g (31.3 %) of chitosan. Chitosan obtained from crab shells exhibited 89.5% degree of deacetylation showing efficiency in reduction and stabilization of silver nanoparticles from the Ag^{+} ions. The UV-Vis spectroscopy showed the formation of spectra with λ_{max} at 420 nm. The scanning electron microscope (SEM) depicted nanoparticles showing spherical morphology with size range of 50 nm. FTIR signals were recorded at 1658 cm^{-1} corresponding to the amide (C=O) bonds, at 1089 cm^{-1} representing secondary alcohol (C-O-C) bonds at 564 cm^{-1} plane with bends NH, plane-out and bends C−O. C-H stretching vibrational signal was noted at 2927 cm^{-1}, a broader band at 3426 cm^{-1} for an overlap between the O−H stretching vibration and the N−H stretching vibration of the oligosaccharide applied in the capping. The intensity of the O−H and N−H stretching bands emanated from the hydroxyl and amino groups thus shifting to 3426 $cm^{-1,}$ implying that chelation of silver with both O−H and N−H groups of chitosan actually took place. The percentages of azo dyes degradation were as follow: 68.4%, 72.5% and 93.1% using electrocoagulation, ITO and ITO-AgNPs coupled electrodes respectively. The results obtained from the two factors ANOVA with replication indicated significant difference (p= 0.0024) when the silver nanoparticles embedded on indium tin oxide electrodes were utilized in the degradation of these azo dyes in the effluent samples. In all the four samples it was noted that, 8 ppm of the silver nanoparticle concentration applied to the ITO thin film electrodes resulted in the least power consumption maximum of 0.4536 watts with average values of 0.0300±0.0023 hours and a current flow of 0.63 A. The average specific consumption of energy at 12 V was 2.110 kWh/m3 compared to 1.318 kWh/m^3 at Pd of 24 V respectively. IR drop was minimized by lowering the created gap within the thin film electrodes to 0.2 cm and raising the surface area of the cross section of electrodes and specific solution conductance. The COD listing for the samples after treatment fell below 100 mg/L which is much lower than the acceptable limits of COD ≤250 mg/L. The BOD for dye effluent from the two-way ANOVA with replication portrayed a significant variation (p=0.0000238) when compared to the one of WHO 2002 with the range of 150±5 mg/L. The colour removal was 99.97% showing that, the optimized process was effective and efficient in the degradation of these azo dyes in the textile wastewaters.

TABLE OF CONTENT

LIST OF FIGURES

LIST OF SCHEMES

LIST OF PLATES

LIST OF ABBREVIATIONS AND ACRONYMS

AMCOW	African Ministers Council on Water
ANOVA	Analysis of Variance
BOD	Biochemical Oxygen Demand
CDs	Compact Discs
Cs	Chitosan
C.I	Colour Index
COD	Chemical Oxygen Demand
DD	Degree of Deacetylation
DNA	Deoxyribonucleic Acid
DO	Dissolved Oxygen
DSA	Dimensional Stable Anode
EC	Electrocoagulation
EM	Effluent from Mombasa

Ef	Effluent Sample
EPA	Environmental Protection Agency
ER	Effluent from Rivatex
ESI	Electrospray Ionization
ESVR	Electrode Surface-to-Volume Ratio
FBC	Fat Binding Capacity
FTIR	Fourier Transform Infrared Spectroscopy
GPS	Global Positioning System
HPLC	High Performance Liquid Chromatography
ITO	Indium Tin Oxide
KNBS	Kenya National Bureau of Statistics
kV	Kilovolt
LC-MS	Liquid Chromatography-Mass Spectrometry
NACOSTI	National Commission for Science, Technology and Innovation
NPs	Nanoparticles
PD	potential difference
pH	Potential of Hydrogen
SEM	Scanning Electron Microscopy
SPR	Surface Plasmon Resonance
Ss	Stainless Steel
TDS	Total Dissolved Solids
UV- Vis	Ultraviolet-visible
UV	Ultraviolet
WBC	Water binding capacity

WRA Water Resources Authority

CHAPTER ONE

INTRODUCTION

1.0 Introduction

Pollution of aquatic ecosystems by industrial effluents containing dyes is a global concern and more so in developing world (Bafana *et al*., 2011a). This pollution, is known to affect aquatic live as well as reduce the quality of water for human consumption (Lee *et al.*, 2021). In lieu of this, world organizations such as: World Health Organization (WHO), Environmental Protection Agency (EPA) in USA, African Ministers Council on Water (AMCOW) in Africa and in Kenya, Water Resource Authority (WRA) and many others in various countries have set policies that regulate pollution of water masses by effluent from the textile factories (Chung, 2016a). Globally, the demand for improved innovations and technologies, that address the removal of industrial water pollutants is enormous, (Saidu *et al*., 2020). There are a variety of innovations that have been applied in several industries involved in the removal of azo dye and related substances, (Brown & De Vito, 1993a). Azo dyes are considered to be one of the most integral component of industrial effluent (Hodaifa *et al.*, 2019), due to their extensive use in industries (Qiao *et al*., 2010). Not less than 15% of the total organic dye mainly azo group is lost and form part of effluents during manufacturing and application processes (Rakness, 2011). This research aimed at addressing the impact of this new technology of ITO- NPs thin film electrodes on effluent quality and its effectiveness in Azo dyes removal and treatment from the textile wastewater before their release to various water bodies.

1.1 Background of the study

Unique water properties is not only considerably fundamental to life support system but also in determining its ecological and chemical predisposition (Hodaifa *et al*., 2019). Most of these

properties are due to its capability to form hydrogen bonding and its polar molecular structure (Venkatadri & Peters, 1993). Water has the highest dielectric constant in comparison to other common liquids. Water is also known to possess higher heat capacity than any other liquid except ammonia with its highest density in its liquid form at 40.0^{o}C. Fundamentally chemical phenomenon of water does not exist in solutions passe' but instead through interacting with other phases for instance, solutes occurring in water molecules (Kavoosi, Rahmatollahi, *et al.*, 2014). For instance, the redox reactions spearheaded by bacteria occurring in their cells has a reducing effect on the dissolved oxygen (DO). This is effect is caused by the cell's chemical or/ and biochemical oxygen demand (Saratale *et al.*, 2011). Generally, during these decay processes, most of hazardous organic compounds are emulsified and reduced into suspensions of tiny particles, that considerably contribute to the total wastes dissolved in water, (Wac\lawek *et al.*, 2019). Wastes compounds are also infiltrated through sedimentary processes into aquatic ecosystems by physical or chemical media resulting into hazardous effects that should be addressed as a matter of urgency (Hashemi & Kaykhaii, 2022). The major producers of waste water pollutants globally is widely believed to be the textile industries, (Bafana *et al.*, 2011b). The waste is generated from their large water volume demands, used in enhancing the activities involving the dyeing of the substrates (Almeida & Corso, 2019). These depositions alters chemistry of the receiving water due to the inclusions of substances such as polymers, organic, inorganic and total dissolved solids (Mantzavinos & Psillakis, 2004). Synthetic dyes used in textile industries are non-biodegradable and have a major challenge in the way they exhibit stability at high temperatures and diurnal light, (Bafana *et al*., 2011c). These factors make it quite a challenge in degrading synthetic dyes majorly azoic groups using conventionally devised treatment methods currently underutilization (Z. U. H. Khan et al., 2018). Besides, the by-products emitted from such industrial procedures during degrading process are very toxic in nature due to incomplete removal by the currently used methods such as electrocoagulation

and electrochemical mineralization (Masomboon *et al.*, 2009). Azo dyes in the textile effluent are not only stable towards light, heat and oxidants but also not easily biodegradable (Singh & Singh, 2017). Dyes can be synthesized in the laboratory or can be obtained from natural sources (de Campos Ventura-Camargo & Marin-Morales, 2013a). The synthetic ones have extensively been utilized as colouring agents over the last few decades in various industries including textile, pulp and paper, leather tanning, pharmaceuticals, paint, cosmetics, printing, plastic and food industries (Brown & De Vito, 1993a). These dyes are also used in photographic activities, as indicators, inks, body arts, biomedical applications, biological strainer, gasoline, many others. All these activities result in discharge of industrial refuse to the aquatic ecosystems and terrestrial habitats (Z. Duan et al., 2020). The presence of industrial dye pollutants can easily be detected even at the lowest levels of <1 mgL^{-1} (Türgay *et al.*, 2011). Their presence even in very low concentration of levels <1 mg L^{-1} reduces sunlight and oxygen penetration, resulting in coloured water, biological attack on the dissolved matter and resisting photochemical reactions (Ganesh *et al.*, 1994). Research shows that some products formed by textile dye effluents pollutants in aquatic ecosystems are carcinogens or/and mutagens (de Campos Ventura-Camargo & Marin-Morales, 2013b). One major component of industrial affluent is coal tar-based hydrocarbons. The coal tar hydrocarbons include; naphthalene, anthracene, benzene, xylene and toluene, making them stable and not easily biodegradable (de Campos Ventura-Camargo & Marin-Morales, 2013a). Textile finishing industry produces large amounts of coloured wastewaters containing synthetic dyes (Brown & De Vito, 1993b). In order to remove all the unfixed dyes, washing the substrates made from polyacrylic is done severally with large volume of water (Chung, 2016b). The process of washing these substrates results into much of the dyes that were not completely utilized during the process of fixation landing in the industrial effluent receiving water bodies, increasing quantities of waste water from the process operations (Kavoosi *et al.*, 2014). Studies have estimated that more than 15% of synthetic dyes applied in the production of fabrics end up in as effluents (Solís *et al.*, 2012).

Bio-degradation of the resulting effluent is made difficult due to the presence of toxic metabolites like aryl amines formed with complex structures (Nateghpoor *et al.*, 2014). Textile industries positively affect the economic development worldwide by creating job opportunities (Aziz *et al.*, 2014). However, challenges majorly associated with textile industries is generation of high volumes of water-based effluents. They are known especially to be containing dyes like vat, direct, reactive, disperse blue and reactive deep components (Kituyi *et al.*, 2016). These dyes and specifically azo dyes are difficult to degrade resulting in chronic health hazard to various organisms living in these surroundings (Y. Liu et al., 2022a). The major aspect for consideration during wastewater studies is TDS which increases due to the common salt and Glauber salt application, thus leading to high levels of osmotic imbalance to the surrounding waters (Lokesh *et al*., 2013). Research carried out in Bangladesh in the year 2016, indicated that the presence of total dissolved solids (TDS) whether high or low concentration in water may affect the osmotic balance, leading to a bulged or dehydrated organisms in aquatic environments (Jolly *et al*., 2016).

In India, study showed that the textile factories consume large quantities of water and in return emit almost similar and proportionate volumes of effluents resulting from their operational processes (Aparna *et al*., 2016). Dogdu *et al*., 2017 noted that several textile industries in Turkey, had these dyes in their aquatic environment which could be detected by the human eye even at very low concentrations of below 0.1 gL^{-1}. This environmental pollutant leads to lack of fresh water for domestic use and aquatic organisms. The report further indicated that a considerable percentage of causes related to cancer reported in Turkey in areas covered by disposed effluent water channels could be attributed to too much foodstuffs and water lased with traces of textile effluents containing azo dyes (Dogdu *et al*., 2017). In Haiti, textile dye effluents containing the organic-colored chromophores which are produced in large quantity and released to the water masses when untreated, are not only considered to be pollutant to the environment but also affect the health condition of the people and other organisms living in

these areas (Sundaram *et al.,* 2013). The various bathing processes involve some heating and even yielding greater concentration of salts above 60 g/L that are included in the discharged refuse to the surrounding water course, increasing the inorganic and organic pollutant load of the effluent (Ramachandran *et al.*, 2013). In East African countries such as Kenya, Tanzania and Uganda, the effect of textile and industrial effluents on living organisms cannot be ignored (Rwiza *et al.*, 2021). According to Chai *et al,*, most of the effluents from textile industries in Tanzania contain dyes which are toxic in nature (Chai *et al*., 2021a). In Arusha for instance, cases of textile dye pollution on the leaves of green vegetation emanating from extracellular respiration have been reported. These pollutants form potential carcinogens, toxins and mutagens capable of interacting with the digestive systems of the organisms living in these areas (Bidu *et al.,* 2021). In Kenya, Rivatex Textile Industry is no exception in discharging these harmful dye effluents and utilizes substantial amount in dissolving chemicals during wetprocessing of textile (Waithaka *et al*., 2017). The relaunching of the Rivatex industry by the government in 2018, resulted in deposition of several recalcitrants (Mwamburi *et al*., 2019). An assessment of Rivatex industry for waste water discharge to the surrounding by the Uasin Gishu County quality assurance revealed that, use of synthetic chemical dyes rose immensely since buy Kenya build Kenya initiative began (Isaboke *et al*., 2021). The initiative further facilitated over application of azo dyes so as to meet the large and growing demand for the locally made fabrics, which led to large quantities of effluents finding their way to the nearby rivers such as Sosiani and Kesses. These untreated effluents containing azo dyes discharged in the nearby water bodies have harmful effects on the well-being and the general health of the residents, animals and aquatic life (Wanjohi *et al*., 2019). Dying 1kg of a commonly used cotton, 60g of reactive dye substance is required with large amount of water of 150L and 800g of NaCl is necessary (Soldan *et al.,* 2014). However, more than 3g/L of the total dye used does not form part of the fixation to the substrate utilized but effluent released to the nearest water bodies (Soldan *et al.*, 2014). These assertions point to the fact that, due to their carcinogenic

and harmful nature, textile effluents need to undergo treatment or degradation before getting discharged to the environment (Belal *et al*., 2021). The process of degrading textile effluent containing azo dyes to less harmful status before releasing to the surrounding is paramount (Haghighi *et al.,* 2016). Degradation process involves the breaking of the complex bond structures of the toxic azo dyes in the effluent by following several physical and chemical methods to ensure toxicity reduction and decolorization of those complex azo dyes (Hussain *et al*., 2021). Nonetheless, degradation of these dyes in textile effluents has not been fully realized due to their coloured components in the textile effluents affect the visibility and the amount of the dissolved oxygen (Ramesh *et al*., 2021). The dye bio-degradation is made difficult by the fact that they contain molecules with complex structures of aromatic hydrocarbon compounds such as phenyl, naphthalene, anthracene and toluene (Ghoreishi *et al.,* 2016). Textile effluents containing azo dyes are also found to be very difficult to degrade due to their high levels of alkalinity caused by the presence of basic compounds of sodium carbonate and sodium chloride (NaCl) that raise solution pH to 10 and very high level of temperatures of about 40.5°C (Shehata *et al.,2016).* The aromaticity in these dyes structures causes high stability and less biodegradability (Ali *et al.,* 2016). The methods currently used for degradation which include electrocoagulation, adsorption and flocculation have several shortfalls and inefficiencies like over polarization and incomplete removal of dyes (Maghanga *et al.,* 2017). This calls for an investigation of a more effective physio-chemical degradation methods using synthesized and characterized silver nanoparticles (AgNPs) electrocatalyst embedded on ITO, $In_4Sn_3O_{12}$ electrodes. These nanoparticles are very vital in the degradation of the textile azo dyes as a result of their wide spectrum and strong antimicrobial functions (Okur *et al*., 2022). The process of catalytic degradation of textile effluents using silver nano-catalysts or particles through reducing agent like Indium Tin Oxide can be demonstrated using the mechanism of electron transfer (Ahmad *et al.,* 2014).

1.2 Statement of Problem

Effluents from the textile factory are a global challenge due to the availability of dissolved recalcitrant containing Azo dye components (Saroha *et al.,* 2013). These Azo dye in the effluents cause pollution of water ecosystems leading to excess deposition of the waste to the environment (Wenhua *et al*., 2016). Some of these azo dyes are reported to be carcinogenic (Schore *et al.,* 2007). There is need to degrade them from textile waste water before releasing to the environment (Bhunia *et al.,* 2016). Coloured substances of azo dyes, inorganic and organic compounds have negative impact on water quality (Uday *et al.,* 2016). It is important that emphasis is made on treatment (Ulanoff *et al.,* 2013). In Kenya, textile industries are the major sources of effluent that contain azo dyes which are classified as a cancer causing agent (Okeke et al., 2022). There are various policies addressing the treatment and disposal of industrial waste developed and gazetted in Kenya, for instance, 1999 Environmental Management and Co-ordination Act, (GOK, EMCA 1999) bestowed the responsibility of maintaining clean surrounding to every other individual within and outside the country. Therefore, any manufacturing industry that produces waste must strictly follow the laws of environment preservation (The water Act cap 372, section 145-147 of the Laws of Kenya) (GOK, 1972). Part ix section 16 of the Public Health Act (Cap 242), (GOK, 1986), requires every industry to uphold and maintain naturally clean environs around and away from the vicinity. This would reduce the burden of pollution caused diseases, toxicities and dangers.

However, the excess wastes in the surrounding water bodies shows that there is laxity in adhering to these stipulated measures by various industries (Kondowe et al., 2022). These policies include; the sessional paper 16 concerning maintenance and standards of public health, Cap 242 of government of Kenya 1986 call upon every factory to ensure proper disposal of waste resulting from their daily operational activities (A. A. Khan *et al.,* 2022). The proper sanitation is aimed at to ensure there is less toxic, mutagenic or carcinogenic substances (Affat,

2021) or any other adverse menace that would otherwise compromise the healthy living (Yüksel *et al*., 2016). This electrolytic method of embedding silver nanoparticles to the ITO thin film conducting material will address the shortfall experienced by the textile industries effluent degradation (Pinheiro et al., 2022a). The currently applied method of treatment of Azo dyes in the industrial effluents involves production of extra flocs in form of sludge (Alsantali et al., 2022). In the electrocoagulation method of azo dye removal, electrodes easily become polarized, hindering efficiency in degradation (Demirer *et al.*, 2014). This study addresses these shortfalls by synthesizing and characterizing silver nanoparticles electrocatalyst, followed by embedment onto indium tin oxide. Silver nanoparticles have electro-catalytic and bactericidal properties towards the waste water (Bundesmann et al., 2021)

1.3 Justification of the Study

Azo dyes in textile effluents are known to possess mutagenic and carcinogenic components (Zafar et al., 2022). Therefore, these Azo dyes contained in waste waters poses serious health threats to people (Maghanga *et al.*, 2017). Azo dye effluents contain large volumes of coloured substances (Wakrim et al., 2022), inorganic materials with high alkalinity levels (Didier de Vasconcelos et al., 2021) and organic recalcitrant affecting quality of water (Gürbulak et al., 2016). In a global landscape, for instance Haiti, India and Turkey Azo dyes have been considered a major challenge (Adegoke et al., 2015) due to their adverse effects when released directly to the surrounding without treatment (Okeke et al., 2022). In Kenya, such textile effluents containing the toxic substances are released to the surrounding environments such as in the cases of Kesses dam and river Sosiani by Rivatex in Eldoret, Uasin Gishu county, Kenya (Maghanga et al., 2017) and Mombasa Textiles Limited in Mombasa County, Kenya. The several cases of cancer related disorders reported in these areas are presumed to be caused by the consumption of food and water contaminated with these Azo dye compounds (Tole *et al.*, 2017). To reduce the toxicity of such textile effluents, different degradation processes and techniques have been applied in various textile industries around the world to eliminate these

dyes (Patel *et al.*, 2017). These include several techniques ranging from biological methods for cationic dye removal (Peng et al., 2021) to physico-chemical (adsorption, coagulation, advanced oxidation processes) which are readily available (Legube & Leitner, 1999). Biodegradation is competitively high in terms of its cost and impact on the environment (Alizadeh et al., 2022). Conventionally aerobic decomposition has proven to lack efficiency (Peng et al.,

2021) and aromatic amines resulting from reduction via fission are carcinogenic in nature (Pandey *et al.*, 2007). Methods such as coagulation are very involving in terms of expenses in degrading coloured components (Abiola, 2019). Treatment of textile effluents is costly and only transfers dye species in the liquid medium to a solid phase OSEMBA (2019), thus other secondary compounds such aryl amines emerge (Kurniawan et al., 2022) advanced oxidation processes (AOP) are potential in decolonizing and reducing recalcitrant organic compounds including surfactants, dyes and auxiliaries substances from textile operational processes (Ghernaout & Elboughdiri, 2020). Nonetheless, these are successful pre-treatment techniques in reducing the levels of toxic organic materials hindering biological removal methods (Hodaifa *et al.*, 2019), the only challenge of using this method, is the generation of flocs which is a major setback as was noted by Thabet (2010). Apparently, these methods currently being applied utilize excess chemicals (Abdullah *et al.*, 2013), which pose again the concern of secondary generation of recalcitrant (Pang *et al.*, 2007). Despite these observations, little attempts have been considered in finding out if azo dyes in these effluents can undergo electrochemical degradation using silver nanoparticles embedded on electrodes (Rahman *et al.*, 2018). This study focused on the essence of synthesizing silver nanoparticles, embedding them on indium tin oxide to be applied in the electrolysis of the said Azo dyes (Silah *et al.*, 2021). The process of optimizing the conditions required for the electrochemical cell was also conducted (Ma et al., 2020). This proposed optimization led to the figuring out impacts of this

technology on effluent quality and its effectiveness in azo dyes removal and treatment from the textile wastewater (Etiégni et al, 2007, Maghanga et al, 2009 a, b).

1.4 Objectives of the Study

The objectives that guided this study are presented below.

1.4.1 Overall Objective

To synthesize and characterize silver nanoparticles electrocatalyst embedded on indium tin oxide for the degradation of azo dyes in the textile effluent.

1.4.2 Specific Objectives

1. To synthesize and characterize chitosan coupled silver nanoparticles then embed them onto indium tin oxide thin film electrodes enhanced electrocatalytic activity.
2. To evaluate the degradation efficiency and changes in physicochemical properties (pH, temperature, COD, BOD, conductivity, and color intensity) of textile industry effluents containing azo dyes before and after treatment processes.
3. To compare the electrochemical performance of unmodified Indium Tin Oxide (ITO) electrodes and silver nanoparticle–embedded ITO (Ag–ITO) electrodes in the degradation of azo dyes, evaluating their efficiency, under identical operating conditions.
4. Evaluate the efficiency of the silver nanoparticle–ITO electrochemical degradation system relative to the conventional electrocoagulation method used in azo dye removal.

1.5 Research Hypotheses

The following hypotheses were tested by the study;

1. **H_0:** There is no significant difference in the degradation levels or physicochemical properties of the textile effluents before and after treatment.

H_1: There is a significant difference in the degradation levels and physicochemical properties of the textile effluents before and after treatment.

2. **H_0**: There is no significant difference in the azo dye degradation efficiency between bare ITO electrodes and ITO electrodes embedded with silver nanoparticles in textile industry effluent.

H_1: ITO electrodes embedded with silver nanoparticles show significantly higher azo dye degradation efficiency in textile industry effluent compared to bare ITO electrodes

3. **H_0**: There is no significant difference in the azo dye degradation efficiency between silver nanoparticles-embedded ITO electrodes and the electrocoagulation method.

H_1: Silver nanoparticles-embedded ITO electrodes achieve significantly higher azo dye degradation efficiency than the electrocoagulation method.

1.6 Limitations and Delimitation of the Study

The limitation of this study included the samples collected from water bodies around Rivatex and Mombasa Textile industries where textile effluents are often discharged. Thus, any other sample which is not related to textile effluent was out of scope, leaving all other recalcitrant that could also be leading to the contamination of the water (Ozgun *et al*., 2013). The study focused on degradation of textile effluents containing Azo dyes using silver nanoparticles electrocatalyst embedded on indium tin oxide thin film electrodes (Escapa *et al.*, 2015). Electrochemical processes, especially in the production industries have not been exhaustively discussed, leaving most of the information in patently owned document (Karim et al., 2022). Likewise, substances that are capable of emitting radiations like Azo dyes, call for special attention which would guarantee safety while interacting with them and during their disposals

(Irene *et al.*, 2018). Textile Industries' effluents constitute an array of pollutants in addition to Azo dyes such as colloidally formed species, particulate matter forms, insoluble components, organic and inorganic materials (Milaković *et al.*, 2020). Additionally, the expected effluent levels and standards varies within pollutant class and industry (Kamali *et al*., 2019). Subsequently, there is no standardized technique for controlling effluent; however, every

industry applies a customized domain in achieving its maximum output (P. Sharma & Kumar, 2021). On a positive side, most technological applications in waste water treatment are fundamental in eliminating most pollutant load and are mostly applied in various areas (Bhattacharjee et al., 2020). In general, a variety of technologies are in use to obtain a reliable degradation method at lower costs (Mahmood *et al.*, 2022). Validating information on textile waste water treatments and experience were obtained from local town data on treatment plants (Xiang *et al.*, 2020). Though, Industrial liquid waste shows similarity to that of wastewater, they can equally record differences in significant ways (N. Ali et al., 2020). Therefore, a commonly designed standards and parameters developed for local town waste water operation should not be utilized for the general industrial waste water treatment (Hemdan *et al*., 2022). Nevertheless, it is advisable to operate smaller piloting in order to be able to conduct testing of the samples with the specific effluent as way of designing the process in the laboratory (ElGendy & Nassar, 2021). Mostly it is important to understand temporal differences in the effluent strength, flow, impact on performance with the diverse discoloration processes of waste components (Bhattacharjee *et al.*, 2020). Industry management officer, in the effort to minimize operational cost, often ignores pilot studies, laboratory tests and only rely on the characteristics of waste from that particular plant (Obotey Ezugbe & Rathilal, 2020). This strategy can easily result in failure emanating from inflated costs, inefficiencies and delays (N. Ali et al., 2020). Subsequently, there might be other wastes components being emitted into the water bodies and this might lead to false information concerning the toxicity levels of effluents in the water bodies (Xiang *et al.*, 2020). Two textile industries were therefore, involved in the study to ensure that proper comparison is done and correct monitoring of the degradation levels of azo dyes (Chai *et al.*, 2021a).

1.7 Operational Definition of Key Terms

Azo Dyes: These dyes consist of diazo amine groups coupling done to the amines and phenols whereby the azoic bonds are attached.

Degradation of Textile Effluent is a process of treating toxic textile effluents to less harmful status before being released to the environment.

Indium Tin Oxide Electrodes refer to an electrode composed of indium, tin and oxygen in the ratios of 37:9:4 by weight respectively. In this study, it will be used due to its transparence, electrical conductivities and optical density, its capability to be deposited in semiconductor electrodes as a thin film is also considered crucial.

Silver Nanoparticles (AgNPs) refers to nanoscale measurement of silver from the range of 1nm and 100nm commonly applied in various industrial processes as a technological advancement in addressing several limitations experienced in the daily running of the industries. In this study the said nanoparticles were utilized in the textile factories considering their unprecedented physical and chemical aspects.

Textile Effluents refer to waste water discharged from textile industries and are highly contaminated with recalcitrant such as dyes, dissolved solids, solid suspensions and harmful metals. They usually cause carcinogenic health effects on the lives of people and other living organisms who consume them.

CHAPTER TWO

LITERATURE REVIEW

This chapter highlights the literature review of the study, based on the classification of textile effluents, degradation of Azo dyes of textile effluents by various methods like reverse osmosis, ozonation**,** advanced oxidation process. Analysis of the levels of textile effluents containing Azo dyes discharged in the water bodies, synthesizing and characterizing of chitosan coupled silver nano-structures, analyzing the levels of dye degradation using Indium Tin Oxide (ITO) thin film electrodes without the silver nanoparticles. Degradation levels of textile effluent dye levels using Indium Tin Oxide with silver nanoparticles electrocatalyst using the UV-Vis

spectroscopy, determination of functional groups and compounds available in the textile effluent dyes before and after treatment using FTIR and LC-MS spectroscopy respectively.

2.1 Classification of Textile Effluents

Textile effluents are classified into various categories based on the functional group they possess. The effluents contain a group of organic components that are applied as coloration in textiles factories (Meyer et al., 2019). Textile effluents containing azo dyes are considered environmental threat globally (Carmen et al., 2012). Disposal of the untreated textile effluent leads to an imminent hazardous substances deposition in that environment (Benkhaya *et al.*, 2020a). These untreated textile effluents are also known to introduce detrimental impact on aquatic organisms (Daniela et al., 2012). There is a fundamental need of degrading toxic recalcitrant that pose debilitating harm to the living things before their release (Kautenburger et al., 2019) into the aquatic ecosystems. Textile effluents are mainly organic compounds infusing colours (M. Osemba et al., 2024) in substrates utilized in synthetic substances including: plastics, clothing, cosmetics, waxy substances, papers and pharmaceutical products (Bhunia et al., 2016). Dye classification in various categories on basis of how they are structured chemically, Colouring index (C.I) and applications (Adegoke et al., 2015). This classification involves; reactive, vat, azo, disperse, mordant, direct, acid and basic dyes

(Prabphane et al., 2015). Over 10,000 dye types are known to exist globally, with more than 70% of the total dyes considered as azo, composed of octahedral or tetrahedral coordination of complexes with metals such as chromium, cobalt and copper (Hassaan *et al.*, 2017, Neeta *et al*., 2018). Dyes possess electron-withdrawing species, together with azo bonding groups (N=N-). The azo groups give them electron-deficient aspect and also considered as xenobiotic in nature (Singh & Singh, 2015). Most textile factories apply reactive dyes to the substrates involved, given that they are high level quality dyes and exhibit characteristics of azo dyes (J. Sharma *et al.*, 2021). Most azo dyes are non-biodegradable and therefore are termed as

environmental pollutants (Deb & Majumdar, 2013, Fahlyani *et al.,* 2013). According to EMCA, the availability of compounds such as 1,4-phenylenediamine, o-tolidine produced by the azo dyes even at low levels are very harmful and toxic to the organisms living in the aquatic environment (Haddal *et al.,* 2014). Azo dyes are synthetic nitrogen-based class of dyes that are most and widely used groups of dyes (El Nemr *et al.,* 2017, & Schore *et al*., 2007). Azo dyes constitute (-N=N-) group as the central component making them highly electron -deficient species (Ratna *et al.,* 2014). They are complex in nature and show carcinogenic evidences of reductive cleavage (Saeedi *et al.,* 2013). Toxicity of ingredients grows with the increase of benzene rings in their structure (Khalvati *et al.,* 2013). Carcinogenicity depends on mechanism of degradation and on the structure of molecule (Gičević *et al.,* 2019). Nitro-compounds especially Azo are degraded in aquatic bodies resulting to carcinogenic amines (Neil *et al.,* 2007). Degraded substances in the azo dyes are known to be aromatic amines with different structures possessing carcinogenic properties (Vollhardt *et al.,* 2007). Carcinogenicity of these dyes is due to their cleaved products such as benzidine (Gičević *et al.,* 2019). Benzidine is a well-known carcinogen affecting the human urinary bladder and causes tumors in humans and animals (Ismail et al., 2019). Structures of these dyes are comprising of conjugation systems containing double bonds with exhibition of aromaticity (Bhatia, Neeta, Ramesh & Joginder, 2018). They have structures that allow much transitions of $\pi \rightarrow \pi^*$ within the UV-visible, possessing strong extinction coefficient forming chromophores (Benkhaya *et al*., 2020c)

2.2 Chemistry of dyes

Chemical syntheses produce synthetic dyes which are aromatic compounds (Haque *et al*., 2021). Aromatic rings in dyes contain different functional groups and also delocated electrons (Ding *et al*., 2020). These dyes possess chromogene-chromophore responsible for colour composition of their structures (acceptor of electrons), whereas their capability of dyeing emanates from the presence of auxochromes (donor of electrons) (Gordon & Gregory, 2022).

The structure of a chromogene is part of the aromatic constitution coupled on naphthalene, anthracene and benzene rings into which the binding of chromophores occur (Riaz *et al.*, 2020). Chromophores constitute conjugation of double bonds showing electron delocalization (Azari *et al*., 2020). Unsaturated chromophores are basically the ones giving these dyes their individual colorations ("chroma" denotes colour and "phore" denotes bearing). The various chromophore alignments could be represented by the following; ethylene (=C=C=), azo (-N=N), carbonyl part (=C=O), methine group (-CH=), carbon-nitrogen (=C=NH; -CH=N-), carbonsulfur (=C=S; ≡CS-S-C≡), nitroso (-N=O) and nitro ($-NO_2$). Auxochrome ("auxo" refers to augments). These are ionizable species that give the dye its 'binding' capacity on to substrates (A. Kumar et al., 2021). An auxochrome is a functional area in atoms attaching itself to the chromophore thus providing electrons to chromophore. These events taking place in the chromophores alter the wavelength and intensity of absorption hence modify their ability towards light absorption (Slama *et al*., 2021). On the other hand, auxochrome usually include the following groups; NH_2 (amino), $-SO_3H$ (sulfonate), -OH (hydroxyl) and -COOH (carboxyl) (Franco *et al.,* 2018). Various chromophore and auxochrome species are represented in Table 2.1.

Table 2. 1: A table showing names of chromophore and auxochrome groups of dyes

Chromophore group	Name	Auxochrome group	Name
-N=N-	Azo	$-NH_2$	Amino
$-N=N^+-O^-$	Azoxy	$-NHCH_3$	Methyl amino
-N=N-NH	Azoamino	$-N(CH3)_2$	Dimethyl amino
-N=O, =N-OH	Nitroso	$-SO_3H$	Sulfonic acid
>C=O	Carbonyl	-OH	Hydroxy
>C=C<	Ethenyl	-COOH	Carboxylic acid
>C=S	Thio	-Cl	Chloro
-NO2	Nitro	$-CH_3$	Methyl
>C=NH, >C=N-	Azomethine	$-OCH_3$	Methoxy
		-CN	Cyano
		$-COCH_3$	Acetyl

$-CONH_2$	Amido

Textile dyes are grouped into two classifications (Benkhaya *et al*., 2020a). These are on:

a) the basis of chemical structure (M. O. Osemba, Ojwang, et al., 2024) for instance, nitro, azo, carotenoid, diphenylmethane, xanthene, acridine, quinoline, indamine, sulfur, anthraquinone, indigoid, phthalocyanine.
b) the application characteristics (these include; - acid, basic, direct, disperse, mordant, reactive, sulfur dye, vat dyes).

Classification of these dyes is outlined in table 2.2. Based on their general structure , they are grouped into:- non-ion, anion and cation dyes. (Benkhaya *et al*., 2020c). Dyes of anionic types are acidic in their composition, direct and reactive dyes (Slama *et al*., 2021). Mostly, the obliterate ones are the water soluble reactive, brightly coloured and acid dyes. This is because they are incapable of undergoing degradation via conventionally utilized techniques in waste management (A. Kumar et al., 2021). Dyes classified as non-ion include disperse because they don't easily dissociate in aqueous solutions located in the environmental discharge points of effluent from textile factories (Benkhaya *et al*., 2020a). Cationic dyes include azo, basic, anthraquinone, disperse and reactive (J. Chen et al., 2021).

Table 2. 2: A Table Showing Classification of Dyes

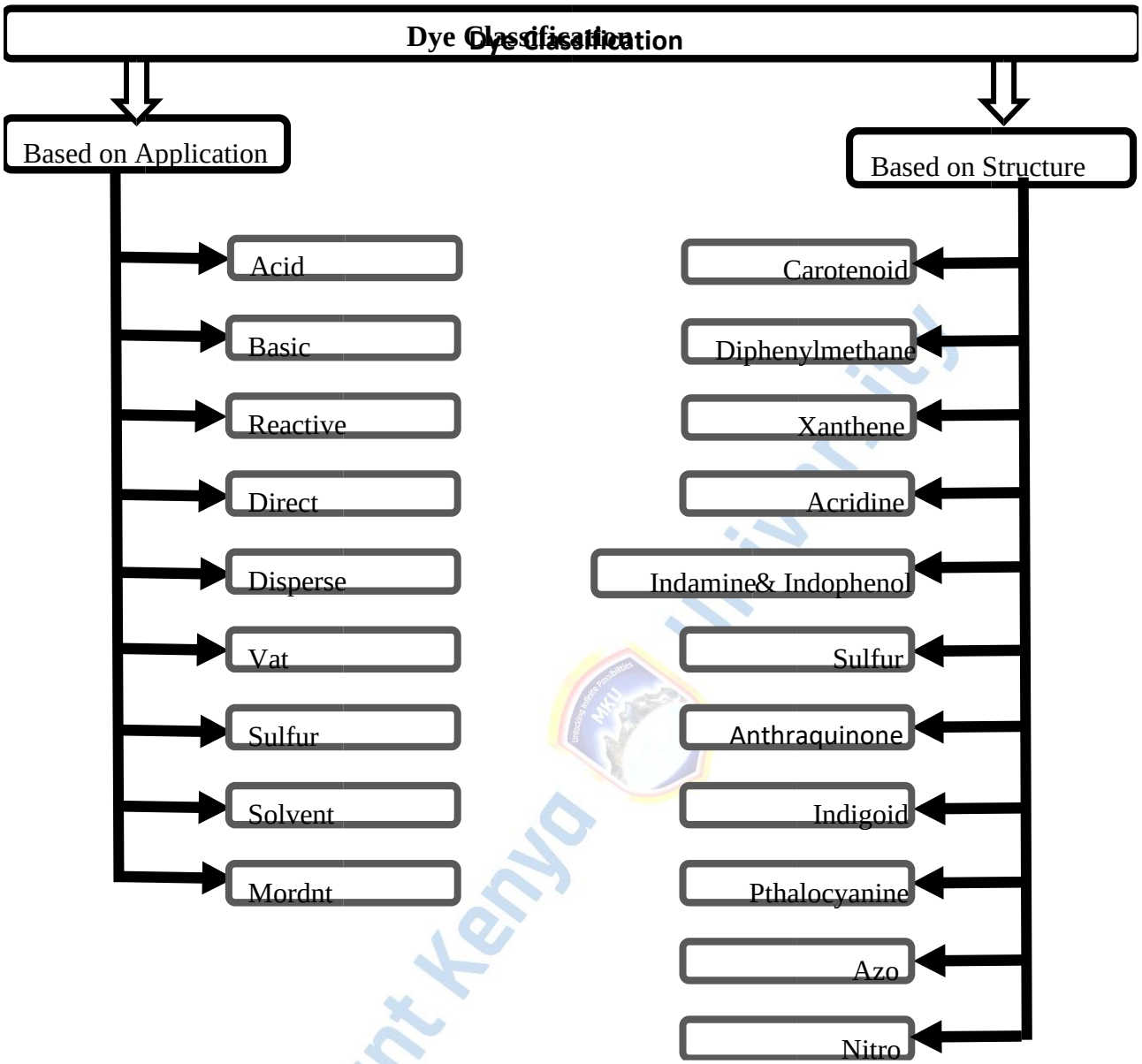

2.2.1 Application-based dye classification

This application dye classification is pegged on the usage or applicability making it a fundamental system through adoption of Colour Index (CI) (Jain & Jain, 2020). Some of the common categories of application-based dyes are detailed below;

2.2.1.1 Acid dyes

They are categorized as anionic dye which are soluble in water. Their application can be done on protein fibres, cotton, nylon, silk, wool, and acrylics (Younis *et al.,* 2020). Moreover, they are also incorporated in leather, inkjet printing, paper dyeing, food technology, and cosmetic industries (Mujumdar *et al*., 2019). These dyes are capable of producing brilliant colours exhibiting excellence in fastness (Osemba et al., 2024). The ability of these dyes to stay attached to the fabrics and not fade away during dry cleaning, or when exposed to light or perspiration and washing is a very vital aspect (Velusamy *et al*., 2021a). Commonly used acid dyes are the families of Acid Yellow, Acid Violet, Acid Blue, Acid Orange, and Acid Red (El Harfi & El Harfi, 2017a).These dyes contain acid that functions well in polyamide fibers (Pirbazari *et al*., 2015). Acid dyes are included in several named stains and possess different commercial naming (Amro *et al.,* 2015). Cotton, silk and nylon are the most common substrates where acid dyes are largely utilized (Ratna *et al.*, 2014). The application of an acid dye to a substrate involves dissolving the dye in water at a temperature range of about 100^{o}C (Kirk *et al*., 2010). Nevertheless, a neutral solution or a strong acid, for instance, chlorine water or sulphuric acid, (Kirk et al., 2010) noted that the different eventual colors of acid dyes vary according to their designs for example, some could exhibit dullness or brilliance in color index (Zawani et al., 2009).

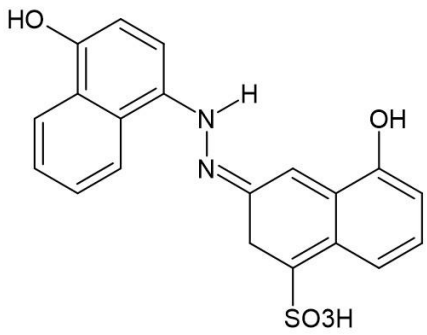

Figure 2.1: Structure of acid red dye

2.2.1.2 Basic dyes

Basic dyes are soluble in water thus classified as cationic (A. Kurniawan *et al.*, 2012). These dyes exhibit brightness in colouring matrix with excellence in regard to its fastness towards light, perspiration, attachment on synthetic fibres and laundry. They tend to portray poor light on natural fibres and fastness to washing (Berradi *et al*., 2019). They are generally used for modified acrylic, acrylic, papers, modified polyesters, protein fibres, modified nylons, cellulosic, and polyacrylonitrile (Chen *et al.*, 2021). Additionally, these dyes are often applied to wool, silk, mordant, tannin–cotton when bright shade is considered vital akin to fastness towards light and in washing (Boudechiche *et al.*, 2019). Basic dyes are composed of basic brown, basic blue, red, violet, yellow, and green basic families (Yin *et al*., 2022).

2.2.1.3 Reactive dyes

They are considered second largest class of dyes with reactive group, and in terms of color Index (Wenhua *et al.*, 2016). The reactive dyes form bonds by chemically reacting directly with the substrate molecules (Zhemin *et al*., 2016). There is a strong covalent bond formation in fibres resulting from the reaction of these dyes with -NH, or -SH (Mahvi *et al.*, 2014). Reactive dyes contain benzene ring which make them exhibit carcinogenic potentiality. The aromatic rings in reactive dyes constitute chlorides, fluorides and vinyl chloride salts as a component in their molecular structures. During fixation processes these groups tend to create some altercations due hydrolysis resulting in effluent being discharged containing coloured components (Bazrafshan *et al.*, 2014). The unique traits of these dyes are in their ability to dissolve and their resistance towards the removal procedures (Zhemin et al., 2014). The challenge tends to complement molecular structures forming these dyes (Yangming *et al.*, 2013). During the synthesis of these dyes, substances that can contain by withstanding the degradation processes are highly recommended (Xuejun *et al.*, 2001). It is important to note that naturally these dyes tend exhibit lower toxicity levels to the living organisms (Zee *et al*.,

2011). However, when a suitable condition like making oxygen a limiting factor, the molecules such as aromatic amines become part of products being formed (Jinpin *et al*., 2016). Reaserch shows that, such molecules tend to show high carcinogenicity levels in organisms consuming them either directly or indirectly (Wenhua *et al.*, 2016). There is formation of strong covalent bond when the aromatic amines react with hydroxylated cellulose, protein fiber in the amino, hydroxylic groups and mercapto compounds in amine polyamides (Vollhardt *et al.*, 2007), making their application suitable in the textile factory (Neil *et al.*, 2017).

These dyes are greatly utilized because of their effectiveness in the wash fastness and their involvement in the facile dye chemistry (Frank *et al*., 2015). Reactive dyes show narrowness in in their absorption spectral lines hence the manifest of their brilliance during dying processes (Zollinger, 1991). Covalent chemical bond is also formed when reactive dyes react with fibre by an ester linkage or ether under suitable conditions (Jain & Jain, 2020). Mostly, this class of dyes contain azo bonds including; triphendioxazine, phthalocyanine, anthraquinone, metallized azo, and formazan (Neves *et al.*, 2018). These molecules are much simple compared to molecular structures found in direct dyes (Boudechiche *et al.*, 2019). Reactive dyes as well produce brighter shades showing excellence in fastness in all aspects, though are difficult in matching the exhibited shades (Younis *et al*., 2020). They are majorly used during cotton fibres printing, and dyeing, though occasionally on nylon and protein fibres as well (Mella *et al.*, 2017). Most widely used reactive dyes are the R.Yellow, Orange, R. Red, and R.Black families (El Harfi & El Harfi, 2017a). Figures 2.2 and 2.3 below show the structures of the reactive dyes.

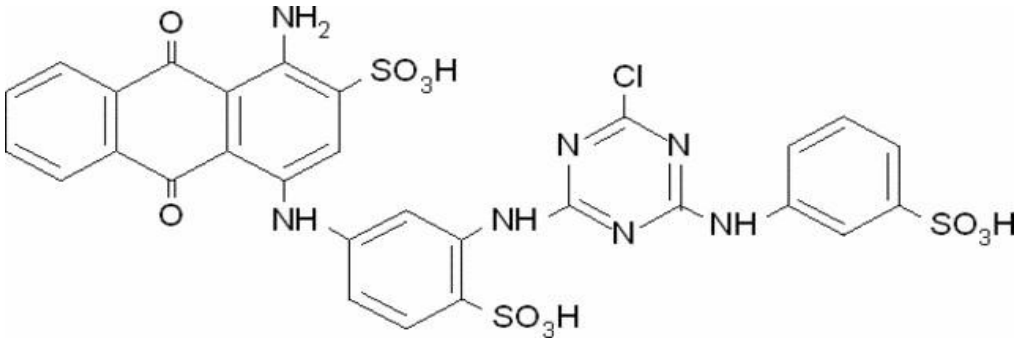

Figure 2. 1.1: Reactive blue structure

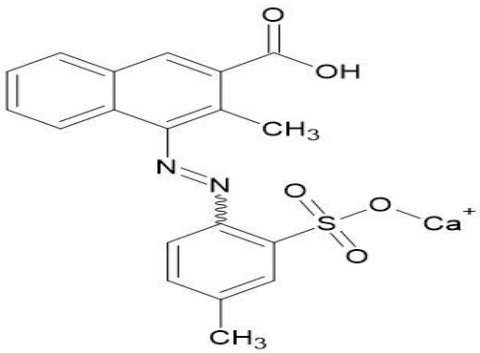

Figure 2:1.2 Lithol rubine structure

2.2.1.4 Direct dyes

Direct dyes are soluble in aqueous solutions and anionic (A. Kurniawan *et al.*, 2012). They possess excellent fastness towards perspiration and dry cleaning and have a high affinity to cellulose fibres, but poor in varied light fastness and fastness to washing (C. Chen & Beigang, 2021). Most direct dyes include polyazo substances, oxazines, phthalocyanines, and stilbenes. These dyes improve wash fastness after frequent chelation with metals like copper and chromium salts are facilitated through application to the substrates (Gillani *et al.*, 2017). Commonly applied dyes from this class in textile industries include the Direct Green, Orange, Yellow and Red categories (C.-C. Wang *et al.*, 2004).

2.2.1.5 Disperse dyes

Disperse dyes were synthesized in 1923 by Hollard Ellis and were used to color for dyeing synthetic fibers such as polyester and related hydrophobic fibres (Padhi *et al.*, 2014), (Kirk *et al*., 2010). Their molecules don't dissolve in aqueous solutions thus, their usefulness indye bath solutions (Ulanoff *et al*., 2013). Disperse dyes contain amino chemicals making them action possible via dispersion of their micro molecules. Their solution is effective even in smaller amounts (Crews *et al*., 2018). These dyes are favorable for use in materials such as polyester, nylon or acetate (Kirk et al., 2010). Furthermore, their particles are very microscopic hence they possess greater tendency to penetrate through the nylon and acetate substrates (Todd *et al*., 2010). Their molecules constitute bonds with the azobenzene or anthraquinone and the –NH, -SH, and –OH (Mahvi *et al.*, 2014). The formed bonds are very strong to ensure that they are durable in the prevailing adversely environmental situation (Thabet *et al*., 2010). The dyes are very much insoluble in water and hence they are referred to as nonionic dyes, thus their application to the hydrophobic fibres is highly recommended during microfine aqueous dispersion (Velusamy *et al*., 2021a). Disperse dyes are predominantly used for nylon, polyester, acrylic, acetate, modacrylic, polyamide, olefin fibres and polypropylene (Y. Zhang et al., 2018). The wash fastness with disperse varies with the kind of fibres. It is excellent on polyester and shows poor results on acetate (Boudechiche *et al.,* 2019). The degree of fastness towards light varies from fair to good, but there is some gas fading on acetate (Benkhaya *et al.*, 2020c), nonetheless, fastness to crocking, perspiration, and dry-cleaning is excellent (Azari *et al.*, 2020). These dyes include; anthraquinonoid and azo containing groups aiding in formation of stable dispersion in solution and possessing low weight in their molecules (Wasim *et al*., 2019). The Disperse Orange, Disperse Red, and Disperse Yellow families are some of the common disperse dye (Cretescu *et al.,* 2017). Examples of these dyes are shown in figures 2.4 and 2.5 below

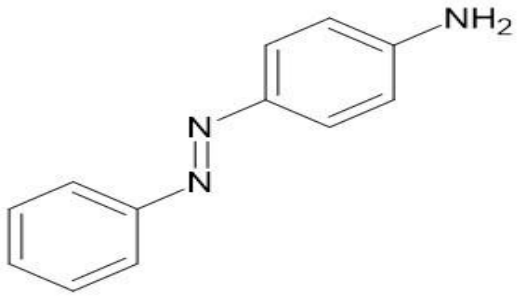

Figure 2. 2: Disperse black structure

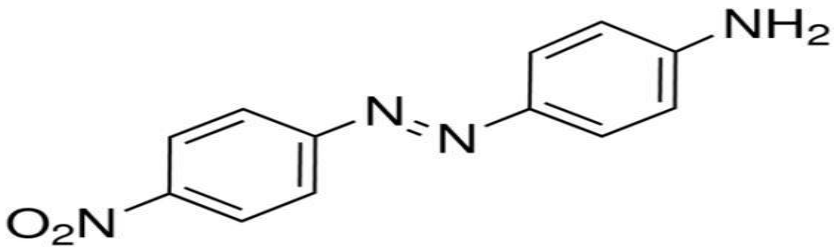

Figure 2. 3: Disperse orange structure

2.2.1.6 Vat dyes

These dyes are classified as as vat dyes based on their method of application in which the dying process takes place in a vat basket, Vat dyes can be applied to cellulose fibre via conversion to leuco components and are water insoluble (Morin, 2017). The former was conducted by reducing and solubilizing with sodium hydrosulfite and NaOH solution called a "vatting process" (Younis *et al.,* 2020). The main functional groups of these dyes composed of indigoid and anthraquinone (Gillani *et al.*, 2017). They show excellence in fastness in all dimensions, especially in bleaches and chlorine, causing them to crock (produce colour when rubbed) if not properly applied (Gillani *et al*., 2017) . Most widely used include; Vat Yellow, Vat Orange, Vat Blue, Vat Red, Vat Black families (Chetyrkina *et al*., 2022).

2.2.1.7 Sulfur dyes

Sulfur dyes are commonly utilized in substrates made of cotton from sodium salts through reducing sodium sulfide under alkaline conditions and are said to be water insoluble (Benkhaya

et al., 2020a). They exhibit great wash fastness characteristics and low cost in the overall dyeing procedures making them economically viable (Bigambo *et al.*, 2021). They are also applied in the cellulosic fibres so as to form dull shades like brown, black, and navy (Atiq *et al.*, 2019). Some sulfur dyes that are most commonly used in textile industries are the Sulphur Blue, Sulfur Black, Sulfur Yellow, Sulfur Red, and Sulfur Green families (Mohtashim & Rigout, 2021).

2.2.1.8 Solvent dyes

Solvent dyes are organic solvent soluble but water insoluble, they possess polar solubility groups for instance, quaternary ammonium, carboxylic or sulfonic acids (Chaudhary & Violet, 2020). Their applications is mainly done on colouring of plastics, waxes, oily substances, and gasoline (Shindy, 2017). Solvent dyes that are regularly used in the factories include; Solvent Violet, Blue, Red, Green, Orange, and Yellow families (Klymchenko, 2017).

2.2.1.9 Mordant dyes

The application of mordant dyes possesses unique features like excellence, for instance in the presence of certain active sites in the molecule (Shindhal *et al.*, 2021). The sites can facilitate the presence of metal residuals by forming coordinate and covalent bonds in a chelate compound (Ye *et al*., 2022). The Al, Cu , Cr, Co, Ni, Sn, and Fe salts are often applied as mordant due to their metallic salts state structure (Baur *et al*., 2022). The mostly applied types of the said dyes include the following; Mordant Black, Brown, Red, Orange, Green, and yellow families.

2.2.2 Dye classification on the basis of chemical composition

This classification includes; nitro, carotenoid, diphenylmethane, xanthenes and acridine dyes (Chuah *et al.*, 2019). Their description is based on the chemical structures they possess (Choong *et al.*, 2009). The following categories are based on their chemical structures.

2.2.2.1 The Nitro dyes

These dyes contain nitro (-NO_2) group (s) as just one or several as their naming implies (Tkaczyk *et al*., 2020). These N=O, N-O groups exhibit equivalence resulting from the resonance. Nitro dyes show conjugation as they resonate with C=C and C-C attached to ring (Ermakova *et al.*, 2018). The aromatic component establishes a chemical equilibrium to the quinonoidone, in the event that the compound is a phenol, (Śmigiel-Kamińska *et al*., 2019). Examples include naphthol yellow S (CI 10316) and Picric Acid (CI 10305). These dyes in the figure below constitute (-NO2) groups (Carmen *et al.*, 2012). N-O or N=O bonding in same groups shows equivalence as a result of the resonance (Daniela *et al*., 2012). They also tend to exhibit conjugation and resonance with C-C and C=C bonding in their aromatic rings (Mavura 2018).

2.2.2.2 Carotenoid Dye

Carotenoid dyes are pigmented chemicals which are naturally occurring in fruits and vegetables. These dyes lack aromatic rings in their structures as shown in the figures 2.4 and 2.5 below. Carotenoid dyes contain isoprene groups (Carmen *et al*., 2012). There are more than three hundred dyes in this category found in plants and just a few are as a result of the industrial processes (Okun *et al.*, 2014). Lycopene is one of the members of carotenoids (Chemeli et al., 20018) This lycopene is mainly found in the tomatoes (Fernandes *et al.*, 2018). Lycopenes constitute of eight units of isoprene arranged in such a way that the conjugation is experienced in the middle part of the formed structured (Daniela *et al.*, 2012).

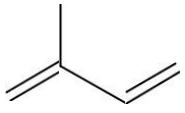

Figure 2. 4: An isoprene unit (2-methyl-1,3-butadien)

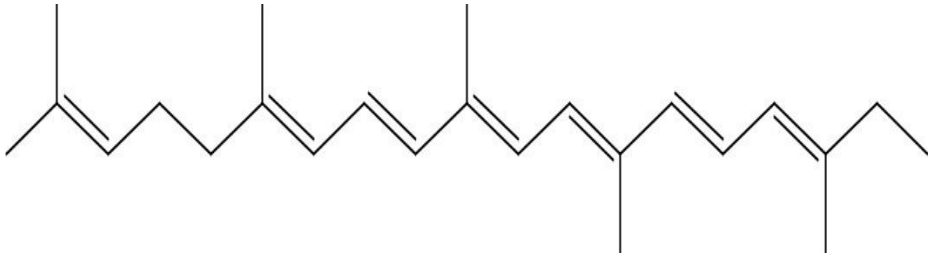

Figure 2.5. Structure of lycopene

Carotenoid structure comprises of eight isoprene units in an alignment that factor in a longer conjugation molecular structure at the central position of the molecule (Supriyanto *et al.*, 2018). In other molecules of this dye type, there exist folding towards the ends of the chains similar to quinonoid or alicyclic, constituting of:- -$OCOCH_3$, -OH and =O groups (Marzorati *et al*., 2020).

2.2.2.3 Diphenylmethane

Diphenylmethane is also known as diarylmethane dye. These dyes contain two aryl rings in which only one subgroup is in use. The dye types are the least commonly found colourant of the cationic classification (Jain & Jain, 2020). Daniela (2012) assert that these dyes are frequently used in the biological field for sole purpose of staining of the biological specimen as shown in the figure 2.6 below.

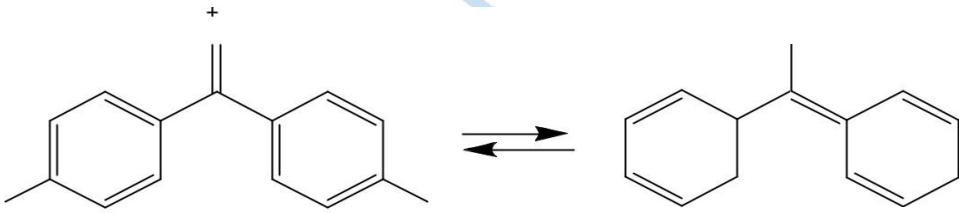

Figure 2. 6: Diarylmethane

2.2.2.4 Xanthenes

These dyes contain oxygen atom in their heterocyclic molecular structure thus the skeletal planarly chromophore-based groups (Daniela *et al*., 2012). Figure 2.7 below represents the structure of xanthene dye. Xanthenes can be used as stains in the biologically staining

processes. There are some that commonly used in the textile industries (El Harfi & El Harfi, 2017b).

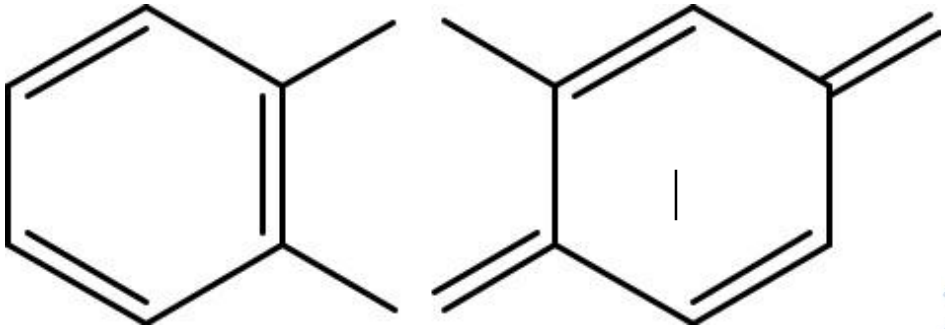

Figure 2.7: Xanthene

2.2.2.5 Acridine Dyes

Acridines are cationic group of dyes. Structurally, acridines and xanthenes show similarities except that in the xanthenes the heteroatom always tends to be oxygen as opposed to the acridine whose heteroatom is the nitrogen atom. They are group of synthetic dyes whose application is mainly for antimicrobial purposes, (Arslan *et al.*, 2016). Figure 2.11below illustrates the structure of acridine dye.

Figure 2. 8: Structure of the acridine dye

2.2.2.6 Quinophthalone

These dyes are commonly known as quinoline, the form an overlapping structure with phthalic anhydride (Arslan *et al*, 2016). Quinoline is applied in

spirit lacquers, polystyrene, polycarbonates, polyamides, acrylic resins, and to color hydrocarbon solvents. It is also applied in drugs and cosmetics and yellow colored smoke formulations. Figure 2.9 below represents an example of the structure of Quinophthalone dye.

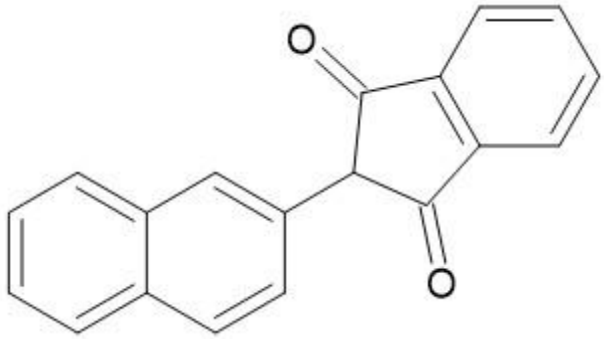

Figure 2. 9: structure of Quinophthalone dye

2.2.2.7 Indamine and Indophenol Dyes

In these classes of dyes, a bridge is formed in between the aromatic and quinonoid chains. It is either the nitrogen or phenolic hydroxyl terminating the chain in the indamine and indophenol dyes (Arslan et al., 2016). These dyes are greatly utilized in the biological analysis as the reagents (Cifti et al., 2008). An indamine (-N=) group forms a bridge between a quinonoid and an aromatic ring (Mustroph & Towns, 2021). Indamine, nitrogen species forms conjugation chain systems, however, indophenol type, shows the existing chain terminating at the quinonoid carbonyl or a phenolic hydroxyl group to one end (Corbett & Gamson, 1972). Some dyes in this category are utilized as analytical reagents, nonetheless, they are rarely applied in the biological stains (Tucker, 1971). Coloured compounds containing indophenol and indamine compounds are considered as end products in various histochemical reactions (Wooster et al., 1938). Example of indamine and indophenol dye is Indophenol Blue.

Figure 2. 10: represents an example of Indophenol Dye.

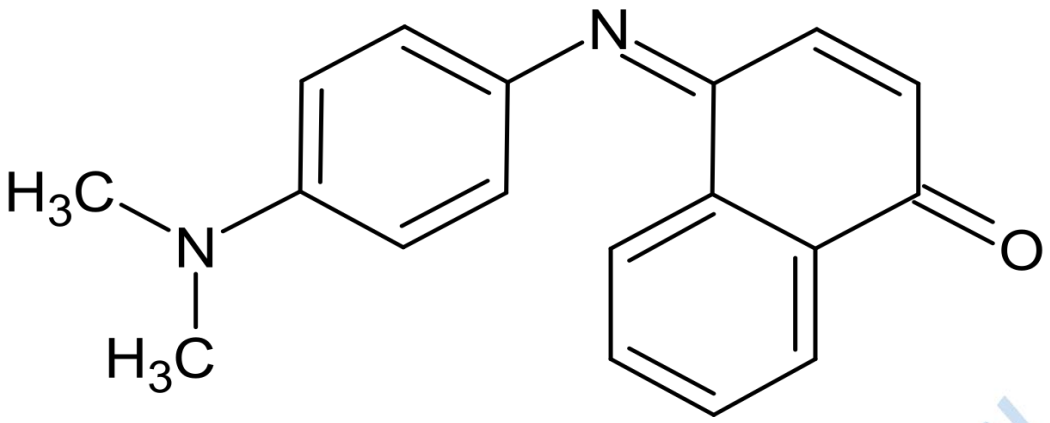

Figure 2. 4: Indophenol Dye

2.2.2.8 Sulfur Dyes

These dyes are commonly applied in cotton manufacture by volume. Being inexpensive, showing excellent wash-fastness, and easily utilized. Predominantly, sulfur dyes are brown, dark- blue and black in colouration, (Saenyi et al., 2008). These dyes are quite inexpensive, shows greater fatness during washing and never complicated in their application (Okun et al., 2014). Figure 2.13: represents an example of sulfur Dye.

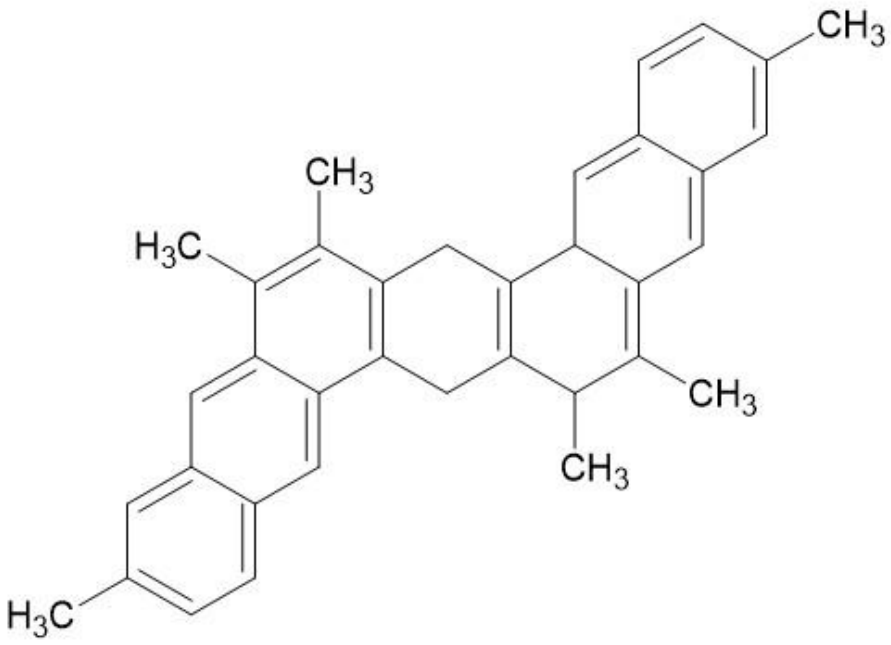

Figure 2. 5: Structure of sulfur Black

2.2.2.9 Indigoid dye

Indigoid dyes possess the carbonyl group in their structures (Verma et al., 2012). These dyes are also special type of the vat dyes. They are said to be one of most ancient dye group. A good example of indigoid dyes is the dibromo indigo (Atul et al., 2012). Figure 2. 14: represents an example of Indigoid Dye.

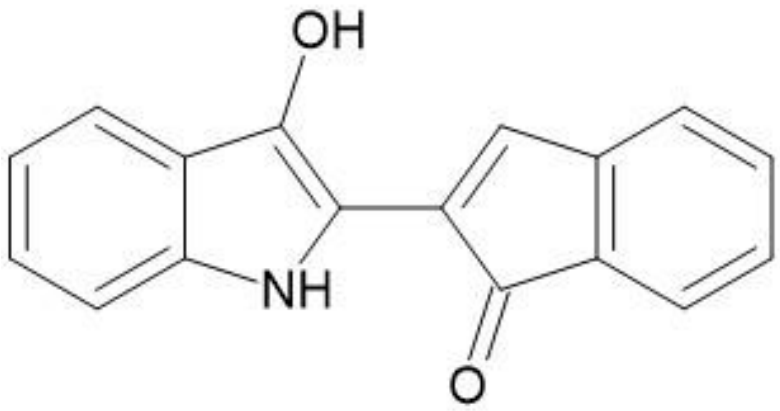

Figure 2. 6: The structure of 6,6'-dibromoindigo

2.2.2.10 Phthalocyanine Dyes

This category of dye exhibits extreme complexity in their structure since they do coordinate with several elements of the periodic table (Demirer *et al.,* 2014). They also show greater intensity in terms of colour shades. Phthalocyanine dyes are mostly utilized in the colouring industries, (Luqman *et al*., 2009). They can as well be applied in the pigmentation process (Atul *et al*, 2012). Figure 2.15 below represents an example of Phthalocyanine Dye.

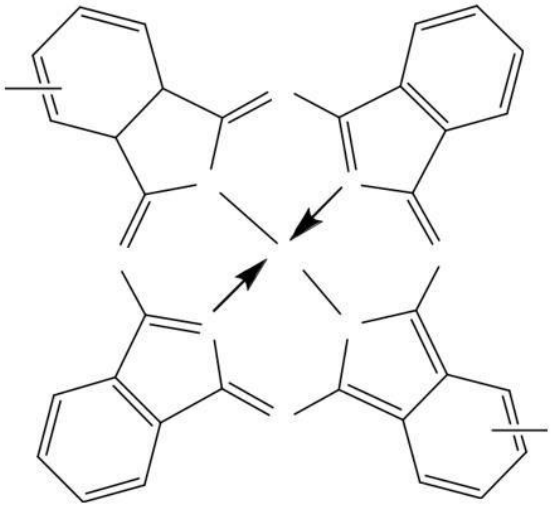

Figure 2. 7: The structure of phthalocyanine

2.2.2.11 Anthraquinone dyes

They are dyeing compounds whose foundation is entrenched upon the fundamentals of anthraquinone structure illustrated below (Epolito *et al*., 2005). They portray several substitutions, incorporating junctions together with fused ring systems (Rafaëlly et al., 2008). Anthraquinone is considered the largest class of carbonyl type of dyes comprising of several components that find their applications in textile plants in different modes (Shahid *et al*., 2019). From an industrial standpoint, the most notables are the anthraquinones and vat in the case of cotton (Nagia & El-Mohamedy, 2007). Figure 2.16 below represents an example of Anthraquinone Dye.

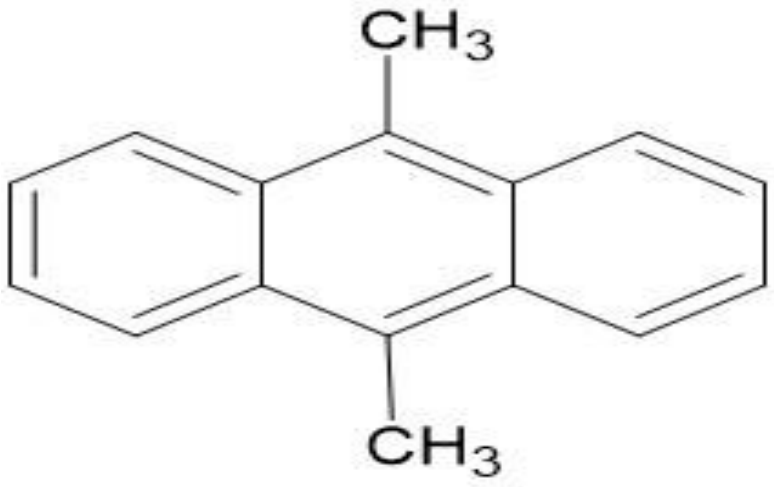

Figure 2. 8: Structure of Anthraquinone

2.2 Azo Dyes

These dyes consist of diazo amine groups coupling done to the amines and phenols whereby the azoic bonds are attached (Atul *et al*., 2012). They constitute over 50 percent of the total amount of dyes produced annually in the global scape (Alkaya *et al*.,2014). Azo dyes are the most commonly applied dyes in the colouration of various textile industrial products, pharmaceutical drugs and various synthetic organic products (Gürbulak *et al.*, 2012). Research reveals that azoic dyes tend to be the most widely applied dyes in the industries, statistically more than 70% of the total textile dyes are simply azo dyes (Demirer *et al.,* 2014). In the printing industries this is the major dye applied due to it brightness in colour and variety of shades possibly emanating from its usage (Choudhary *et al.,* 2012). Furthermore, about 15% of the total azo dyes utilized in the industries end up in the surrounding environments, this was about 280,000 tons by the year 1980 (Reid *et al.,* 1996). These types of dyes are commonly applied because they have shown excellent fixation to the textile fibres and their unparalleled solubility in the aqueous suspensions (Yüksel *et al.*, 2018). Therefore, the application of these azoic dyes results in about 85% of the total final pollutants that are emitted to the surroundings,

making them the most commonly encountered dye emission to the surrounding environments (Alkaya *et al.*,2014). Figure 2.17: represents an example of Azo Dye.

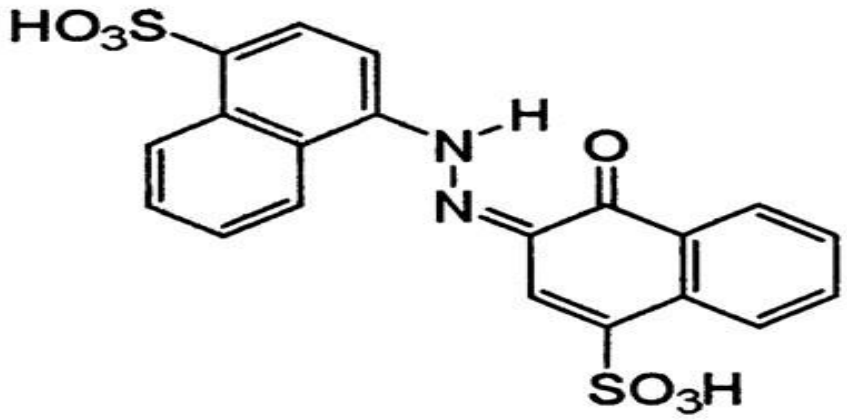

Figure 2. 9: The structure of azo dye

Their concentration in the textile effluent wastewater produced is considered to be the most polluting by various industrial sectors (Reid and Green, 1996). Azo group possess synthetic aspects due to the complexity in their aromatic rings making them most stable and almost impossible undergoing biodegradation (Gürbulak *et al.*, 2012).

Azo dyes by design tend to be very resistant to fading notwithstanding, chemicals or light (Janossy & Kosa, 1992). They also show a lot of resilience when it comes to increased temperature and enzymatic actions resulting from detergents applied during washing (Lin *et al.*, 2003). Therefore, as a result of the aforementioned reasons, biodegradation of azo dyes has proven to be a slow process (Aziz *et al.*,2014). The textile effluent containing azo dyes must therefore, get treated properly before releasing to the environment (Hameed *et al.*, 2014). Azo dyes even at lower levels have great impact on colour which consequently alters the aesthetic nature in receiving sources (Zhao *et al.*, 2016). Azo dyes possess harmful components which are toxic to the aquatic life and humans in these surroundings (Gičević *et al.*, 2019)

2.2.1 Effects of azo dyes on environment and human health

Azo dyes are known to have adverse effect environment and human health. The methods of pollution by azo dyes are either direct or indirect. For instance, besides the adverse outcomes emanating from food and water contamination, the personnel operating in textile factories tend to experience exposure through direct contact to the toxic dye components, hence suffer dermal tissues absorption (Woo & Jhung, 2021). Likewise, the living organisms in these areas suffer exposure via the food chain processes, from when the said dyes find their way into the digestive systems through consumption of the poorly treated water or aquatic organisms resulting in contamination (Klymchenko, 2017). Although there are well laid up regulatory environmental statutory and coordination mechanisms to curb health risks posed by the discharged dye effluent to the environment, environmental pollution by untreated industrial effluents containing azo dyes is still a global concern and Moreso, in developing countries. One of the ways to address this challenge is by bringing forth better treatment techniques of textile waste water containing azo dyes (Chetyrkina *et al*., 2022).

2.2.1.1 Mutagenic effect

Azo dyes generate severe toxicity complicating health situation right from lower organisms like bacteria to human beings (Yusuf, 2019a). The mutagenic, genotoxic and cytotoxic impact of these dyes for instance CI Disperse Blue 291, illustrates dose-dependent causative effects of azo group of dyes. Deoxyribonucleic acid (DNA) fragments, influences the micronuclei generation, thus raising levels of apoptotic index in human hepatoma cells (Alderete *et al*., 2021). Several studies have indicated that these dyes generate mutagenic outcomes in mammals' assay systems and Salmonella, and it has also been noted that their potencies relies on exact positioning of aromatic rings, amino nitrogen molecule and their general nature (Mohtashim & Rigout, 2021). Therefore, it important noting that 2-methoxy-4aminoazobenzene is a weak mutagen, however with the same factors, 3-methoxy-

4aminoazobenzene is a potent hepatocarcinogen in rats and a strong mutagen in Escherichia coli and Salmonella typhimurium (Saini, 2017).

2.2.1.2 Effect of metabolites of azo dyes

The carcinogenic, mutagenic and toxic impacts of azo dyes results from the generated free radicals and aryl amine emanating from reduction and biotransformation in their bonding cleavage (Rajashekarappa *et al.*, 2022) or the action within the component involved, nonetheless, can also result from metabolites formed from the oxidation through cytochrome (Tara *et al.*, 2021). Study conducted by Sisley indicated that metabolism of azoic components in mammalian systems by 1911. She further discovered that sulfanilic acid present in dogs' urine after consumption of Orange I. Therefore, this was a demonstration that azo components are easily metabolized through reduction cleaving of azo group (Gu *et al*., 2021). Ingestion of these dyes results in their reduction to free aromatic amines via anaerobic intestinal microflora, this happens due to the presence azo reductase located in the intestinal wall or the liver (Franca, Vieira, *et al*., 2020). This kind of biotransformation readily take shape in several species of mammals, for instance not only in the Rhesus monkeys but also in humans (Franca *et al.*, 2020). The generated aromatic amines are quite carcinogenic thus they easily get accumulated in various environmental food chains (Sevastre & Hodorog, 2021). Biphenyl amines, like in the case of benzidine and 4- biphenylamine, their presence in the surrounding is conspicuously detectable where they pose severe health threatening conditions to organisms living in the said ecosystem (Shanmugam *et al.,* 2020). Nitroanilines are also other forms of aromatic amines frequently formed whenever biodegradation of azoic group dyes occur in condition influenced by the presence of anaerobes via reductive cleavage of the chemical bonds present in these dyes (–N=N–) in the textile effluent (Chittal *et al.,* 2019). Therefore, it is notably important to realize that various aromatic amine metabolites are non-biodegradable in nature hence exhibit difficulty as far as degradation process is concerned (Q. Zhang *et al*., 2021), resulting in an enormous toxicity levels into the aquatic and higher organisms involved (Shanmugam *et al*.,

2020).

2.3 Degradation of Textile Effluents

Textile Effluent degradation involves the physical breakdown and disintegration of substances into significantly smaller fragments. There is great concern when it comes to pollution emanating from the textile dyeing industry, being one of the intensively chemical utilizer on earth, considered the most polluter of water sources after agriculture (Mehra *et al.*, 2021). Only 80 percent of the dyestuffs applied is retained on fabrics, whereas the other 20% goes through the trench (Benkhaya *et al.*, 2020b). The release of waste fluids containing synthetic dyes causes significant side effects to the organisms living in these aquatic ecosystems, with severe consequences during the photochemical processes (Lellis *et al.*, 2019). Because of the toxic nature of these chemicals and their resistance to natural deterioration such as light, acid, base, and oxygen, the dye's color becomes permanent (Srivastava & Sofi, 2020). Several forms of azo dyes show higher solubility in water, making them easier for the body to absorb through inhalation and ingesting of dust, as well as other methods (Manzoor & Sharma, 2020). Azo dyes tend to be very toxic to aquatic organisms and causing adverse challenges in these water bodies (**scheme 2.1**).

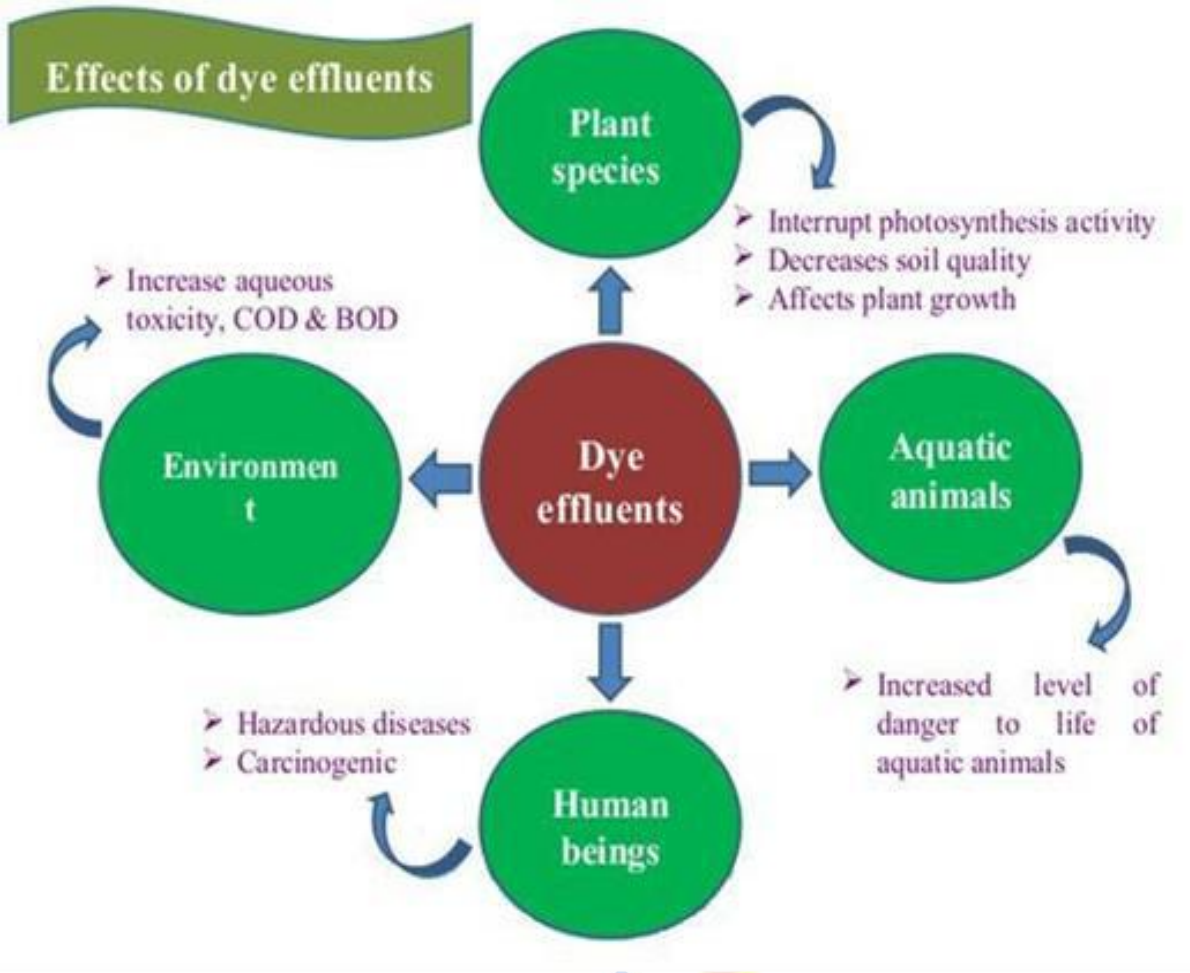

Scheme 2. 1: ***Effect of textile dye effluents on the environment (Yusuf, 2019b)***

This part presents the literature review on different methods and processes for the removal dyes and other pollutants from textile effluents. The various methods currently being used for degradation of textile effluents are discussed below.

2.3.1 Electrocoagulation

Electrocoagulation (EC) refers to a technique used for treating wastewater, wash water, industrially processed water, and medical treatment. The EC involves generation of metal hydroxide flocs inside the textile effluents in the process of electrochemical dissolution of the anode comprising of the aluminum and irons (Syam Babu *et al.*, 2020). This technology has highly been employed in degradation of wastewater containing proteins' components, heavy metallic components, textile effluents, water containing dissolved fluoride compounds and dye solutions from the textile industries worldwide (Nawarkar & Salkar, 2019). The

electrocoagulation process proceeds in a series of phases such as electrolysis on the conductive material surface (A. Kumar et al., 2018), coagulation in solution phases, adsorption of dissolved pollutants get eliminated by sedimentation procedure (Ebba *et al*., 2021). Equations 2.1 and 2.2 below describes reactions that occur at the electrodes during electrocoagulation;

Anode: $Al_{(s)} \rightarrow Al^{3+}(aq) + 3e^{-}$ Eq (2.1)

Cathode: $3H_{(2)}0 + 3e \rightarrow {}_2H_2(g) + 3OH^{-}$ Eq (2.2)

Al^{3+} and OH^{-} ions formed by electrode reaction equation 2.1 and equation 2.2 which react to form various monomeric species such as $Al(OH)^{2+}$, $Al(OH)_2^{+}$, $Al_2(OH)_2^{4+}$, $Al(OH)_4^{-}$, and polymeric species such as $[Al_6(OH)_{16}]^{3+}$, $[Al_7(OH)_{17}]^{4+}$, $[Al_8(OH)_{20}]^{4+}$, $[Al_{13}O_4(OH)_{24}]^{7+}$ which finally transforms into $Al(OH)_{3(s)}$ (Al-Qodah *et al*., 2020) according to complex precipitation reaction as shown in equation 2.3 below.

$$Al^{3+}(aq) + 3H_2O(l) \rightarrow Al(OH)_3(s) + 3H^{+}(aq) \quad \text{Eq (2.3)}$$

The main weakness of the electrocoagulation method is the production of residues such as flocs which call for treatment before disposal due to their complexity in nature (Sher *et al*., 2020).

2.3.2 Biological Techniques

This is a kind of clean up method which involves maintenance of environmentally friendly ecosystem through biodiversity preservation technology globally (Pang *et al*., 2013). Biological technique is accomplished by constructing wetlands where textile dye effluent is introduced in a series of water-weeds contained in ponds (Alkaya *et al.*, 2014). The selection of the said weeds involves considering the nutrition habits for instance those that depend on NO_3^- or PO_4^{3-} and the capability to oxidize effluent released via their roots (Aziz *et al.*, 2014). The COD and BOD are generally realized, however, removing coloured components proves to be a major challenge facing textile industry (Hameed *et al*, 2014). Mostly, biological methods depend on microbial remediation within the effluent for the removal of dyes involved (Ahmad

et al.,2014). Naturally, these azo dyes dissolved in the textile effluent are resistant to natural disintegration (Njau *et al.,* 2021). Therefore, the toxicity of the dissolved compounds responsible for the biological pollution and resistant to this kind of treatment makes this method inefficient (Mwamburi *et al.,* 2019). Resistant type of organic compounds calls for the mineralization as the medium for purification and incorporation of oxygen, raising heat content and UV rays (Isaboke *et al*., 2019).

2.3.3 Adsorption Techniques

This method forms a higher quality resultant water in terms of quality via the adsorption of cations, mordant and acid dyes contained in the textile effluent (Velusamy *et al.,* 2021b). Adsorption method has greatly been applied in the textile industries globally due to its stability in removing the earlier mentioned dye type (Shahedi *et al*., 2020). Adsorption technique is limited to types and number of dyes it can eliminate during the textile effluent treatment (Hao *et al.*, 2019). Removal of coloured dyes by this method is based on two major aspects which include, surface adsorption and ion exchange (Van Tran *et al.*, 2018). This technique is however affected by several physio-chemical aspects, for instance the interaction of dye and sorbent, surface of the sorbent, sizes of particles involved, temperature of the components, solution pH, and overall time of particles contact (Chai *et al.*, 2021b). Nonetheless, activation of carbon and other crucial components such as peat, fly ash, wood chips, bentonite clay and fly ash were found to have an impact on the said discoloration (Zhao *et al.*, 2016). After synthetically processing the textile effluent, fly ash generally does the treatment of stains including malachite green, methylene blue and rhodamine B. Grassis 2016 asserted that ash is commonly applied since it not exorbitant in terms of cost, thus, can be availed even in larger quantities. It was also noted that adsorption method demands for unique situations like the concentration of the solution required, right pH level, proper heating, and sufficient time of contact must be provided (Grassis *et al.*, 2016). To obtain different adsorbents, research on rice

husks was carried out to determine adsorption efficiency in order to eliminate components of methylene blue (Saleemi *et al*., 2017).

The fundamental factors involved included; solution pH, presence of salts, low rate, forms of the bed, and methylene blue concentration (Prabhakar & Samadder, 2019). Applying the model formulated by Thomas, the cutoff curve identification can easily be done whereas, process parameters exhibited in a regression line (Han *et al.,* 2016). Moreover, leaves of Ficus religiosa are powdered to serve as absorbent for substances like hexavalent Cr and Pb metal (Qaiser *et al*., 2017). This method therefore does not address the removal of azo dyes sufficiently which are major component of the textile effluent (Maghanga *et al*., 2017)

2.3.4 Cationic Coagulation / Flocculation

This is a technique of treating textile effluent through the neutralization of electrically charged components of the dye by applying coagulating chemicals (Abdo *et al.*, 2020a) . Electrolysis of the solutions is conducted, Gases (like O_2, H_2) produced are attached to the pollution causatives such as fatty and oily substances towards bubbles of gas generated then directed to the solution top where they can easily collect and get eliminated (Othmani *et al*., 2020). Increased electro-production of effervescence during the electro-flotation generation optimizes the said bubbling activity separately from conditions surrounding the solution (P. Hu, Zhuang, *et al*., 2021a). In the event that hydrogen gas is liberated at cathode when an anode is made of iron (Fe) or aluminum (A1) then it follows that Fe ~+ or $A1^{3+}$ ions emanating via oxidation at anode would probably react with the hydroxyl (OH^-) ions generated at cathode with the production of insoluble OH^- capable of precipitation, thus the adsorption of effluents targeted, for instance Cr(vi) from the aqueous solution resulting in coagulation (J. Ma *et al.*, 2019a). The slag in solid form released was noted to be very much in contact with each other compared to those acquired through chemical means (Mcyotto *et al.*, 2020). Nonetheless, the availability of Fe^{2+} ions, like in water mixed oil from emulsification results in flocculation coalescing to form particles with colloids during neutralization of negatively charged substances causing

repulsive forces between colloids formed; hence, impacting emulsion destruction (L. Chen *et al.,* 2019a). Electric fields can also enhance the flow of the charged particles in colloids formed in aqueous solution, raising probability that collision would occur (Veréb *et al.,* 2019a). Yielding up to 99% decrease in the COD, 91% decrease in BOD, 99% elimination of suspended matter, 100% removal of $PO^{3}{}_{4}$- and 100% de-coloration using electro-coagulation and electroflotation when treating effluents of different industries have been recorded (M. Xu et al., 2021). To minimize on expenses, iron scrap utilization as the anode was advised when carrying out electrocoagulation to obtain 98-100% elimination of dye components (Veréb *et al.,* 2019a). This method effectively removes direct dyes in the textile effluent when chemicals such as iron sulphate or iron chloride is applied (Cho *et al.,* 2014), Flocculation or coagulation method unfortunately does not help in the elimination of acid dyes (Mahmud *et al.,* 2015). There is also aspect of high cost of iron (II) sulphate and iron (II) chloride involved in the process making it unviable when large scale application is required (Folkard *et al.,* 2017). In this method, application of polyamide or cationic coagulants is preceded by the settling of physicochemical procedures at full-scale levels to acquire greater efficiency in colour substance elimination. Aluminum, iron (III) and calcium are some of the coagulating agents, necessary for textile effluent degradation (N. Chen *et al.,* 2020a). Mechanisms involved in the coagulation include; charge adsorption process, neutralization, flocs sweeping process and insoluble substances formation. It was further noted that the said chemical reactions have an impact on solution pH, coagulant saturation and the availability of solids in solution (P. Hu, Shen, *et al.*, 2021a).

2.3.5 Membrane Technology Method

This technology is capable of categorizing, concentrating and continuously separating dyes from the effluent (Wilts *et al.,* 2018). Recently, membrane-centered technologies have achieved commercial successes, for instance, in the separation of liquids, gaseous components

and in the concentration of biological and chemical substances (Abdo *et al*., 2020b). There are outlined industrial achievements during the commercial application of this technology however, still there are several unhandled issues which significantly remain as untapped opportunities for the advancement of the technology including new developments (B. Liu *et al*., 2018). Electrodialysis is a major membrane-type of separation process in commercial use in the most recent (El-Naggar *et al.*, 2018). This technique involves separating and purifying electrolytes on the basis of electromigration via ion resin exchange pores (P. Hu, Zhuang, *et al.*, 2021b). Alternating arrangement of cation and anion membranes is centralized within the conducting material separated with screens of insulations (J. Ma et al., 2019b). The alternation in the membrane arrangement enables ions penetration through one and become obstructed by the consequent membrane (L. Chen *et al.*, 2019b). Solution collection in the membranes is conducted through the stacks formed which cellulose acetate get frequently applied together with nafron - a polymer of polysulfone and polyacrylonitrile (L. Chen *et al*., 2019b).

Electrodialysis is considered applicable in the following areas:

(i) Removal of the ionizing solids from one solution and concentrate them in other (N. Chen *et al.*, 2020b)

(ii) Removal of an electrolyte from non-electrolyte for instance organic process in the stream having waste incorporated.

The migrating charged particles from the non-charged components is the force driving the whole logistical transmission modalities (Veréb *et al*., 2019b). The concentration, fractionation and desalting of the waste from metal final products represented by a technology which could benefit largely from the technology of membrane science and electrochemistry congruence (P. Hu, Shen, *et al*., 2021b). The use of permselective membranes and ion-exchange in chemical processing and separations is a rapidly growing field (van Reis & Zydney, 2007). In the most recent past, there have been some developments in the ion exchange membranes technologies as a result of decreasing the mass transport resistance, chemical stability and increased

selectivity. Ion-selective membranes including; Flemion ®, Nation® and the Dow membranes tend to be perfluorinated polymers that underwent development initially for the chlorine-alkali industry (Asad *et al*., 2020). A revolutionized electrochemical aspects occurred from the developed permeable, ion-selective membrane technologies with the capabilities of reaching the targeted substances (Baker, 2002). Therefore, there have been a review in the fields of soil decontamination by applying electrokinetic processes during the effluent treatment (Banerjee *et al*., 2018). The method has several vital features that resist adverse temperatures and extreme chemical compositions Duim (2014). However, it faces a challenge of concentrated flocs and residues during separation which are very difficult to dispose (Nasrollahi *et al*., 2021). This disposal problem associated with this technology hinder its usage as a result of the run-away costs incurred (Achterberg *et al*., 2018). The method is only important to the factory if the effluent has vey levels of dyes (van Putten *et al*.., 2016). Reverse osmosis and ultra-filtration involved in this technology have been in application from 1970 and having proven efficiency in eliminating the recalcitrant present in textile effluent streams (Nicolaisen, 2003). High cost of membranes and their fouling activities have rendered this technique uneconomical in the pulp and paper mill effluent removal (C. Y. Tang *et al*., 2018).

2.3.6 Colloidal Dispersions and Destabilization

Colloidal dispersions suspend nanoparticles (1–200 nm) by combining electric charge and hydration (Patel *et al*., 2017). Colloids are stable in a liquid, or solution, because of electrostatic repulsion between the particles (Ulanoff *et al*., 2013). There is no agglomeration of this dispersion. Particles with a higher zeta potential are one example. Hydrophilic colloids take on a positive charge from aqueous solutions, but hydrophobic ones have their own (Hunt *et al*., 2013). The stability of hydrophobic colloids is reduced when electrolytes are added. When the electrolytes' double-layer of charge on the colloids is suppressed, the particles bond (Voice *et*

al., 2013). Hence, aggregation happens due to the combination of nearly twenty Van der Waals attractive forces (Pirbazari *et al*., 2013). It has been shown that multimodal ions with a charge opposite to that of a colloid particle are the most effective electrolytes (Weber *et al*, 2013).

2.3.7 Floating Air Techniques

Colour can be removed and suspended solids can be diminished via air flotation (Achterberg *et al*., 2018). The underlying concept is an air flotation involves de-linking procedure (Folkard *et al*., 2017). The use of membranes during the effluent treatment includes in the pulp, kraft, and paper industries and which is greatly facilitated by their incorporation into the pretreatment of the wastewater by air flotation (De Boer *et al*., 2014). Ultrafiltration is used to get rid of the chromophores, and flotation of dissolved gases is used to get rid of the suspended particles, especially the colloidal debris that causes membrane fouling. Wenhua (2016).

2.3.8 Applications of Biological Technique

This waste water treatment process is highly favored, because lower costs are involved with less impact on the surroundings (Choi *et al*., 2007). The technique's credibility rests on the ability of the microbes involved in the process to convert organic dye components into carbon dioxide, ammonia, and heat energy as a byproduct of the growth process (Chipasa & Mdrzycka, 2006). These bacteria' ability to degrade pollutants relies on the presence of enzymes like reductases and oxidases (Wu *et al*. 2012). For instance, azo dyes require azo-reductases to cleavage the azo bindings and to liberate the aromatic amines, which are then degraded by bacteria using oxidases (Janossy & Kosa, 1992). The difficulty lies in identifying microorganisms or microbial consortiums that possess these enzymes and can breakdown a large diversity of the dyes, while thriving in conditions involving the presence of salts commonly applied to the textile effluents. Therefore, there is a growing trend towards investigating the natural habitats such as textile wastewater and wastewater treatment plants (WWTPs) to discover suitable microbes for use in industrial wastewater treatment (Moosvi *et al*. 2015; Asad et al. 2017; Mahmood *et al*. 2011; Pokharia & Ahluwalia 2023). Several aerobic

and anaerobic microbes, like bacteria, fungi, and algae, are found to include enzymes with azo reducing activity, such as azo-reductases, peroxidases, laccases, and polyphenol oxidases (Singh *et al*. 2015). They possess the ability to remove and convert over 70% of organic matter into biosolids. These biological treatments are widely regarded as an effective technique of treating organic matter-rich wastewater (Zheng *et al*. 2013). However, the current compounds' low water solubility and high molecular weight make biodegradation difficult since they prevent the chemical from passing through biological cell membranes (Pearce *et al*. 2013). Additionally, the substituents and their location on the chromophore can have a major impact on biodegradability. Dyestuffs having nitro, sulfo, methoxy and/or methyl groups tend to take longer to breakdown than ionic dyes containing azo with amino or hydroxyl groups (Paszczynski *et al.,* 2022; Nigam *et al.,* 2016). Dyes with hydroxyl, amino, acetamido, or nitro groups in the non-ionic for instance disperse, solvent, and vat dyes biodegrade more quickly than unsubstituted chromophores (Spadaro *et al*., 2018). There are three types of biological treatments: aerobic, anaerobic, and combination anaerobic/aerobic. Organic molecules are degraded by microorganisms in the presence of free dissolved oxygen in the wastewater during aerobic treatment, while methane and carbon dioxide are produced during anaerobic treatment. Using a hybrid anaerobic/aerobic treatment strategy allows for the efficient removal of COD and volatile suspended particles while also providing energy in the form of biogas from highly concentrated waste (Chan *et al*., 2019). Aerobic treatment continues with the degradation of dye residual products such aromatic amines, whereas the anaerobic component is responsible for the reduction and cleaving of these dyes (for example, azo dyes) in the textile effluent (dyes) treatment (Van der Zee & Villaverde 2015).

2.3.9 Ozonation

In comparison with other oxidants like chlorine with reduction potential of 1.36 V and hydrogen peroxide with 1.78 V, ozone (which was discovered in the 1970s; Collivignarelli *et al*., 2017) is a far more effective oxidant as a result of its instability (2.07 V) (Heeb *et al*., 2017).

Chlorination of hydrocarbons, insecticides, phenols and aromatic compounds can all undergo oxidation via ozonation technique (G. Chen *et al*., 2020). The total colour and residual COD, measures the capacity of water to utilize oxygen in the process of the degradation of organic material and during the oxidation of chemicals like ammonia and nitrites which are inorganic in nature, thus reducing the residual forms and sludge (John *et al*., 2022). Harmful metabolites determine the appropriate dosage application to the said effluent containing dyes (Gorito et al., 2021). The ozonation process removes all color and chemical oxygen demand, making the effluent safe for release into environmental rivers (Y. Liu *et al*., 2021). Double-bonded dye molecules are favored by this procedure (Gomes *et al*., 2017). As a result of this high reaction with several azo dyes by degrading azo ink (-N=N-), ozonation has been found to be efficient in cleaning wastewater containing azo colors (C. Wei *et al*., 2017). When its application is in gaseous condition, it doesn't elevate reaction volume and sludge while still being effective at removing color (Mecha & Chollom, 2020). Low chemical oxygen demand elimination; short half-life; continual ozonation necessary; limited toward dispersion dyes and those insoluble in water; high cost of ozone; short half-life; normally roughly 20 minutes (J. Zhang et al., 2021).

Stability is altered by salts, pH, and temperature, and the presence of dyes can further reduce the half-life (Y. Liu *et al*., 2021). Ozone degradation is also hastened in alkaline conditions, therefore it's important to keep an eye on the pH of the effluent (Malakootian et al., 2020).

2.3.10 Indirect Oxidation

Strong oxidizing agents are created on-site during the electrochemical reaction can degrade organic contaminants like dyestuffs, causing their whole or partial deterioration. This process is known as indirect electro-oxidation (Ketut *et al*., 2018).

In one of the two most used approaches, active chlorine is employed to speed up the electrooxidation process (Jogi *et al*., 2015). The organic component in the effluents is oxidized by free-chlorine gas thereto producing chlorine-oxygen substances, for instance HClO or

hypochlorite ClO^- pegged on their pH (Chiang *et al*., 2011). First step is the dye-treatment process, in which the active chlorine undergoes oxidation in order to produce chlorine gas, thus reacting with water molecules to produce hypochlorite ions (Nidheesh *et al*., 2020). Equations 2.5 - 2.7 represents this process. Long term, the dye molecules are degraded by the hypochlorite into intermediate components, and ultimately carbon dioxide (Syam Babu & Nidheesh, 2021).

$$2Cl^- \rightarrow Cl_{2(aq)} + 2e^- \quad \text{Eq (2.5)}$$

$$Cl_{2(aq)} + H_2O \rightarrow ClO^- + Cl^- + H^+ \quad \text{Eq (2.6)}$$

$$Dye + ClO^- \rightarrow dye\ intermediates \rightarrow CO_2 + H_2O + Cl^- \quad \text{Eq (2.7)}$$

Another option is the electro-Fenton approach (Cai et al., 2018), in which catalytic Fe^{2+} and H_2O_2 are used to electro-generate hydroxyl radicals (OH•) for color removal (Rahmani *et al*., 2019). Equations 2.8 - 2.11 shows the entire procedure for eradicating the dye:

$$O_{2(g)} + 2H^+ + 2e^- \rightarrow H_2O_2 \quad \text{Eq (2.8)}$$

$$H_2O_{2(g)} + Fe^{2+} + .\ H^+ \rightarrow Fe^{3+} + OH\cdot + H_2O \quad \text{Eq (2.9)}$$

$$Dye + OH\cdot \rightarrow CO_2 + H_2O + H^+ \quad \text{Eq (2.10)}$$

$$4Fe^{3+}e^- \rightarrow Fe^{2+} \quad \text{Eq (2.11)}$$

In addition, as has been demonstrated up to this point, Fe^{3+} can be reduced by acquiring electron(s) to produce Fe^{2+}. The difficulty of the indirect oxidation approach is that it is optimal only in highly acidic environments (Martnez-Huitle & Panizza, 2018). Certain reactive dyes, such as those with an alkaline pH, need acidic solutions added to the degradation process to make it work more effectively (Syam Babu & Nidheesh, 2021). As a result of its application for neutralization of the reactive dyes that experienced degradation, the entire process raises the alkalinity of the effluents being released (Nidheesh *et al*., 2020). The absence of a need to add a chemical reagent makes I above preferable for treating effluents with high chloride concentrations (Fieser, 1930). Procedure X, however, requires the use of Fenton reagent (ii). Nonetheless, when the treated water is enhanced further in a biological set

up to remove haloforms, method I is employed through electrolysis to liberate haloforms like chloroform. It has been proven that the concentration of haloforms in treated water is quite low (48 mg L^{-1}), and that these haloforms have no harmful effect on the microorganisms found in biological plant media (Jogi *et al*., 2015). Instead, UV radiation can be applied to the electrochemical cell to eliminate the haloforms (Parsa & Abbasi, 2017), or H_2O_2 can be added to the wastewater to neutralize the haloforms before the UV radiation is applied (Chamruspollert *et al*., 2002). It has been observed that the kinetic rates of electrochemical degradation of some reactive azo dyes at titanium coated by platinum oxide (Ti/PtO) electrodes can be enhanced by employing the first strategy (Malakootian *et al*., 2020). In acid dyes (Chiang et al., 2011) or dispersion dyes, the electrochemical technique utilizing chlorine was found to be successful (Maljaei *et al*., 2019). Method (ii) has shown improved performance for phthalocyanine dye degradation when combined with photo-electrochemistry (Collivignarelli *et al*., 2017), in this instance, the metal ions freed as Cu is eliminated.

2.3.11 Reverse osmosis

At least 90% of most ionic chemicals are retained by reverse osmosis membranes, and the permeate they generate is of very high quality (Couto *et al*., 2020). Reverse osmosis can be used to decolorize dye house wastewater and remove chemical auxiliaries all at once (Torii et al., 2019). Mineral salts, reactive dyes hydrolyzed and chemically constituted auxiliaries are filtered out using reverse osmosis (Qasim *et al*., 2019). The osmotic pressure plays a larger role and great deal of energy is required in this elimination procedure with the concentration of dissolved salt skyrocketing (Albergamo et al., 2019).

2.3.12 Filtering purification

Microfiltration, nanofiltration, and ultrafiltration are only some of the filtration techniques that have been used to these problems (Bolisetty *et al*., 2020). These filtration techniques have dual utility in the textile sector, serving both filtration and recycling needs. Including both wastewaters containing a lot of pigment and wastewaters used to remove it (Jaspal & Malviya, 2020). The filter's type and porosity must be adjusted according to the temperature and

chemical makeup of the effluent (Park *et al*., 2020). Investment expenses and short lifespan (before membrane fouling), both of which must be factored into any economic analysis of filtration operations, are their primary drawbacks (Arola *et al*., 2021). Also, the secondary waste streams produced by the possible membrane fouling necessitate additional treatment (Nascimben Santos *et al*., 2020).

2.3.13 Exchanging Ions technique

This method of separation is very useful in the wastewater treatment (Ipekci *et al*., 2020). The accumulation of flocs in the sludge, is a major problem for this separation procedure because it reduces its efficiency and makes it impractical to use (Goldfeld *et al*., 2020). As this ionexchange technique is limited in the types of dyes it can effectively remove, it has also become apparent that it is not the method of choice for cleaning up textile effluent (Luo *et al*., 2020).

The ion exchange resin is directed to the effluent until all of the exchange sites are full (Modarresi *et al*., 2021). The aforementioned procedures allow for the removal of cations and anions present in the textile dye containing effluents (Reynier *et al*., 2022). The elimination of all water-soluble color compounds is possible thanks to this separation approach, and there is no adsorbent loss during the treatment processes (Lebron *et al*., 2021). Disperse dyes, which make up the vast majority of azo dyes in textile effluents, are notoriously difficult to remove with this process, and it also requires the use of costly organic solvents (Scriba, 2019).

2.3.14 Irradiation

Degradation of organic components in textile effluents can be aided by irradiation thanks to the use of adequately dissolved oxygen (Abd Rani *et al*., 2020). The organic dye matter in the aforementioned textile industry waste streams is instantly consumed by this process in an effort to decompose it (Y. Wang *et al*., 2020). The ongoing cost of operations is a key drawback of using this technology (El-Sayyad *et al*., 2020). Hence, dye-containing textile effluents are

permitted to pass through a dual-tube bubbling reactor (Wei *et al*., 2020). The oxidation of the phenols and organic dye components by the irradiation approach provides further confirmation that it is possible to treat some textile dyes by scaling laboratories effectively (Sujatha *et al*., 2020).

2.4 Electrochemical degradation of Textile dye effluents

Effluent from textile dyes is electro-degraded via anodic oxidation, producing metallic hydroxides in the process (Bani-Melhemc *et al*., 2019). Several types of effluents have been treated effectively using the method (Duim *et al*., 2014). Electrolytic reactions take happen in sequence at electrode surfaces, where the chemical reactions take place (Xuejun *et al*., 2016). Many industrial effluents are amenable to treatment by the electrochemical technique (Xuejun *et al*., 2016). To improve the efficiency of electrolysis in the degradation of textile dye effluents, catalysts are introduced in this process (Yangming *et al*., 2016). Electrodes are the sites of reactions that precipitate various colored ions (Patel *et al*., 2017). Electro-coagulation for the degradation of dye effluent is reported as a highly effective tool, with high COD and color removal effectiveness (Patel, 2017). This technology is convenient due to its low learning curve, high efficiency, low impact on the environment, and high capacity to process big volumes of wastewater (Nandi *et al*., 2016). Titanium dioxide has been utilized in photochemical processes during the destruction of colored substances, making electrocoagulation the most typical approach involving thin film surface reactions (Al-AAnbera *et al*., 2019).

2.4.1 Degradation of azo dyes

These dyes are distinguished from the rest by their possession of two radicals, in which at least one is often an aromatic group (naphthalene rings or benzene) (Mapukata *et al*., 2019). These double bonds between nitrogen atoms are written as – N=N-. The azo bonds and the auxochromes and chromophores they're linked to are what give azo-dyes their distinctive hues (Shandilya *et al*., 2021). Most of the oxidation and reduction of azo-dye compounds occurs at

the Azo bonds, which can be mediated by a positive hole, an electron from the conduction band, or a hydroxyl radical (Han *et al*., 2018). The aforesaid bonds are the one responsible for the bleaching of colours. Solar light irradiating a TiO_2 catalyst has been used in the study of photocatalysis in the degradation of azo dyes in their aqueous solutions for instance in the case of acid Orange (Porter, 1989). The said dye primarily appears in different tautomeric forms like hydrazone and the azo type. The hydrazone, however, predominates in water (Nqombolo *et al*., 2018). It was discovered that this causes decolorization of the water and, ultimately, it totally mineralizes the aqueous dye solution due to its photocatalytic property in degradation (El Mragui *et al*., 2021). The sulfonate together with the two oxygen atoms forming the hydrazone in AO7 all contribute to the increased absorptivity on the photocatalytic surface (C. Bhattacharjee *et al*., 2017). First of all, the dye molecule is cleaved around the azo link when exposed to the sunlight, and then benzene-type rings and naphthalene-containing molecules are produced (Hassanien *et al*., 2019). Figure 2. 10 shows tautomerism of acid orange 7 conformers in aqueous solution.

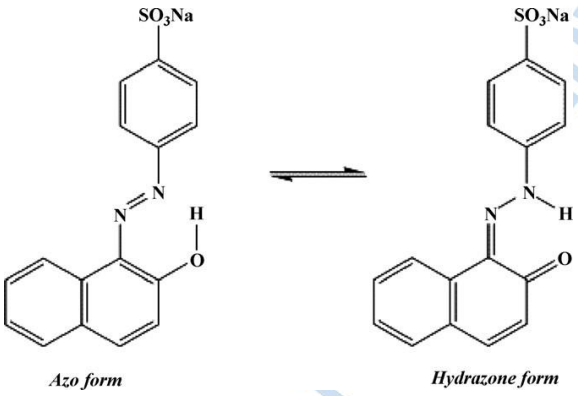

Figure 2. 11: Acid Orange 7 tautomerism conformers in aqueous solution.

Although the chemical oxygen demand is not much reduced, this process takes shape in a larger part through the photosensitization mechanisms, resulting in the decolorization of the aqueous dye effluent (Waghmode et al., 2019). It was discovered that the principal reaction intermediates go through a series of sequential oxidation stages, first by producing aromatic compounds and subsequently aliphatic ones by increasingly lowering the molecular weight

(Waheed et al., 2020). As a consequence, there was a rise in the solution conductivity and a drop in the pH value. It is also noted that at some point, all of the carbon, nitrogen, and sulfur heteroatoms are converted into their respective compounds of interest (CO2, SO42-, NH4+, and NO3- ions) (Baker, 2002). Acid Red 18, Methyl Orange, and other azo dyes have all been studied for their potential degradation by TiO2 (El Mragui et al., 2021), both mono-azo and diazo dyes were among them (Bilal et al., 2018). Dye color loss and total organic carbon removal rates can be used as proxies for their degradation rates (C. Y. Tang et al., 2018). Diazo dyes are shown to be less biodegradable than mono-azo dyes on this basis. In these analyses, phenolic compounds, aromatic amines, and organic acids were found to be major intermediates (El Mragui et al., 2021). The outcome further indicated that adsorption of the dye to TiO2 is a key component when determining the level of degradation of azo dyes in photocatalytic system (El Mragui et al., 2021). According to a recent theory (Rashidi et al., 2019), illustrated the insertion of electron from the dye to conduction band as a minor contributor to the degradation process, occurring primarily by oxidation via •OH and reduction by conduction band electron. Figure 2. 12 below show azo dye degradation pathway.

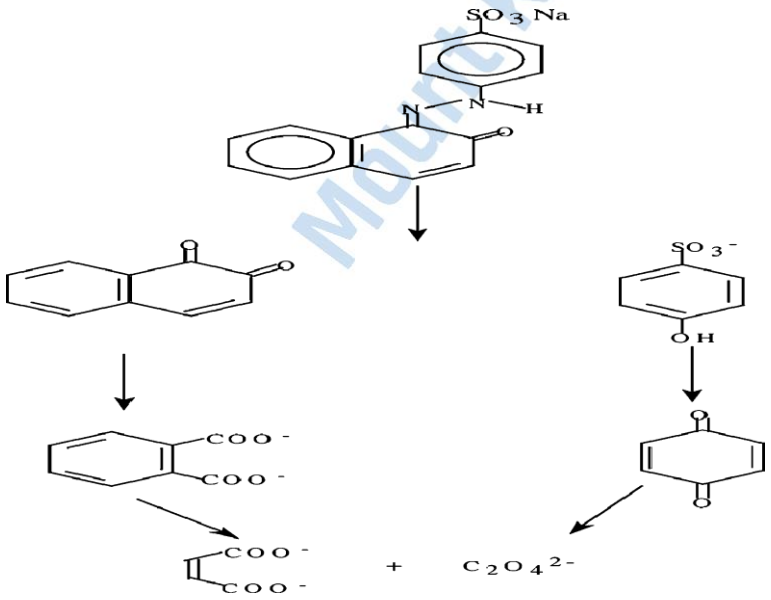

Figure 2. 13: Azo dye degradation pathway.

2.4.2 Thin Film Surface Reactions of Titanium Dioxide (TiO_2)

The absorption of photons, results in the liberation of energy of similar amount or higher compared to the one generated when a semiconductor oxide is applied. The titanium dioxide (TiO_2) constitutes a band gap of ca.3.2 eV for anatase. Followed by the generation of pairs of electron-hole.

$$TiO_2 h\nu \rightarrow e^-_{cb}(TiO_2) + h^+_{vb}(TiO_2) \quad \text{Eq (2.12)}$$

Redox reaction, taking place causes species involved in the solution to bind with these electrons and the holes possessing positive charges as shown in the equation 2.12 above. The outcome shows that these radicals are charged and ready to part in the reaction (Ghattavi & Nezamzadeh-Ejhieh, 2021).

2.4.2.1 Principles of photocatalysis and mechanistic pathways

Advance oxidation processes involves the degradation of the components involved photo catalytically proving to be a sufficient technology in the treatment of these organic dye substances compared to other AOPs (Ji et al., 2020). This technique is more effective because semiconductors can effectively mineralize several organic components and inexpensive too (Omrani & Nezamzadeh-Ejhieh, 2020). The photocatalytic degradation of the dyes is known to occur following the illustrated mechanism below, which involves exposing a catalyst to a radiation containing UV. The electrons get promoted from the valence band to the conduction band resulting in an electron–hole pair being formed as illustrated in the equation 2.13 below (Tafreshi et al., 2019) .

$$\text{Catalyst} + hU \rightarrow e^-_{cb} + h + vb \quad \text{Eq (2.13)}$$

Here, e−cb and h+ vb are the conduction band electrons and the vacant electrons occupying the valence band, accordingly (N. Sharma et al., 2019). There is a tendency by the generated species to attach themselves to the surface of the catalyst from where oxidation and reduction reactions with other entities present occur on the surface (Y. Hu et al., 2020). Nonetheless,

h+vb reacts quickly to the surface bound water in order to form OH species, while, e^{-}сь interacts with oxygen liberating superoxide anion species as indicated in the equation 2.14(a) and 2.14 (b) (Kovacic et al., 2020).

$$H_2O + h + vb \rightarrow {}^{\circ}OH + H \qquad \text{Eq (2.14 (a))}$$

$$O_2 + e^{-}_{cb} \rightarrow O_2^{-\circ} \qquad \text{Eq (2.14(b))}$$

These interactions hinder the association between the electron and the hole generated at the initial step. These radicals (°OH and O_2^{-}°) formed have a possibility of reacting in the same way with dyes to generate other components hence being responsible for the dye colour elimination as illustrated in the equation 2.14(a)-2.14(f) below (B. Liu *et al*., 2019).

$$O^{-}{}_2{}^{\circ} + H_2O \rightarrow H_2O_2 \qquad \text{Eq 2.14 (c)}$$

$$H_2O_2 \rightarrow 2 \cdot OH \qquad \text{Eq 2.14 (d)}$$

$$\cdot OH + \text{dye} \rightarrow \text{dye ox } (k = 10^9 - 10^{10} M^{-1} S^{-1} \qquad \text{Eq 2.14 (e)}$$

$$\text{Dye} + e^{-}_{cb} \rightarrow \text{dye red} \qquad \text{Eq 2.14 (f)}$$

The oxidative species production in a photocatalytic mechanism is represented by scheme 2.2.

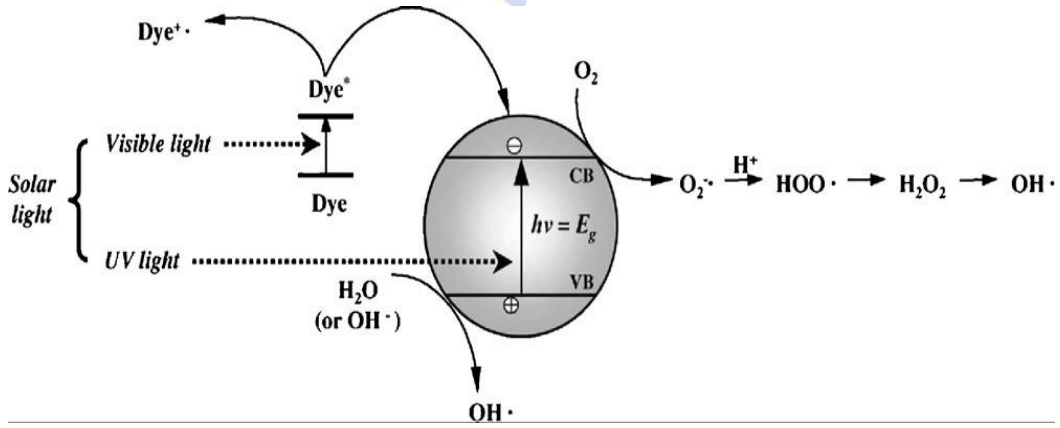

Scheme 2. 2: Schematic illustration of the oxidative species production in a photocatalytic mechanism (G. Duan *et al*., 2023).

2.5 The Development of Nanotechnology

Little particles of colored metals, most notably silver, was added to glass windows in the recent past in order to achieve a glassy yellow hue (Solomon *et al*., 2007). Although nanomaterials have been around for a while, the last twenty years have seen significant advancements in the field of nanoscience (Leon *et al*., 2020). Nobel Laureate Richard Feynman introduced for the first time in history the nanotechnology concept in 1959 while speaking at the Technology Institute of California (Prasad *et al*., 2021). In his article titled "There is lots of room at the bottom," published in 1960, Richard Feynman introduced the concept of nanomaterials. If information required only 100 atoms, he realized, every book ever written could fit into a cube 0.02 inches on a side (Chanu & Singh, 2022). This technology was later on explained by Norio Taniguchi in 1970. To paraphrase what he said, "Nanotechnology basically constitute of the separation, processing, distortion, and consolidating a fabric an atom or by a molecule" (Enescu *et al*., 2019). In addition, in 1980, K. Eric Drexler advocated for the importance of nanotechnology. Most significantly, at the nanoscale, particle characteristics diverge significantly from those at the bulk size (Ariga, 2021). The sizes and shapes of the metal particles in colloids take a fundamental role in several applications for instance in magnetic preparation, electronics, wound fixation, anti-microbial organic phenomenon, and within the manufacture of bio-composites. Therefore, these nanoparticles find their application in many areas like in electrical appliances, biological treatments, textile industries, and chemistry in general (Z. P. Xu, 2022). The optical, catalytic, and electromagnetic properties of colloids composed of metallic elements which are directly related to the particle sizes and forms (Gottardo *et al*., 2021). It is essential to have a firm grasp on the synthesis procedures for creating colloidal nanoparticles with a predetermined morphology (Shnoudeh et al., 2019).

2.5.1 Nano Materials

Nanotechnology refers to a branch of materials-focused engineering and science (Azharuddin *et al*., 2019). Particle sizes range of 1 and 100 nanometer is the focus in the nanoscience, and

nanomaterials are defined as having a minimum of one structured component with a dimension less or equal to 100 nanometers (Prasad *et al*., 2021). The high conductivity by the nano-metals has resulted in a great deal of research interest in nanostructures created from the nanoparticles during the past decade, especially when contrasted to nanoparticles derived from metal oxides (El-Seedi *et al*., 2019). Nanoparticles are defined as solitary components fringing between 1 and 100 nanometers in size and do not indicate a metal-metal link (Leon *et al*., 2020). In comparison to bulk metal particles, metal nanoparticles are remarkably unique in features because due to their nanoscale dimensions, large surface area to volume ratio and degenerated density in their energy states (Azharuddin *et al*., 2019). Catalysts are desirable due to their high chemistry and selectivity in comparison to the bulk metal species (Jamkhande *et al*., 2019). These nanoparticles are much different from their bulk counter-parts in terms of their overall chemistry, electrical conductivities, optical, magnetic, and mechanical, properties brought about by the quantum effects they possess (Shnoudeh *et al*., 2019). Many fields, including electronics, photovoltaics, drug delivery, catalysis, fuel cells, LEDs, industrial lithography, quantum dots, quantum wires, quantum devices, optical analogues, and quantum computing, have contributed to research interest significantly starting with the nanomaterials due to their unique values and diversity in terms of their applications (Bayda *et al*., 2019). Amazing nanoparticle qualities are highly sensitive to factors like as nanoparticle form, size, environment, and production technique (Behzad *et al*., 2021). As a result, researchers are keen to investigate the potential of metal nanoparticles in domains including catalysis, electronics, sensor, and device fabrication by focusing on their creation into a variety of shapes and sizes (Prasad *et al*., 2021). Many in the nanotechnology community view nanoparticles (NPs) as fundamental components of the field (Chanu & Singh, 2022). The nanotechnology subfield draws from a range of disciplines in science, including physics, biology, chemistry, medicine, and material science (Canaparo *et al*., 2020). In the most recent years, various physical and chemical techniques have been reported for synthesizing metal nanoparticles (Azharuddin *et*

al., 2019). It is crucial to establish environmentally safe protocols in nanomaterial synthesis because the use of chemical procedures and energy-intensive pathways renders these options eco-hazardous and prevents them from being used in the biological, medical, and therapeutic fields (Gottardo *et al*., 2021). Nanotechnology has given rise to biotechnology, the targeted integration of bio and nano-techniques for the production of NPs (Saravanan *et al*., 2021). These nano-products stand out from the crowd not only because of their novel treatment approach, but also because of their distinct particle size, physical, biological, and chemical properties, and wide variety of potential uses (Chanu & Singh, 2022). To meet the rising demand in a variety of sectors, it was important to develop a low-cost, safe, and environmentally acceptable method of producing metal nanoparticles (Kamran *et al*., 2019).

2.5.2 Nanoparticle Metal Synthesis

Top-down and bottom-up methods have been developed for the synthesis of nanoparticles, respectively (Gómez-Graa *et al*., 2017). In the top-down method, nanoparticles are first synthesized by reducing their size from a suitable starting material (Manimaran & Kannabiran, 2017). Because the surface chemistry and, by extension, the other physical characteristics of nanoparticles, are heavily dependent on the surface structure, imperfections generated by a topdown approach inside the surface structure of the nanoparticles are often a major constraint (Rodrigues *et al*., 2019). Nanoparticles with smaller entities are generated first, and then assembled to supply the ultimate particles, in a process known as bottom-up synthesis, in which smaller entities are connected with one another and fabricated (Abdussalam-Mohammed, 2019). To achieve a bottom-up strategy, it is common to use chemical and biological techniques (Azharuddin *et al*., 2019). When compared to biological approaches, chemical and physical methods for synthesizing nanoparticles are environmentally harmful due to the usage of toxic compounds and high energy requirements (Gómez-Graa *et al*., 2017). Although biological methods require more time to synthesize metal nanoparticles than chemical ones, this time has been reduced with the use of the most suitable microorganisms or organisms (Alavi & Rai,

2019a). Hence, biological procedures are preferable to chemical and physical ones because of their low cost, little impact on the environment, and scalability. Nanoparticle synthesis without the use of potentially hazardous amounts of energy, heat, or chemicals (Gottardo *et al*., 2021). It has been extensively reported that nanoparticles can be synthesized from microbes using biological processes (Siddiqi *et al*., 2018). In contrast to the cheaper production and handling of plant extracts, the generation and handling of microorganisms is more expensive when synthesizing nanoparticles using microbes (Some *et al*., 2018). (Mohanta *et al*., 2017). Scheme

2. 3 below shows the various approaches for fabrication of Metal Nanoparticles. As reported by Moradi *et al*. (2021), chitosan-mediated metal nanoparticle synthesis is a beneficial and inexpensive alternative for industrial-scale metal nanoparticle synthesis (Some *et al*., 2018). It has been suggested that biomolecules included in crab extracts are responsible for the reduction of metal ions and a stabilizer for metal nanoparticles throughout the manufacturing process (Renuka *et al*., 2020). Extracts from the neem crab contain biomolecules such terpenoids, nimbaflavone, sugars, etc., that can be used as capping agents to reduce metal ions (Siddiqi *et al*., 2018). As crab-shell chitosan extract may be easily obtained and inexpensive, that's why we decided to include it in our nanoparticle synthesis (AbdelRahim *et al*., 2017).

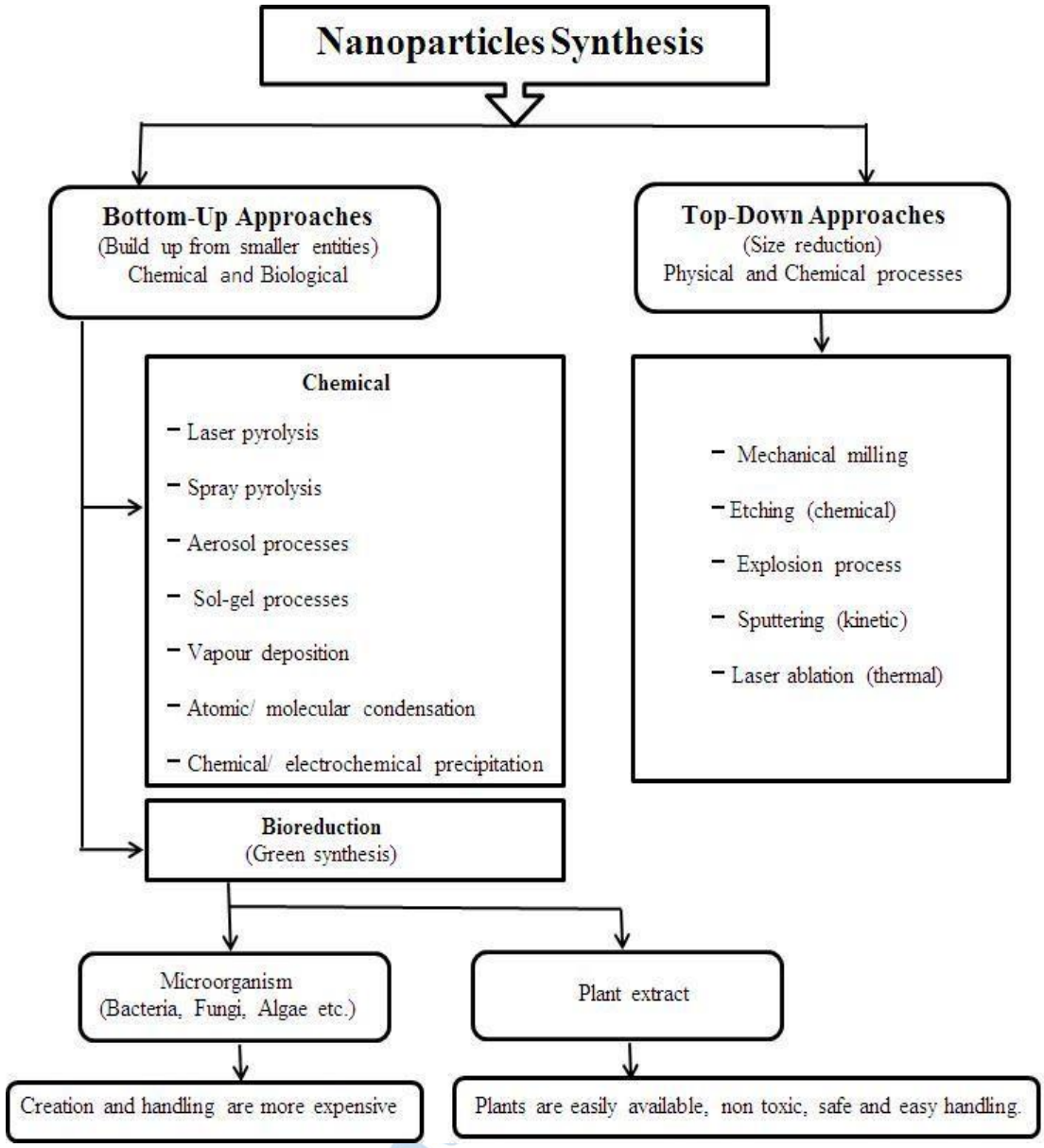

Scheme 2. 4: Various approaches for fabrication of Metal Nanoparticles

2.5.3 Synthesis of Nanoparticles by Bio-reduction

The application of chemicals and physical techniques have been in use for a very long time to produce metal nanoparticles (Cui *et al*., 2017). Yet, only recently has the possibility of biological manufacturing of metal nanoparticles been investigated (Vijaya *et al*., 2017). It has been common knowledge since the early 1900s that plant extract can be utilized as a biological reduction for metal ions (Some *et al*., 2018). The reduction products haven't been explored for

practical applications, but natural processes and chemical or physical procedures have been shown to produce metal nanoparticles with similar properties (Mohanta *et al*., 2017). Increased chemical, biological, and therapeutic aspects of the produced nanoparticles have led to a wide utilization of plant extracts in the green synthesis methods (Renuka *et al*., 2020). The noticeable impacts of these nanoparticles can be attributed not only to their reduced sizes and form diversity, but also the ease with which they can be synthesized (Patil & Kim, 2017). There is such an urgent need for environmentally recognized technologies in material synthesis, this has made biosynthesis as a method to receive much attention (Gorito *et al*., 2021). The result of developing environmentally friendly routes for nanoparticle synthesis without the use of toxic chemicals is becoming an increasingly pressing issue (AbdelRahim *et al*., 2017). Moreover, cutting-edge techniques have been presented for the ecologically benign production of the said nanoparticles (Siddique *et al*., 2022). They cover such ground in the areas such as bio-reduction, development and stability of the nanoparticles (Raja et al., 2017). Nanoparticles of metal that have been manufactured in such a friendly method require low-maintenance and are affordable (Nagar & Devra, 2018). The method is not only suitable for a large-scale synthesis but also discourages the process of handling microbial cultures (Beyene *et al*., 2017). The scheme 2. 5 below shows biosynthesis of metal nanoparticles.

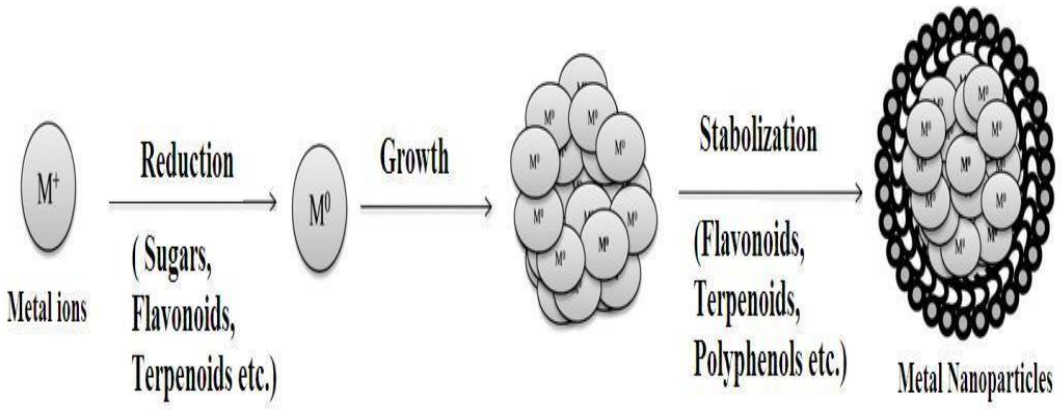

Scheme 2. 6: Biosynthesis of metal nanoparticles (Vijaya *et al*., 2017).

2.5.4 Silver nanoparticles

One of the most exciting developments in nanotechnology is silver nanoparticles (Zekic *et a*l., 2018). Currently, nanotechnology research relies heavily on the development of reliable procedures for the development of the nanoparticles (Dlamini *et al*., 2019). Green synthesis is one example of such a promising procedure (Yazdi *et al*., 2020). There are also a number of, chemical and biological routes of synthesizing silver nanoparticles (L. Xu *et al*., 2020). Recently, green synthesis has replaced several fast chemical processes in order to reduce process toxicity and boost product quality (Deshmukh *et al*., 2019). Glass makers used silver nanoparticles for their exceptional optical characteristics as early as the Roman Empire (Kefeni & Mamba, 2020). The so-called Lycurgus cup, is a prime example of this green synthesis and on display in the British Museum (T. Naseem & Durrani, 2021). Silver nanoparticles of 40 nm diameter consisting of 70% silver and 30% gold alloy were found in its bronze-mounted insets of glass in a study conducted in the late 20th century (Guilger-Casagrande & Lima, 2019). This explains why this bowl seems red or grey in different light media, a striking optical effect (Pareek *et al*., 2018). Before the 1980s, scientists and engineers became interested in silver nanoparticles due to the possibility that they could be applied sufficiently as dispersed support for amplifying signals emerging from organic substances within the Raman spectroscopy (John *et al*., 2022). This glass containing nano silver was prepared (Li *et al*., 2021). Silver nanoparticles, as shown by basic experiments conducted over the past three decades, have a unique and important set of properties, including surfaces development, catalysis, double layer high electrical capacitance, and more (Salleh *et al*., 2020). This is why they have become an integral part of research into next-gen electrical, optical, and sensor technologies (Akter *et al*., 2018). There has been a dramatic growth in scholarly articles dedicated to the production and various aspects of silver nanoparticles for the last two decades, thanks to the consequent need to modernize technological processes (Handoko *et al*., 2019). Common applications for silver nanoparticles as catalysts include the conversion of methanol to formaldehyde, oxidation of

ethylene to ethylene-oxide (Yazdi *et al*., 2020). Unique qualities of colloidal silver such as high conductivity, chemical stability, catalytic activity, and antimicrobial properties, make it an intriguing substance (Liao *et al*., 2019). Although surface enhanced spectroscopy (SERS) in part requires electrical conducting surface, silver colloids are essential substances for this technique (Alavi & Rai, 2019b).

2.5.5 Chitosan-coupled silver nanoparticles

Chitosan (CS) is a polysaccharide that features a b-1-4- glycosidic bond between glucosamine and N-acetyl glucosamine (Crini *et al*., 2013). CS is a biopolymer that is both harmless and biodegradable by enzymes found in the human body (Badot *et al*., 2013). Crystallinity is a crucial factor in adsorption efficiency, and commercial CSs are semicrystalline polymers (Gupta *et al*., 2014). Polymer CS has broad-spectrum antibacterial effect because it binds to the negatively charged bacterial cell wall and then attaches to the DNA, preventing replication of the bacterium (Bajpai *et al*., 2014). Chitosan is an antimicrobial biopolymer (Joginder *et al*., 2018). Chitosan's bioactivity can be enhanced by combining it with other bioactive compounds, such as medicines. The antimicrobial and healing functions of silver nanoparticles (AgNPs) are well-established (Neeta *et al*., 2018). They are highly effective against many different types of bacteria, and this is true even at extremely low concentrations (Ramesh *et al*., 2018). It was found that silver nanoparticles have promising applications in cancer therapy (Gupta *et al*., 2014). However, the main drawback of employing silver alone is that it is poisonous to normal cells when exposed for extended periods of time when the normal size of silver utilized is (Gupta *et al*., 2014). Using chitosan as a carrier for silver nanoparticles, this research hopes to overcome this obstacle. Since the chitosan in the nanocomposite is highly selective for cancer cells, it is one of the few composite materials to have the potential to be employed as a biosensor and in the addressing the issue of cancer (Crini *et al*., 2013). Silver's effectiveness on damaged cells is increased, while normal cells are protected (Badot *et al*., 2013). This nanocomposite also has the added benefit of being biodegradable, meaning it can be broken down by enzymes

and chemical auxiliaries found in textile effluent (Gupta *et al*, 2014). In this research, silver nanoparticles (AgNPs) will be synthesized and characterized before their application to indium tin oxide to form a nanocomposite electrode.

2.5.6 Roles of Silver Nanoparticles

It is used in a variety of fields, including air filtration and quality management, biosensing, imaging, and drug delivery (Dang *et al*., 2020). Silver nanoparticles generated biologically have various potential uses, such as antimicrobials, optical receptors, catalysts in chemical detection reactions, bio labels, and coatings for solar power absorption (Fahmy *et al*., 2019). Despite their cytotoxicity, silver nanoparticles find widespread use in sectors as diverse as bimolecular analysis of high-sensitivity, diagnostics, antibacterial and therapies, catalysis, and micro-electronics chips (Liao *et al*., 2019). Applications in medicine, such as wound dressings, contraceptive devices, surgical equipment, and bone prosthesis, have been proposed (Rodrguez-Serrano *et al*., 2020). Other possible uses include in diagnosis and bio-imaging, optical densities imaging, and bio-implants e.g., heart valves. Several large consumer goods companies are currently making domestic products that make use of silver nanoparticles' antibacterial qualities (Das *et al*., 2020). Silver nanoparticles are utilized in a variety home appliance, including refrigerators, air conditioners, and washers (Ferdous & Nemmar, 2020a). Nanoparticles have unique physicochemical qualities that make them ideal candidates for various applications. These characteristics include a large surface area to volume ratio, mechanical strength, optical property, and their overall chemistry (Syafiuddin *et al*., 2017). To prevent the spread of disease, silver nanoparticles are incorporated in an inorganic antibacterial agent (Jeong *et al*., 2015). It has been hypothesized that the ions of silver have both a bacteriostatic (growth inhibition) and bactericidal (antibacterial) effect (Vázquez-Rodrguez *et al*., 2020), hence the term "oligodynamic" to characterize silver. Silver nanoparticles have various biological uses for instance antibacterial medicines are resistant to bacterial infection, enable wound healing and possess anti-inflammatory effects (Taylor *et al*., 2017). They are

also toxic towards microorganisms, by showing potent biocidal effect on different types of bacteria (Castillo-Henrquez *et al*., 2020), although they are rather non-lethal to mammalian cells. Thus, dental resin composites, bone cement, natural process fibers, and coatings for medical equipment all include silver ions, an antibacterial component (Ferdous & Nemmar, 2020b). Electronic effects coming from the localized electronic structure on the surface of nanoparticles are responsible for their bactericidal action (Barkat *et al*., 2018). These modifications are thought to increase silver nanoparticle surface reactivity (Yaqoob & Ibrahim, 2019). The ionic form of silver has been shown to inhibit vital enzymes by forming strong interactions with their thiol groups (Löffler *et al*., 2021). It is also hypothesized that after interacting with silver ions, bacteria's DNA loses its capacity to replicate (Orlowski *et al*., 2018). By attacking the bacterial membrane, silver nanoparticles disrupt the cell wall potential and accelerate intracellular (ATP) depletion, ultimately killing the bacteria (Dhayalan *et al*., 2018). Silver nitrate and silver sulfadiazine, two common silver compounds, are used to kill bacteria in water, to sterilize surfaces, and in burn care (Agarwal *et al*., 2019). For antibacterial functionality, it is costeffective to incorporate polymers, textiles, and catheters with silver nano-composites (Vázquez-Rodrguez *et al*., 2020). Ag NP is potently antibacterial against a wide variety of bacteria, including the ubiquitous E. coli found in the kitchen. According to the proposed mechanism, silver nanoparticles kill bacteria by interacting with their outer membrane and blocking their ability to breathe, as well as a few other metabolic pathways (Panpaliya *et al*., 2019). Because to recent technological advancements, silver compound may now be chemically reduced to nanoscale sized particles, allowing for its incorporation into an expanded range of materials, such as plastics, coatings, foams, and both natural and synthetic fibers. Antimicrobial protection offered by nano-sized silver is more longlasting, sometimes lasting the lifespan of the product (Mustapha *et al*., 2020). The pharmaceutical and medical industries have entered a new era thanks to the discovery of inorganic nanoparticles with effective antibacterial capabilities (Löffler *et al*., 2021). The promise of silver's antimicrobial

properties makes it the metal of choice (S. Tang & Zheng, 2018). It has recently come to light that silver nanoparticles are a promising antibacterial agent with a wide spectrum of extracellular and intracellular target locations (Roy *et al*., 2019).

2.5.7 Nano-catalysis

If metal nanoparticles have high surface energy, then they are productive catalytic medium.(Noël *et al*., 2021).According to Zhou *et al*. (2018), small silver particles are simpler catalysts than stable colloidal particles. These nano-catalysts have been shown to efficiently reduce several organic dyes, such as borohydride, as noted by K. Naseem *et al*. (2019). This catalytic process occurs via the transfer of electrons from the reducing agent to the dye, facilitated by the particles, according to Kharisov *et al*. (2019). The sizes of these particles, the E1/2 of the dye, and the interaction between the dye and the particles all affect the catalytic property of silver nanoparticles, as pointed out by Slepička *et al*. (2019). Li *et al*. 2021, noted that sizes of nanoparticles can be used to control their catalytic activity, as the redox potential is dependent on the nanoparticle size. Bilal *et al*. 2021, suggested that the structure, shape-based properties, nanoscale size, and composition of nanoparticles determine the catalytic activity of nanomaterials. They have received significant attention both industrial and academic researchers as a result of their potential benefits (Dawood *et al*., 2022). Scheme 2. 7 below illustrates the nano catalysis applications.

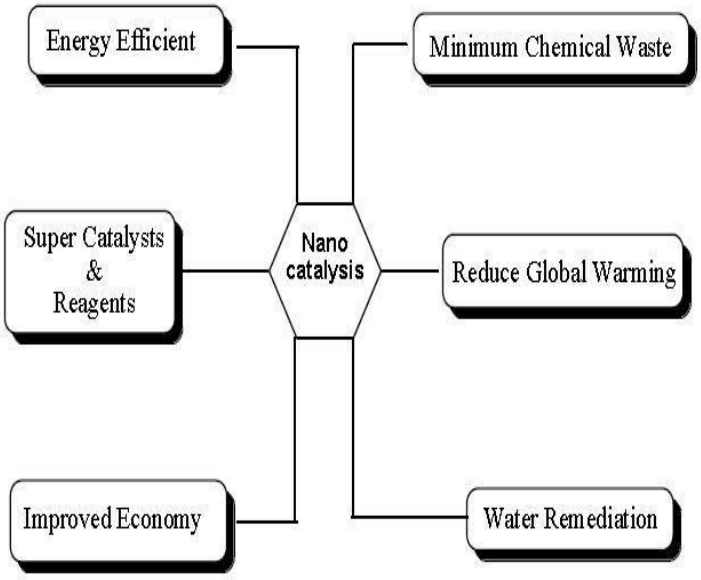

Scheme 2. 8: Illustration of nano catalysis applications (Zhou *et al*., 2018).

Homogeneous catalysis in solution (Kharisov *et al*., 2019) and heterogeneous catalysis on supported nanoparticles (Kharisov *et al*., 2019) are two types of nano-catalysis (Zhou *et al*., 2018). Solid nano-catalysts, such as iron, platinum, and nickel nanoparticles supported on clays, silica, alumina, and zeolites, or biowaste materials, carbon fibers, are also viable options for heterogeneous systems (Syafiuddin *et al*., 2017). To be effective, heterogeneous catalysts need extreme conditions, which might be challenging to transport in large quantities (H. Xu *et al*., 2017). In contrast to numerous homogeneous catalysts, however, their catalytic activity and selectivity are generally quite low (Li *et al*., 2021). Suspensions of nanoparticles dissolved in a solvent make up the nano-catalyst in a homogenous system (Willis, 2019). When constructing a nano-catalyst for use in a wellestablished solution catalyzed reaction, the system should incorporate strategies to prevent its aggregation (Bao *et al*., 2019). The vast surface area, catalytic activity, and other benefits of nanoparticles are lost when they agglomerate and cluster together to form larger particles (Gallego *et al*., 2017). The best results, especially in terms of product solutions, can be achieved by a process in which biomolecules are used to stabilize nano-particles and prevent their aggregation (Isbrandt *et al*., 2019). In contrast, the large

number of atoms in direct contact with the surface of metal colloids makes them potent catalysts (Begum *et al*., 2019). Quasi-homogeneous nanoparticle catalysts are the common name for this type of catalytic system (Chand *et al*., 2020). Colloidal nanoparticles are a possible solution, but they must be stable enough to prevent nanoparticle aggregation and recyclable enough to be environmentally friendly (Khaleghi *et al*., 2023). Because of their necessity for high activity, selectivity, and simple separation for re-use, quasi-homogeneous catalysts are potential catalysts for industrial application (Guo *et al*., 2022). To define catalytic processes, scientists use a category known as "quasi-homogeneous catalysis," which serves as a bridge between homogeneous and heterogeneous catalysis (Safaripour *et al*.,

2023).

2.5.8 Dye Degradation by Nanoparticle as Electrocatalysts

When released without sufficient treatment, organic coloring compounds can cause damage to aquatic ecosystems (Khalvati-Fahlyani *et al*., 2013). Many other approaches, including cremation, bioremediation, and ozonation, have been tried to deal with these dyes (Vikal *et al*., 2023). Both bioremediation approach and the incineration method have been shown to have drawbacks when used independently, such as the release of volatile and toxic chemicals (Saeedi *et al*., 2013). Complete elimination of colors in waste waters was made possible by employing metal oxide nanocatalysts with zinc dioxide semiconductor (Fahlyani *et al*., 2013). The organic nature of these coloured components is converted by the aforementioned nanoparticles into water, carbon dioxide, and less toxic chemicals like ammonia (Al-Qodaha *et al*., 2019). Because of their environmental friendliness and simplified method of synthesis, semiconductors like TiO_2 and ZnO are often utilized to improve the degradation aspect of the effluents (Wahab *et al*., 2022). Indium tin oxide (ITO) electrodes will be used in conjunction with silver nanoparticles (AgNPs) as the electrocatalyst to degrade textile effluents dye in this research (Qumar *et al*., 2021).

2.6 Electrochemical properties of Indium tin oxide (ITO) electrodes

There have been many attempts in the last two decades or so to create electrodes with dimensional stability (H. Wang *et al*., 2022), transparency, the ability to degrade organic colorants (S. Kumar *et al*., 2022), and the ability to undergo a variety of changes in properties as a result of electrochemical manipulation (Peafiel-Vicua *et al*., 2020). A tiny coating of indium tin oxide, which is responsible for the device's electrical conductivity, separates the two electrodes (Si *et al*., 2020). Both the switchable property and the auxiliary function of potential applications are demonstrated by these electrodes (Kusmierek, 2020). These semiconductor electrodes, which are essential to DSA, have a band gap greater than 3.5 eV. (Y. Ma *et al*., 2022). Because of the large tin (Sn) components exceeding 10 atoms% within the In_2O_3 oxide crystalline lattice, film electrodes made of indium (In) and tin (Sn) oxides deposited on a solid substrate as a thin film enhance its conductivity, which upon appropriate doping could rise up to a metallic level (Sezemsky *et al*., 2021). The electronic conductivity of indium tin oxide (ITO) is due to n-type doping, which is caused when tin (Sn) atoms substitute for indium (In) atoms in the bulk oxide structures (Zeng *et al*., 2020). Despite this, ITO electrodes exhibit nonstoichiometry in their oxide synthesis, as vacancy in oxygen deficit of the O2 ions may be readily observed via its conduction band (Kusmierek, 2020). The tin compounds formed in this electrode have been proven in various studies to be composed of oxides of Sn (IV) and Sn (II) (Peafiel-Vicua *et al*., 2020). Annealing ITO in an oxidizing environment is required for low sheet resistance good conductivity after deposition, even when using oxide targets (Gui *et al*., 2019). As a result of this reaction, the Sn (IV)/Sn (II) ratio in indium tin oxide (ITO) was altered, and overall conductivity of the material is raised (Xian *et al*., 2019). Indium tin oxide (ITO) electrodes and other oxide-type thin film conductors, such as SnO_x, undergo charge transfer via external Redox pair dissolution in electrolyte and deposition on the electrode surfaces, resulting in characteristic electrochemical behavior (Nehate *et al*., 2018). Since the structure of the electrode affects its electrochemical performance, these sorts of electrodes are

classified as organic material oxidizers (Kusmierek, 2020). (Sujatha *et al*., 2020). The present results from Granite and Ni are inappropriate (Tran *et al*., 2018). The addition of phenols is a useful technique for rendering the Pt anode useless. As a result, the rate of organic decomposition is slowed by these deposited oligomers (Abd Rani *et al*., 2020). The degrading process for organic compounds has advanced greatly thanks to the development of indium tin oxide (ITO) anodes in the last two decades (Y. Shen *et al*., 2020).

2.7 Water quality

Kenya's National Environmental Management Authority (NEMA) has established rules on water purity. Domestic water quality guidelines and discharge monitoring guidelines can be found in the Environmental Management and Coordination Act of 2006. Schedule 4 identifies biochemical oxygen demand (BOD), total suspended solids (TSS), chemical oxygen demand (COD), color/dye/pigment, temperature, oil and grease as the most important characteristics to track when observing textile discharge (GOK, 2006).

2.7.1 Alkalinity

Water's alkalinity measures its inherent capacity to prevent the acidity of its dissolved components (Ahmed *et al*., 2018). All the fundamental components that can be determined in a given sample using titrimetric analysis are included (Drumm *et al*., 2022). The alkalinity of textile effluent is caused entirely by the presence of dissolved carbonates (CO_3^{2-}), hydrogen carbonates ($HCO_3^{-)}$, and hydroxyls (OH^-) (Rathod & Pathak, 2018). The alkaline nature of textile effluents is also contributed to by other chemicals, such as PO_4^{3-}, BO_3^{3-}, and SiO_3^{2-} (Dos Santos et al., 2018). Waste water treatments, such as those used for irrigation or the addition of pesticides, are governed in part by the effluents' alkalinity (Al-Ansari *et al*., 2022a). According to (APHA, 2002), the alkalinity of textile industry effluent is primarily $CaCO_3$ (Bilinska *et al*., 2020).

2.7.2 Chemical oxygen demand

Dissolved oxygen (DO) levels drop as a result of chemical processes, leading to chemical oxygen demand (COD) (Pessoa *et al*., 2019). In most cases,COD is applied to gauge the extent of organic material contamination in textile effluents (Aleem *et al*., 2020). Thus, this suggests that the demand for dissolved oxygen (DO) by water channel to which the discharge is done increases proportionally with the chemical oxygen demand (COD) (Al-Sakkaf *et al*., 2020). COD is regarded to be representing the quantity of dissolved oxygen (DO) needed to reduce components like S^{2-}, CH_4 measured in units where comparable formulation of kinetics is utilized in many waters' quality models (Ataş et al., 2020). (Raj *et al*., 2021).

2.7.3 Biochemical oxygen demand

This is the sum of the chemical and biological oxygen used up by water microorganisms at a given temperature from the dissolved oxygen in the water (Abdalla & Hammam, 2014). Hence, textile effluents' BOD refers to the overall amount of dissolved oxygen (DO) necessary to promote the full degradation of organic components (Hur *et al*., 2010). To break down these organic molecules, the participating bacteria require oxygen (Dogan *et al*., 2009). Chemically activated processes involving nitrifications can also lead to oxygen depletion (Jouanneau *et al*., 2014). It also refers to a measure of how much oxygen an organism needs, although it is not a physically or chemically driven process (Agtaş *et al*., 2020). Using biochemical oxygen demand to assess water quality ensures that water is treated before releasing to the environment (Al-Sakkaf *et al*., 2020).

2.8 Instrumental Techniques

The fundamental theories and methods behind the most common types of analysis and characterization are covered in this section. This section also discusses the specifics instrumental methods -microscopy, Liquid chromatography mass spectrometry, Furiour Transform infrared spectroscopy, UV-Visible spectroscopy, used to characterize chitosan,

nanoparticles, and the removal of dyes in the presence of nanocatalysts embedded on indium tin oxide (ITO) electrodes.

2.8.1 A photo of Ultraviolet-Visible Spectrophotometer

Scheme 2. 9: (a): A photo of Ultraviolet-Visible Spectrophotometer taken from Pwani University Biological lab

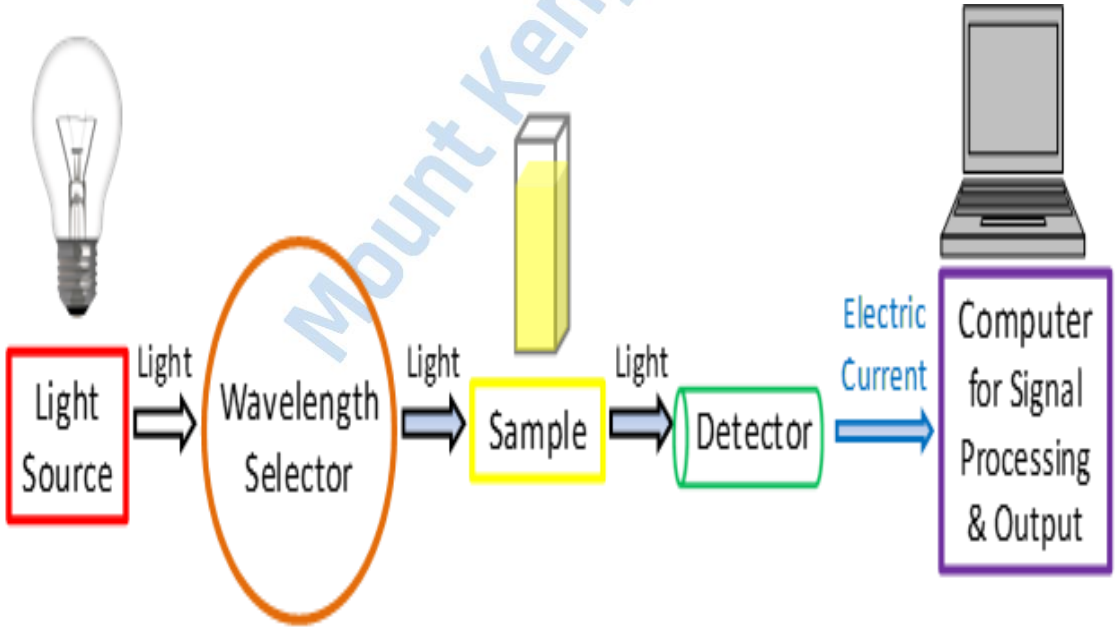

Scheme 2. 10: (b): ***Ultraviolet-Visible Spectrophotometer (Nardino et al., 2023)***

Absorption and reflectance spectroscopy are both components of UV-Vis or UV/Vis spectroscopy. It employs visible and ultraviolet light. The substances' hue is determined by how much light they absorb or reflect within the visible spectrum. Atoms and molecules undergo electronic transitions at these frequencies. It is possible for molecules with electrons or non-bonding electrons (n-electrons) to absorb energy in the form of UV or light if these electrons are excited in higher anti-bonding molecular orbitals. There are four different kinds of transitions ($\sigma \rightarrow \sigma^*$, $n \rightarrow \sigma^*$, $\pi \rightarrow \pi^*$and $n \rightarrow \pi^*$), and they are typically ranked as follows: - $\sigma \rightarrow \sigma_*$ > $n \rightarrow \sigma_*$ > $\pi \rightarrow \pi_*$ >$n \rightarrow \pi_*$. Analytical chemists use ultraviolet-visible (UV-Vis) spectroscopy to quantitatively work out various analytes, like metal ions, organic compounds conjugation, and biochemical involving macromolecules. This system also makes it possible to easily determine drug concentrations, review reaction rates, and calculate rate equations, which are often used to propose a mechanism. Although spectroscopy is most commonly used with liquid solutions, it can also be applied to the study of solids and gases (Tian *et al*., 2021). Analysis of metal nanoparticles distributed in a fluid or embedded in an insulator matrix can benefit from UV-Vis spectroscopy. In this investigation, the metal nanoparticles' surface plasmon resonance (SPR) is responsible for the absorption of incoming radiation. When light waves contact with the free electrons of a metal, a phenomenon known as surface plasmon resonance occurs (Milanović et al., 2021). Changes in color or brightness from reactants to products are necessary for kinetic analysis of reactions in solution. Measurements of the UV-Vis absorbance spectrum at known times are commonly used to calculate the degradation rate constant of a dye. Therefore, first order rate law integral, ln [A] (time t) = kt + ln[A] (time t), may apply if the reaction is first order (initial). ln [A] over duration yields a line having a slope of k, where k is negative of the speed constant. Different integrated rate laws correspond to different rate orders, which is consistent with the reaction mechanism. Changes in absorbance were used as an indicator of dye degradation in a kinetics study.

2.8.2 Centrifuge

The process of centrifugation involves utilizing pressure to segregate mixtures. This device is driven with an electric motor rotating an object, like a rotor via fixed axis. The process of centrifugation is based on sedimentation, which causes materials to separate based on their density under the influence of gravity maximum relative centrifugal force (RCF): ~1,600 g. In this particular research, a Remi C-854/6 Laboratory centrifuge with 8x15 swings out heads was utilized to prepare metal nanoparticles. The nanoparticles were held in tubes and 3500 rpm of centrifugation done for 15 minutes to create purified pellets, then underwent dispersion in deionized water. The process of centrifugation and re-dispersion were done three times, ensuing that separate species were obtained. The resulting pellets were filtered using Whatman paper and dried for further use in FT-IR spectroscopy.

2.8.3 Scanning Electron microscopy

Scanning electron microscopy is a very high and versatile technique applied in obtaining highly detailed with high level resolution images on surface information of the samples. This microscopy applies a focal beam, high-energy electrons in its signal generation from a specimen in solid phase (Rydz *et al*., 2019). These signals are formed when specimens and electron beams interact and thus are capable of revealing morphological texture, chemical constitution, structural crystals and how the components orient themselves in samples. The scheme 2.8 below shows a photograph of scanning electron microscope (J. Liang *et al*., 2021).

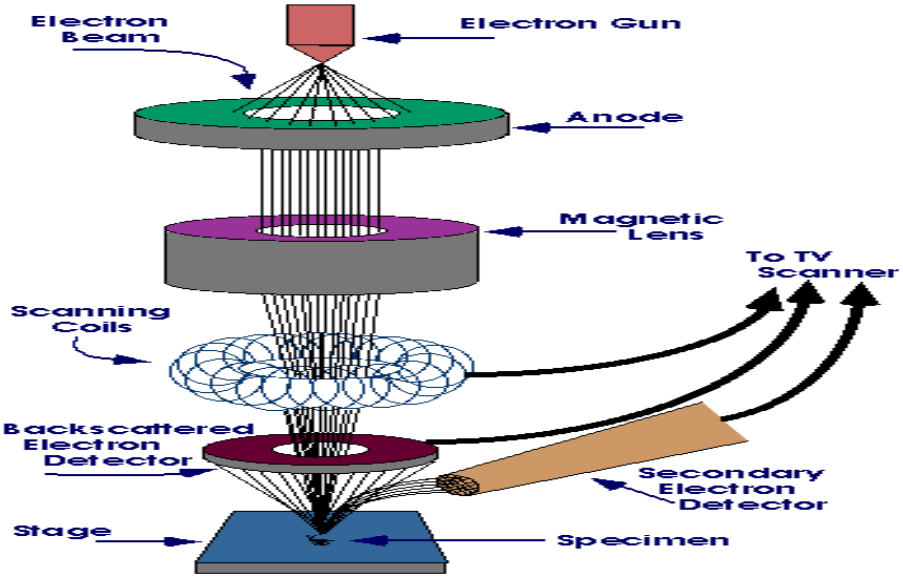

Scheme 2. 11: ***Scanning Electron microscopy (Fang et al., 2022)***

In most cases imaging through scanning electron microscopy involves two dimensions of the materials in the samples (Brahim Belhaouari *et al*., 2020). The displaying can spatially cut across the properties mentioned earlier on. An area range of between 1-5 micron in breadth can be imaged by magnification range of 20 - 30,000 X at 50 -100 nm resolution (Smith & Starborg, 2019). The scanning electron microscopy (SEM) can also image specified locant positions through sample under study (Pesaresi et al., 2020), a vital procedure to qualify and quantify components chemically, crystallized(Ullah *et al.*, 2022) orientation and crystal structures of the substances constituting the sample (Behbahani *et al*., 2019).

2.8.4 Fourier Transform Infrared Spectrophotometer (FT-IR)

FTIR as a spectrophotometer is crucial when it comes to identification of bond types in various molecules (Valand *et al.*, 2020). Scheme 2.9 below shows a photograph of a fourier transform infrared spectrophotometer. It is applied bring into perspective the composition of unknown mixtures and to analyze gas, liquid and solid samples (Hou *et al.*, 2018). It converts data from interference patterns to a spectral pattern (da Silva *et al.*, 2020).

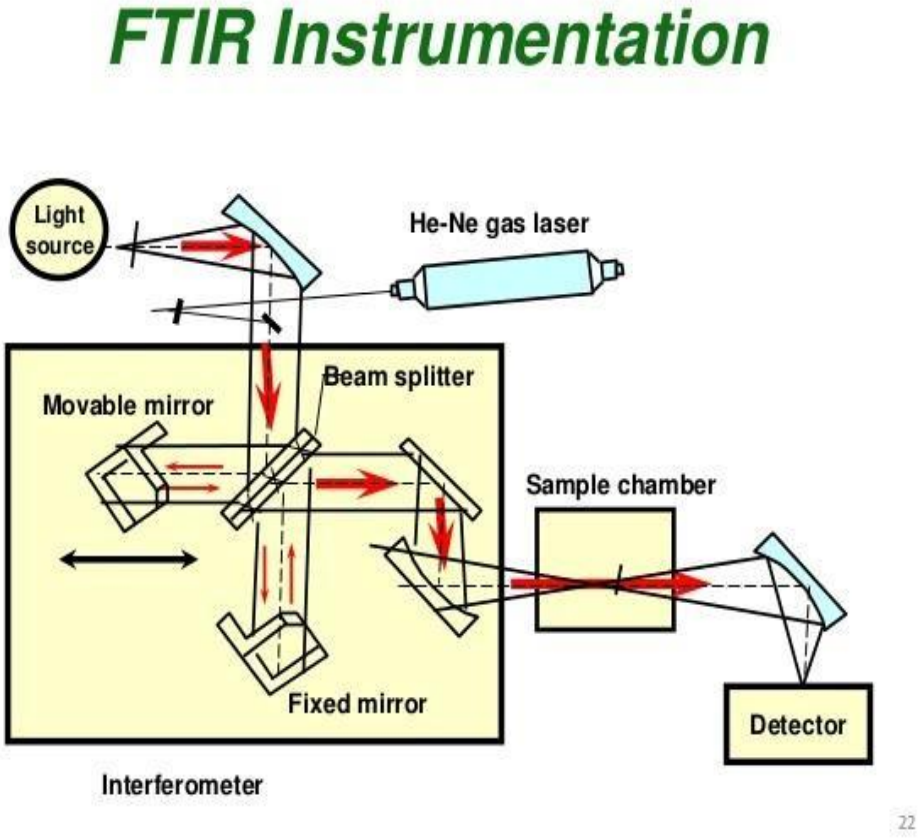

Scheme 2. 12: ***Fourier Transform Infrared Spectrophotometer*** **(Willans et al., 2023)** Furiour Transform Infrared Spectroscopy has a fingerprint for each chemical bond existing in a molecule making it an important tool in identification whenever applied since it would produce an infrared spectrum with specific molecular fingerprints (Cabernard *et al.*, 2018). The absorption by the chemical bond in the infrared spectrum occurs at specific wavelengths (Veerasingam *et al*., 2021). Bond types present in molecules occasionally vibrate at several frequencies and this depends on their presence in molecules and angles of their vibrations. Any chemical bond is capable of vibrating on various specified frequencies (Su & Lee, 2020). Quantum physics shows that these frequencies are related with the lowest and highest frequencies. This technique involves a method that focuses on the frequency of a molecular vibration to an extent of excitation as these chemical bonds undergo absorption of light energy (Y. Chen *et al.*, 2020). The light energy absorbed causes transitions, in which the energy

emitted is equivalent to the difference in energies between the lowest and highest frequencies (Sadat & Joye, 2020).

2.8.4 Liquid Chromatography –Mass spectrometry

Liquid chromatography-mass spectrometry (LC-MS) is an analytical chemistry technique which is predicated on the combinations of the physical separation abilities of liquid chromatography with the mass analysis capabilities of mass spectrometry (MS) (Ye *et al*., 2022). The standard LC-MS system may be a combination of HPLC with MS using interface (ionization source). The sample is separated by LC, and therefore the separated sample species are sprayed into the air pressure ion source, to ions converted within the gas phase. The mass analyzer is employed to categorize ions according to their mass to charge ratio (R. Zhang *et al.*, 2022). The separated ion identifies and quantifies directed to a photograph or tube detector amplifies the signal generated from each ion. Results of spectrum (a plot of the ion signal as a function of the mass-to-charge ratio) is generated, which is employed to work out the basic nature of a sample, the masses of particles of molecules, and to elucidate the chemical structures of molecules (Baur *et al*., 2022).Scheme

2.10 below shows a photograph of liquid chromatography–mass spectrometry (chick et al., 2023).The advantages of this technology include its sensitivity, specificity, and precision as analysis is completed at the molecular level. This system is often capable of determining inorganic, organic and biochemical compounds commonly found in complex samples of environmental and biological origin (Zhao *et al*., 2022). An interface is present in LC-MS that efficiently transfers the separated components from the LC column into the MS ion source. While the mobile introduces an LC system may be a pressurized liquid, the MS analyzers commonly operate under vacuum. Therefore, the eluate directly pumped from the LC column into the MS source isn't possible (Shen *et al*., 2022).

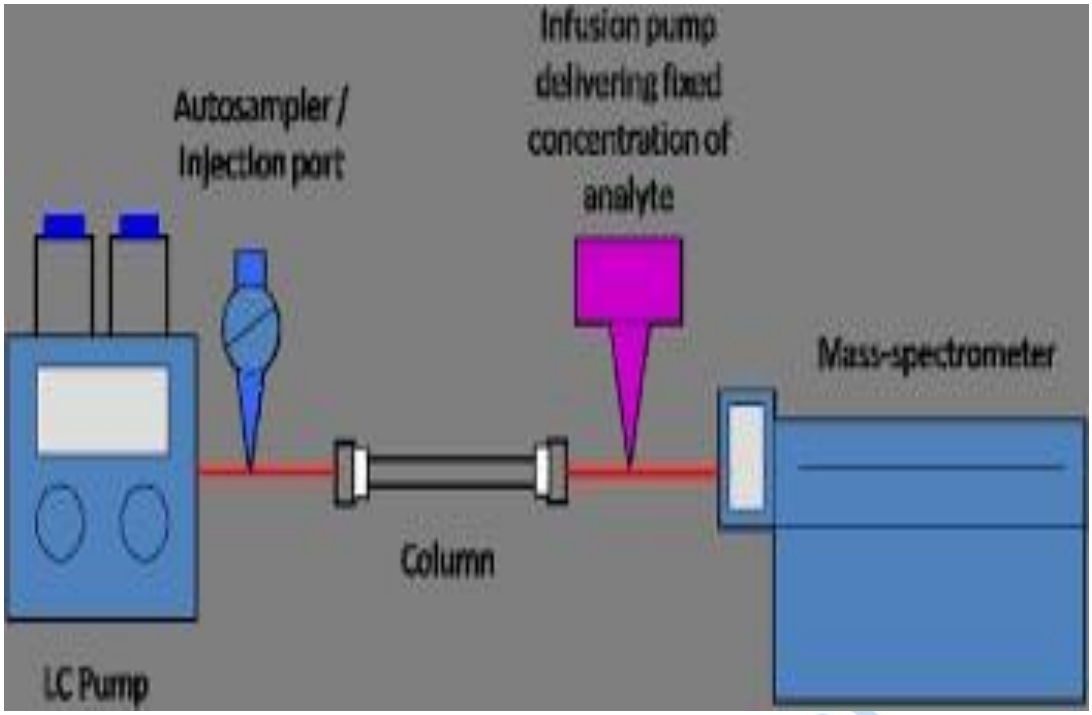

Scheme 2. 13*: Liquid Chromatography –Mass spectrometry* (Chick *et al*., 2023)

LC-MS interfaces are grounded on air pressure ionization (API) strategies like electronspray ionization (ESI), air pressure chemical ionization (APCI), and air pressure photoionization (APPI) (BALKAN, n.d.). Intermediates and end products obtained during dye degradation process were detected by LC-MS technique. Mass/charge ratio is employed to work out the molecular ions of unknown products. When fragmentation voltage of LC-MS increases, more fragments are observed to facilitate product determination (Holness *et al*., 2022).

CHAPTER THREE

MATERIALS AND METHODS

3.0 Introduction

This chapter presents the research methodology adopted in the study. It describes the experimental design, study site, materials and apparatus used, synthesis and characterization procedures, and data analysis techniques. The section also outlines measures taken to ensure reliability, validity, and ethical compliance in the research process.

3.1 Experimental designs

This research utilized an experimental approach in which the design established the cause-andeffect relationship relation towards the independent and dependent variables This study design was informed by Mi Yan et al., "Experimental study on the catalytic supercritical water oxidation of oilfield sludge" (2022) – Process Safety and Environmental Protection. The article presented an experimental study of catalytic degradation of oil-field sludge via supercritical water oxidation. It examined temperature, reaction times, oxidation coefficients, and catalyst usage. They determined the removal efficiencies (total organic carbon, carbon conversion) of up to ~96% under optimal conditions, and also examined catalyst regeneration. The findings were useful since it was a full experimental paper and not just a review in environmental engineering, it also applied real hazardous waste (sludge), catalytic process and gave parameter variation. It was further utilized in the designing experiments, benchmarking degradation efficiencies and catalyst selection for sludge/oil-waste. Throughout a 12-month period, 41 and 42 samples of industrial effluent were randomly collected from Rivatex textile industry, Uasin Gishu county, Kenya and Mombasa Textile Industry, Mombasa County, Kenya respectively. The samples were collected at discharge points and the specific locations were determined using a GPS MAP 64SX. A global positioning system was used to pinpoint the precise collection site and guarantee that future samples would be obtained from the same area. The gathered samples were stored in stored in amber glass bottles to prevent photodegradation until they were analyzed. The Azo dye concentrations in the collected samples were analyzed before treatment, during the pre-treatment and after the actual degradation. After testing and confirming the presence of Azo dyes in the control (untreated effluent), there were effluent samples treated with ITO electrode, AgNPs-ITO electrode and with electrocoagulation method.

3.1.1 Geometry of the applied Electrodes

In this study, it was important to determine the geometry of the applied electrodes during the electrolysis because electrodes have impact on the operational parameters (Kusmierek, 2020). In the electrolysis setup, indium tin oxide (ITO) electrodes were typically used as planar, transparent conducting substrates. Each electrode consisted of a flat glass plate coated on one side with a thin conductive ITO layer, thickness range between 100 to 300 nanometers. The conductive surface was smooth and uniform, allowing for a well-defined electrochemical interface. During electrolysis, two ITO electrodes were positioned parallel to each other, facing their conductive sides inward. The distance between the electrodes was precisely controlled—often on the order of a few millimeters—to ensure a uniform electric field across the electrolyte solution. The active area of each electrode (the region in contact with the electrolyte) was rectangular section, between 1–4 cm^2, on the cell design. The electrodes were typically mounted vertically and slightly inclined within a cell chamber that holds the electrolyte solution. Electrical connections were made to the ITO coating via copper clips, silver paint, and conductive adhesive tape attached to the unexposed edge of the coating, ensuring minimal obstruction of the optical path if optical measurements are needed. The transparent nature of the ITO allows in situ optical observation or spectroscopic analysis during electrolysis (Ligorio *et al*., 2020).

3.1.2 Scale up issues

Scaling up is defined as the possibility for the expansion and replication of the study. Scaling up is an integral aspect in the implementation of any scientific research. Scaling up ITO electrodes from small research samples to large-area devices presents a range of difficulties related to uniformity, cost, and process compatibility. One of the foremost challenges is achieving consistent film thickness and electrical conductivity over large substrates. In smallscale sputtering or evaporation setups, parameters such as target-substrate distance,

deposition rate, and temperature can be tightly controlled. However, as substrate dimensions increase, it becomes harder to maintain uniform film composition and surface morphology, often resulting in variations in sheet resistance and optical transmittance across the surface (Xian *et al*., 2019). Another major issue concerns the mechanical fragility of ITO films. ITO is inherently brittle, and when deposited on flexible substrates (used in flexible electronics or large-area displays), it tends to crack or delaminate under strain. This mechanical limitation becomes more pronounced when scaling up to flexible or roll-to-roll processing, where films must endure bending, thermal cycling, and handling stresses. Deposition throughput and cost are also significant considerations. The sputtering process commonly used to deposit ITO requires vacuum systems, high energy input, and expensive indium targets. Scaling these systems up for mass production leads to high capital and operational costs. Moreover, indium is a relatively scarce and costly element, creating supply chain and sustainability concerns for large-scale deployment. Thermal processing steps used to optimize film crystallinity and conductivity also introduce difficulties. ITO typically requires annealing at temperatures above 300 °C to achieve good performance, but many flexible polymer substrates cannot withstand such heat. This limits the choice of substrates or requires alternative low-temperature processing methods, which often compromise film quality. Finally, integrating large-area ITO coatings with complex device architectures—such as multilayer organic LEDs, solar cells, or touch panels— demands precise patterning. Conventional photolithography or etching becomes cumbersome and expensive at scale, while alternatives like laser ablation can introduce edge defects or surface damage(El-Naggar *et al.*, 2018).

3.1.3 Current density

Current density is the current delivered to the electrode divided by the active area of the electrode and is achieved by varying the current. It determines both the rate of electrochemical metal dosing to the water and the electrolytic bubble density production. Current densities

ranging from 10 to 2000 A / m^2 have been used; however current density in the range 10 to 150 A / m^2 has proved efficient (Cheng, 2004). Different current densities are desirable in different situations. High current densities are desirable for separation processes involving flotation cells or large settling tanks, while small current densities are appropriate for electrochemical cell set ups that are integrated with conventional sand and coal filters (Reynier *et al*., 2022)). A systematic analysis is required to define and refine the relationship between current density and desired separation effects. Current density was determined from the surface area of the electrodes applied to volume ratio of the azo dye solution from the textile effluent.

3.2 Chemicals, reagents and electrodes

Chemicals and reagents utilized were analytical grade obtained from Sigma Aldrich Laboratory suppliers. Solution preparations were conducted in the postgraduate research laboratory of Pwani University, Kilifi County, Kenya. All solutions were prepared using distilled de–ionized water. Indium tin oxide (ITO) thin film conductive materials were obtained from Sigma Aldrich Laboratory suppliers, whereas, textile effluent was acquired from Rivatex, Textile Factory Uasin Gishu County, Kenya and Mombasa textile industries, Mombasa County, Kenya discharge points. Specific locations for collections for the sample acquisition were determined using global positioning systems (GPS MAP 64SX). Chemical reagents included: - dichloromethane, sodium sulphate, propylene glycol, hexane, sulfuric acid (H_2SO_4), sodium hydroxide, pH buffer, phosphate buffer, magnesium sulphate, calcium chloride, iron (III) chloride, potassium dichromate ($K_2Cr_2O_7$), silver sulphate, ammonium sulphate, salicylic acid, sodium nitrate, **s**odium dihydrogen phosphate (NaH_2PO_4), copper sulphate, zinc sulphate and 1,10-phenanthroline monohydrate, silver nitrate, chitosan, sodium chloride.

3.2.1 Solution pH

An optimal pH exists for a given pollutant, with optimal pH values ranging from 6.5 to 7.5 for the textile effluents (Holt *et al.,* 2006). The solution pH used in this study was maintained at 6.5, based on its reported efficiency in azo dye removal (Patidar & Srivastava, 2022). This pH

was used to determine the speciation of metal ions. The pH has an influence on the state of other species in solution and the solubility of products formed (Koulini *et al*., 2022). Thus, solution pH influences the overall efficiency and effectiveness of electro-coagulation.

3.2.2 Electrode Material

The electrodes used in this research included indium tin oxide embedded with silver nanoparticles. Stainless steel electrodes were also applied during the electrocoagulation in order to correlate their effectiveness in comparison to the new technology. The most commonly used electrodes in the recent past during treatment of the textile effluent boron doped diamond (BDD), indium tin oxide (ITO) and/or iron plates Novikova and Shkorbatova (2012) . Comparison of the performance of BDD, iron and ITO electrodes for removing colour from dye-containing solutions indicated that optimal electrochemical conditions needed to be varied with the choice of electrode, which in turn determines the initial pollutant concentration (Vik et al. (2011)), pollutant type and stirring rate (Do and Chen, 1994).

3.2.3 Electronic Balance

Analytical balance (model- CX 220 manufactured by Citizen Scale (I) Pvt Ltd) was used for weighing reagents. The weighing range of balance is 0.0001 g and 220 g respectively.

3.2.4 Magnetic Stirrer with Hot Plate

In this research, a magnetic stirrer with a hot plate (Model MSW-313, MAC)at 600 rpm (range 0-1200 rpm) was used for precision in temperature control and efficiency in mixing of the liquids involved. The stirrer works on 220/230 volts AC supply and temperature 0.0350.0 °C. They were used for mixing reagents and samples to form homogeneous solution.

3.2.5 Motic Light Microscope

The BA210 version with the digital features of an integrated 3MP camera with Motic Images 3.0 software were incorporated in order to view images of the ITO electrode before and after

embedment with silver nanoparticles (AgNPs). The resolution was varied between 20x, 60x and 100x magnifications.

3.3 Study Area

The study area included industrial effluent discharge areas of Rivatex Textile Factory in Eldoret, Uasin Gishu County and Mombasa Textile Industry in Mombasa County, Kenya. For Rivatex textile industry, the samples were collected from rivers Sosiani and Kesses which are the main discharge sites for textile effluents from Rivatex Textile Industry located in Eldoret County, country. The Eldoret municipality, covering an area of 35 km^2 with approximate population of 475, 716 people (KNBS, 2019). The town lies at 0° 30' 51.3972" N and 35° 16' 11.2044" E (KNBS, 2019). The main economic activities in Eldoret Town include agriculture and the town is also a local manufacturing hub hosting manufacturing industry such as Raiplywoods, Rupa Textiles, Rivatex Textiles, Kenya Pipeline Company, Kenya Co-operative Creameries as well as corn, wheat and pyrethrum factories all within the town (Maghanga *et al.*, 2017). Mombasa textiles lie in the coastal region in Mombasa County, Kenya. Mombasa city, is an island surrounded by Indian ocean. The major economic activities of people living in Mombasa include: - trade, tourism and manufacturing. The Mombasa textiles industries include the Apparel and Hantex. These industries discharge textile effluents to the surrounding water bodies. These effluents are discharged into rivers Mwachi, Mombona and Chasimba which in turn drain their waters to the Indian ocean. According to Wanjohi *et al.*, 2019 most of the cancer-related ailments and disorders among residents living around Rivatex Textile Industry could be attributed to the consumption of foodstuff containing traces of textile effluents (Wanjohi *et al.*, 2019). Efforts to mitigate these challenges have not yielded much remarkable progress, hence the focus on Rivatex and Mombasa Textiles as the study site (Mwasi *et al.*, 2019). Figure 3.1 and Figure 3.2 below show the maps of the two study areas.

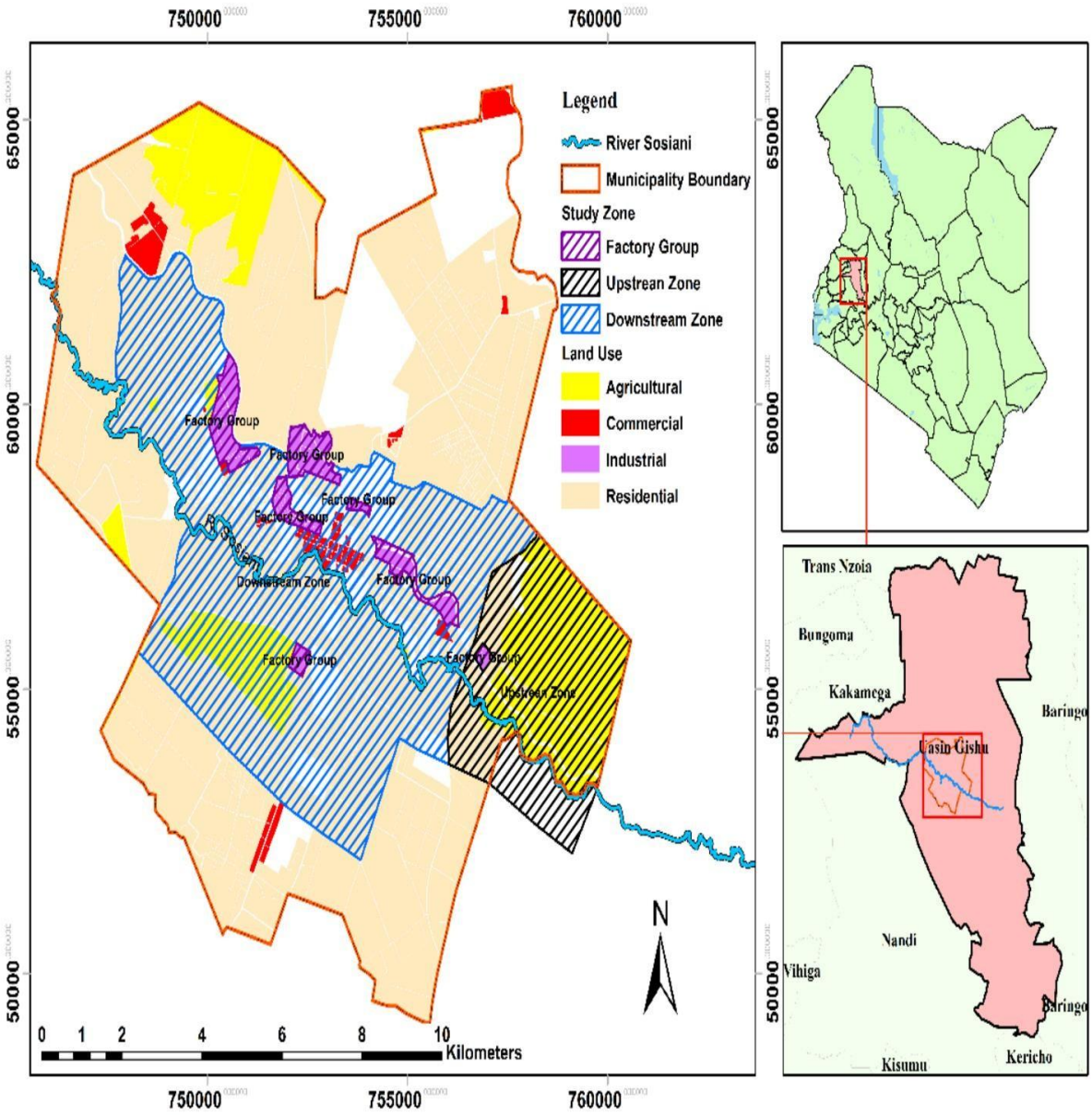

Figure 3. 1: Map of Uasin Gishu county Showing the location of River Sossiani that receives Textile effluents (Mumbi & Watanabe, 2021)

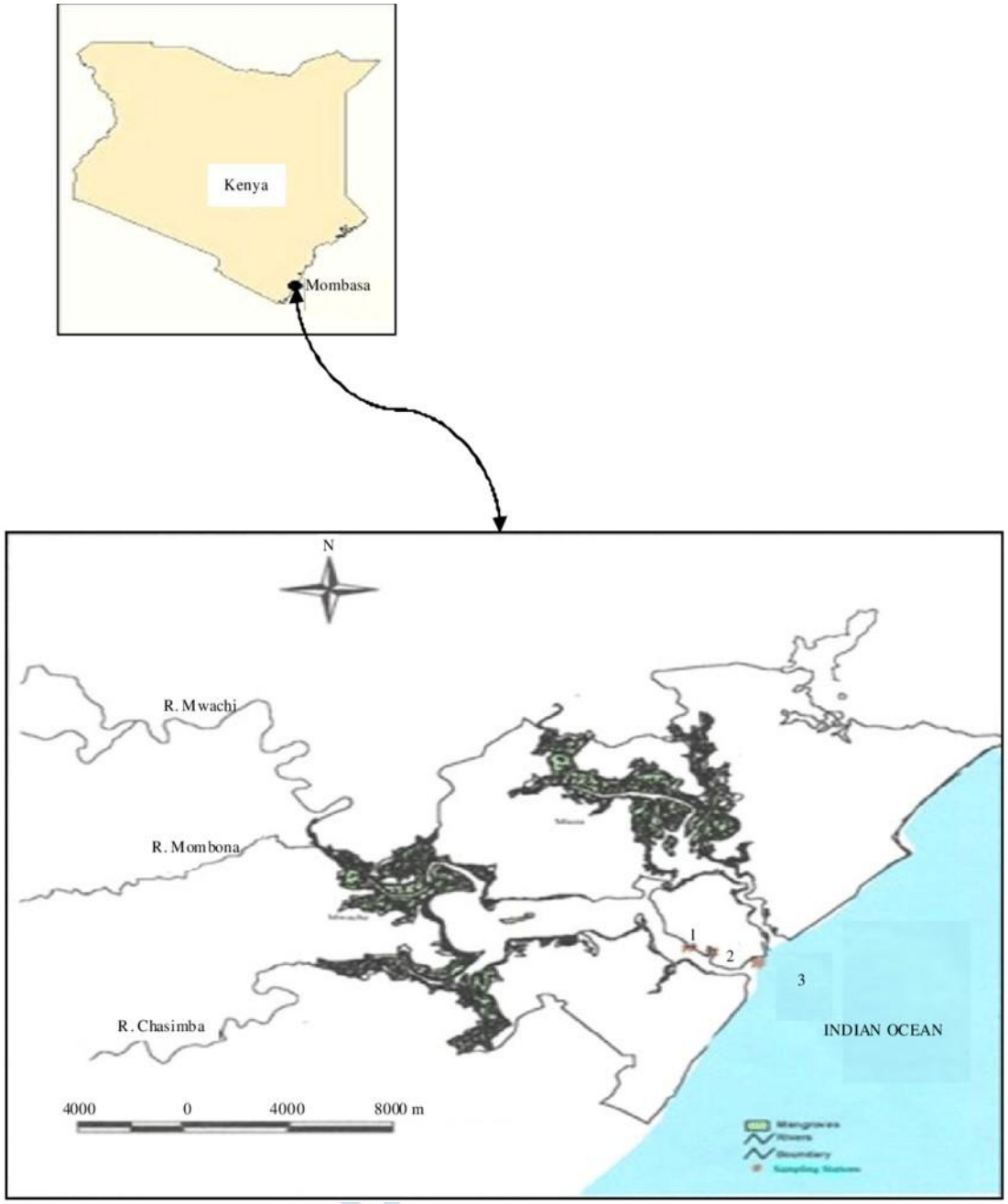

Figure 3. 2: Map of Mombasa County Showing the location of Rivers Mwachi, Mombasa and Chasimba that receives Textile effluents (Wanjohi *et al.*, 2019).

3.4 Sample and sampling Procedures

Sample size for this particular study was calculated using this experimentally determined

formula, $N = \frac{E}{Z_2 2PT}$

Where;

N= sample size

P= percentage distance (from point of discharge)

E= sampling error (SE) or margin of error (ME)

Z= Z-score (reliability and validity factor of study area)

T = period of study

$$N = \frac{96^2 x 0.5(1-0.5)}{0.003^2 x 365} \quad 1.$$

$1 + (1.96)^2 \times 0.5(1-0.5) / (0.003)^2 \times 365$

N=43.09 samples.(Qi et al., 2023).

Therefore, 86 samples were obtained from water bodies around Rivatex and Mombasa Textile Industries which were be labeled as ER1 to ER43 and Em1 to Em43 in which letters R represents Rivatex and M Mombasa textiles. The samples were collected from points of discharge of textile effluents and to the points where living organisms including humans interacts with these aquatic ecosystems for a period of twelve months using global positioning system (GPS MAP 64SX) to ensure that the same location used for acquisition of the samples. The collected samples were packaged in a one-liter double cap acid-washed plastic bottles and then transported to the Pwani University laboratory, Kilifi County by Wells Fargo transport service provider within 24 hours of the dispatch. Each of the sample was stored in Pwani University Postgraduate Research Laboratory at room temperature and pressure for a period not more than 30 days. Before sampling, every bottle was washed with acid water and double distilled water then rinsed with effluents to be sampled. Every sample was analyzed in triplicates to ensure accuracy was achieved.

3.5 Experimental analysis and Laboratory Techniques

All the experiments for this study were conducted in the following institutions' laboratories: Mount Kenya university, Kenya, Pwani university Kilifi County, Kenya, Kemfri and Government Chemistry Mombasa County, Kenya.

3.5.1 Preparation of chitosan

3.5.1.1. Materials and Chemicals

The materials used in this research includes; crustacean, crab shells, freezer (-16˚C), hydrochloric acid, sodium hydroxide and acetone, Glutaraldehyde (GA) solution 25% in water as a cross-linking agent and 100% (v/v) glacial acetic acid as a solvent, an oven, grinder.

3.5.1.2. Extraction of chitin from crab shells

Crab shells were collected from Malindi Marine Biotechnology Industry. The permit to collect the samples was obtained from the Department of Agriculture, Livestock Development and Fisheries Directorate (REF: KCG/MSC/FL/VOL.1/10) as shown in the appendix I. Crab shells were washed several times with distilled de-ionized water and then dried at 40 °C in an oven. Dried shells were powdered by a GRTA-2903 grinder and stored in a tightly closed glass bottle in Pwani University Research Laboratory at room temperature. Extraction process began through the demineralization procedures, where 40.0 g of powdered sample got reacted with 2.0 M hydrochloric acid solution for 24 h at 80.0 °C in order to eliminate all the minerals in the sample. Secondly deproteinization procedures were done, whereby, the sample was reacted with 2.0 M sodium hydroxide at 110.0 ºC for 20 hours at a solid to solution ratio of 1:10 to remove all the proteins present in the sample. After demineralization and deproteinization, the sample were treated with acetone to remove colour. Finally, filtration was done to the sample, then washing with distilled de-ionized water severally and with drying at 40.0 °C in an oven (Joginder *et al.,* 2018).

3.5.2 Production of chitosan from extracted chitin

The extracted chitin was by applied with 50% concentrated sodium hydroxide at 150.0 °C after 4 hours at a solid to solution ratio of 1:10 (w/v). This process was used for the removal of the acetyl group attached to the extracted chitin. Therefore, this procedure allowed for the process of deacetylation to take place. The deacetylated sample was filtered using a Whatman filter paper of 0.35 mm thickness and thorough washing was done using distilled de-ionized (DD) water, this was done to obtain a neutral pH which is very fundamental in the extraction of chitosan. The extracted chitosan was the allowed to dry for further application. 2.00 mL of chitosan solution was prepared in (6%, v/v) acetic acid solution and mixed until the solution became homogeneous and clear. 1.00 mL of glutaraldehyde (GA) solution (1, 3 and 6%, v/v) was poured to the prepared chitosan solutions. The polymer and cross-linker mixture were immediately poured into a plastic syringe and placed into the cryostat. The mixture was incubated in the cryostat at -16.0 °C for 2 hours and stored in the freezer at the same temperature for 24 hours (D. Liang *et al*., 2023).

3.5.3 Characterization of chitin and chitosan Yield

Percentage production of chitin calculations was done by dividing the weight of extracted chitin to initial dry crab shell weight. On the other hand, the percentage production of chitosan was done by dividing the weight of yielded chitosan to dry chitin weight before deacetylation. Yield calculations were done as follow:

Production of chitin (%) = [yielded chitin (g)/Crab shells (g)] x100 …… equation 3.5(a)

Production of chitosan (%) = [yielded chitosan (g)/Chitin (g)] x100…… equation 3.5 (b)

3.5.4 FT-IR analysis of chitin and chitosan

The infrared spectral analysis of the extracted chitosan samples was measured using Fourier Transform Infrared Spectrometry, FT-IR (Frontier Spectrometer, Perkins Elmer, USA) in the

wavelength range of 450 - 4000 cm^{-1} at a resolution of 4 cm^{-1} (Sadat & Joye, 2020). For preparation of pellet from the sample, the following were used; - pellet holder, pestle, mortar, drier. The 2.0 g of the extracted sample was washed with 80.00 mL alcohol at 1:4 ratio. The dried sample was then centrifuged using a Remi C-854/6 centrifuge at 3500 revolutions per minute (rpm). Then KBr was ground using a pestle and mortar. The ground

KBr was placed in FT-IR to hide the rock bottom in pellet disc and pressed at 0-10 Tones. The pressed sample was then carefully remove from the disc and place in sample holder for FTIR analysis (Zhuang *et al*., 2020).

3.5.5 Solubility of chitosan

A volume of 10.0 mL 1% acetic acid solution was added to a centrifuge tube containing 0.100 g of produced chitosan. The sample was centrifuged using a Remi C-854/6 centrifuge at 10,000 rpm for 30 minutes. The supernatant was poured away and the undissolved part of chitosan was washed with 25.0 mL of distilled de-ionized water and then centrifuged at 6,000 rpm. The supernatant liquid was poured away and the undissolved solid was dried at 60 °C for 24 h in an oven. The dried solid was stored in a dry petri dish. It was then weighed and the percentage of solubility determined. To determine the water uptake capacity (WUC), 10.0 mL of distilled water was put in a centrifuge tube containing 0.5 g of produced chitosan. The sample was mixed on a vortex about 5 minutes until the sample was dispersed. Then, the dispersed sample was vortexed for 5 seconds in every 10 minutes (for a total of 30 minutes) and centrifuged at 3500 rpm for 30 minutes. After Centrifugation, the supernatant was poured into a glass petri dish and then the sample was weighed (Abhinaya et al., 2021). Water uptake capacity (WUC) was calculated as follows:

$$\text{WUC}\ (\%) = \left[\frac{\text{Bound water (g)}}{3.5\ (\text{c})\ \text{Initial chitosan weight (g)}}\right] \text{x}\ 100 \qquad \text{Eq}$$

3.5.6 Oil uptake capacity (OUC)

To determine the oil uptake capacity, 10.0 mL of sunflower oil was added into a centrifuge tube containing 0.5 g of produced chitosan. Then sample of sunflower oil and chitosan was mixed on a vortex for up to 5 minutes until the sample was dispersed. It was eventually vortexed for another 5 seconds every 10 minutes (for a total of 30 minutes) and centrifuged at 3500 rpm for 30 minutes. After Centrifugation, the supernatant was poured away for disposal and the sample of was weighed to determine oil uptake capacity. OUC was calculated as follows: -

$$\text{OUC}\ (\%) = \left[\frac{\text{Bound oil (g)}}{\text{Initial chitosan weight (g)}} \right] \times 100 \qquad \text{Eq 3.5 (d)}$$

3.5.7 Preparation of chitosan coupled silver nanoparticles

Stable silver nanoparticles were synthesized using chitosan acting as both reducing and stabilizing agent without using any toxic chemicals. This reaction was carried out in an autoclave at a pressure of 15 psi and 120.0 ^{o}C temperature by varying the time. Analytical grade silver nitrate was purchased from the commercial suppliers (Sigma-Aldrich). 0.200g of the chitosan was dissolved in 1 % acetic acid solution followed by magnetic stirring for 30 minutes. The mixture solution was then filtered to obtain clear solution of chitosan- acetic acid mixture. Then 3.0 mL of 0.1M solution of freshly prepared of silver nitrate was added to the mixture. 100 µL of 1.0 M sodium hydroxide was also added and then the mixture was stirred for 10 hours using a magnetic stirrer at 90.0°C. Centrifugation was then carried out at 3500 rpm for 30 minutes to isolate the silver nanoparticles formed (Joginder *et al.,* 2018).

3.5.8 Characterization of the silver nanoparticles

UV-visible spectral analysis of the silver nanoparticles was accomplished using UV-Vis spectrophotometer (Shimadzu UV 2500 Japan model) for determination of maximum absorption spectrum, which should occur between 410-420 nm of wavelength. Fourier

Transform Infrared (FT-IR) spectroscopy analysis for functional group determination using IR spectrophotometer (Shimadzu model 8400). Scanning electron microscopy was then used for the visualization of the morphology of the nanoparticles using (JEOL 2010).

3.5.9 Loading silver nanoparticles on the electrodes

Drop casting method was applied in embedding silver nanoparticles to the indium tin oxide electrodes. Electrode was modulated by changing the sizes of the drop and concentration of the silver nanoparticles dispersed in the solution. Direct modification of the nanoparticles by the aid of the selected sensors on to the working electrode. Current density of 0.2 mA cm^{-2} was applied for homogeneous flower like structures deposits on the thin film conducting material.(Milanović *et al*., 2021).

3.6 Electrochemical degradation of Azo dyes

The scheme 3.1 below shows a photo diagram representing a setup for the electrochemical cell applied in conducting the process of electrolysis. The photo was taken from Pwani University post graduate chemistry laboratory. The setup was completed using the following equipment: - power supply, AC-DC multimeter, rheostat, hot plate, magnetic stirrer, connecting wires and the electrodes. The instrument cell was used for enhancing degradation of the azo dyes from the textile effluent placed in 250 mL glass beaker.

Scheme 3. 1: Electrochemical cell set up for Azo dye degradation, a photo taken from Pwani University Chemistry laboratory

All textile dyeing effluent samples was treated with coagulating agent PAC (Analytical Reagent Grade). Samples of 100 mL was placed into 250 mL glass beaker. Indium tin oxide thin conductive materials coated with silver nanoparticles was suspended to create an inter-electrode distance using an insulator. The ITO electrodes were suspended into the solution and connected in series with an ammeter and rheostat. Potential difference was applied using an AC – DC converter and current, time and absorbance was recorded at end of electrolysis. Power consumption was calculated using the relationship;

$$P = Vit \qquad \text{Eq 3.6 (a)}$$

The reaction will continue to complete removal of colour while recording current.

Measurements of absorbance was taken at an interval to monitor colour removal progress. This was repeated using stainless steel electrodes. The electrodes were mechanically polished underwater with abrasive paper, cleaned in 0.2 M HCl solution for 2 minutes and rinsed with distilled water to eliminate any interference and ensure surface reproducibility during EC. The absorbance was then measured using UV-Vis spectrophotometer. Percentage of color removal was calculated using the following equation:

$$\% \text{ of color removal} = \frac{A_0 - A_f}{A_0} \times 100\% \qquad \text{Eq 3.6 (b)}$$

where A_o and A_f are the initial and final absorbance of the effluent, respectively.

The specific energy consumption of the four samples each from Rivatex and Mombasa Textiles were determined at the effluent pH of 4.0, 6.0, 7.0 and 8.0 respectively. They were then allowed to settle for about 30 minutes. The solution was then filtered. All these tests were performed at temperature of 30°C because this temperature is fundamental parameters on concentration and viscosity of textile effluent solution (Koulini *et al*., 2022)

3.7 Physico- chemical processes

The removal of COD, BOD and colour from test reagents by electrolysis was investigated basing on the parameters described below. The COD and BOD analysis were carried out using the standard methods for examination of water as outlined in the APHA (2000).

3.7.1 Chemical oxygen demand (COD)

A 2.50 mL textile effluent sample containing azo dyes was measured and transferred into a 100 mL glass beaker and 1.50 mL of digestion solution were added. 3.70 mL of sulphuric acid also added to the sample in the beaker. Contents were stirred thoroughly and heated to 110.0 ^{o}C. The heated sample was placed on a block digester and refluxed for two hours, and then cooled to room temperature. The tubes containing the samples were placed on a settling rack and allowed to settle. The tube contents were then transferred into an Erlenmeyer flask on a magnetic stirrer. Two drops of ferroin indicator were added and then titrated with 0.1M

ferrous ammonium sulphate (FAS). The determination of the chemical oxygen demand was done using the equation below.

$$\text{COD} = (\text{A} - \text{B}) \text{ x M x } 8000 \text{ ml of sample} \qquad \text{Eq 3.7}$$

Where:

A= mL FAS for blank

B = mL FAS for sample

M = molarity of FAS.

3.7.2 Biochemical oxygen demand (BOD)

The BOD analysis was carried out using standard methods for examination of water and waste water as outlined in the APHA (2000). Standard 20.00 mL of distilled water was siphoned into two BOD bottles, which served as blank for initial dissolved oxygen (control). 1.00 mL of the nutrient was added to dilution water. The nutrients were standardized by phosphate buffer solution containing magnesium sulphate, calcium chloride and ferric chloride. A 5 % of the seed was added to the dilution water and well mixed. The 20,00 mL mixed dilution water was then siphoned into one litre volumetric flask containing the sample and filled to the mark. The content of the volumetric flask was siphoned into two BOD bottles. One incubated and the other used for the determination of initial dissolved oxygen in the mixture. The bottles were stoppered tightly and incubated for 5 days at 20.0 ^{o}C. The BOD bottles were sealed throughout the five-day period. Equation 3.8 below was used to determine BOD after determining initial and final dissolved oxygen of the blank and sample.

$$\text{BOD} = (\text{D1} - \text{D2}) - (\text{B1} - \text{B2}) \times \frac{1000}{\quad} \qquad \text{Eq 3.8 v}$$

Where: -

D_1 is dissolved oxygen in sample 15 minutes after preparation.

D_2 is dissolved oxygen in sample 5 days after preparation.

V is the volume (mL) of the sample used

B_1 is concentration of oxygen in the seeded dilution water or blank 15 minutes after preparation.

B_2 is concentration of oxygen in the seeded dilution water after incubation at 20 ^oC for 5 days.

3.8 Effect of Process Parameters

This section is mainly concerned with the impact of varying parameters such as the shaking speed, potential difference, surface area to volume ratio, initial dye concentration, support electrolytes, current density, contact time, change in pH and temperature. The focus is on how these changes bring about variation on specific energy consumption during the azo dye degradation.

3.8.1 Determination of the Effect of Potential Difference

Potential difference was varied at 2 different levels of 12 and 24V. Optimum voltage for complete chromophore degradation were established and used in all the subsequent reactions involving the other variations such as surface area to volume ratio, contact time. (APHA, 1992). The voltage applied is indeed essential in determining the effectiveness and the efficiency in colour chromophore removal time (Wei *et al*., 2022).

3.8.2 Determination of the Effect of Shaking Speed

Shaking speed by magnetic stirrer was varied at five different levels of 150, 200, 250, 300 and 350 rpm using 20 ppm wastewater. The optimum speed was used for subsequent experiments involving the variation of azo dye concentration, support electrolyte, contact time, current density and surface area to volume ratio (APHA, 1992). Shaking speed enhances well and intensely mixed azo based dye effluents thus showing measurements which optically integrated (Sillanpää *et al*., 2023).

3.8.3 Determination of the Effect of Surface Area to Volume Ratio (S/V)

Surface area to volume ratios as a parametric condition was varied at five different levels during the electrolysis process which included: - 10, 15, 20, 25 and 30 m^2/m^3 using 20 ppm textile effluent wastewater. The optimum S/A was established and used for further experimental and tabulation of the relevant data in the areas of current density, change in temperature and pH variation (APHA, 1992). Surface to volume ratio of the electrode facilitates the length diffusion thus reducing heat generation by the current collector, this has an impact of lowering the local heating (Zeng *et al*., 2023).

3.8.4 Determination of the Effect of Initial Dye Concentration

Concentrations of the textile effluent samples considered from 0, 20, 40, 60 and 80 parts per million (ppm) from the 200-ppm stock using distilled de-ionized water and electrolysis was carried out at the determined conditions from the varied parameters such as contact time, temperature change and pH variation. The initial dye concentration determines which level of variation is suitable for effective degradation with the shortest time possible

3.8.5 Determination of the Effect of Support Electrolytes

Sodium chloride as a support electrolyte was applied to support the electro-catalysis of the textile effluent azo dyes at a varied concentration of 5, 10, 15, 20 and 25 ppm while using a dye concentration of 20 ppm (APHA, 1992). The support electrolyte has a synergistic impact on the electrodes and are also found to vital in chemical mediation during the electrochemical process (König *et al*., 2019).

3.8.6 Determination of the Effect of Current Density

Current density was adjusted to 0, 10, 20, 30 and 40 A/M^2 using a stabilized variable rheostat connected in series and the power utilized to completely degrade the textile effluent dyes was noted (APHA, 1992). In azo dye degradation current density facilitates the process of transferring electrons in reaction system (Y. Xu *et al*., 2021).

3.8.7 Determination of the Effect of Contact Time

The effect of contact time was investigated at intervals of 5 minutes until complete decolorization occurs. A 2 mL sample was obtained using a dropper and its absorbance measured at the constant parametric conditions (APHA, 1992). It's widely understood from Rate Laws that rate of reaction decreases with time since the reactants level decimates due to their conversion to products and vice versa (Rahmani *et al*., 2022).

3.8.8 Determination of the Effect of pH

The initial pH of 200 mL textile effluent wastewater was adjusted to various values using both acidic and basic conditions ranging from 1 to 7 and then from 8 to 14 by applying either NaOH and HCl of the determined concentrations and the electrochemical degradation of the textile effluent dyes and consequent power consumption recorded (APHA, 1992).

3.8.9 Effect of Temperature

The temperature of the textile effluent wastewater was varied at five different values with the 20-ppm starting from 25.0, 50.0, 75.0, 95.0 and 115.0 ^{o}C using a thermostatic water bath. The optimal temperature for complete colour degradation was tabulated and power consumption for the dye degradation calculated using formula:

$$\text{Power} = \text{Current (A)} \times \text{Potential Difference (V)} \times \text{Time (hours)} \qquad \text{Eq 3.9}$$

3.9 Characterization

Both spectroscopic and microscopic techniques were applied in this study for the characterization of the synthesized samples. They include the following: - Furiour transform infrared (FT-IR), ultraviolet (UV-Vis) and liquid chromatography mass (LC-MS) spectrometry, scanning electron microscope (SEM) and Motic light microscope. The samples were analyzed for functional groups by FT-IR spectroscopy, SEM analysis for visualizing the morphology.

Images of the ITO electrode before and after embedment with silver nanoparticles (AgNPs) were viewed under Motic light microscope. The dyes were then analyzed for the levels of azo dyes before and after degradation using UV-Vis spectroscopy and LCMS.

3.9.1 FT-IR analysis

Fourier transform infrared spectroscopy was applied in the analysis of the chitosan, silver nanocomposite film electrodes. The spectra were obtained over 16 scans covering the 4000-400 cm^1 wave-number range at 4 cm^{-1} resolution and at 25.0 using a Thermo Scientific Nicolet iS10

FTIR spectrometer.

3.9.2 UV-Vis spectroscopic analysis

The study of the degradation of dye and optical characterization of the synthesized metallic nanoparticles was observed during this research work with the assistance of a double beam 3000+ LABINDIA, UV-Vis spectrophotometer and a cell of 1.0 cm path length within the spectral range 200-800 nm. Effect of temperature on kinetic study of reaction was studied by a Peltier accessory (temperature-Controller) model PTC-2 is linked with the UV-Visible spectrophotometer. Two lamp combinations are utilized in double beam spectrophotometer one is deuterium lamp used for UV part and second is tungsten lamp used for the visible part. Sample cell is formed by Quartz and lightweight beam travels a distance of 1 cm through the sample. For obtained UV spectra of our sample first done baseline by reference in order that other reagent peaks were nullified, then obtain the spectra

3.9.3 LC-MS analysis.

LC-MS was used for the analysis of the concentration of azo dyes dissolved in textile effluent before and after the degradation.

3.9.3.1 Sample preparation

10 g of homogenized sample was weighed, then followed by the addition of 10 mL acetonitrile to the said sample. Magnetic stirring was done at 900 rpm and shaking allowed for 10 minutes. 10 mL of distilled de-ionized water was then added to the sample as stirring proceeded. Centrifugation was carried out at 4000 rpm for a timeline of 5 minutes. Filtration of supernatant through a 0.45-µm membrane filter was done. Finally, transfer of 1 mL of the prepared sample into an amber auto-sampler vial was performed. Nonetheless, the analysis by LC-MS/MS was carried out.

3.9.3.2 Instrumentation setup

Chromatographic conditions for LC-MS/MS included Agilent LC-MS/MS 6460 coupled to 1260 HPLC. The HPLC column was set up as follow: - Zorbax Eclipse plus C18, sizes of 100 mm, 2.1 mm, 3.5 mm. Flow rate was conducted at 0.3 mL/min. Mobile phase was made of A = 5mM ammonium formate in H_2O+0.01 % formic acid and B = 5mM ammonium formate in MeOH+0.01 % formic acid.

3.9.3.3 Mass Spectrometric conditions

Electron spray ionization (ESI) positive mode was set; gas temperature was recorded at 300 ^oC with gas flow of 7 L/min done. Nebulizer was set at 45 psi, sheath gas temperature of 350 ^0C recorded with sheath gas flow of 10 L/min carried out. Its capillary was recorded at 4 kV.

3.10 Dye removal efficiency

For electrocoagulation reactions, a 2.00 mL sample was drawn at intervals of 2 minutes and their absorbance measured using a UV-VIS spectrophotometer at a pre – determined λ_{max}. For the electrochemical degradation samples was centrifuged at 4000rpm using centrifuge machine 6 tubes for 15minutes and their absorbance measured at a pre – determined λ_{max} of the dye. The amount of dye degraded or removed will be calculated using the equation 4.0,

$$= \frac{o \quad O}{} * 100 \quad A - A$$

% Eq 4.0 A_0

Where, R% is the amount removed, A_0 is the initial dye absorbance, A_e is the final absorbance (mg/L)

(APHA, 1992).

3.11 Data Analysis Procedures

The collected samples were be analyzed for some major parameters of the textile dyeing effluents including pH, EC, TSS, TDS, COD, BOD, chlorides, bicarbonates, sulphates and heavy metals. TDS and TSS of the effluents were be measured by the gravimetric oven drying method at 105.0 °C. BOD of the effluents was determined by incubating the sample at 20.0 °C for 5 days followed by titration. COD by the closed reflux method. Bicarbonates, chlorides, and sulphates were determined by complexometric titration, argentometric titration, and turbidity method, respectively. All the parameters after the treatment with PAC coagulants were measured, followed by the same methods above. To analyze the effectiveness of silver nanoparticles on degradation of textile effluents, descriptive statistics such as frequencies and percentages was applied. Inferential analysis was undertaken using 2-ANOVA to test the hypotheses by testing the difference in levels of textile effluents in the wastewater discharge before and after treatment with AgNPs using ITO electrodes. The findings of the study were presented using tables and charts. In the entrapment experiment, each entrapment data point represents the mean value of three measurements and the standard deviation value was calculated. Linearity of a relation was assessed based on both the random pattern in the corresponding residual plot and the statistical significance of the correlation coefficient at the 95% confidence level using Student's *t*-test. Uncertainties associated with the slopes and ordinate intercepts of all linear relations are denoted by the 95% confidence intervals and □= 0.005 for addressing the uncertainties associated with the slopes and ordinate intercepts of all linear relationships.

CHAPTER FOUR

RESULTS AND DISCUSSIONS

This chapter entails the research findings, data analysis and discussions.

4.1 Results

4.1.1 Results from the synthesis and characterization of chitosan

The chitin was extracted by applying 50% concentrated sodium hydroxide at 150.0 °C for 4 hours after which a solid to solution ratio of 1:10 (w/v) was recorded. The processing of the 40.0 g of powdered crab shells resulted in the formation of 23.0 g of chitin after undergoing the demineralization to eliminate the minerals available in the crab shells. The removed minerals from the crab shells constituted 17.0 g (39.53%) of the total dry weight in the crab shell. The extracted chitin was further reacted with 50% concentrated sodium hydroxide at 150.0^{o}C after 4 hours at a solid to solution ratio of 1:10 (w/v) in order to carry out deacetylation for the removal of the acetyl group attached to the extracted chitin. The deacetylated sample was filtered using a Whatman filter paper of 0.35 mm thickness and thorough washing was done using DD water resulting in the formation of 7.20 g (31.3 %) of chitosan as shown in the table 4.1 below. Similar results were obtained by Pakizeh in his previous studies on "Chemical extraction and modification of chitin and chitosan from shrimp shells" (Pakizeh *et al.*, 2021).

Table 4. 1: Percentage of extracted crab chitosan

Initial weight (g)	Final weight (g)	% of extracted Chitosan
23	7.2	31.3

The FTIR spectra of both chitin and chitosan presented a distinct absorption bands corresponding to characteristic functional groups. Chitin exhibited a strong band near 1655 cm^{-1}, attributed to the amide I (C=O stretching) vibration, and a weaker band at 1550 cm^{-1}, corresponding to the amide II (N–H bending) vibration. After deacetylation, the intensity of these amide peaks significantly decreased, while a new prominent band appeared near 1590 cm^{-1}, assigned to the N–H bending of primary amines ($–NH_2$). The broad absorption band

around 3400 cm^{-1} in both spectra corresponds to O–H and N–H stretching vibrations, while the bands at 1070 cm^{-1} are attributed to C–O stretching in the polysaccharide backbone. The reduction of the amide I band intensity and the appearance of a stronger amine peak confirm the successful removal of acetyl groups and the formation of chitosan (No & Meyers, 1995).

4.1.2 The results of physicochemical properties of the chitosan

Solubility of the prepared chitosan was determined by dissolving 0.100 g of the extracted chitosan in (6%, v/v) acetic acid, 1.00 mL of glutaraldehyde (GA) solution (1, 3 and 6%, v/v) was poured to the prepared chitosan solutions to act as a crosslinker and then centrifuged using a Remi C-854/6 centrifuge at 10,000 rpm for 30 minutes. The supernatant was poured away and the undissolved part of chitosan was washed with 25.0 mL of distilled de-ionized water and then centrifuged at 6,000 rpm. The dried solid was stored in a dry petri dish, weighed and the percentage of solubility determined. The extracted chitosan solution was also noted to possess a yellow colouration implying results were positive , this corresponded to the findings from the shrimp shells after the removal of the acetyl and mineral components (Kou *et al*., 2021). The table 4.2 below shows physio-chemical properties used in determining quality and effectiveness of chitosan extracted in reduction of metals to nano-metals (Zhuang *et al*., 2020).

Table 4. 2: Physicochemical properties of the extracted chitosan

Properties	Chitosan in %
Water binding capacity (WBC)	69.0
Fat binding capacity (FBC)	56.0
Moisture content	59.6
Deacetylation degree	89.5

The water binding capacity (WBC) was found to be 69 % as shown in the table 4.2 above. The WBC % was determined by putting 10.0 mL distilled deionized water in a centrifuge tube containing 0.5 g of produced chitosan, mixed on a vortex about 5 minutes until dispersed and then centrifuged at 3500 rpm for 30 minutes. The fat binding capacity (FBC) was found to be

56 % as also shown in table 4.2 above. The percentage FBC was determined by adding 10.0 mL of sunflower oil into a centrifuge tube containing 0.500 g of the extracted chitosan. After Centrifugation, sunflower oil and chitosan were placed on a vortex for up to 5 minutes until the sample was dispersed and centrifuged again at 3500 rpm for 30 minutes. Chitosan obtained from these crab shells exhibited 89.5% degree of deacetylation (DD) which was noted to be effective and efficient in reducing and stabilizing silver nanoparticles from the Ag^{+} ions because these were value trends that were also obtained in previous studies when shrimp shells were used in synthesis of silver nanoparticles (Carrera *et al*., 2023). The wide range usage of chitosan in reducing the nanoparticles is due to its low levels of toxicity, biodegradability and its capability of being biocompatible (Innocent & Padikasan, 2023).

4.1.3 Results of the characterization of chitosan using Fourier Transform Infrared (FTIR) Spectroscopy

Characterization of chitosan was accomplished using, FT-IR (Frontier Spectrometer, Perkin Elmer, USA). Analysis was carried out in the wavelength range of 450 - 4000 cm^{-1} at a resolution of 4 cm^{-1}. 2.000 g of extracted, washed, and dried chitosan was centrifuged. KBr was placed in FT-IR to hide the rock bottom in pellet disc. Sample pellets were prepared using KBr salts due to their transparent nature, hence allowing greater resolution of spectra (Faix, 1991). The FT-IR spectrum for the characterization of 2.0 % chitosan is shown in Figure 4.1 below.

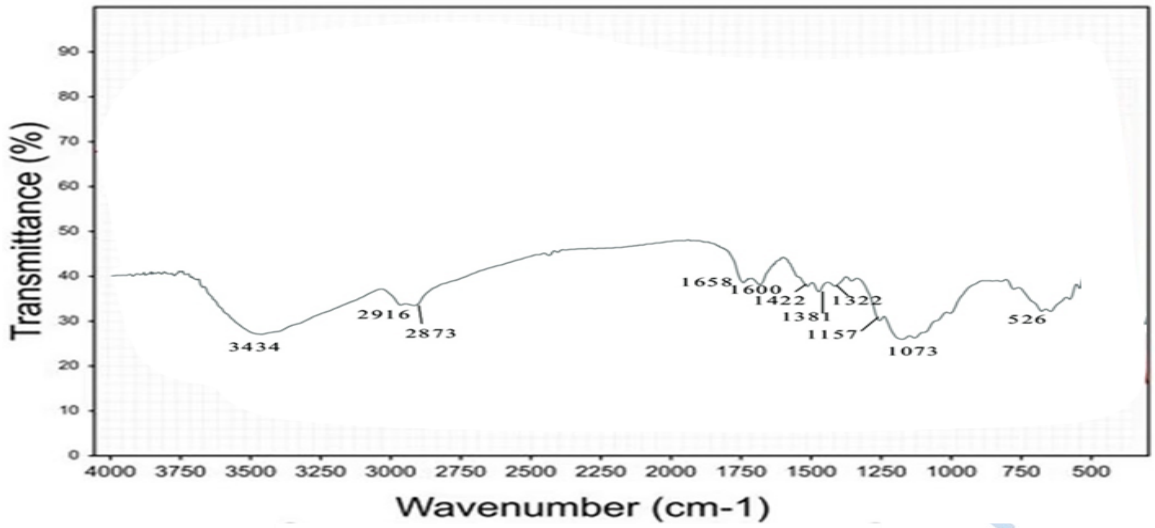

Figure 4. 1: A graph showing FT-IR spectrum of 2.0 % chitosan

In the figure 4.1 above, the x-axis represents the wave-number in (cm^{-1}) of infrared spectra. The absorption bands, correspond with different vibrations of atoms in the sample applied when it was exposed to the infrared region of the electromagnetic spectrum, whereas, y-axis represents the transmittance (%). The signal shown at 526 cm^{-1} corresponds to the plane with N-H bends overlapping with C−O plane-out and bends in stretching bonds vibrations. The chitosan spectra showed a peak at 863 cm^{-1} corresponding to carbon - nitrogen (C−N) stretch, absorption spectral peaks between 1019 and 1073 cm^{-1} represented bending of C−O in glucose, whereas, 1422 cm^{-1} corresponded to C−H bend side chain. The signal shown at 1157 cm^{-1} corresponded to C− O−C stretching vibrational bond, C-H stretching included 2873 cm^{-1} and 2916 cm^{-1}, a broader band at 3434 cm^{-1} for an overlap between the O−H stretching vibration and the N−H stretching vibration of the oligosaccharide was recorded. The amide, C=O bond showed its vibrational stretching mode at 1658 cm^{-1}. The signal at 1381 cm^{-1} corresponded to the C−O starch in the primary alcohols. The patterns of vibrational mode acquired from FT-IR spectrum indicated that the functional groups available included carbon, nitrogen, and oxygen. The bands obtained from the FT-IR spectra occurred in the range between 4000 and 400 cm^{-1} frequencies, basing on the fact that, it is ranging within the electromagnetic spectrum where

several molecules absorb electromagnetic radiation (J. Zhang *et al*., 2022). FT-IR is therefore, essential in identification of the molecular groups in the organic compounds (Hazeena *et al*., 2022). Therefore, it is worth noting that the amino groups in the chitosan facilitated the formation of complexes with metallic ions, thus making it a super effective polymeric chelating agent with the silver (Ag^{+}) ions (Mei *et al*., 2023). These results agree with those obtained from the studies carried out by Rafaëlly which indicated that FT-IR analysis of shrimp shells and chitosan showed spectral lines at 1073 cm^{-1} confirming the presence of the amino groups located on the second carbon in the glucosamine (Rafaëlly et al., 2008). Saraswathi *et al*.2021 noted a major absorption band between 1220 cm^{-1} and 1020 cm^{-1} which represented free amino group ($-NH_2$) in the glucosamine in the same locant position as earlier established.

4.1.4 Results of the characterization of silver nanoparticles using FT-IR Spectroscopy

The characterization of silver nanoparticles was achieved using FT-IR (Frontier Spectrometer, Perkins Elmer, USA). These silver nanoparticles were dried at a temperature of 80^{o}C, then ground with anhydrous KBr for the formation of pellets for easier characterization in the Furiour transform infrared spectroscopy within the absorption frequency range of between 4000 cm^{-1} to 400 cm^{-1}. FT-IR analysis provided spectra with different peaks as shown in figure 4.2 below. These vibration signals were useful in the identification of the functional groups found in the silver nanoparticles samples applied in the research study.

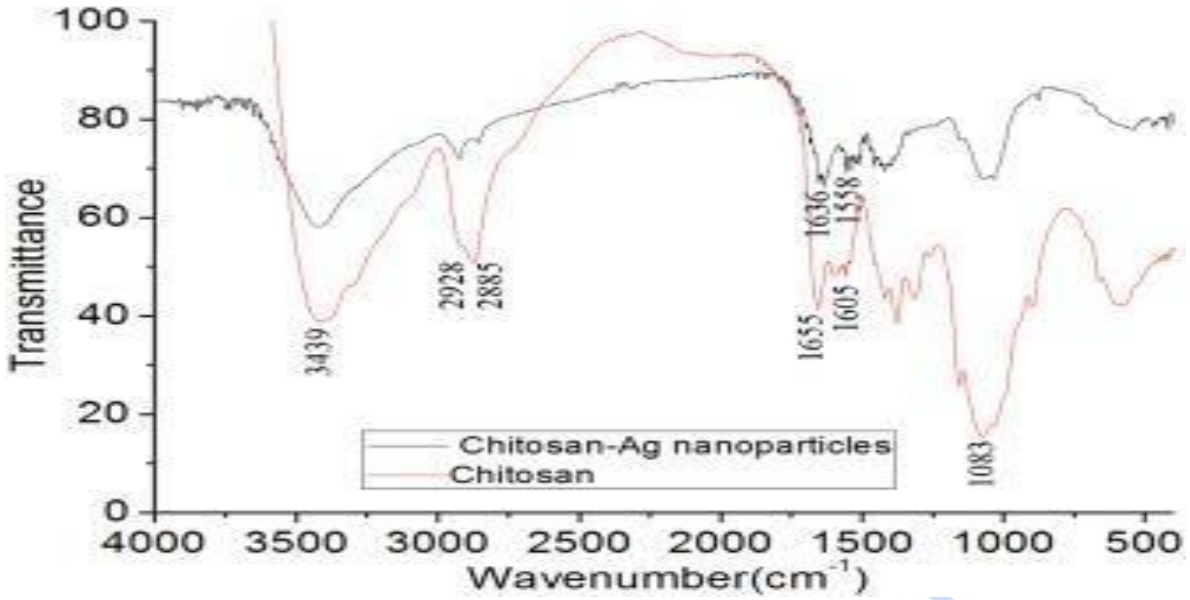

Figure 4. 2: Showing FT-IR spectrum of silver nanoparticles capped chitosan

Figure 4.2 shows an FT-IR graph whose x-axis represents the wave-numbers (cm^{-1}) of infrared spectra whereas, y-axis represents the transmittance (%) of the sample applied. The absorption bands, correspond to different vibrations of atoms in the sample applied when it was exposed to the infrared region of the electromagnetic spectrum. The results obtained envisaged a strong symmetrical stretching at the range of 1400 cm^{-1} to 1200 cm^{-1} with the major peaks recorded at 1390 cm^{-1} and 1380 cm^{-1}, indicating the presence of nitro component in the sample. The following signals presented in the spectrum in figure 4.2 below were obtained from the FT-IR analysis. The signal at 1658 cm^{-1} corresponded to the amide (C=O) bonds stretching vibrations. The signal shown at 1089 cm^{-1} represents secondary alcohol (C-O-C) bonds whereas, the peaks show sharpness at 564 cm^{-1} planes with bends NH, plane-out and bends C−O. C-H stretching vibrational signal was noted at 2927 cm^{-1}, a broader band at 3426cm^{-1} for an overlap between the O−H stretching vibration and the N−H stretching vibration of the oligosaccharide applied in the capping. The obtained results are in agreement with the previous findings on the functional groups found in silver nanoparticles formed in the bio-reduction techniques in which, chitosan macro-molecules are found to be acting not only as reducing but also capping agent (Ateeb et al., 2023). It is important to note that the intensity of the O−H and N−H

stretching bands emanated from the hydroxyl and amino groups thus shifting to 3426 cm^{-1} from 3439 cm^{-1} wave number of the chitosan in the FT-IR spectrum as shown in figure 4.2, implying that chelation of silver with both O−H and N−H groups of chitosan actually took place.

4.1.4.1 Results when different levels of chitosan is applied during the synthesis of silver nanoparticles

The impact of concentration of chitosan on transmittance during the synthesis of silver nanoparticles was done using 0.5%, 1.0%, 1.5% and 2.0% solutions. The results obtained using FT-IR. (Fourier Transform Spectrometer, Perkins Elmer, USA), were presented in figures 4.3.-4.6 below. Analysis was carried out in the wavelength range of 450 - 4000 cm^{-1} at a resolution of 4 cm^{-1}.

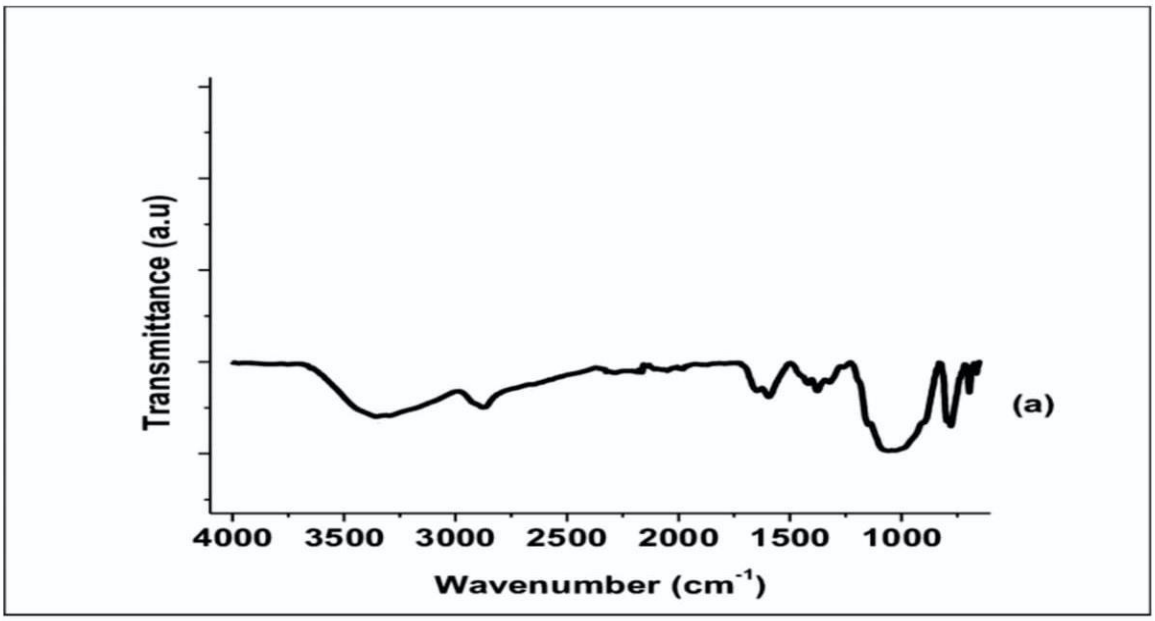

Figure 4. 3: Showing FT-IR spectrum of silver nanoparticles capped with 0.5% chitosan

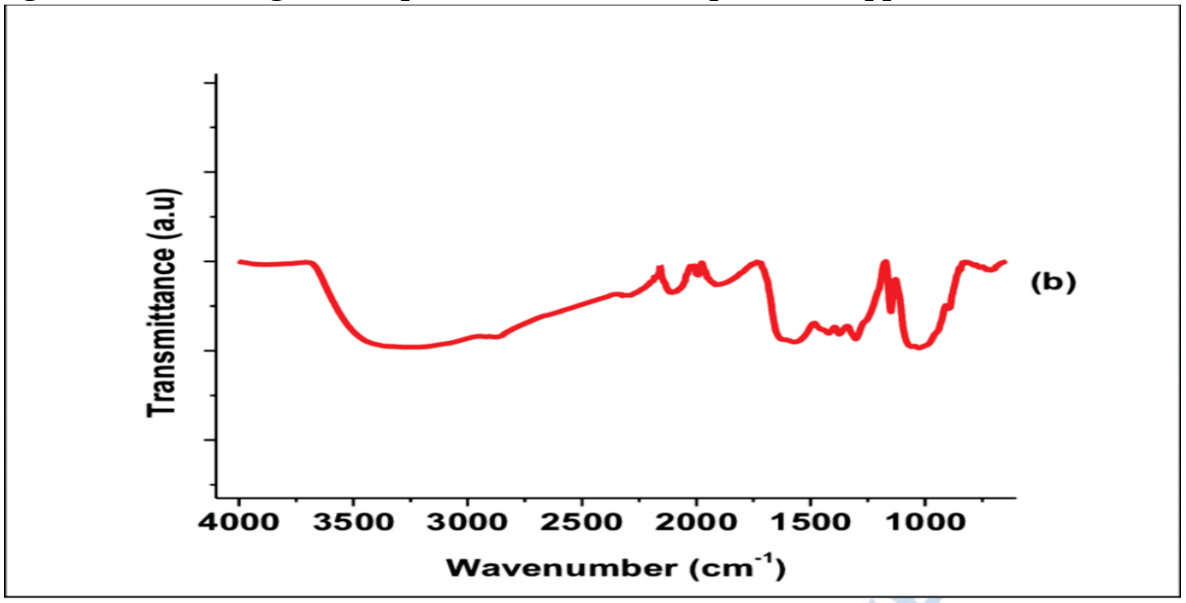

Figure 4. 4: Showing FT-IR spectrum of silver nanoparticles capped with 1.0 % chitosan

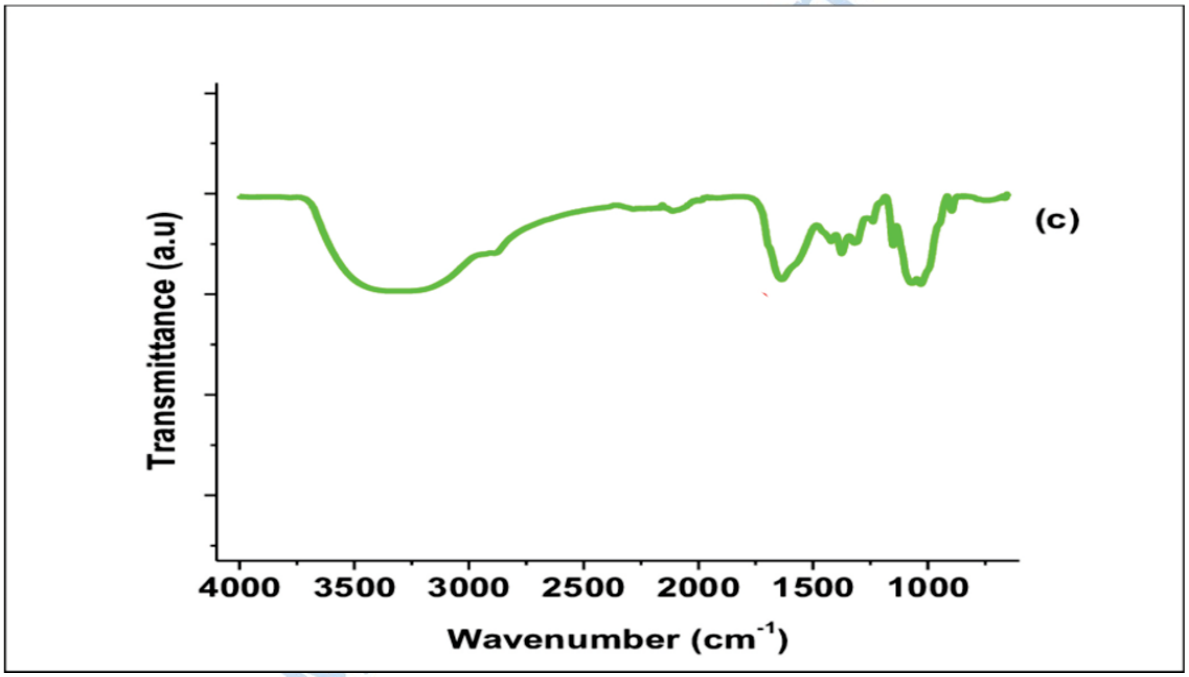

Figure 4. 5: Showing FT-IR spectrum of silver nanoparticles capped with 1.5 % chitosan

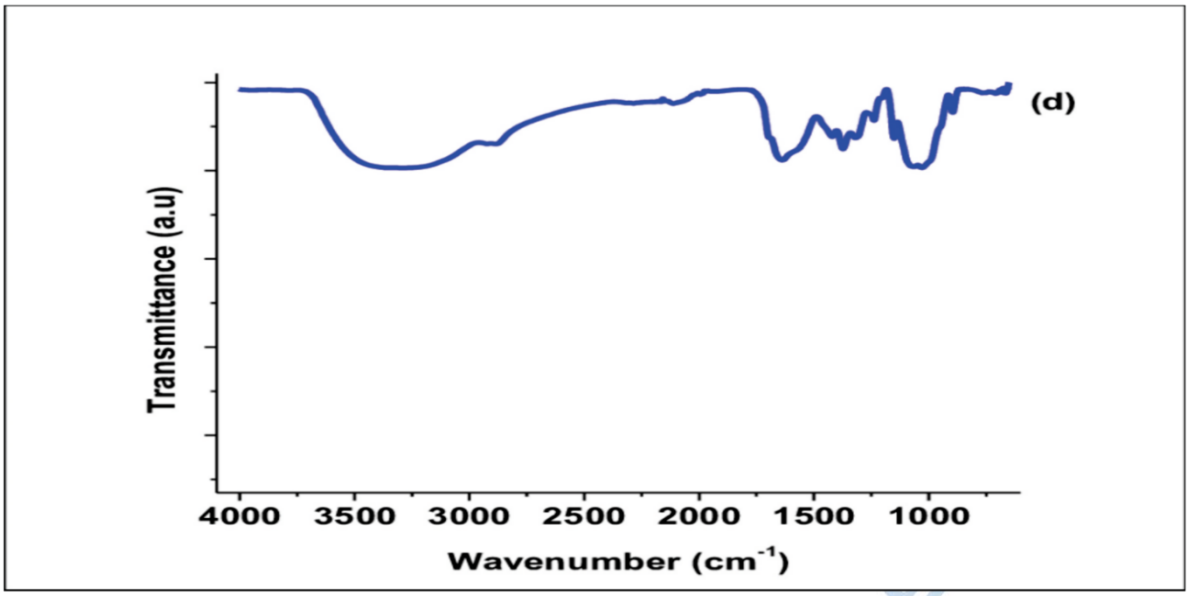

Figure 4. 6: Showing FT-IR spectrum of silver nanoparticles capped with 2.0 % chitosan

The Figures 4.3- 4.6 above represent the data obtained from the FT-IR and interpreted using the spectral lines of infrared by comparing the correlation of bands in the absorbance spectrum to that of the silver nanoparticles samples capped with 0.5, 1.0, 1.5 and 2.0 % chitosan respectively and applied during the experiment. It was also noted that intensity of transmittance was much elaborate at 2.0 % chitosan capping compared to the least at 0.5 %. FT-IR spectroscopy was able to effectively determine the formation of silver nanoparticles. During this characterization it was confirmed that the breadth and intensities of peaks taken from infrared spectrum, explicitly depended on the sizes of silver nanoparticles under scrutiny. The observation confirmed that as nanoparticles sizes increase, the peak width declines, nonetheless, resulting in an escalation of their intensities.

4.1.5 Results of the characterization of synthesized silver nanoparticles using UV-Vis spectroscopy

The characterization of the synthesized silver nanoparticles was performed using a UVVis spectrophotometer (double beam 3000+ LABINDIA) and a cell of 1.0 cm path length within the wavelength range of 200-800 nm. Two lamp combinations are utilized in double beam spectrophotometer in which one is deuterium lamp used for UV part and second is tungsten lamp used for the visible part. Sample cell was formed by Quartz and lightweight beam travels

a distance of 1 cm through the sample. For UV spectra of the sample to be obtained, first and foremost, a baseline by reference was done in order to nullify peaks for any other reagent present, then obtain the spectra for the sample of the silver nanoparticles. The figure 4.7 below represents synthesized silver nanoparticles scanned between 400 nm to 500 nm wavelength using the UV-Vis spectrophotometer. The maximum absorbance from the UV-Vis spectrophotometer showed the formation of silver nanoparticles with λ_{max} of 418 ± 2 nm. The synthesized silver nanoparticles were analyzed using UV-Vis spectroscopy, the analysis exhibited spectral line readings at different time intervals commencing with the initiation stage of the reaction (Panda *et al*., 2021). Ultraviolet-visible spectroscopy allows the resonance of the oscillation by conducting electrons within the interfaced band occurring at the negative and positive permittance in the materials undergoing stimulation through incidence of light (Barbhuiya *et al*., 2022). Surface plasmon resonance, highly depended on the sizes of the silver nanoparticles present. The study showed that the shape of these nanoparticles played a very crucial role in actualizing the surface plasmon position of the band formed. Technically, the applications of silver nanoparticles and the control in process utilizes the in-situ model of concentration determination, distribution in size and the dielectric aspects (B. Kumar *et al*., 2021). The absorption spectral lines of silver nanoparticles are optically over shadowed by SPR, this is in line with other finding in the earlier studies. Therefore, longer wavelengths were determined in the cases where particle sizes had shown increase. This study confirmed that position and shape in the absorbance within the surface plasmon resonance of silver nanoparticles are greatly dependent on the sizes of particles and surfaces of the species adsorbed (Mahy *et al*., 2023). The readings obtained from the UVVis in the figure 4.7 below showed that the maximum wavelength of 420 nm, gave the highest absorbance for the silver nanoparticles synthesized through the reducing and stabilizing property of the chitosan. This wavelength is line with the previous findings which opined that silver nanoparticles exhibit a

UV–Vis absorption maximum within the range of 400–500 nm due to their surface plasmon resonance (Hossain *et al*., 2022).

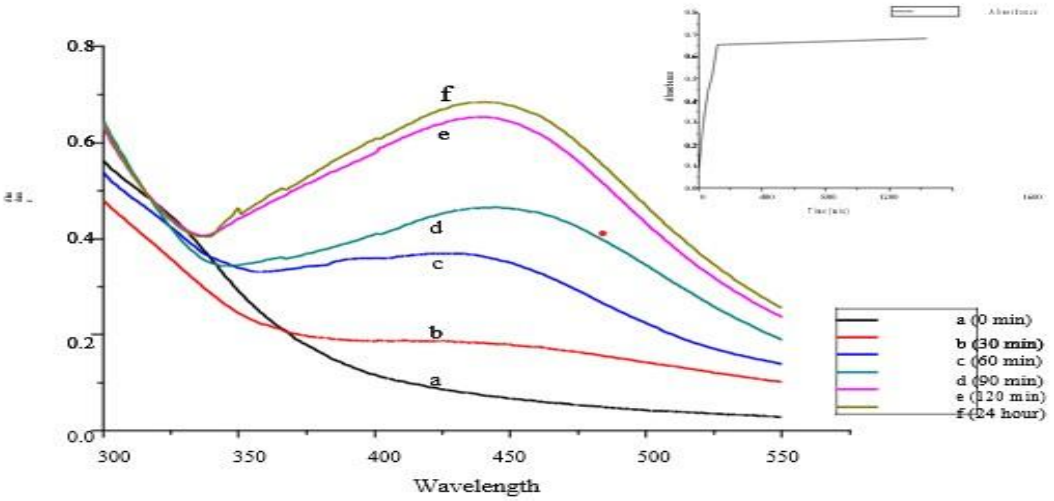

Figure 4. 7: UV-Vis spectra recorded at different wavelengths with respect to chemical reactions in relation to absorption as synthesis of AgNPs at various time intervals The reaction occurred rapidly as the formation of these nanoparticles took place steadily from 100 minutes with the increase in time showing a zero shift in wavelength peaks. After a period of 10 hours, there was no more rise in the absorption spectra due to the reason that each single ion had been consumed during the reduction phase. The UV-visible spectroscopic analysis confirmed the presence of the synthesized silver nanoparticles (AgNPs) via the reduction method of silver ions in the solution when reacted with chitosan extracted from crab shells (Mistry *et al*., 2021). They exhibited raw sienna colored in the aqueous media due to surface plasmon resonance (SPR). The colour turned from clear to faint then yellow brown solution demonstrating the formation of the silver nanoparticles as shown in plate 4.1 below

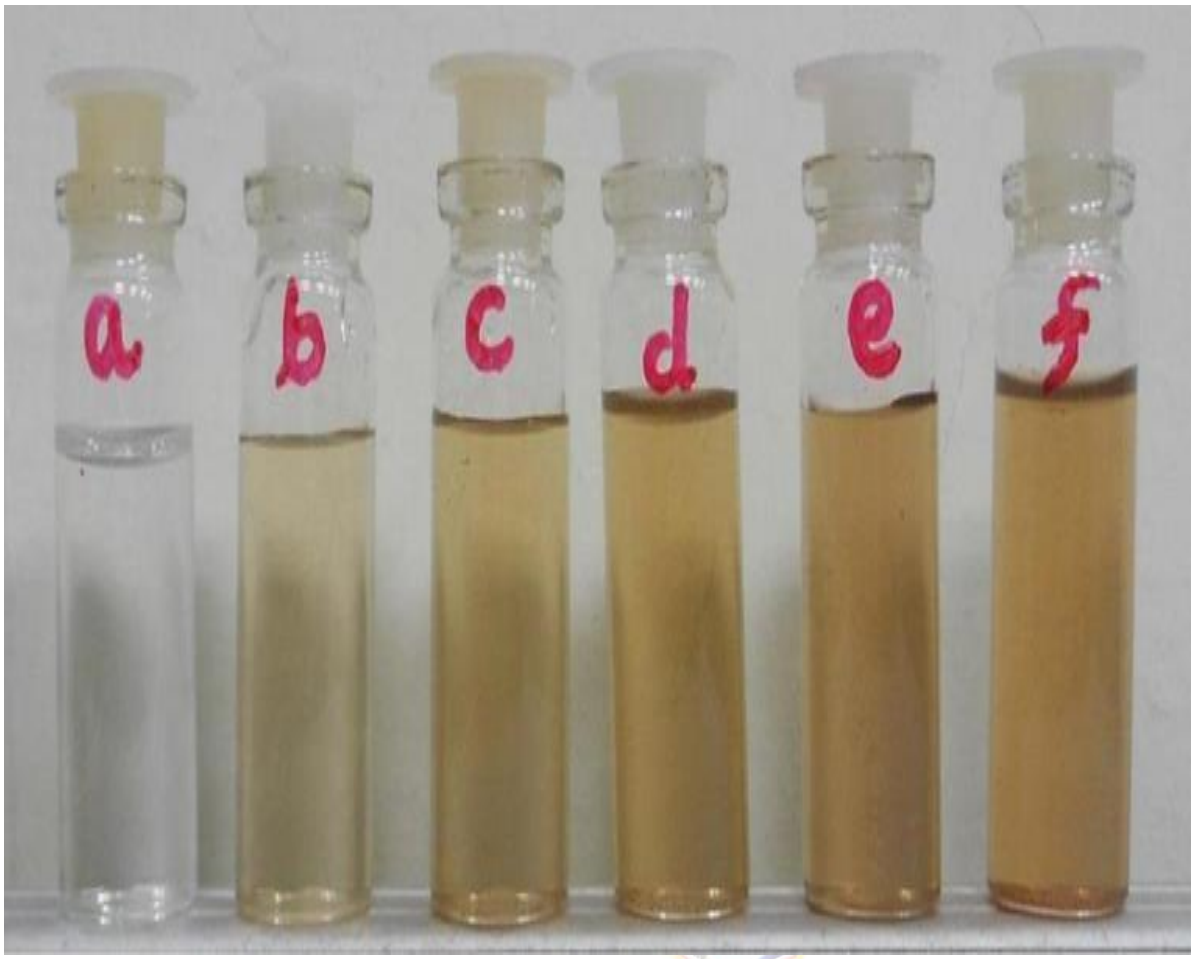

Plate 4. 1: Observing colour change in the process of silver nanoparticles (AgNPs) formation with variation of time intervals starting from 0 - 600 minutes (a) 0 minutes (b) 100 minutes (c) 300 minutes (d) 400 minutes (e) 500 minutes (f) 600 minutes.

These colour changes were consistent with the reported colour in the previous studies related to the extraction of silver nanoparticles (Nawabjohn *et al*., 2021). The plate 1 below shows the change in color of silver nanoparticles synthesized with respect to change in time. The variation in coloration was brought about by visible light when refracted by the various sizes of nanoparticles formed in relation to the difference in time (Renuka *et al*., 2021).

4.1.6 Results of absorbance at different levels of the synthesized silver nanoparticles using UV-Vis spectroscopy

Concentration of the silver nanoparticles samples was varied at three different levels starting from 1 mL Ag^+, 10 mL Ag^+ and 15 mL Ag^+. On the other hand, the variations in chitosan concentration were conducted at 2.5, 5.0,10.0 and 15.0 ppm and applied to three different samples containing silver ions. The impact of increasing the concentration of chitosan solution on the three different levels of silver ions was monitored using UV-Vis spectroscopy. Figures 4. 8 - 4.10 below show the UV-Visible spectral lines of AgNPs formed at 1 mL Ag^+ ion concentration with variations in concentrations of chitosan: a) 2.5 ppm b) 5 ppm c) 10 ppm d) 15 ppm. The results from the UV-Vis spectrophotometer showed an increasing trend in the absorbance as both solution's concentration was stepped up confirmed that absorbance is directly proportional to the concentration of the substance. The higher the concentration, the higher its absorbance (Rachtanapun *et al*., 2021) . These observations were found to be consistent with the findings that chitosan acts both as a reducing and stabilizing agent. Therefore, an increase in the amount of silver ions and chitosan concentration elevated the reacting species in that system (Mohan *et al*., 2022). The results obtained in the figure 4.10 below was therefore, considered most efficient in terms of time required for the formation of silver nanoparticles. From the data presented below, for quick synthesis of these nano-catalysts, 20 ppm of chitosan with 15 mL Ag+ ions solution proved to be the most efficient and sufficient. Therefore, for the production of silver nanoparticles similar trend was also established in the previous studies done using chitosan as a reducing agent for the reaction (Innocent & Padikasan, 2023).

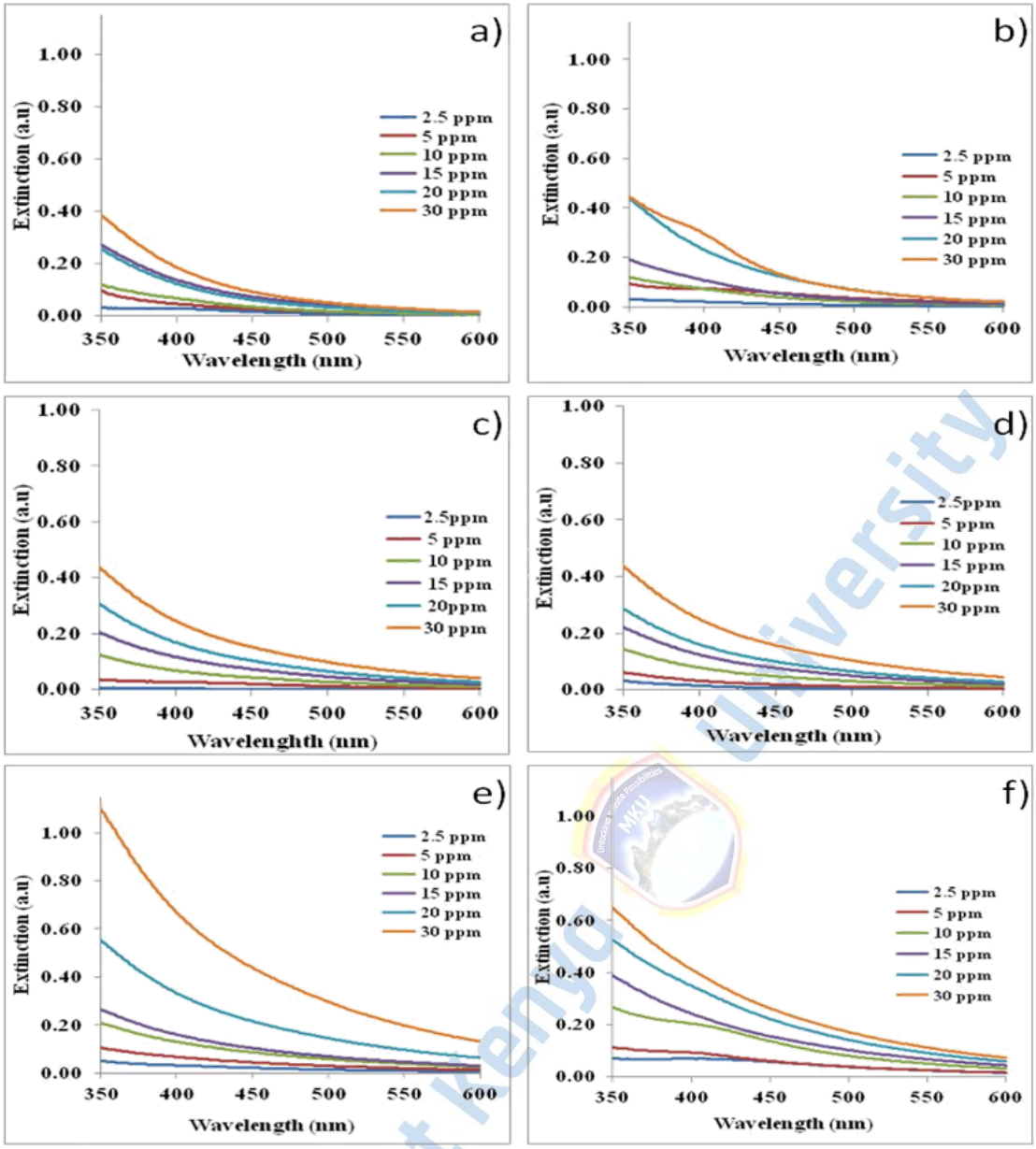

Figure 4. 9: UV-Visible spectral lines of Ag NPs formed at 1 mL Ag+ ion conc. With variations in concentrations of chitosan a) 2.5 ppm b) 5 ppm c) 10 ppm. d) 15 pmm

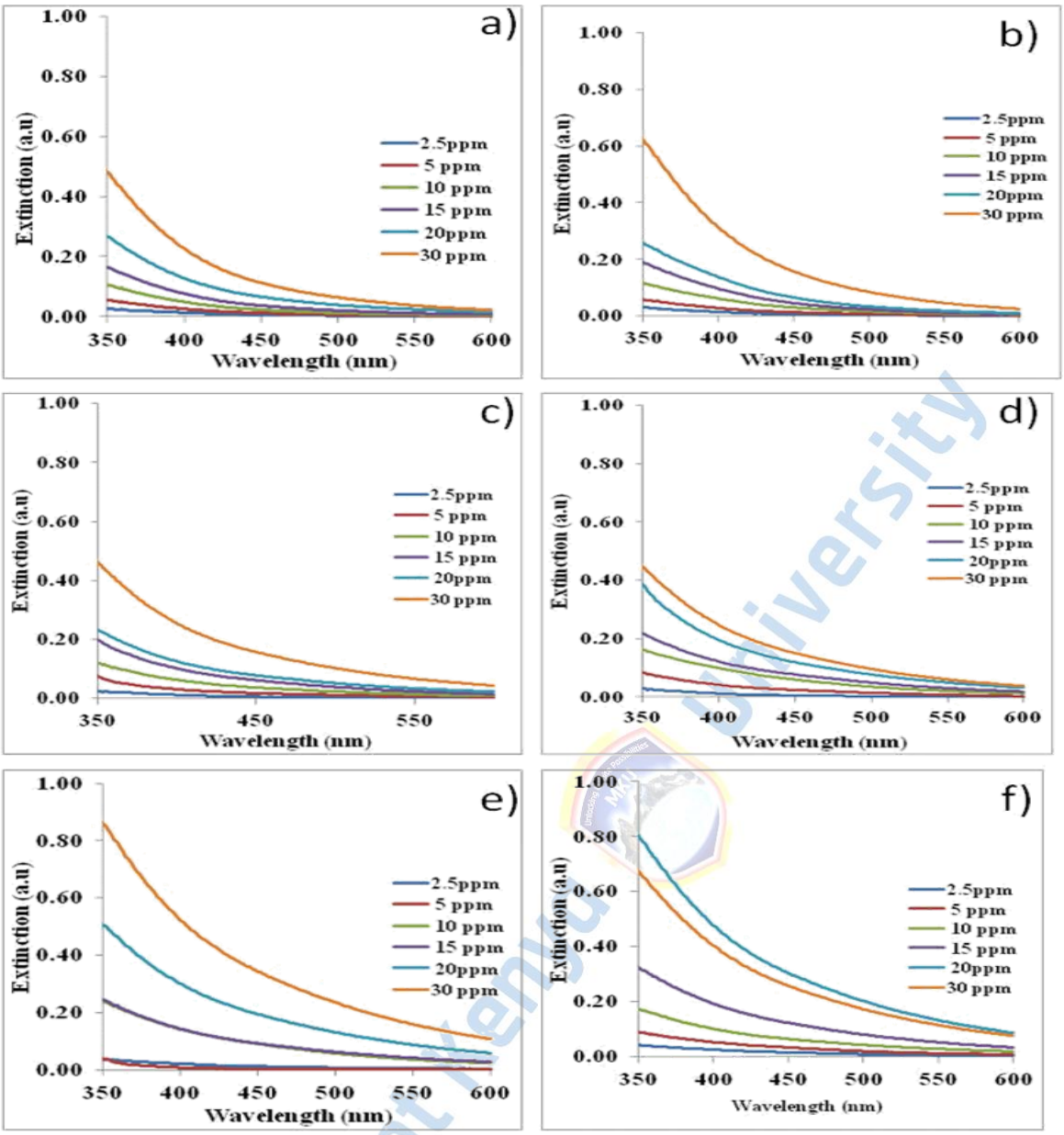

Figure 4. 10: UV-Visible spectral lines of AgNPs formed at 10 mL Ag ion conc. With variations in concentrations of chitosan a) 2.5 ppm b) 5 ppm c) 10 ppm. d) 15 ppm e) 20 ppm and f) 30 ppm

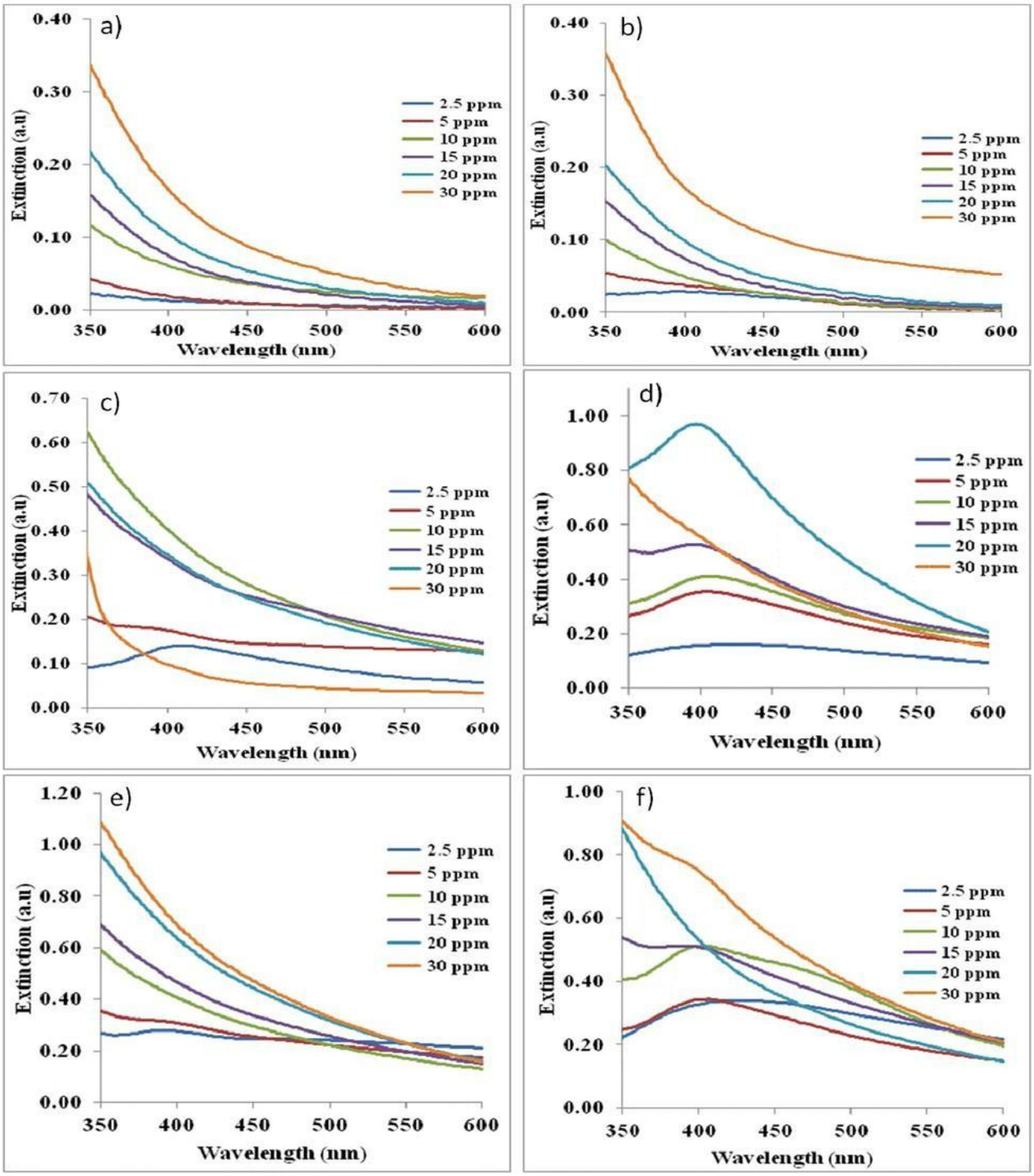

Figure 4. 11: UV-Visible spectral lines of AgNPs formed at 15 mL Ag+ ion conc. With

variations in concentrations of chitosan a) 2.5 ppm b) 5 ppm c) 10 ppm. d) 15 pmm

4.1.7 Scanning Electron Microscopy characterization of silver nanoparticles

Scanning electron microscopy (SEM) applies a high energy electron beam so that it undergo scanning on the surface and back scattering of the electrons in order to resonate (Dhar *et al*., 2021) . Therefore, the interaction between the atoms in the sample and high energy beam of electrons leads to the production of the signals providing details on the kind of surface topography, components present and the dialectical aspects of the silver nanoparticles (Agarwal *et al*., 2021). Initial size characterization of the silver nanoparticles synthesized using chitosan as a reducing method was done using UV-Vis spectroscopy. Scanning electron microscope was used to validate the characterization of the morphology of silver nanoparticles in this study. These images of silver nanoparticles obtained were scanned at 500 nm using the scanning electron microscopy. The plates 4.2 -4.4 below indicated that silver nanoparticles exhibit a size range of 10-50 nm which are in agreement with the earlier findings on the right sizes at different resolutions between 0.5 to 4 nm. (Chinni *et al*., 2021).These results from SEM together with those from the UV-Vis studies gave a clear affirmation of the presence of silver nanoparticles. The scanning electron microscope technique was directly applied to detect and characterize silver nanoparticles, due to the ability of SEM to image silver nano-structures, by directly determining their sizes. Furthermore, SEM presented more information on the orientation and the spherical shapes of the silver nanoparticles, even though it had a limitation on the number of particles detected within a given time duration (Jomehzadeh *et al*., 2021).

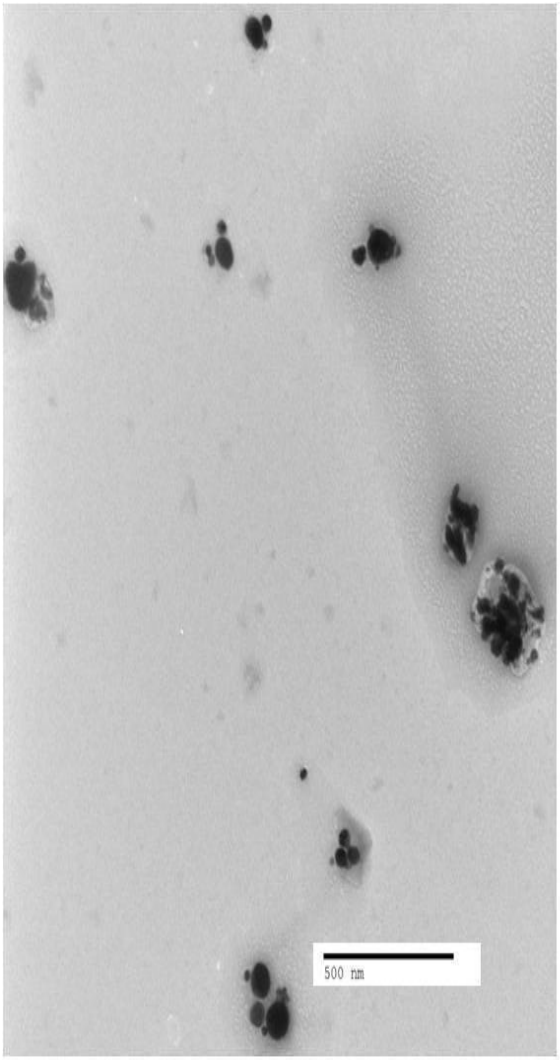

a)

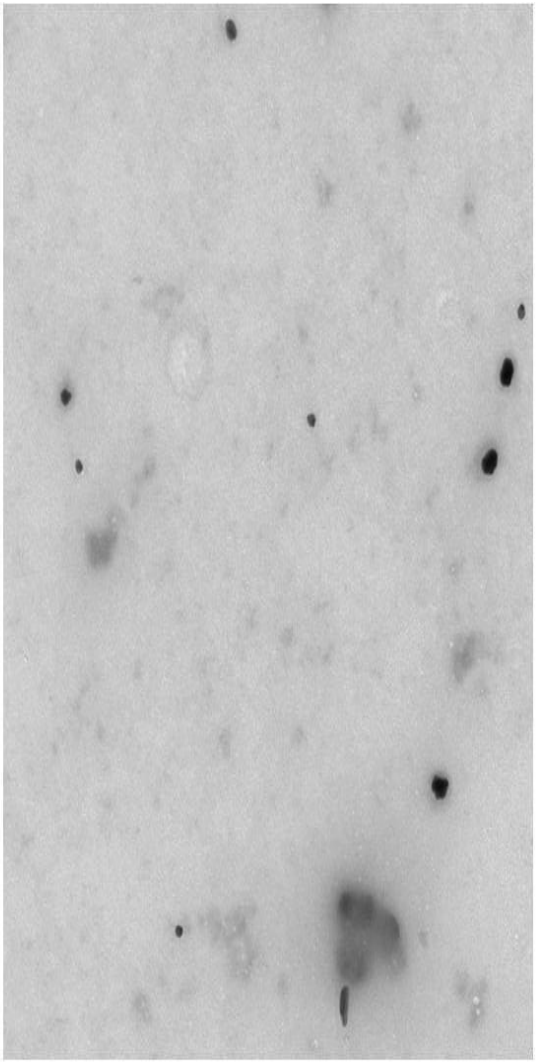

b)

Plate 4. 2: Scanning electron microscope image of synthesized Silver Nanoparticles

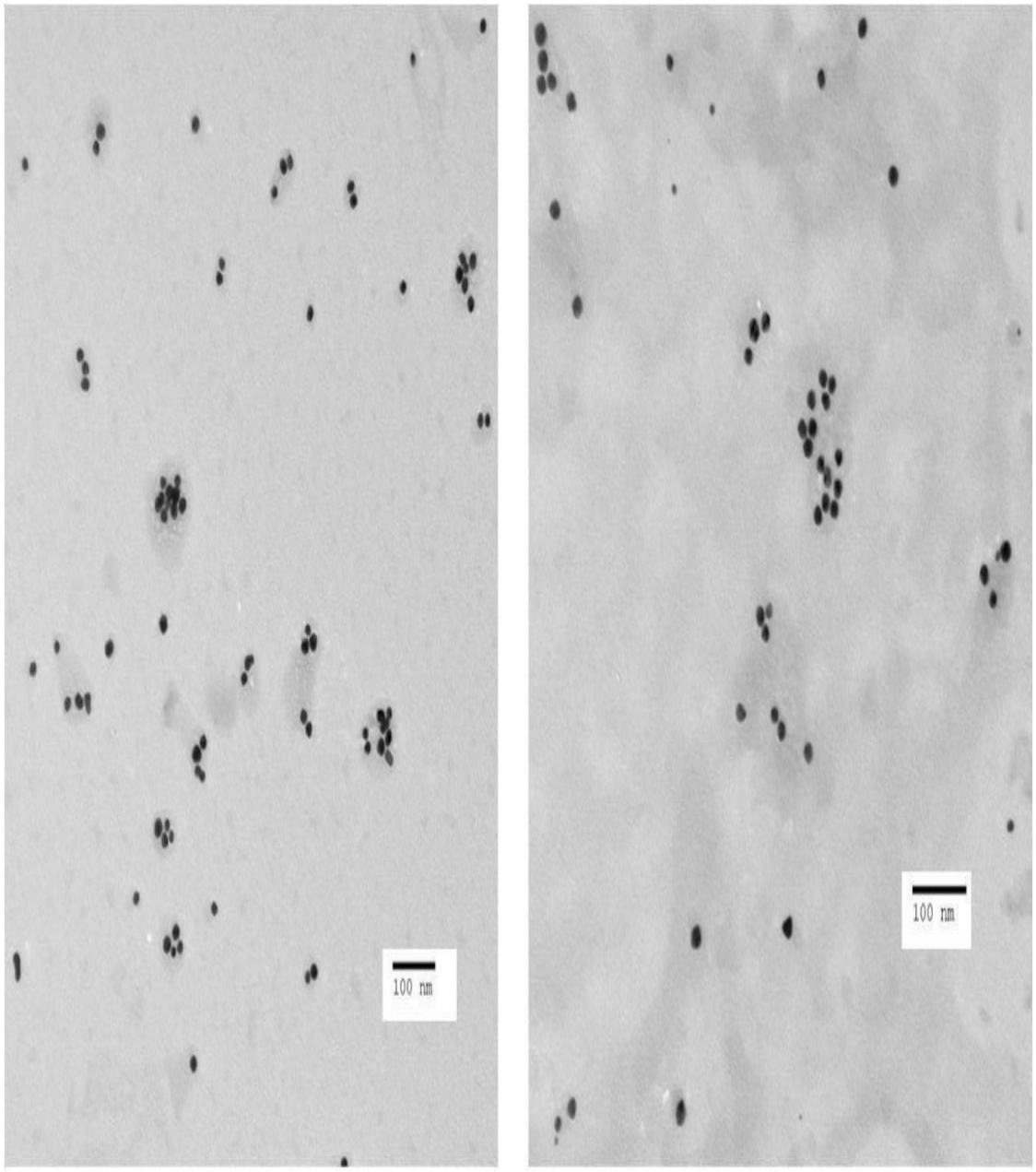

Plate 4. 3: Scanning electron microscope image of synthesized Silver Nanoparticles

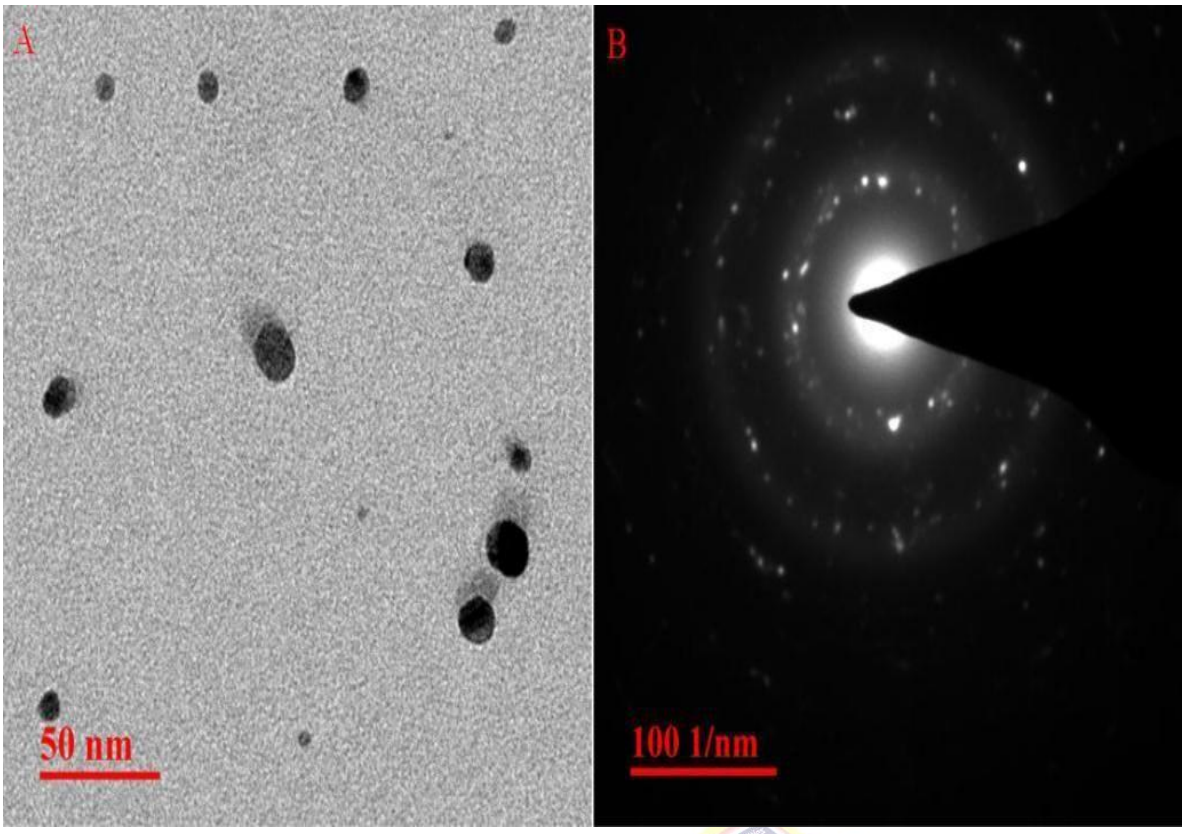

Plate 4. 4: Scanning electron microscope image of synthesized Silver Nanoparticles

4.1.8 Results of loading silver nanoparticles on indium tin oxide electrodes

Drop casting method was applied in embedding silver nanoparticles to the indium tin oxide electrodes (G. Duan *et al*., 2023). The indium tin oxide electrode was modulated by changing the sizes of the drop and concentration of the silver nanoparticles dispersed in the solution (Song *et al*., 2023). Direct modification of the nanoparticles was made possible by the aid of the selected sensors on to the working electrode (J. Shi *et al*., 2023). A current density of 0.2 mA cm^{-2} was applied for homogeneous flower like structures deposits on the thin film conducting material. Plates 4.5 -4.6 below show image of ITO electrode before embedment of AgNPs whereas, the plates 4.7 -4.10 show after embedment of AgNPs using Motic light microscope. Milanović also reported similar results in his study (Milanović *et al*., 2021).

Plate 4. 5: Image of ITO electrode before embedment of AgNPs using Motic light microscope

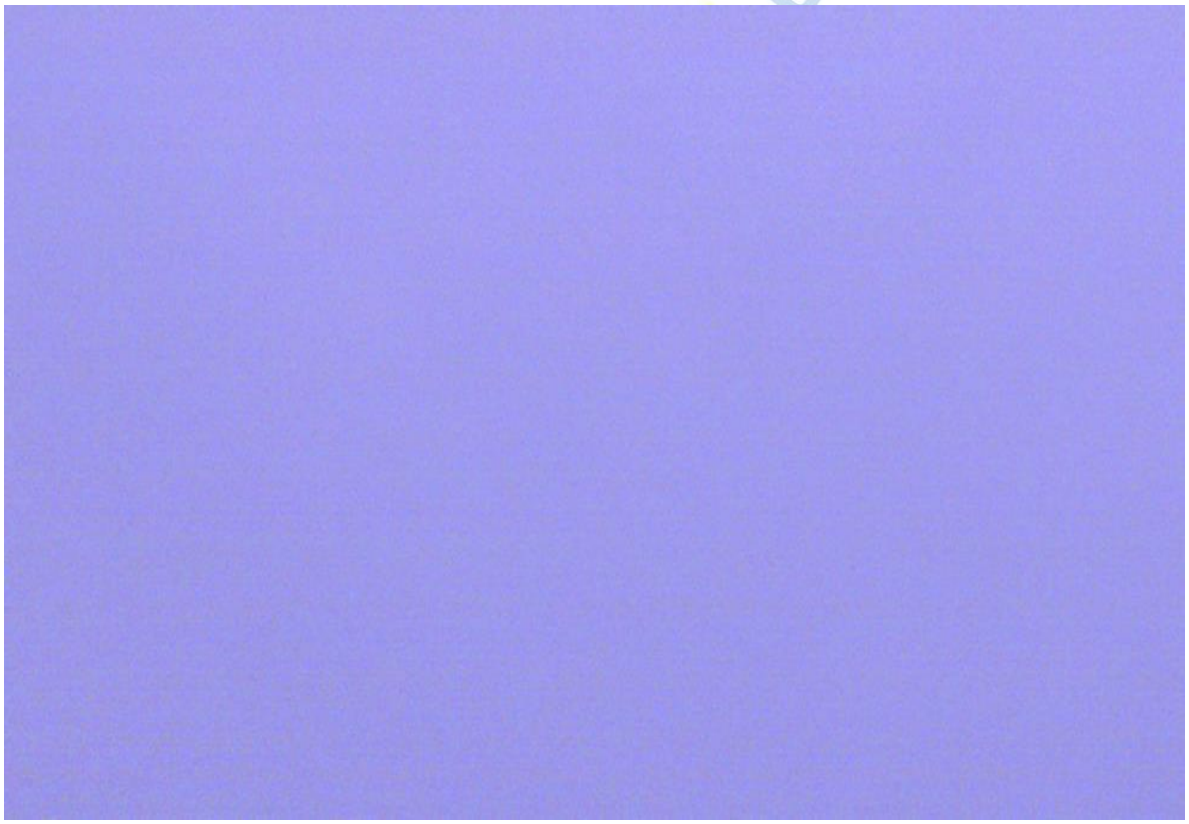

Plate 4. 6: Image of ITO electrode before embedment of AgNPs using Motic light microscope

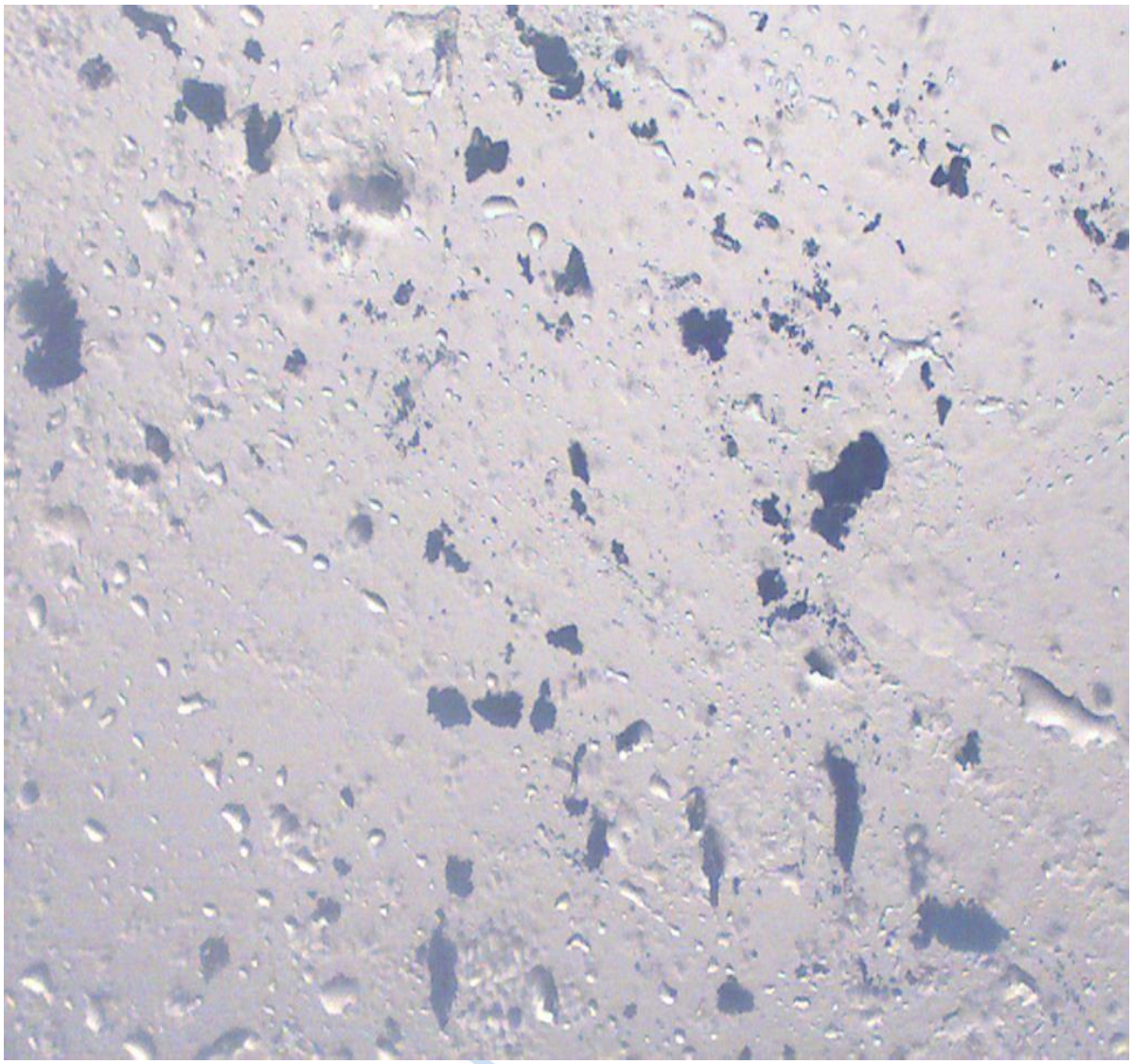

Plate 4. 7: Image of ITO electrode after embedment of AgNPs using Motic light microscope

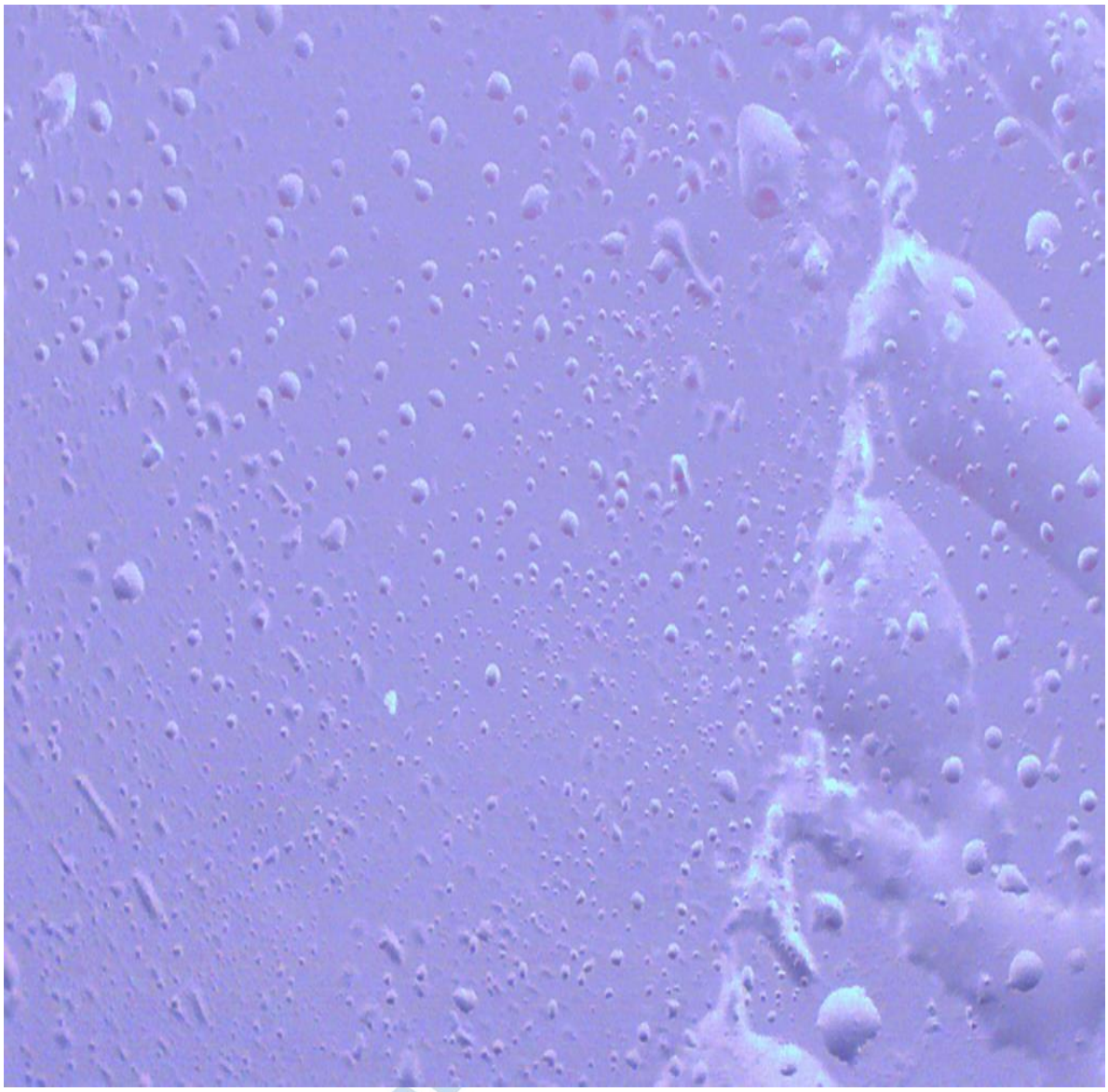

Plate 4. 8: Image of ITO electrode after embedment of AgNPs using Motic light microscope

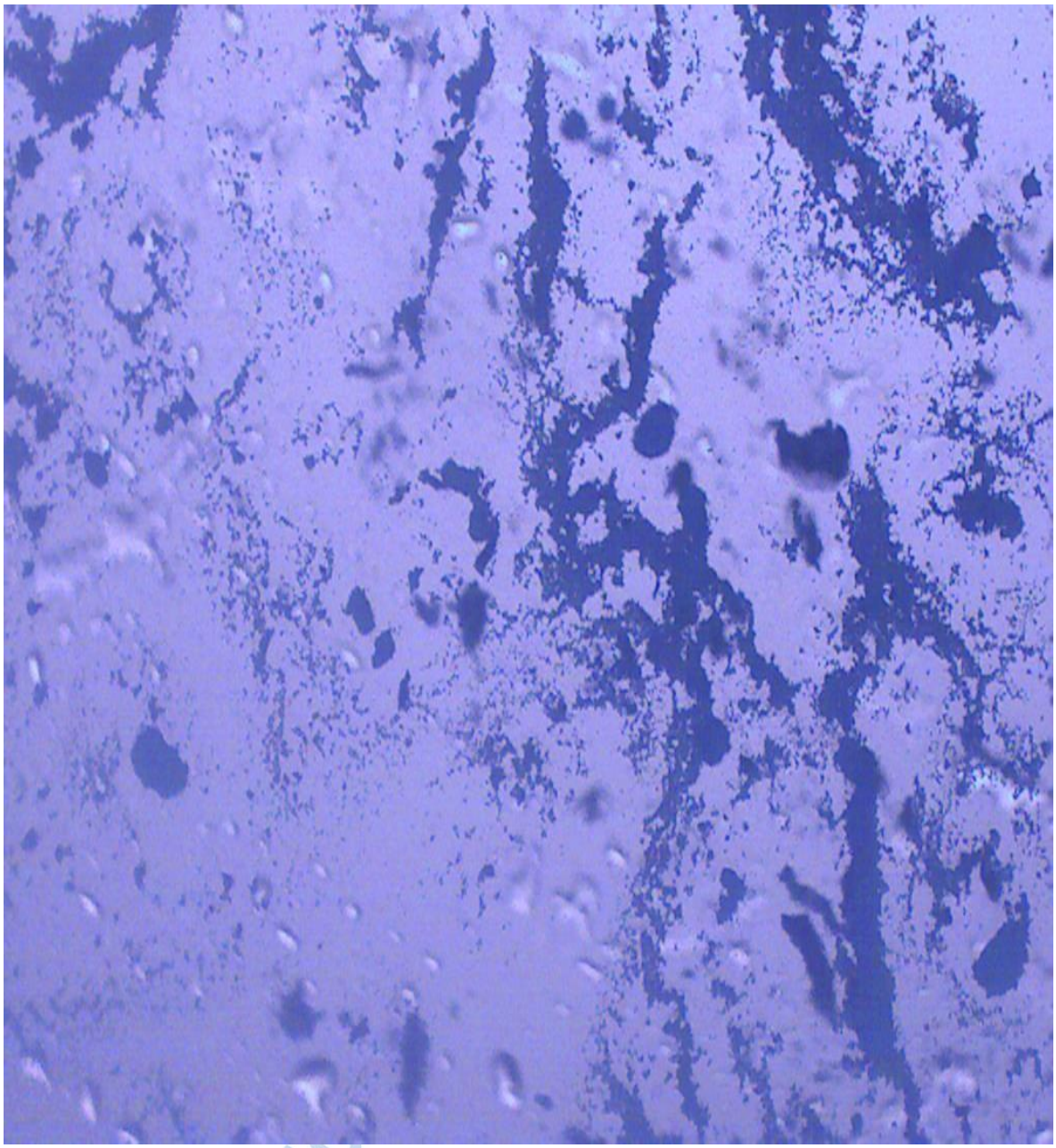

Plate 4. 9: Image of ITO electrode after embedment of AgNPs using Motic light microscope

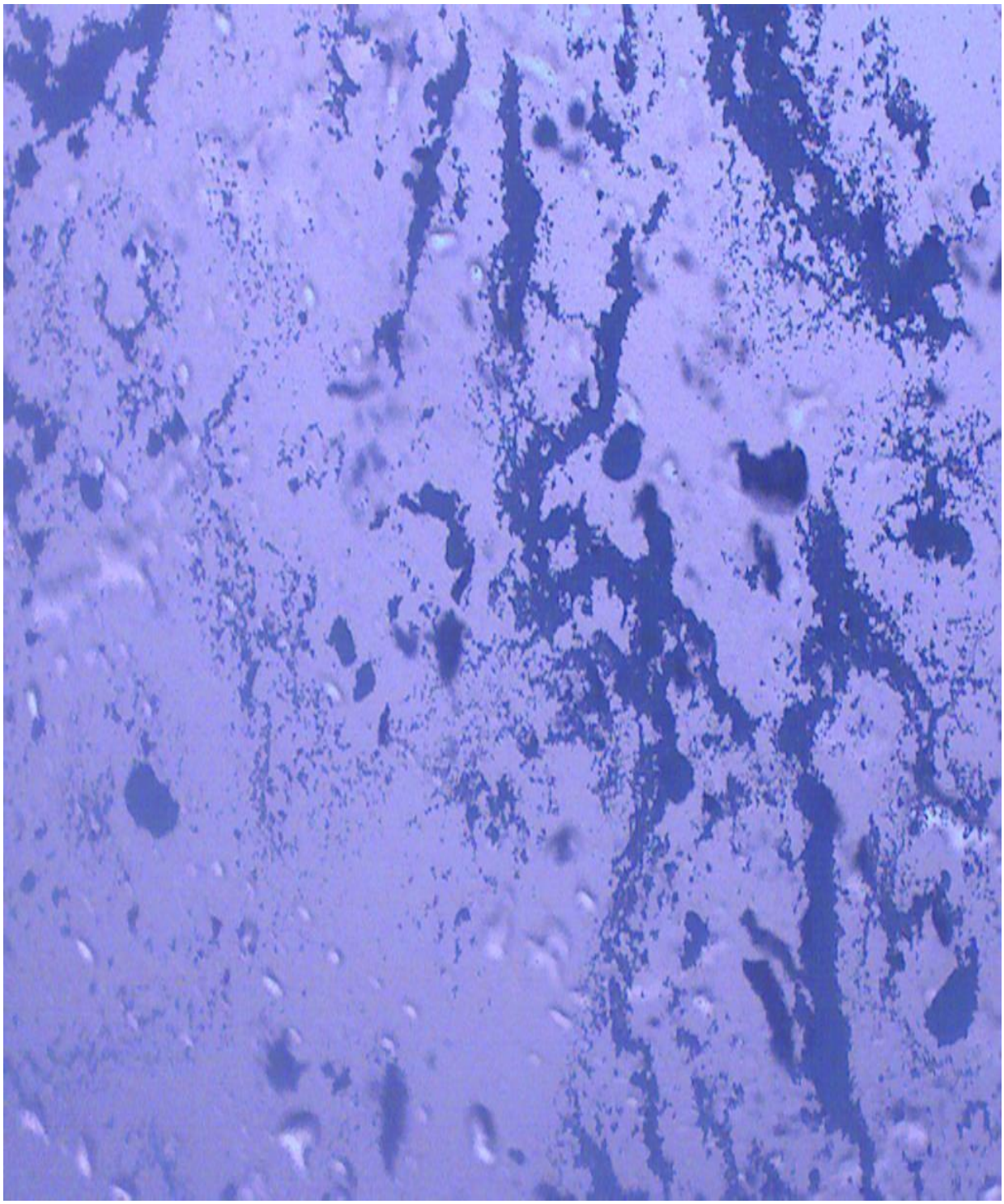

Plate 4. 10: Image of ITO electrode after embedment of AgNPs using Motic light microscope

The modified ITO electrodes exhibited relative insensitivity towards the interference by the electro-active species dissolved in the textile azo dyes effluent. Similar findings were also recorded by Azwatul (Azwatul *et al*., 2023). The electrodes presented in plates 4.7 - 4.10 *above* further demonstrated their stability over a long period of time. They also showed selectivity, reproducibility with greater resistivity towards conducting material fouling, which was in line with the earlier findings (Ameen *et al*., 2023), which are the fundamental amperometry in nanoparticle biosensor that can be applied in matrices that are complex in nature (Alduraihem *et al*., 2023). These electrochemical biosensor electrodes derived from the application of silver nanoparticles demonstrated their possession of vital chemical and physical aspects like elevated surface area, mass transport and catalysis in azo dye degradation.

4.2 Results of degrading Azo dyes using silver nanoparticles embedded on ITO electrodes

The textile wastewaters are coloured due to the presence of the azo group (-N=N-) of the dye that enhances its visible colour (Zee, 2002). In this study four azo dyes were used which included two disperse and two reactive dyes namely: disperse black, disperse blue, reactive red and reactive deep. The disperse blue, black dye, reactive deep and red are some of the examples of commonly used industrial azo dye types (Anliker, Clarke and Moser, 1981). A 100ppm stock solution of the four azo dyes was prepared and used to determine their respective maximum absorption spectra using UV-VIS spectroscopy. The absorption spectra of these azo dyes were determined between 200nm to 800 nm wavelength range using the Uv-vis spectroscopy. The figure 4.11 below shows the λ_{max} for the four Azo dyes obtained by scanning at different wavelengths in the UV-VIS spectroscopy.

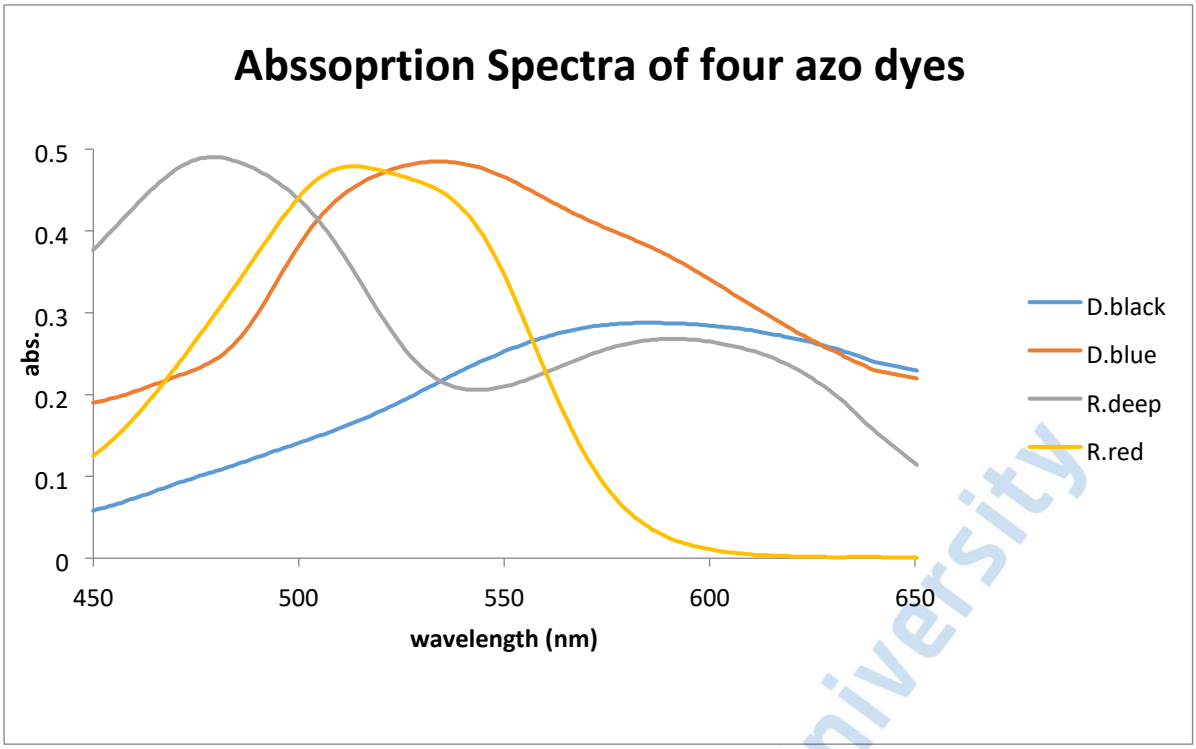

Figure 4. 12: A graph showing absorption spectra of the 4 azo dyes.

The four dyes showed difference in their λ max; disperse black showed its highest absorption spectrum at a wavelength of 586nm, disperse blue showed its highest absorption spectrum at a wavelength of 532nm, reactive deep showed its highest absorption spectrum at a wavelength of 476nm, and reactive red showed its highest absorption spectrum at a wavelength of 512nm. These values implied that light absorbed by azo compounds in the textile effluent is within the visible range of the electromagnetic spectrum. These wavelengths: - 476, 512, 532 and 586 nm are in line with the findings of Zee (2002) which reported that all aromatic compounds absorb electromagnetic radiation, however, only those that absorb light within the wavelengths in the visible range are coloured.

4.3 Degradation efficiency from UV-Vis spectral analysis

The determination of levels of azo dye in the textile effluents discharged by Rivatex Textile Industry, Uasin Gishu County, Kenya and Mombasa Textile Industry, Mombasa County, Kenya before and after treatment was conducted using ultraviolet visible (UV-Vis) spectroscopy. The spectral signals in the figures 4.12 - 4.17 below illustrate the degradation efficiency obtained through monitoring the changes that occurred in terms of absorbance of

azo dyes dissolved in textile waste waters dyes using various electrodes. The UV-Vis spectrum obtained in the figure 4.12, involved the degradation of azo dyes in the effluent using solely ITO electrode whereas, figures 4.13 - 4.15 involved degradation with the ITO coupled with silver nanoparticles and Figure 4. 13 - 4.17 involved electrocoagulation. The degradation efficiency was much higher when the nanocomposites electrode was applied. These figures below therefore, illustrated the wavelengths and their absorption maxima (λ_{max}) for the Azo dyes from effluents obtained from Rivatex and Mombasa textile industries respectively. The percentage of azo dyes degradation using the formula earlier stated were as follow:- 68.4%, 72.5% and 93.1% using electrocoagulation, ITO and ITO-AgNPs coupled electrodes respectively, these values are in agreement with the findings of (Zhou et al., 2021). The effectiveness of this analytical instrument was tested by considering its capability to monitor the decolorization aspect of these coloured textile Azo dyes (Laouini *et al*., 2021). The variation of the colours along the visible spectrum gave an indication of their intensities in terms of curves and spectral lines formation. In all the values presented, there was a general decrease in the intensity of the coloured chromophores with respect to amount of dye degradation time (Masarbo & Karegoudar, 2022). Therefore, in the case these measurements, there was no compulsion for calibration in optical illumination for the purposes of obtaining absolute values for irradiation, because relative values for spectral signals gave a significant outcome, thus was in for consideration (Alsamhary et al., 2022). When the measurement for normalization of the absorption maximum for the samples were taken, they showed a gradual decrease in absorbance as the coloured chromophores were being removed during the process of treating (Khaled *et al*., 2022). It was therefore, proven that, scattering resulting from ITO-AgNPs coupled electrodes effectively performed the role of degrading the color in these Azo dyes dissolved in the textile effluents, these findings are in line with the earlier studies on the same subject (Esmaeili *et al*., 2020)..

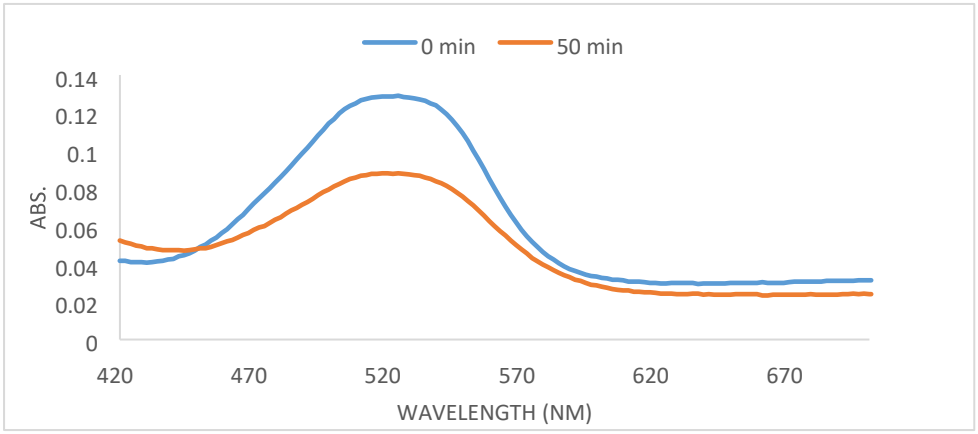

Figure 4. 14: Textile azo dye effluent degradation using ITO electrodes without embedding silver nanoparticles electrocatalyst at 24 V for 50 minutes.

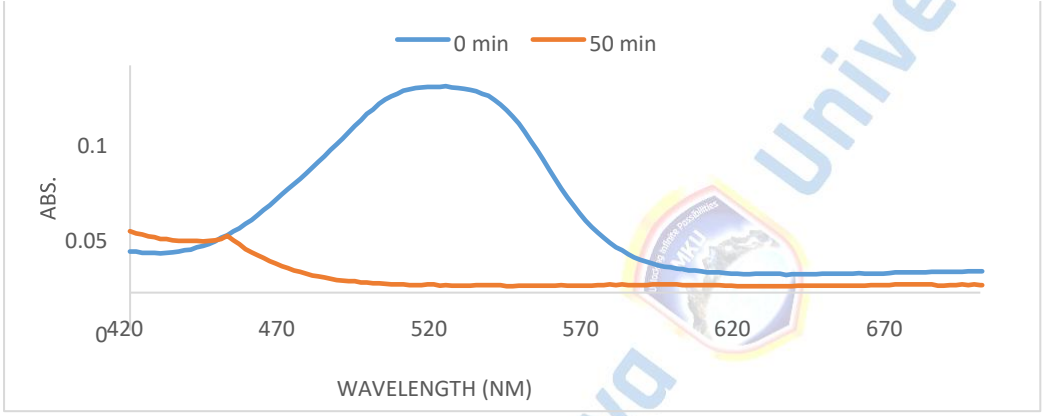

Figure 4. 15: Textile azo dye degradation using silver nanoparticles (AgNPs) embedded on ITO electrodes at 24 V for 50 minutes.

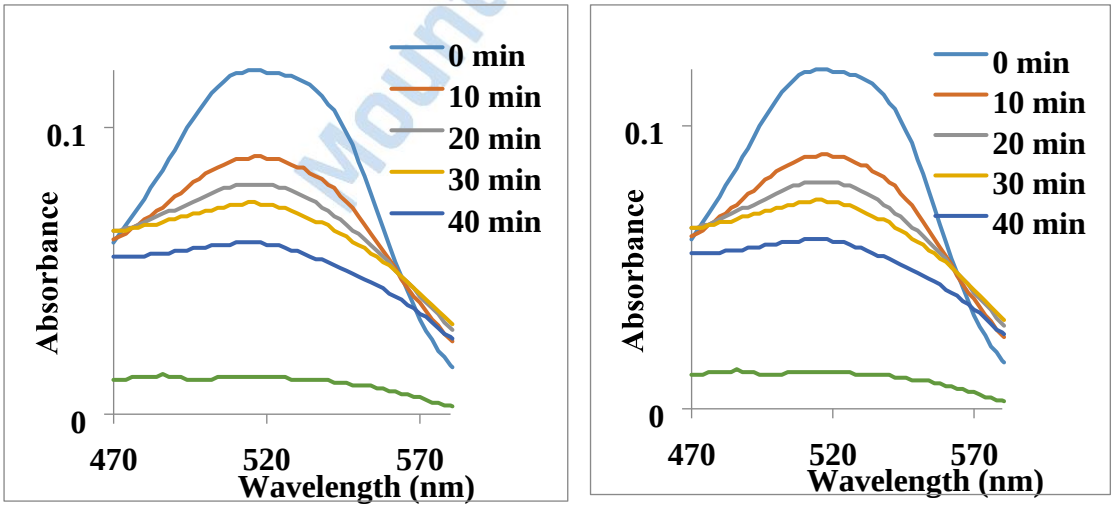

Figure 4.16: Rivatex Azo dye effluent degradation using ITO electrodes embedded with

silver nanoparticles electrocatalyst at 24 V for 40 minutes

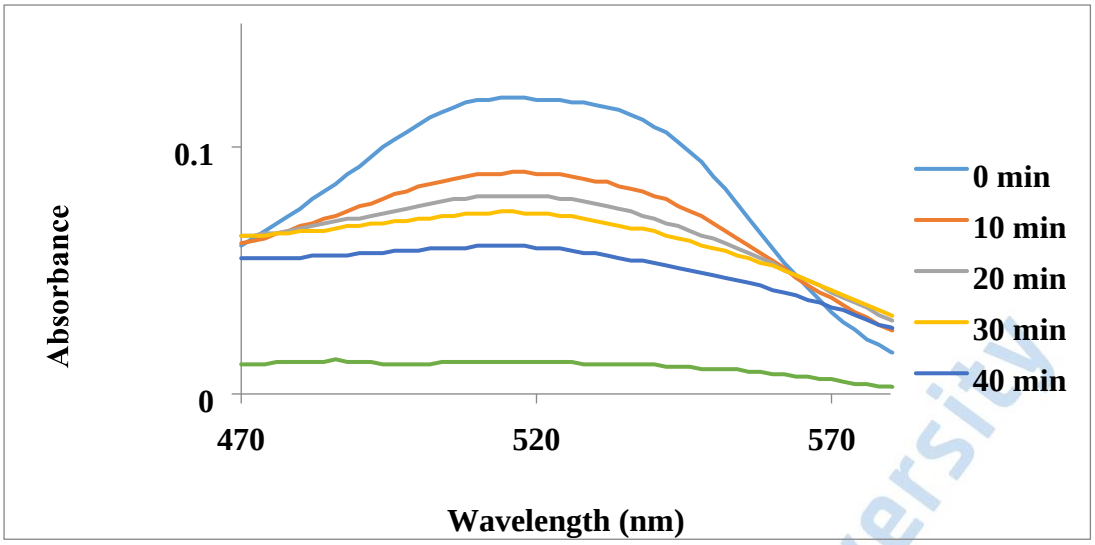

Figure 4. 17: Mombasa Textiles' Azo dye effluent degradation using ITO electrodes embedded with silver nanoparticles electrocatalyst at 24 V for 50 minutes.

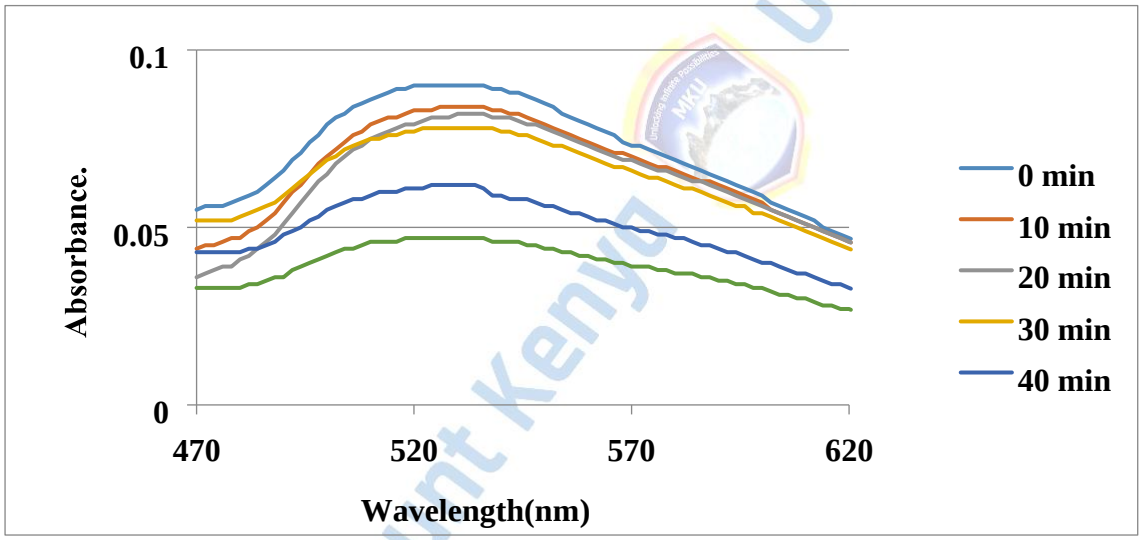

Figure 4. 18: Rivatex Textiles' Azo dye effluent electrocoagulation using stainless steel electrodes at 24 V for 40 minutes.

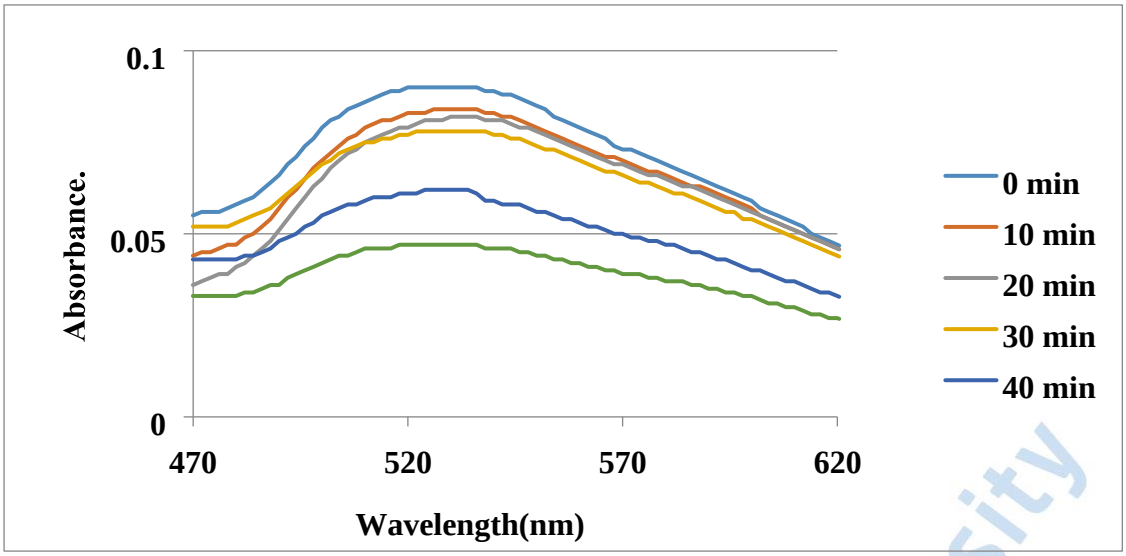

Figure 4. 19: Mombasa Textiles' Azo dye effluent electrocoagulation using stainless steel electrodes at 24 V for 40 minutes

4.4 Results of the level of azo dye in the textile effluents before and after treatment from LC-MS spectrometry

The figure 4.20 below demonstrates the levels of azo before and after degradation using electrocoagulation method and electrochemical technique of applying silver nanoparticles embedded on indium tin oxide electrodes. Twelve total number of samples were prepared for the for the LC-MS analysis. Eight of the samples were treated before the analysis, where four were degraded by electrocoagulation method while the other four degraded using silver nanoparticles embedded on the ITO conductive material. The remaining four sample were not treated so as to monitor the concentration of these samples before and after treatment. The liquid chromatography column was set up, possessing the following dimensions; - 100 mm, 2.1 mm, 3.5 mm with 0.30 mL/min as the flow rate. The mobile phase had 5mM ammonium formate in dissolved in distilled de-ionized water containing 0.01 % formic acid and 5mM ammonium formate in methanol containing 0.01 % formic acid. Then 10 mL acetonitrile was added to 10 g of homogenized with magnetic stirring at 900 rpm for 10 minutes. 10 mL of distilled de-ionized water was then added to the sample as stirring proceeded. Centrifugation

was performed at 4000 rpm for 5 minutes. Filtration of supernatant through a 0.45 µm membrane filter was done. 1 mL of the prepared textile effluent sample containing azo dyes was transferred into an amber auto-sampler vial at 300 ^{o}C with gas flow of 7 L/min and nebulizer was set at 45 psi and 4 kV sheath capillary.

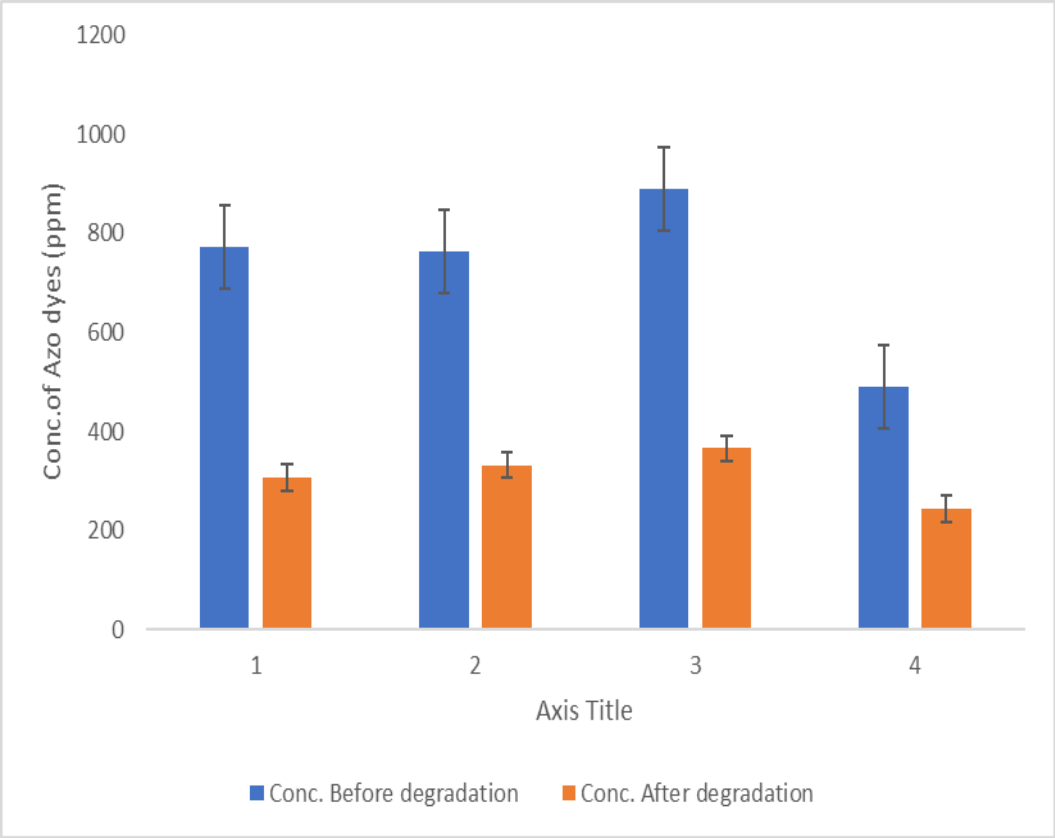

Figure 4. 21: Concentration of azo dye in the textile effluent before and after degradation using electrocoagulation method at 24 V for 50 minutes.

The figure 4.18 above shows a higher concentration in parts per million of the azo dyes before treatment in all the four samples and a decrease in the concentration after treatment. Results from the two factors ANOVA with replication indicated that there was a significant difference (P= 0.016) when the electrocoagulation was applied in the treatment of these effluent samples. On the hand figure 4.19 below illustrated a scenario of a higher concentration in parts per million of the azo dyes before treatment in all the four samples and very low concentrations after treatment compared to the previous outcome. The results obtained from the 2-Way ANOVA, indicated that there was a significant difference (P= 0.0204) when the silver

nanoparticles embedded on indium tin oxide electrodes were utilized in the degradation of these azo dyes in the effluent samples.

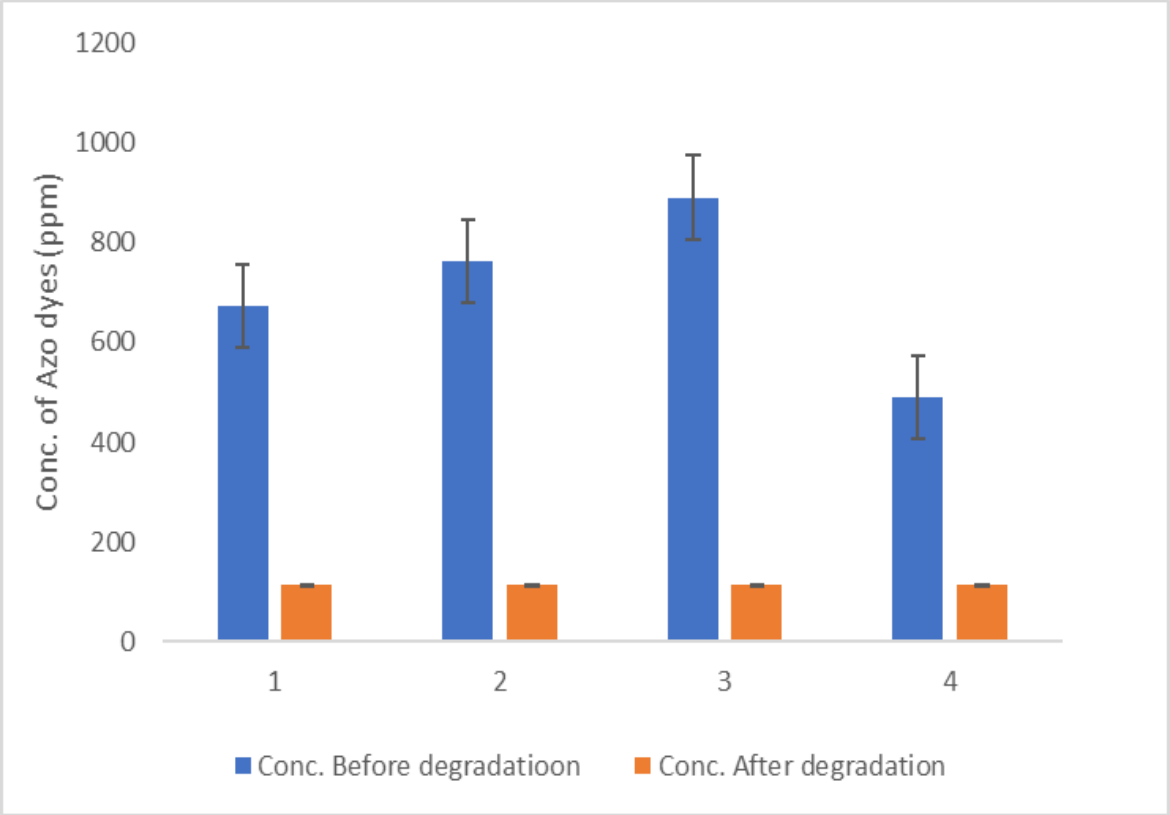

Figure 4. 22: Concentration of azo dyes in the textile effluent sample before and after degradation using ITO electrodes embedded with silver nanoparticles at 24 V for 50 minutes.

4.4.1 Results on the impact of inter-electrode gap on specific energy consumption

The indium tin oxide was used both as cathode and anode at different spacing i.e., at 2 cm, 4 cm, 6 cm and 8 cm. There was an insulator applied between the two electrodes to create a gap. The role of this spacing was to monitor the impact of varying inter- electrode distance on current and power consumed during the degradation process of these Azo dyes.

Electrolysis was then performed at a potential difference of 24 V. The table 4.3 illustrates the impact of inter-electrode gap on current and power consumption using ITO-AgNPs coupled electrodes whereas, table 4.4 provides information on the impact of the inter-electrode gap on current and power consumption using ITO electrodes solely. The result illustrates that specific

energy consumption during the azo dye degradation is greater in the table 4.4 compared to those obtained in the consecutive table 4.3 where the ITO electrodes were coupled with AgNPs. The tabulated results indicated that an increase in the inter-electrode distance led to an increase in specific energy consumption. Power utilization greatly increased with the electrode gap in both cases. It was also noted in both samples that, smaller inter-electrode distance of 2 cm consumed the least energy and the vice versa. Nonetheless, this minimal specific energy consumption could have resulted from lower over-potentials occurring during the electrochemical degradation process (Sleptsov *et al*., 2022). Increased inter spacing led to high specific energy consumption due to less interactions of the azo dyes in the effluent with the few hydroxyls (OH) liberated hence reducing the efficiency of eliminating the coloured chromophores (Shy *et al*., 2021). These fundings were in agreement with those of (Maghanga *et al*., 2015) who stated that increased distance between the electrodes lowered degradation efficiency from 99.0% to 90.0%.

Table 4. 3: A table showing the impact of inter-electrode gap on current and power consumption using ITO-AgNPs coupled electrodes

Sample	Electrode gap (cm)	Time (hours)	Current (A)	Power (watt)	
				Min	Max
ER 1	2	0.043±0. 04	0.87±0.02	0.897	0.996
	4	0.076±0.02	0.99±0.01	1.806	2.022
	6	0.451±0.01	0.45±0. 57	4.871	4.947
	8	1.045±0.03	0.23±0. 19	5.768	5.834
EM 1	2	0.039±0. 05	1.18±0.02	1.102	1.273
	4	0.064±0.08	0.88±0.06	1.351	1.616
	6	0.451±0. 01	0.45±0. 57	3.863	3.948
	8	1.045±0.03	0.23±0.05	5.243	5.636

Table 4. 4: A table showing the impact of the inter-electrode gap on current and power consumption using ITO electrodes

Sample	Electrode gap (cm)	Time (hours)	Current (A)	Power (watt)	
				Min	Max
ER 2	2	0.025±0.012	1.23±0.014	0.738	0.782
	4	0.063±0.013	0.92±0.005	1.391	1.428
	6	0.546±0.007	0.65±0.003	8.518	8.664
	8	0.723±0.005	0.58±0.005	10.064	10.213
EM 2	2	0.030±0.009	1.31±0.120	0.943	1.328
	4	0.0792±0.001	0.87±0.009	1.654	1.694
	6	0.651±0.009	0.67±0.021	10.467	10.960
	8	1.876±0.005	0.49±0.003	22.061	22.923

Increasing the gap between the two electrodes increases the reduction potentials of the setup cells, up scaling resistance resulting in adverse impact on textile effluent treatment (Guo *et al*., 2022). These findings are also in line with Ohm's law elaborating on the relationship between the quantity of electricity in form of current passed through a metallic conductor in a circuit, which happens to have a direct proportionality with the voltage applied for any amount of temperature allowed. The Ohm's expression drops on potential (IR drop) brought about by the resistivity of the solution therefore, leads to a varying potential causing the movements of mobile ions in the dye solution. This drop is Potentially instrumental on the electrochemical aspects of the applied factors. Potential drop is calculated using Equation 4.1

$$IR = I \frac{d}{\quad} \qquad \text{Eq 4.1 A.k}$$

Here: I = current (A) d = inter-electrode distance (m) A = active anode surface area (m^2) κ = specific conductivity (102.9 mS/m)

Equation 4.1 suggests that drop in potential (IR) increases whenever the spacing between the electrodes is increased. The increased distance causes the current flow to consequently drop thus the necessity to step up the voltage to contain the required current passed. This decrease in power consumption with increased electrode gap occurs as a result of increased Ohmic loss (IR drop). Therefore, this facilitates a decrease in oxidation rate taking place at the anode during the degradation of the azo dye components in the textile effluent samples. Most importantly, it is worth noting that an increased distance between the ITO electrodes raises the chances of IR drop increasing thus lowering efficiency of the electrolytic degradation of the Azo dyes (Gandi *et al*., 2022). Therefore, IR drop shows a relationship to the gap within the ITO electrodes, surface area (m^2) of the conductor, specific conductance of the electrolyte and current. Minimizing the IR drop is easily achieved by lowering the created gap within the electrodes and raising the surface area of the cross section of electrodes and specific solution conductance (Tanveer *et al.*, 2023).

4.4.2 Results on the impact of AgNPs concentration on specific energy consumption

Table 4.5 illustrated the impact of AgNPs concentration on time, current and power consumption during azo dye degradation using ITO electrodes. The general trend showed that specific energy consumption and time taken to degrade the azo dyes in the textile effluent declined with increased silver nanoparticle concentration application. When testing was done to determine the relationship at 95% confidence level on the hypothesis as to whether there was an impact of varying the concentration of AgNPs applied on the Indium tin oxide (ITO) on average specific energy consumption, H0: CE =0 Vs. H1: CE≠0. The outcome from the 2-way ANOVA analysis in appendix VI (c) showed that the value (p=0.002384) appeared to be less than (p= 0.05). This implied that, varying silver nanoparticles concentration in electrode embedment, brought the difference in specific energy consumption. These results are consistent

with the previous of Ganeshan *et al*., 2018 findings that silver nanoparticles have plasmon effects when embedded to the counter electrode in order to enhance greater performance in dye degradation (Ganeshan *et al.,* 2018). The AgNPs concentration had direct proportionality impact on the level of azo dye in the textile effluent degradation. A similar experiment was conducted on improving the efficiency of the organic solar cell on a photo-conductor layer doped by silver nanoparticles and it gave similar result (A. M. Ali *et al*., 2020). In both samples from Rivatex and Mombasa Textiles, data recorded on the table below demonstrated that 8 ppm of the nanoparticles applied to the ITO electrodes resulted in lower average power consumption maximum of 0.7533 watts-hr. The highest power consumption was noted which was not economical in terms of cost effectiveness in all the cases of 0 ppm application of silver nanoparticles to the ITO electrodes. Silver nanoparticles embedded on ITO electrodes had the ability to exhibit electro-catalysis, an aspect emanating from their nano sizes with large surface area to volume ratio (Wulandari *et al*., 2018). This explanation advances the findings on the fundamental catalytic properties of silver nanocomposites supported on the silica spheres and silver nanoparticles-embedded nano-paper as a colorimetric chiral sensing platform (Zor, 2018). Zero application of AgNPs to the electrodes, resulted in lower current generation and power over utilization. Increased current production lowers the amount of watts applied because the reaction takes minimal duration in degrading chromophores in the azo dyes as earlier noted (Matsukatova *et al*., 2020).

Table 4. 5: A table showing the impact of AgNPs concentration on time, Current and power consumption during azo dye degradation using ITO electrodes

Sample	**AgNPs (ppm)**	**Time (h)**	**Current (A)**	**Power (watt-hr)**	
				Min	**Max**
ER 3	0	0.16±0.01	0.51±0. 11	1.959	2.120
	2	0.08±0. 05	0.57±0. 01	1.090	1.163
	4	0.07±0.01	0.54±0. 09	0.908	0.936

	6	0.05±0.07	0.60±0. 06	0.720	0.908
	8	0.031±0.05	0.64±0. 06	0.476	0.488
EM 3	0	0.18±0.010	0.48±0.01	2.074	2.215
	2	0.11±0.023	0.58±0.02	1.530	1.879
	4	0.10±0.010	0.57±0.012	1.369	1.534
	6	0.10±0.010	0.54±0.002	1.296	1.433
	8	0.09±0.011	0.42±0.001	0.907	1.142

4.4.3 Results on the effect of potential difference on specific energy consumption

Potential difference was varied at 2 different levels of 12 and 24V. Optimum voltage for complete chromophore degradation was established and used in all the subsequent reactions involving the other variations such as surface area to volume ratio, contact time. Table 4.6 showed the effect of varying potential difference on current generation and specific energy consumption using ITO-AgNPs coupled electrodes while table 4.7 represented the results of potential difference variation where ITO electrodes were not coupled.

Table 4. 6: A table showing the effect of varying potential difference (Pd) on current (I) generation and specific energy consumption using ITO-AgNPs coupled electrodes

S/N	Sample	Time (h)	Pd (V)	Current (A)	Power (watt-hour)	
					Min	Max
1 a)	**ER 4**	0.83±0.18	12	0.30 ±0.21	3.00	3.02
(b)	**ER 5**	0.12 ±0.26	24	0.52±0.03	1.45	1.50
2 a)	**EM 4**	1.17±0.81	12	0.30±0.01	4.20	4.27
(b)	**EM 5**	0.14±0.19	24	0.52±0.33	1.75	1.89

Table 4. 7: A table showing the effect of varying potential difference (Pd) on current (I) generation and specific energy consumption using ITO electrodes

S/N	Sample	Time (h)	Pd (V)	Current (A)	Power (watt-hour)	
					Min	Max
1 a)	**ER 6**	0.78±0.01	12	0.30±0.09	2.81	2.89
(b)	**ER 7**	0.10±0.08	24	0.52±0.17	1.23	1.33
2 a)	**EM 6**	0.73±0.03	12	0.30±0.37	1.06	2.69
(b)	**EM 7**	0.16±0.10	24	0.52±0.01	1.90	2.02

Result in tables 4.6 and 4.7 above shows that when the potential difference was stepped up from 12 V to 24V, specific energy consumption in both effluent samples was consistent by 16.19%, 15.23% and 21%, 17.7% for ITO-AgNPs coupled and ITO electrodes respectively. This showed that, the specific energy consumption was much higher at lower voltage application compared to a higher voltage. The average specific energy consumption at 12 V was 2.110 kWh/m^3 compared to 1.318 kWh/m^3 at Potential difference of 24 V. In both cases of electrochemical degradation procedures, voltage application is a fundamental parameter in determining the reaction rate of the components in the system (Sleptsov *et al*., 2022). The potential difference of the direct current using the direct multimeter was varied at the two levels of because these voltages have proven favorable for efficient reaction (Sleptsov *et al*., 2022).

This variation was also supplied to ensure effective and sufficient achievement for the voltage required to completely degrade azo dyes in the textile effluent samples. The time and current quantity needed to process the chromophore elimination was factored into consideration to facilitate the optimal conditions required. The outcome from the potential difference applied; time taken, current and power utilization at 12 and 24 V were tabulated. The results obtained in the tables 4.6 and 4.7 indicated that increased potential difference resulted in a decrease in specific energy consumption. Similar results were obtained by (J. Tang *et al*., 2022), he concluded that when samples are subjected to an increased potential difference more power

consumption is realized thus high voltage acts as a powerful driving force in the electrochemical reactions involving organic components in the recalcitrant involved (R.-F. Chen *et al*., 2021). From the Two- Way ANOVA analysis at 95% significant level in the appendix VI (d) used to test the correlation between the effect of varying Pd on specific energy consumption, H0: CE =0 Vs. H1: CE≠0. Results (p=0.989778) shows that there was no significant difference in the current generated as a result of applying different voltages in the range of 12 to 24V. This outcome established that 24V generated much more current per unit time, compared to 12 V. The current generated through ITO-AgNPs coupled electrodes for each of the Azo dye effluent samples were much higher in comparison to the one generated by ITO without silver nanoparticles embedment. These finding are in agreement with the observation made by Zhuo 2022, who found that, higher voltages tend to increase current generation, as a parameter during the electrochemical degradation of the organic compounds, causing a linear increase in the reaction rate (Zhuo *et al*., 2022). Therefore, the impact of voltage on the reduction rate constants, facilitates thermodynamic driving force in that chemical reaction where the elimination of contaminants rate increases with an upsurge in voltage, holding chemical kinetics as limiting rate path (Ren *et al*., 2023).

4.5 Results for the impact of surface area to volume ratio on specific energy consumption

Surface area to volume ratios as a parametric condition was varied at five different levels during the electrolysis process which included: - 10, 15, 20, 25 and 30 m^2/m^3 using 20 ppm textile effluent wastewater. The results in the table 4.8 below showed that there is direct proportionality between the power consumption and the surface area to volume ratio. This relationship was also realized by Maghanga (2017). The results in table 4.8 below shows that there was a decrease in specific energy application from 12.8 to 9.4 watt-h with a decrease in S/V from 34.0 m^2/ m^3 to 14.0m^2/ m^3. However, an increase in specific energy consumption from 14.5 to 40.0 watt-h as the S/V ratio decreased from 22.0 m^2/ m^3 to 14.0 m^2/ m^3 with the use of ITO-AgNPs coupled electrodes. On the other hand, higher specific energy requirement

was noted in the case of SS electrodes application, at S/V ratio of 34.0 m^2/ m^3 to 26.0 m^2/ m^3 the output range was 25.0 to 14.3 watt-h. The trend of surface area on specific energy consumption was similar in both cases of ITO-AgNPs coupled and SS electrodes application. The implication of surface area to volume ratio of the electrodes towards the specific energy consumption is supported by the findings by Zeng *et al*., 2023, who asserted that, surface to volume ratio of the electrode facilitates the length of diffusion thus reducing heat generation by the current collector, this has an impact of lowering the local heating (Zeng *et al*., 2023).These results also showed that, the current generation in both techniques was at a constant of 0.13 translating to 22.0 A/m^2 and 19 A/m^2 current densities respectively. This range is in agreement with the acceptable range of 20 - 25 A/m^2 for proper sustainability of electrode life (Chen, 2010). The surface area to volume ratios were found to vary in terms of the nature of effluent (Maghanga *et al*., 2015). In summary this research found that, an increase in the surface area, had a significant reduction in the current generation due to its distribution to a larger surface thus decreasing the ratio of current densities in both ITO-AgNPs coupled and SS electrodes.

Table 4. 8: A table showing effect of surface area to volume ratio on dye removal from the effluent samples

	Power (watt –hr)	
Surface area to volume ratio m^2/m^3	**ITO-AgNPs coupled electrodes**	**SS electrodes**
34.0	12.8	25.0
30.0	10.7	19.1
26.0	9.4	14.3
22.0	14.5	18.2

18.0	16.6	23.0
14.0	40.0	35.0

4.5.1 Results of colour removal level during Azo dye electrochemical degradation

The colour of azo dyes in the textile effluent samples ER 8, ER 9, EM 8 and EM 9 were analyzed using the standard methods of platinum-cobalt (Pt-Co) colour units provided by APHA. The table 4.9 provides data on the determination of colour removal level of the Azo dyes in the textile effluent before and after treatment using different electrodes. Spectrophotometer (HACH DR 2000) normally applied to determine the colour levels in various samples (Shindhal *et al*., 2021). Table 4.9 below shows that ER 8 effluent sample had the highest colour value recorded with the platinum-cobalt units of 2004±0.5 whereas, EM 9 showed the least platinum-cobalt colour units of 1003±0.2 during the electrochemical degradation process. These values are within the range of the findings by Asfaha who noted that platinum-cobalt colour units' range of the azo dyes in the textile effluent is 950-2050 (Asfaha *et al*., 2022). In the four effluent samples, ER 8, ER 9, EM 8 and EM 9, the colour removal was 99.97% in the case of ITO electrodes coupled with AgNPs, showing that this technique optimized was very effective and efficient in the degradation of *azo* dyes in the textile wastewaters. It is a requirement that any technique applied should be able to eliminate the coloured chromophores emanating from Azo dyes to undetectable levels (Bustos-Terrones *et al*., 2021).

The Two-way Anova analysis was conducted at 95% confidence levels recorded in the appendix VI (e), indicated a significant difference between the samples before and after degradation using the silver nanoparticles embedded on the ITO electrodes (p=0.000441). These outcomes are in agreement with the findings from DSA electrodes utilized in azo dyes degradation (Ozturk *et al*., 2021). Furthermore, the findings are also in agreement with the earlier statement that, electrocoagulation alone as a method of textile effluent treatment is not efficient in the degradation of azo dyes due to the regeneration of flocs (Okur *et al*., 2022*).*

Table 4. 9: A table showing determination of colour removal level of the Azo dyes in the

textile effluent before and after treatment using different electrodes

Samples	Pt-Co colour units before treatment	Pt-Co colour units after tre - ITO electrodes coupled with AgNPs	SS electrodes
ER 8	2004±0.5	0.047	180.7
ER 9	1981±1.5	0.087	129.0
EM 8	2317±2.0	0.054	298.3
EM 9	1003±0.2	0.076	91.6

4.5.2 Results of chemical oxygen demand of the Azo dyes in the textile effluent

The collected textile effluent sample containing azo dyes was measured, into 2.50 mL then placed in digestion bottle then reacted with 1.50 mL of digestion solution and 3.70 mL of 2.0 M sulphuric acid at 110.0 ^{o}C. Table 4.10 below shows the COD of azo dyes in the textile effluent before and after treatment using different electrodes. The amount of oxygen utilized in reactions involving chemicals is often referred to as chemical oxygen demand (COD). It gives details on the quantities of organic components present in effluents occurring in various water bodies. The COD measurement is crucial by the way it facilitates total removal of harmful organic components by oxidizing them to non-toxic substances such as CO_2, NH_3 and H_2O in the prevailing acidic conditions. The oxidizing agent in this case is the $K_2Cr_2O_7$ due to its ability to convert ammonia formed to nitrates through further oxidation process. The table 4.10 of the COD values illustrates increased levels compared to the biochemical oxygen demand for the same textile effluent. This result implies that, chemical oxygen demand is always greater compared to biochemical oxygen demand since more organic compounds require chemical oxidation and not biological oxidation.

Table 4. 10: A table showing COD of the azo dyes in the textile effluent before and after treatment using different electrodes

Effluent sample	COD (mg/L) before treatment	COD mg/L of the effluent after treatment using: - SS electrodes

		ITO electrodes coupled with AgNPs	
ER 10	834 ±5.78	82.8±3.84	167.8±3.12
ER 11	693±8.74	96.6±7.25	156.6±1.23
EM 10	793±6.47	87.2±2.26	147.2±2.20
EM 11	592±3.79	68.0±4.96	145.0±4.31

The two-way ANOVA recorded in the appendix VI (f) indicated that a significant difference (p=0.014206) existed in the chemical oxygen demand (COD) of the azo dyes dissolved in the textile effluent after treating with silver nanoparticles embedded on the ITO electrodes to the actual levels accepted by the world health organization (WHO 2002) of 250±5 mg/L. The 2Way ANOVA analysis at 95% confidence interval in the same appendix VI (f) further recorded (p=0.014251) after degradation of azo dyes in the waste water. This analysis confirmed that there was significant difference in the chemical oxygen demand after degrading them using SS in the electrocoagulation method. Table 4.10 further shows that COD was not reduced to an acceptable level when SS electrodes applied as the only method of treatment. The results on the table 4.10 also indicated that ITO electrodes coupled with AgNPs was sufficient in lowering the competition for the dissolved oxygen (DO) in these water bodies as required by the environmental and coordination act (Yehuala *et al.*, 2022). Exhausting the dissolved oxygen endangers aquatic lives hence immediate measures for treating before discharge is very fundamental in conserving biodiversity (Hemalatha & Sanjay, 2023). The four samples ER 10, ER 11, EM 10 and EM 11 depicted a very negligible variation in terms of their chemical oxygen demand (COD), this is in line with the earlier finding (Shy *et al.*, 2021). The highest chemical oxygen demand was noted in ER 10 at 834 ±5.78 mg/L before degradation process and 90.07 % removal was realized. The COD listing for the samples after treatment with ITO-AgNPs coupled electrodes reached the acceptable limits of COD ≤250 mg/L (Xiao *et al.*, 2022). These

results supported the observation that electrolysis of textile effluent containing azo dye is efficient when silver nanoparticles embedded on indium tin oxide is applied to eliminate the COD (C. Wang *et al.*, 2021).

4.5.3 Results of Biochemical oxygen demand of the azo dyes in the textile effluent

The quantitative measurement of the oxygen gas utilized by bacteria while decomposing organic substances aerobically is termed as biochemical oxygen demand (Waffo *et al.*, 2022). Every textile factory is mandated to ensure there is reduction or even complete removal of the BOD before discharging the said effuse to the nearby water bodies (Aguilar-Torrejon *et al.*, 2022). Competition for the dissolved oxygen in aquatic biodiversity is lessen when the BOD is completely lowered before releasing textile effluents to these water courses (Yadav *et al.*, 2023). The table 4.11 below illustrates biochemical oxygen demand before and after degradation using the indium tin oxide coated with the silver nanoparticles.

Table 4. 11: A table showing BOD of the Azo dyes in the textile effluent before and after treatment using different electrodes

Effluent sample	BOD (mg/L) before treatment	BOD mg/L of the effluent af treatment using: -	
		ITO electrodes coupled with AgNPs	SS electrodes
ER 12	189±5.21	26±1.52	107.8±1.17
ER 13	186±4.83	24±3.25	96.6±3.32
EM 12	163±2.63	18±1.77	77.2±2.69
EM 13	171±6.30	22±2.21	100.0±2.11

The Two-way ANOVA analysis of the sample at 95 % confidence levels documented on the appendix VI (g), portrayed a significant variation (p=0.0000238) in biochemical oxygen demand for the Azo dyes dissolved in the textile effluent before degrading to an acceptable level according to the world health organization (NEMA, 2002) range of 150±5 mg/L. Moreover, this significant difference (p=0.0000238) existed between biochemical oxygen demand for the azo dyes in the textile waste waters after the degradation with silver

nanoparticles embedded on the ITO electrodes. These results showed a similar trend to the previous finding on the role of nanoparticles when embedded on DSA towards the mineralization of organic components in the waste waters (Arlyapov *et al*., 2022). In this study it was also noted that, the biochemical oxygen demand for all the four samples was ER 12, ER 13, EM 12 and EM 13 was generally high, with sample Ef1 registering highest BOD of 189±5.21 mg/L before degradation and lowest in Ef3 with 163±2.63 mg/L. Similar data range was obtained by Mohammadi earlier in which he noted that the BOD values were above 150±5 mg/L but much lower compared to those obtained for COD (Mohammadi et al., 2023). Furthermore, the above results indicated that BOD was perfectly lowered through degradation of the azo dyes in these effluent samples with ITO -AgNPs coupled electrodes. This technique of treating textile effluent resulted to a safer way of preserving dissolve oxygen by enhancing acceptable BOD prior to the waste discharge to the nearby water bodies. This principle is in line with studies carried out to determine the sustainable BOD towards the dissolved oxygen (DO) in the aquatic ecosystems (Yadav *et al*., 2023).

4.5.4 Results of the effect of effluent pH on azo dye degradation

The pH of 100 mL of the initial textile effluent sample before the degradation was adjusted to various values using both acidic and basic conditions ranging from 1 to 7 dilute hydrochloric acid of the determined 2.0 M concentrations. The electrochemical degradation of the textile effluent dyes and consequent power consumption was recorded. The impact of pH variation on specific power consumption and removal of coloured chromophores was recorded by adjusting the pH of textile effluents to 4.0, 5.0, 6 and 7.0 as shown in the table 4.12 below. The selected pH range was established to be the most effective in azo dye removal from the textile effluent (Ramzan *et al*., 2022). The table 4.12 below indicated that application of silver nanoparticles embedded on the ITO electrode at various pH values had lower specific energy consumption compared to the cases of electrocoagulation by use of SS electrodes. The 2-way Anova results in the appendix VI (h) conducted at 95% confidence interval level (p=001292) exhibited some

statistical significance in variation between the pH applied and power consumed in the samples under the study. The amount of current produced showed an inverse proportionality to strength of acid (Schallemberger *et al*., 2023). These results are synonymous with the findings that, current production is more powerful in acids and bases in comparison to neutrally build solutions of organics substances. Nonetheless, a change in pH of any solution affects the general efficiency and effectiveness of the degradation (Maghanga *et al.*, 2017). Specific energy applied for complete chromophore degradation became higher then dropped gradually as the pH increased towards 6.5 these results are synonymous to the observations made earlier correlating to the recalcitrant organic constituents pH (Al-Ansari *et al*., 2022). Nevertheless, lowest average specific energy consumption effective in azo dye degradation was determined at pH of 6.5, which agrees with the optimum pH range for the organic pollutants during the electrochemical degradation using DSA electrodes (Tibebe *et al.*, 2022). Studies have shown that initial pH of any solution is a fundamental part of determining the efficiency and feasibility of the electrochemical degradation (Kuokkanen *et al*., 2018). Textile effluent pH not only facilitates speciation of metallic ions but also helps in influencing the properties of these components in aqueous solution together with their products of solubility formation (Ikram *et al.*, 2022). It was also noted in various studies that pH of a solution was not constant during the electrolysis but depends on the type of electrodes applied (Allabakshi *et al.*, 2023).

Table 4. 12: A table showing impact of pH on power consumption at a pd of 24 V

Electrode	pH	Time (h)	Current (A)	Power (watt –hr.)	
				Min	Max
ITO electrodes coupled with AgNPs	7.0	0.51±0.04	0.35±0.04	4.29	4.83
	6.0	0.49±0.04	0.29±0.09	3.37	3.53
	5.0	0.46±0.09	0.33±0.07	3.65	3.79
	4.0	0.68±0.08	0.31±0.56	5.06	5.23

SS electrodes	7.0	0.73±0.01	0.34±0.06	5.96	6.08
	6.0	0.75±0. 49	0.34±0.02	6.12	6.21
	5.0	0.60±0. 87	0.34±0. 32	5.07	5.69
	4.0	0.89±0.09	0.30± 0.08	6.41	6.64

Lower pH, results in speciation of iron (ii) (Fe^{2+}), whose stability depends on acidic medium (Zhang *et al.*, 2022). Therefore, a pH range of 6.0 – 6.5 results in the formation of iron (iii) hydroxide [$(Fe(OH)_3$] most stable hydroxide of iron in its complex form (Y. Liu *et al*., 2022b). The stability of a complex is determined by its ability to possess lower crystal field stabilization energy (CFSE) thus, as seen in the case of Fe (III) contrary to Fe (II) constituting large energy, since iron (II) belongs to d6 system whereas, Fe (III) to d5 in periodic table systems (Pinheiro *et al*., 2022b). At pH 6.5 iron (III) is the most commonly occurring complex due to its stability that has been elaborated on (Dihom *et al*., 2022a). Mostly, recalcitrants emanating from the textile effluents are weakly organic acids and bases, causing the pH of the H_2O to interfere with the pollutant properties in these textile wastewaters (Wang *et al.*, 2022). These reactions were favored mainly in acidic conditions due to the fact that azo dyes found in the textile effluent do experience buffering activities under alkaline conditions, preventing degradation efficiency (Patidar & Srivastava, 2022).

4.5.5 Results of the Effect of temperature on Azo dyes in textile effluent degradation

The temperatures of the effluent samples were adjusted from 30.0^{o}C- 45.0^{o}C through the application of the heated thermostatic plate. These values were guided by the established optimum temperature ranging occasioned by dimensional stable nature shown by the ITO thin film conducting materials (Vilchis-Carmona *et al*., 2021). Table 4.13 below shows effect of temperature on Azo dye removal from the effluent.

Table 4. 13: A table showing effect of temperature on Azo dye removal from the effluent

Sample	Temp. (^{0}C)	Time (h)	Current (A)	Power (watt –hr.)	
				Min	Max
ITO	30	0.16±0.05	0.38±0.01	1.46	1.51
electrodes coupled with AgNPs	35	0.11±0. 18	0.42±0.04	1.12	1.21
	40	0.19±0.02	0.40±0.53	1.83	1.99
	45	0.17±0.71	0.40±0.89	1.63	1.81
SS electrodes	30	0.34±0.04	0.38±0.06	3.10	3.59
	35	0.29±0.08	0.38±0.75	2.65	2.88
	40	0.26±0.33	0.38±0.03	2.34	2.54
	45	0.23±0.02	0.40±0.07	2.21	2.27

Temperature is a fundamental operating parameter which affects the efficiency of azo dyes degradation in the textile effluent (Sreedharan *et al*., 2021). Two-way Anova analysis in the appendix VI (i) conducted at 95% confidence levels for the effluent samples showed significant difference in power usage (p=0.0007831) resulting from the steady rise, from 30-45.0ºC. There was an increase ion transfer from the electrode surface to the solution bulk leading to high viscosity and consequently ion diffusivity took place (Sreedharan *et al*., 2021). Temperature elevation causes an increase in resistance, lowering the voltage consequently lowering the consumption in terms of power an observation noted in all the samples. The group mean for the specific energy consumption decreased with an increase in solution temperature similar to trend noted by Carmona (Vilchis-Carmona *et al*., 2021). The effectiveness in turbidity elimination from abattoir effluents was conducted through the electrolytic cell thus elevating the temperature of aqueous substances containing the organic components. The current generated, time and specific energy consumption were documented in table 4.13 above. The tabulated data depicted a consistent trend of a decrease in power consumption with an increase

in temperature of the effluent sample. This is consistent with the understanding that resistance and voltage have a direct proportionality (Dihom *et al*., 2022b), and therefore, elevating temperature raises the resistance due to the increased vibrational energies of the existing molecule in sample (Oyetade *et al*., 2022).

CHAPTER FIVE

SUMMARY, CONCLUSION AND RECOMMENDATIONS

5.1 Summary

In summary, this investigation was conducted in order to establish the effectiveness of silver nanoparticles embedded on indium tin oxide (ITO) thin film conducting material on the textile azo dyes effluent degradation. The overall objective was to synthesize and characterize silver nanoparticles electrocatalyst embedded on indium tin oxide for the degradation of azo dye in the textile effluent. The study also involved four specific objectives; first was to synthesize and characterize chitosan coupled silver nanoparticles electrocatalyst then embed them on the indium tin oxide thin film electrodes. Secondly, to determine the levels of azo dye in the textile effluents discharged by Textile Industry, Kenya before and after treatment. Thirdly, to correlate the levels of azo dye degradation in textile industry effluent using Indium Tin Oxide (ITO) thin film electrodes with degradation of azo dyes in textile industry effluent using Indium Tin Oxide embedded with silver nanoparticles electrocatalyst. Lastly to compare the degradation of azo dyes using this technology of silver nanoparticles embedded on indium tin oxide with the electrocoagulation the commonly applied method.

5.2Conclusion

The 40.000 grams of powdered crab shells resulted in 23.000g of chitin after demineralization and 7.200 g (31.3 %) of chitosan. Chitosan obtained from crab shells exhibited 89.5% degree of deacetylation showing efficiency in reduction and stabilization of silver nanoparticles from the Ag^{+} ions. It was also imperative to compare the efficiency of the ITO when coupled with

silver nanoparticles and the commonly applied technology of electrocoagulation using stainless steel electrodes. The results from UV-Vis spectroscopy showed the formation of silver nanoparticles with λmax of 418 ± 2 nm. The readings indicated that the maximum wavelength at 420 nano-meters, gave the highest absorbance for the silver nanoparticles synthesized through the reducing and stabilizing property of the chitosan. Moreover, the examination of the results obtained from the scanning electron microscope (SEM) depicted a picture of these nanoparticles exhibiting spherical morphology with size range of 100 nm. FTIR signals were recorded at 1658 cm^{-1} corresponding to the amide (C=O) bonds, at 1089 cm^{-1} representing secondary alcohol (C-O-C) bonds at 564 cm^{-1} plane with bends NH, plane-out and bends C−O. C-H stretching vibrational signal was noted at 2927 cm^{-1}, a broader band at 3426cm^{-1} for an overlap between the O−H stretching vibration and the N−H stretching vibration of the oligosaccharide applied in the capping. It is worth noting that the intensity of the O−H and N−H stretching bands emanated from the hydroxyl and amino groups thus shifting to 3426 $cm^{-1,}$ implying that chelation of silver with both O−H and N−H groups of chitosan actually took place. In all the four samples it was noted that, 8 ppm of the nanoparticles application to the ITO thin film electrodes resulted in the least power consumption maximum of 0.4536 watts with average values of 0.03±0.0023 hours and a current flow of 0.63±0.0001 amperes. The average specific consumption of energy at 12 V was 2.110 kWh/m3 compared to 1.318 kWh/m3 at Pd of 24 V respectively. IR drop was minimized by lowering the created gap within the thin film electrodes 0.2 cm and raising the surface area of the cross section of electrodes and specific solution conductance. The COD listing for the samples after treatment fell below 100 mg/L which is much lower than the acceptable limits of COD ≤250 mg/L. The BOD for dye effluent portrayed no significant variation (p=0.835) when compared to the one of WHO 2002 with the range of 150±5 mg/L. The colour removal was 99.97% showing that, the optimized process was effective and efficient in the degradation of these azo dyes in the textile wastewaters.

5.3 Recommendations

From the findings of this research, the following recommendations have been deduced:

1. The indium tin oxide coupled silver nanoparticles can be incorporated together with the electrocoagulation and both applied in the textile industries for the colour removal, COD and BOD reduction.
2. There should be a study carried to on removal mechanisms of the other dye types, for instance reactive, disperse and vat dyes.
3. There is need to study the effects of different cations and anions on ITO degradation efficiency including Fe (II).
4. There is need to carry out more studies to identify alternative conducting thin films that can be cheaper than ITO based on dimensionally stable anodes (DSA).
5. There is need to carry out more spectroscopic and electrochemical analysis to understand the interactions of dye and the metallic hydroxide and degraded products using, Transmission electron microscopy (TEM), Zeta potentiometer.

REFERENCES

Abdo, S. M., Mahmoud, R. H., Youssef, M., & El-Naggar, M. E. (2020a). Cationic starch and polyaluminum chloride as coagulants for River Nile water treatment. *Groundwater for Sustainable Development*, *10*, 100331.

Abdo, S. M., Mahmoud, R. H., Youssef, M., & El-Naggar, M. E. (2020b). Cationic starch and polyaluminum chloride as coagulants for River Nile water treatment. *Groundwater for Sustainable Development*, *10*, 100331.

Abiola, O. N. (2019). Polymers for coagulation and flocculation in water treatment. In *Polymeric materials for clean water* (pp. 77–92). Springer.

Affat, S. S. (2021). Classifications, advantages, disadvantages, toxicity effects of natural and synthetic dyes: A review. *University of Thi-Qar Journal of Science*, *8*(1), 130–135.

Agarwal, H., Kumar, S. V., & Rajeshkumar, S. (2021). Antidiabetic effect of silver nanoparticles synthesized using lemongrass (Cymbopogon Citratus) through

conventional heating and microwave irradiation approach. *Journal of Microbiology, Biotechnology and Food Sciences*, *2021*, 371–376.

Aguilar-Torrejon, J., Hernández, P. B., Roa-Morales, G., & Barrera-Diaz, C. (2022). Electrochemical Sensors in the Determination of Biochemical Oxygen Demand. A Revision of the Last Decade. *ECS Transactions*, *106*(1), 15.

Al-Ansari, M. M., Li, Z., Masood, A., & Rajaselvam, J. (2022). Decolourization of azo dye using a batch bioreactor by an indigenous bacterium Enterobacter aerogenes ES014 from the waste water dye effluent and toxicity analysis. *Environmental Research*, *205*, 112189.

Alderete, B. L., da Silva, J., Godoi, R., da Silva, F. R., Taffarel, S. R., da Silva, L. P., Garcia, A. L. H., Júnior, H. M., de Amorim, H. L. N., & Picada, J. N. (2021). Evaluation of toxicity and mutagenicity of a synthetic effluent containing azo dye after Advanced Oxidation Process treatment. *Chemosphere*, *263*, 128291.

Alduraihem, N. S., Bhat, R. S., Al-Zahrani, S. A., Elnagar, D. M., Alobaid, H. M., & Daghestani, M. H. (2023). Anticancer and antimicrobial activity of silver nanoparticles synthesized from pods of Acacia nilotica. *Processes*, *11*(2), 301.

Ali, A. M., Said, D. A., Khayyat, M., Boustimi, M., & Seoudi, R. (2020). Improving the efficiency of the organic solar cell (CuPc/C60) via PEDOT: PSS as a photoconductor layer doped by silver nanoparticles. *Results in Physics*, *16*, 102819.

Ali, N., Azeem, S., Khan, A., Khan, H., Kamal, T., & Asiri, A. M. (2020). Experimental studies on removal of arsenites from industrial effluents using tridodecylamine supported liquid membrane. *Environmental Science and Pollution Research*, *27*(11), 11932–11943.

Alizadeh, A., Rajabi, Y., & Bagheri–Mohagheghi, M. M. (2022). Effect of crystallinity on the nonlinear optical properties of indium–tin oxide thin films. *Optical Materials*, *131*, 112589.

Allabakshi, S. M., Srikar, P., Gomosta, S., Gangwar, R. K., & Maliyekkal, S. M. (2023). UVC photon integrated surface dielectric barrier discharge hybrid reactor: A novel and energy-efficient route for rapid mineralisation of aqueous azo dyes. *Journal of Hazardous Materials*, *446*, 130639.

Almeida, E. J. R., & Corso, C. R. (2019). Decolorization and removal of toxicity of textile azo dyes using fungal biomass pelletized. *International Journal of Environmental Science and Technology*, *16*(3), 1319–1328.

Al-Qodah, Z., Al-Qudah, Y., & Assirey, E. (2020). Combined biological wastewater treatment with electrocoagulation as a post-polishing process: A review. *Separation Science and Technology*, *55*(13), 2334–2352.

Alsamhary, K., Al-Enazi, N. M., Alhomaidi, E., & Alwakeel, S. (2022). Spirulina platensis mediated biosynthesis of Cuo Nps and photocatalytic degradation of toxic azo dye Congo red and kinetic studies. *Environmental Research*, *207*, 112172.

Alsantali, R. I., Raja, Q. A., Alzahrani, A. Y., Sadiq, A., Naeem, N., Mughal, E. U., Al-Rooqi, M. M., El Guesmi, N., Moussa, Z., & Ahmed, S. A. (2022). Miscellaneous azo dyes: A comprehensive review on recent advancements in biological and industrial applications. *Dyes and Pigments*, *199*, 110050.

Ameen, F., Al-Homaidan, A. A., Al-Sabri, A., Almansob, A., & AlNAdhari, S. (2023). Antioxidant, anti-fungal and cytotoxic effects of silver nanoparticles synthesized using marine fungus Cladosporium halotolerans. *Applied Nanoscience*, *13*(1), 623–631.

Arlyapov, V. A., Plekhanova, Y. V., Kamanina, O. A., Nakamura, H., & Reshetilov, A. N. (2022). Microbial Biosensors for Rapid Determination of Biochemical Oxygen Demand: Approaches, Tendencies and Development Prospects. *Biosensors*, *12*(10), 842.

Asad, A., Sameoto, D., & Sadrzadeh, M. (2020). Overview of membrane technology. In *Nanocomposite membranes for water and gas separation* (pp. 1–28). Elsevier.

Ateeb, M., Asif, H. M., Ali, T., Baig, M. M., Arif, M. U., Farooq, M. I., Kaleem, M., & Shaukat, I. (2023). Photocatalytic and Antibacterial activities of bio-synthesised silver nanoparticles (AgNPs) using Grewia asiatica leaves extract. *International Journal of Environmental Analytical Chemistry*, 1–19.

Atiq, M. S., Rehman, A., Iqbal, K., Safdar, F., Basit, A., Ashraf, M., Maqsood, H. S., & Khan, A. (2019). Salt Free Sulphur Black Dyeing of Cotton Fabric after Cationization. *Cellul. Chem. Technol*, *53*, 155–161.

Azari, A., Nabizadeh, R., Nasseri, S., Mahvi, A. H., & Mesdaghinia, A. R. (2020). Comprehensive systematic review and meta-analysis of dyes adsorption by carbonbased adsorbent materials: Classification and analysis of last decade studies. *Chemosphere*, *250*, 126238.

Azwatul, H. M., Uda, M. N. A., Gopinath, S. C., Arsat, Z. A., Abdullah, F., Muttalib, M. F. A., Hashim, M. K. R., Hashim, U., Isa, M., & Uda, M. A. (2023). Plant-based green synthesis of silver nanoparticle via chemical bonding analysis. *Materials Today: Proceedings*.

Bafana, A., Devi, S. S., & Chakrabarti, T. (2011a). Azo dyes: Past, present and the future. *Environmental Reviews*, *19*(NA), 350–371.

Bafana, A., Devi, S. S., & Chakrabarti, T. (2011b). Azo dyes: Past, present and the future. *Environmental Reviews*, *19*(NA), 350–371.

Bafana, A., Devi, S. S., & Chakrabarti, T. (2011c). Azo dyes: Past, present and the future. *Environmental Reviews*, *19*(NA), 350–371.

Baker, R. W. (2002). Membrane technology. *Encyclopedia of Polymer Science and Technology*, *3*.

BALKAN, T. (n.d.). Determination of pesticide residues and risk assessment in some vegetables grown in Tokat province. *Plant Protection Bulletin*, *62*(2), 26–35.

Banerjee, P., Das, R., Das, P., & Mukhopadhyay, A. (2018). Membrane technology. In *Carbon Nanotubes for Clean Water* (pp. 127–150). Springer.

Barbhuiya, R. I., Singha, P., Asaithambi, N., & Singh, S. K. (2022). Ultrasound-assisted rapid biological synthesis and characterization of silver nanoparticles using pomelo peel waste. *Food Chemistry*, *385*, 132602.

Baur, S., Bellé, N., Hausladen, H., Wurzer, S., Brehm, L., Stark, T. D., Hücklhoven, R., Hofmann, T., & Dawid, C. (2022). Quantitation of Toxic Steroidal Glycoalkaloids and Newly Identified Saponins in Post-Harvest Light-Stressed Potato (Solanum tuberosum L.) Varieties. *Journal of Agricultural and Food Chemistry*.

Behbahani, B. A., Noshad, M., & Falah, F. (2019). Cumin essential oil: Phytochemical analysis, antimicrobial activity and investigation of its mechanism of action through scanning electron microscopy. *Microbial Pathogenesis*, *136*, 103716.

Belal, R. M., Zayed, M. A., El-Sherif, R. M., & Ghany, N. A. A. (2021). Advanced electrochemical degradation of basic yellow 28 textile dye using IrO2/Ti meshed electrode in different supporting electrolytes. *Journal of Electroanalytical Chemistry*, *882*, 114979.

Benkhaya, S., M'rabet, S., & El Harfi, A. (2020a). A review on classifications, recent synthesis and applications of textile dyes. *Inorganic Chemistry Communications*, *115*, 107891.

Benkhaya, S., M'rabet, S., & El Harfi, A. (2020b). A review on classifications, recent synthesis and applications of textile dyes. *Inorganic Chemistry Communications*, *115*, 107891.

Benkhaya, S., M'rabet, S., & El Harfi, A. (2020c). Classifications, properties, recent synthesis and applications of azo dyes. *Heliyon*, *6*(1), e03271.

Berradi, M., Hsissou, R., Khudhair, M., Assouag, M., Cherkaoui, O., El Bachiri, A., & El Harfi, A. (2019). Textile finishing dyes and their impact on aquatic environs. *Heliyon*, *5*(11), e02711.

Bhattacharjee, G., Gohil, N., Vaidh, S., Joshi, K., Vishwakarma, G. S., & Singh, V. (2020). Microbial bioremediation of industrial effluents and pesticides. In *Bioremediation of Pollutants* (pp. 287–302). Elsevier.

Bigambo, P., Carr, C. M., Sumner, M., & Rigout, M. (2021). Investigation into the removal of pigment, sulphur and vat colourants from cotton textiles and implications for waste cellulosic recycling. *Coloration Technology*, *137*(6), 604–614.

Boudechiche, N., Fares, M., Ouyahia, S., Yazid, H., Trari, M., & Sadaoui, Z. (2019). Comparative study on removal of two basic dyes in aqueous medium by adsorption using activated carbon from Ziziphus lotus stones. *Microchemical Journal*, *146*, 1010–1018.

Brahim Belhaouari, D., Fontanini, A., Baudoin, J.-P., Haddad, G., Le Bideau, M., Bou Khalil, J. Y., Raoult, D., & La Scola, B. (2020). The strengths of scanning electron microscopy in deciphering SARS-CoV-2 infectious cycle. *Frontiers in Microbiology*, *11*, 2014.

Brown, M. A., & De Vito, S. C. (1993a). Predicting azo dye toxicity. *Critical Reviews in Environmental Science and Technology*, *23*(3), 249–324.

Brown, M. A., & De Vito, S. C. (1993b). Predicting azo dye toxicity. *Critical Reviews in Environmental Science and Technology*, *23*(3), 249–324.

Bundesmann, C., Bauer, J., Finzel, A., Gerlach, J. W., Knolle, W., Hellmich, A., & Synowicki, R. (2021). Properties of indium tin oxide thin films grown by Ar ion beam sputter deposition. *Journal of Vacuum Science & Technology A: Vacuum, Surfaces, and Films*, *39*(3), 033406.

Cabernard, L., Roscher, L., Lorenz, C., Gerdts, G., & Primpke, S. (2018). Comparison of Raman and Fourier transform infrared spectroscopy for the quantification of microplastics in the aquatic environment. *Environmental Science & Technology*, *52*(22), 13279–13288.

Carrera, C., Bengoechea, C., Carrillo, F., & Calero, N. (2023). Effect of deacetylation degree and molecular weight on surface properties of chitosan obtained from biowastes. *Food Hydrocolloids*, *137*, 108383.

Chai, W. S., Cheun, J. Y., Kumar, P. S., Mubashir, M., Majeed, Z., Banat, F., Ho, S.-H., & Show, P. L. (2021a). A review on conventional and novel materials towards heavy metal adsorption in wastewater treatment application. *Journal of Cleaner Production*, *296*, 126589.

Chai, W. S., Cheun, J. Y., Kumar, P. S., Mubashir, M., Majeed, Z., Banat, F., Ho, S.-H., & Show, P. L. (2021b). A review on conventional and novel materials towards heavy metal adsorption in wastewater treatment application. *Journal of Cleaner Production*, *296*, 126589.

Chaudhary, B., & Violet, T. E. (2020). Chemistry of synthetic dyes: A review. *J. Interdiscipl. Cycle Res*, *12*(390), 390–396.

Chen, C., & Beigang, L. I. (2021). Characterization of Fe 3 O 4@ SA/Ce microspheres and their adsorption characteristics for direct dyes. *Environmental Chemistry*, *3*, 799–807.

Chen, J., Li, X., Huang, A., Deng, W., & Xiao, Y. (2021). Nonionic surfactants based hydrophobic deep eutectic solvents for liquid–liquid microextraction of Sudan dyes in tomato chili sauces. *Food Chemistry*, *364*, 130373.

Chen, L., Sun, Y., Sun, W., Shah, K. J., Xu, Y., & Zheng, H. (2019a). Efficient cationic flocculant MHCS-gP (AM-DAC) synthesized by UV-induced polymerization for algae removal. *Separation and Purification Technology*, *210*, 10–19.

Chen, L., Sun, Y., Sun, W., Shah, K. J., Xu, Y., & Zheng, H. (2019b). Efficient cationic flocculant MHCS-gP (AM-DAC) synthesized by UV-induced polymerization for algae removal. *Separation and Purification Technology*, *210*, 10–19.

Chen, N., Liu, W., Huang, J., & Qiu, X. (2020a). Preparation of octopus-like lignin-grafted cationic polyacrylamide flocculant and its application for water flocculation. *International Journal of Biological Macromolecules*, *146*, 9–17.

Chen, N., Liu, W., Huang, J., & Qiu, X. (2020b). Preparation of octopus-like lignin-grafted cationic polyacrylamide flocculant and its application for water flocculation. *International Journal of Biological Macromolecules*, *146*, 9–17.

Chen, R.-F., Wu, L., Zhong, H.-T., Liu, C.-X., Qiao, W., & Wei, C.-H. (2021). Evaluation of electrocoagulation process for high-strength swine wastewater pretreatment. *Separation and Purification Technology*, *272*, 118900.

Chen, Y., Wen, D., Pei, J., Fei, Y., Ouyang, D., Zhang, H., & Luo, Y. (2020). Identification and quantification of microplastics using Fourier-transform infrared spectroscopy: Current status and future prospects. *Current Opinion in Environmental Science & Health*, *18*, 14–19.

Chetyrkina, M., Talalaev, F., Kameneva, L., Kostyuk, S., & Troshin, P. (2022). Vat Dyes: Promising Biocompatible Organic Semiconductors for Wearable Electronics Applications. *Journal of Materials Chemistry C*.

Chick, C. N., Sasaki, Y., Kawaguchi, M., Tanaka, E., Niikura, T., & Usuki, T. (2023). LCMS/MS quantitation of elastin crosslinker desmosines and histological analysis of skin aging characteristics in mice. *Bioorganic & Medicinal Chemistry*, *90*, 117351.

Chinni, S. V., Gopinath, S. C., Anbu, P., Fuloria, N. K., Fuloria, S., Mariappan, P., Krusnamurthy, K., Veeranjaneya Reddy, L., Ramachawolran, G., & Sreeramanan, S. (2021). Characterization and antibacterial response of silver nanoparticles biosynthesized using an ethanolic extract of Coccinia indica leaves. *Crystals*, *11*(2), 97.

Chittal, V., Gracias, M., Anu, A., Saha, P., & Rao, K. B. (2019). Biodecolorization and biodegradation of azo dye reactive orange-16 by marine Nocardiopsis sp. *Iranian Journal of Biotechnology*, *17*(3), e1551.

Chung, K.-T. (2016a). Azo dyes and human health: A review. *Journal of Environmental Science and Health, Part C*, *34*(4), 233–261.

Chung, K.-T. (2016b). Azo dyes and human health: A review. *Journal of Environmental Science and Health, Part C*, *34*(4), 233–261.

Corbett, J. F., & Gamson, E. P. (1972). Benzoquinone imines. Part XI. Mechanism and kinetics of the reaction of p-benzoquinone di-imines with aniline and its derivatives. *Journal of the Chemical Society, Perkin Transactions 2*, *11*, 1531–1537.

Cretescu, I., Lupascu, T., Buciscanu, I., Balau-Mindru, T., & Soreanu, G. (2017). Low-cost sorbents for the removal of acid dyes from aqueous solutions. *Process Safety and Environmental Protection*, *108*, 57–66.

da Silva, V. H., Murphy, F., Amigo, J. M., Stedmon, C., & Strand, J. (2020). Classification and Quantification of Microplastics (< 100 μm) Using a Focal Plane Array–Fourier Transform Infrared Imaging System and Machine Learning. *Analytical Chemistry*, *92*(20), 13724–13733.

Dawood, S., Ahmad, M., Zafar, M., Asif, S., Klemeš, J. J., Bokhari, A., Mubashir, M., Han, N., Ibrahim, M. M., & El-Bahy, Z. M. (2022). Biodiesel synthesis from Prunus

bokhariensis non-edible seed oil by using green silver oxide nanocatalyst. *Chemosphere*, *291*, 132780.

de Campos Ventura-Camargo, B., & Marin-Morales, M. A. (2013a). Azo dyes: Characterization and toxicity-a review. *Textiles and Light Industrial Science and Technology*, *2*(2), 85–103.

de Campos Ventura-Camargo, B., & Marin-Morales, M. A. (2013b). Azo dyes: Characterization and toxicity-a review. *Textiles and Light Industrial Science and Technology*, *2*(2), 85–103.

Dhar, S. A., Chowdhury, R. A., Das, S., Nahian, M. K., Islam, D., & Gafur, M. A. (2021). Plant-mediated green synthesis and characterization of silver nanoparticles using Phyllanthus emblica fruit extract. *Materials Today: Proceedings*, *42*, 1867–1871.

Didier de Vasconcelos, G. M., Mulinari, J., de Arruda Guelli Ulson de Souza, S. M., Ulson de Souza, A. A., de Oliveira, D., & de Andrade, C. J. (2021). Biodegradation of azo dyecontaining wastewater by activated sludge: A critical review. *World Journal of Microbiology and Biotechnology*, *37*(6), 101.

Dihom, H. R., Al-Shaibani, M. M., Mohamed, R. M. S. R., Al-Gheethi, A. A., Sharma, A., & Khamidun, M. H. B. (2022a). Photocatalytic degradation of disperse azo dyes in textile wastewater using green zinc oxide nanoparticles synthesized in plant extract: A critical review. *Journal of Water Process Engineering*, *47*, 102705.

Dihom, H. R., Al-Shaibani, M. M., Mohamed, R. M. S. R., Al-Gheethi, A. A., Sharma, A., & Khamidun, M. H. B. (2022b). Photocatalytic degradation of disperse azo dyes in textile wastewater using green zinc oxide nanoparticles synthesized in plant extract: A critical review. *Journal of Water Process Engineering*, *47*, 102705.

Ding, J., Pan, Y., Li, L., Liu, H., Zhang, Q., Gao, G., & Pan, B. (2020). Synergetic adsorption and electrochemical classified recycling of Cr (VI) and dyes in synthetic dyeing wastewater. *Chemical Engineering Journal*, *384*, 123232.

Duan, G., Zhang, H., Zhang, C., Jiang, S., & Hou, H. (2023). High mass-loading α-Fe2O3 nanoparticles anchored on nitrogen-doped wood carbon for high-energy-density supercapacitor. *Chinese Chemical Letters*, 108283.

Duan, Z., Hou, S., Xiao, J., & Li, B. (2020). Study on the essential properties of recycled powders from construction and demolition waste. *Journal of Cleaner Production*, *253*, 119865.

Ebba, M., Asaithambi, P., & Alemayehu, E. (2021). Investigation on operating parameters and cost using an electrocoagulation process for wastewater treatment. *Applied Water Science*, *11*(11), 1–9.

El Harfi, S., & El Harfi, A. (2017a). Classifications, properties and applications of textile dyes: A review. *Applied Journal of Environmental Engineering Science*, *3*(3), 00000–00003.

El Harfi, S., & El Harfi, A. (2017b). Classifications, properties and applications of textile dyes: A review. *Applied Journal of Environmental Engineering Science*, *3*(3), 00000–00003.

El-Gendy, N. S., & Nassar, H. N. (2021). Phycoremediation of phenol-polluted petro-industrial effluents and its techno-economic values as a win-win process for a green environment, sustainable energy and bioproducts. *Journal of Applied Microbiology*, *131*(4), 1621–1638.

El-Naggar, M. E., Samhan, F. A., Salama, A. A., Hamdy, R. M., & Ali, G. H. (2018). Cationic starch: Safe and economic harvesting flocculant for microalgal biomass and inhibiting E. coli growth. *International Journal of Biological Macromolecules*, *116*, 1296–1303.

Epolito, W. J., Lee, Y. H., Bottomley, L. A., & Pavlostathis, S. G. (2005). Characterization of the textile anthraquinone dye Reactive Blue 4. *Dyes and Pigments*, *67*(1), 35–46.

Ermakova, Y. G., Sen, T., Bogdanova, Y. A., Smirnov, A. Y., Baleeva, N. S., Krylov, A. I., & Baranov, M. S. (2018). Pyridinium analogues of green fluorescent protein chromophore: Fluorogenic dyes with large solvent-dependent Stokes shift. *The Journal of Physical Chemistry Letters*, *9*(8), 1958–1963.

Escapa, A., San-Martín, M. I., Mateos, R., & Morán, A. (2015). Scaling-up of membraneless microbial electrolysis cells (MECs) for domestic wastewater treatment: Bottlenecks and limitations. *Bioresource Technology*, *180*, 72–78.

Esmaeili, M., Koushki, E., & Mousavi, H. (2020). Nonlinear optical re-orientation and photoacoustic properties of indium tin oxide nanoparticles. *Physica E: LowDimensional Systems and Nanostructures*, *120*, 114063.

Fang, K., Tang, H., Li, C., Su, X., An, P., & Sun, S. (2022). Centrifuge modelling of landslides and landslide hazard mitigation: A review. *Geoscience Frontiers*, 101493.

Fernandes, A. S., do Nascimento, T. C., Jacob-Lopes, E., De Rosso, V. V., & Zepka, L. Q. (2018). Carotenoids: A brief overview on its structure, biosynthesis, synthesis, and applications. *Progress in Carotenoid Research*, *1*, 1–17.

Franca, R. D. G., Pinheiro, H. M., & Lourenço, N. D. (2020). Recent developments in textile wastewater biotreatment: Dye metabolite fate, aerobic granular sludge systems and engineered nanoparticles. *Reviews in Environmental Science and Bio/Technology*, *19*(1), 149–190.

Franca, R. D. G., Vieira, A., Carvalho, G., Oehmen, A., Pinheiro, H. M., Crespo, M. T. B., & Lourenco, N. D. (2020). Oerskovia paurometabola can efficiently decolorize azo dye Acid Red 14 and remove its recalcitrant metabolite. *Ecotoxicology and Environmental Safety*, *191*, 110007.

Franco, J. H., da Silva, B. F., Dias, E. F. G., de Castro, A. A., Ramalho, T. C., & Zanoni, M. V. B. (2018). Influence of auxochrome group in disperse dyes bearing azo groups as chromophore center in the biotransformation and molecular docking prediction by reductase enzyme: Implications and assessment for environmental toxicity of xenobiotics. *Ecotoxicology and Environmental Safety*, *160*, 114–126.

Gandi, V. K., Verma, R., Warrier, M., & Sharma, A. (2022). Effect of Electrode Profile and Polarity on Performance of Pressurized Sparkgap Switch. *Plasma*, *5*(1), 130–145.

Ganesh, R., Boardman, G. D., & Michelsen, D. (1994). Fate of azo dyes in sludges. *Water Research*, *28*(6), 1367–1376.

Ganeshan, D., Xie, F., Sun, Q., Li, Y., & Wei, M. (2018). Plasmonic effects of silver nanoparticles embedded in the counter electrode on the enhanced performance ofy desensitized solar cells. *Langmuir*, *34*(19), 5367–5373.

Garcia-Becerra, F. Y., & Ortiz, I. (2018). Biodegradation of emerging organic micropollutants in nonconventional biological wastewater treatment: A critical review. *Environmental Engineering Science*, *35*(10), 1012–1036.

Ghattavi, S., & Nezamzadeh-Ejhieh, A. (2021). A double-Z-scheme ZnO/AgI/WO3 photocatalyst with high visible light activity: Experimental design and mechanism pathway in the degradation of methylene blue. *Journal of Molecular Liquids*, *322*, 114563.

Ghernaout, D., & Elboughdiri, N. (2020). Advanced oxidation processes for wastewater treatment: Facts and future trends. *Open Access Library Journal*, *7*(2), 1–15.

Gičević, A., Hindija, L., & Karačić, A. (2019). Toxicity of azo dyes in pharmaceutical industry. *International Conference on Medical and Biological Engineering*, 581–587.

Gillani, S. S., Qureshi, E. I., & Munawar, M. A. (2017). Synthesis of Direct dyes based on noncarcinogenic amines for leather and textile industry. *Lahore Garrison University Journal of Life Sciences*, *1*(04), 284–305.

Gordon, P. F., & Gregory, P. (2022). Organic chemistry in colour. In *Organic Chemistry in Colour*. De Gruyter.

Gorito, A. M., Pesqueira, J. F., Moreira, N. F., Ribeiro, A. R., Pereira, M. F. R., Nunes, O. C., Almeida, C. M. R., & Silva, A. M. (2021). Ozone-based water treatment (O3, O3/UV, O3/H2O2) for removal of organic micropollutants, bacteria inactivation and regrowth prevention. *Journal of Environmental Chemical Engineering*, *9*(4), 105315.

Gu, M., Yin, Q., & Wu, G. (2021). Metagenomic analysis of facilitation mechanism for azo dye reactive red 2 degradation with the dosage of ferroferric oxide. *Journal of Water Process Engineering*, *41*, 102010.

Guo, Y., He, H., Peng, R., Guan, M., Yan, X., Si, X., Gu, M., Lei, Y., & Luo, L. (2022). Silver Nanocatalyst Based Clock Reaction for Multi-mode Detection of Tetracycline Antibiotics. *ChemistrySelect*, *7*(9), e202200045.

Hao, X., Hua, G., Jiangtao, F., Dan, W., Zhengwei, L., Yu, W., & Wei, Y. (2019). electrochemical oxidation combined with adsorption: A novel route for low concentration organic wastewater treatment. *Int. J. Electrochem. Sci*, *14*, 8110–8120.

Haque, M. M., Haque, M. A., Mosharaf, M. K., & Marcus, P. K. (2021). Decolorization, degradation and detoxification of carcinogenic sulfonated azo dye methyl orange by newly developed biofilm consortia. *Saudi Journal of Biological Sciences*, *28*(1), 793–804.

Hashemi, S. H., & Kaykhaii, M. (2022). Azo dyes: Sources, occurrence, toxicity, sampling, analysis, and their removal methods. In *Emerging freshwater pollutants* (pp. 267–287). Elsevier.

Hemalatha, H. N., & Sanjay, N. S. (2023). Real silk textile wastewater treatment using 2-D electrochemical coagulation and estimation of electrical energy consumption. *Brazilian Journal of Chemical Engineering*, *40*(1), 151–158.

Hemdan, B., Garlapati, V. K., Sharma, S., Bhadra, S., Maddirala, S., Varsha, K. M., Motru, V., Goswami, P., Sevda, S., & Aminabhavi, T. M. (2022). Bioelectrochemical systemsbased metal recovery: Resource, conservation and recycling of metallic industrial effluents. *Environmental Research*, *204*, 112346.

Hodaifa, G., Gallardo, P. A. R., García, C. A., Kowalska, M., & Seyedsalehi, M. (2019). Chemical oxidation methods for treatment of real industrial olive oil mill wastewater. *Journal of the Taiwan Institute of Chemical Engineers*, *97*, 247–254.

Holness, J. L., van der Westhuizen, D. J., Davids, M. R., & Warwick, J. M. (2022). Measurement of glomerular filtration rate and its current status in African countries. *African Journal of Nephrology*, *25*(1), 74–81.

Hossain, M. A., Paul, B., Khan, K. A., Paul, M., Mamun, M. A., & Quayum, M. E. (2022). Green synthesis and characterization of silver nanoparticles by using Bryophyllum pinnatum and the evaluation of its power generation activities on bio-electrochemical cell. *Materials Chemistry and Physics*, *282*, 125943.

Hou, X., Lv, S., Chen, Z., & Xiao, F. (2018). Applications of Fourier transform infrared spectroscopy technologies on asphalt materials. *Measurement*, *121*, 304–316.

Hu, P., Shen, S., Zhao, D., Wei, H., Ge, J., Jia, F., Zhang, X., & Yang, H. (2021a). The influence of hydrophobicity on sludge dewatering associated with cationic starch-based flocculants. *Journal of Environmental Management*, *296*, 113218.

Hu, P., Shen, S., Zhao, D., Wei, H., Ge, J., Jia, F., Zhang, X., & Yang, H. (2021b). The influence of hydrophobicity on sludge dewatering associated with cationic starch-based flocculants. *Journal of Environmental Management*, *296*, 113218.

Hu, P., Zhuang, S., Shen, S., Yang, Y., & Yang, H. (2021a). Dewaterability of sewage sludge conditioned with a graft cationic starch-based flocculant: Role of structural characteristics of flocculant. *Water Research*, *189*, 116578.

Hu, P., Zhuang, S., Shen, S., Yang, Y., & Yang, H. (2021b). Dewaterability of sewage sludge conditioned with a graft cationic starch-based flocculant: Role of structural characteristics of flocculant. *Water Research*, *189*, 116578.

Hu, Y., Zhan, F., Wang, Q., Sun, Y., Yu, C., Zhao, X., Wang, H., Long, R., Zhang, G., & Gao, C. (2020). Tracking mechanistic pathway of photocatalytic CO2 reaction at Ni sites using operando, time-resolved spectroscopy. *Journal of the American Chemical Society*, *142*(12), 5618–5626.

Hussain, S., Khan, H., Khan, N., Gul, S., Wahab, F., Khan, K. I., Zeb, S., Khan, S., Baddouh, A., & Mehdi, S. (2021). Process modeling toward higher degradation and minimum energy consumption of an electrochemical decontamination of food dye wastewater. *Environmental Technology & Innovation*, *22*, 101509.

Ikram, M., Naeem, M., Zahoor, M., Hanafiah, M. M., Oyekanmi, A. A., Ullah, R., Farraj, D. A. A., Elshikh, M. S., Zekker, I., & Gulfam, N. (2022). Biological degradation of the azo dye basic orange 2 by Escherichia coli: A sustainable and ecofriendly approach for the treatment of textile wastewater. *Water*, *14*(13), 2063.

Innocent, S., & Padikasan, I. A. (2023). Biotransformation of Chitin to Chitosan using Bacillus cereus JCM44 isolated from Kanyakumari, India and its Characterization. *Journal of Pure & Applied Microbiology*, *17*(1).

Irene, A., Martín, J., Santos, J. L., & Alonso, E. (2018). Determination of Pharmaceutical Compounds in Sewage Sludge from Municipal Wastewater Treatment Plants: Current State, Perspectives, Limitations, and Opportunities. In *Life Cycle Assessment of Wastewater Treatment* (pp. 171–198). CRC Press.

Jain, S., & Jain, P. K. (2020). Classification, chemistry, and applications of chemical substances that are harmful to the environment: Classification of dyes. In *Impact of textile dyes on public health and the environment* (pp. 20–49). IGI Global.

Janossy, I., & Kosa, T. (1992). Influence of anthraquinone dyes on optical reorientation of nematic liquid crystals. *Optics Letters*, *17*(17), 1183–1185.

Ji, Y., Fan, T., & Luo, Y. (2020). First-principles study on the mechanism of photocatalytic reduction of nitrobenzene on the rutile TiO 2 (110) surface. *Physical Chemistry Chemical Physics*, *22*(3), 1187–1193.

John, A., Brookes, A., Carra, I., Jefferson, B., & Jarvis, P. (2022). Microbubbles and their application to ozonation in water treatment: A critical review exploring their benefit and future application. *Critical Reviews in Environmental Science and Technology*, *52*(9), 1561–1603.

Jomehzadeh, N., Koolivand, Z., Dahdouh, E., Akbari, A., Zahedi, A., & Chamkouri, N. (2021). Investigating in-vitro antimicrobial activity, biosynthesis, and characterization of silver nanoparticles, zinc oxide nanoparticles, and silver-zinc oxide nanocomposites using Pistacia Atlantica Resin. *Materials Today Communications*, *27*, 102457.

Kamali, M., Suhas, D. P., Costa, M. E., Capela, I., & Aminabhavi, T. M. (2019). Sustainability considerations in membrane-based technologies for industrial effluents treatment. *Chemical Engineering Journal*, *368*, 474–494.

Karim, S., Ahmad, N., Hussain, D., Mok, Y. S., & Siddiqui, G. U. (2022). Active removal of anionic azo dyes (MO, CR, EBT) from aqueous solution by potential adsorptive capacity of zinc oxide quantum dots. *Journal of Chemical Technology & Biotechnology*, *97*(8), 2087–2097.

Kavoosi, G., Nateghpoor, B., Dadfar, S. M. M., & Dadfar, S. M. A. (2014). Antioxidant, antifungal, water binding, and mechanical properties of poly (vinyl alcohol) film

incorporated with essential oil as a potential wound dressing material. *Journal of Applied Polymer Science*, *131*(20).

Kavoosi, G., Rahmatollahi, A., Dadfar, S. M. M., & Purfard, A. M. (2014). Effects of essential oil on the water binding capacity, physico-mechanical properties, antioxidant and antibacterial activity of gelatin films. *LWT-Food Science and Technology*, *57*(2), 556–561.

Khaled, J. M., Alyahya, S. A., Govindan, R., Chelliah, C. K., Maruthupandy, M., Alharbi, N. S., Kadaikunnan, S., Issac, R., Murugan, S., & Li, W.-J. (2022). Laccase producing bacteria influenced the high decolorization of textile azo dyes with advanced study. *Environmental Research*, *207*, 112211.

Khaleghi, N., Forouzandeh-Malati, M., Ganjali, F., Rashvandi, Z., Zarei-Shokat, S., TaheriLedari, R., & Maleki, A. (2023). Silver-assisted reduction of nitroarenes by an Agembedded curcumin/melamine-functionalized magnetic nanocatalyst. *Scientific Reports*, *13*(1), 5225.

Khan, A. A., Gul, J., Naqvi, S. R., Ali, I., Farooq, W., Liaqat, R., AlMohamadi, H., Štěpanec, L., & Juchelková, D. (2022). Recent progress in microalgae-derived biochar for the treatment of textile industry wastewater. *Chemosphere*, 135565.

Khan, Z. U. H., Khan, A., Chen, Y. M., Shah, N. S., Khan, A. U., Muhammad, N., Tahir, K., Shah, H. U., Khan, Z. U., & Shakeel, M. (2018). Enhanced antimicrobial, anti-oxidant applications of green synthesized AgNPs-an acute chronic toxicity study of phenolic azo dyes & study of materials surface using X-ray photoelectron spectroscopy. *Journal of Photochemistry and Photobiology B: Biology*, *180*, 208–217.

Kingslin, A., Kalimuthu, K., Kiruthika, M. L., Khalifa, A. S., Nhat, P. T., & Brindhadevi, K. (2023). Synthesis, characterization and biological potential of silver nanoparticles using Enteromorpha prolifera algal extract. *Applied Nanoscience*, *13*(3), 2165–2178.

Klymchenko, A. S. (2017). Solvatochromic and fluorogenic dyes as environment-sensitive probes: Design and biological applications. *Accounts of Chemical Research*, *50*(2), 366–375.

Kondowe, B. N., Masese, F. O., Raburu, P. O., Singini, W., & Walumona, R. J. (2022). Water quality and ecology of Lake Kanyaboli, Kenya: Current status and historical changes. *Lakes & Reservoirs: Research & Management*, *27*(1), e12401.

König, M., Vaes, J., Klemm, E., & Pant, D. (2019). Solvents and supporting electrolytes in the electrocatalytic reduction of CO2. *Iscience*, *19*, 135–160.

Kou, S. G., Peters, L. M., & Mucalo, M. R. (2021). Chitosan: A review of sources and preparation methods. *International Journal of Biological Macromolecules*, *169*, 85–94.

Koulini, G. V., Laiju, A. R., Ramesh, S. T., Gandhimathi, R., & Nidheesh, P. V. (2022). Effective degradation of azo dye from textile wastewater by electro-peroxone process. *Chemosphere*, *289*, 133152.

Kovacic, Z., Likozar, B., & Hus, M. (2020). Photocatalytic CO2 reduction: A review of ab initio mechanism, kinetics, and multiscale modeling simulations. *ACS Catalysis*, *10*(24), 14984–15007.

Kumar, A., Dixit, U., Singh, K., Gupta, S. P., & Beg, M. S. J. (2021). Structure and Properties of Dyes and Pigments. In *Dyes and Pigments-Novel Applications and Waste Treatment*. IntechOpen.

Kumar, A., Nidheesh, P. V., & Kumar, M. S. (2018). Composite wastewater treatment by aerated electrocoagulation and modified peroxi-coagulation processes. *Chemosphere*, *205*, 587–593.

Kumar, B., Smita, K., Sánchez, E., Debut, A., & Cumbal, L. (2021). Plukenetia volubilis L. Seed flour mediated biofabrication and characterization of silver nanoparticles. *Chemical Physics Letters*, *781*, 138993.

Kumar, S., Kumar, A., Malhotra, T., & Verma, S. (2022). Characterization of structural, optical and photocatalytic properties of silver modified hematite (α-Fe2O3) nanocatalyst. *Journal of Alloys and Compounds*, *904*, 164006.

Kurniawan, A., Sutiono, H., Indraswati, N., & Ismadji, S. (2012). Removal of basic dyes in binary system by adsorption using rarasaponin–bentonite: Revisited of extended Langmuir model. *Chemical Engineering Journal*, *189*, 264–274.

Kurniawan, S. B., Imron, M. F., Chik, C. E. N. C. E., Owodunni, A. A., Ahmad, A., Alnawajha, M. M., Rahim, N. F. M., Said, N. S. M., Abdullah, S. R. S., & Kasan, N. A. (2022). What compound inside biocoagulants/bioflocculants is contributing the most to the coagulation and flocculation processes? *Science of The Total Environment*, *806*, 150902.

Laouini, S. E., Bouafia, A., Soldatov, A. V., Algarni, H., Tedjani, M. L., Ali, G. A., & Barhoum, A. (2021). Green synthesized of Ag/Ag2O nanoparticles using aqueous leaves extracts of Phoenix dactylifera L. and their azo dye photodegradation. *Membranes*, *11*(7), 468.

Lee, J.-W., Cho, J. Y., Kim, M. J., Kim, J. H., Park, J. H., Jeong, S. Y., Seo, S. H., Lee, G.-W., Jeong, H. J., & Han, J. T. (2021). Synthesis of silver nanoparticles embedded with single-walled carbon nanotubes for printable elastic electrodes and sensors with high stability. *Scientific Reports*, *11*(1), 1–10.

Legube, B., & Leitner, N. K. V. (1999). Catalytic ozonation: A promising advanced oxidation technology for water treatment. *Catalysis Today*, *53*(1), 61–72.

Lellis, B., Fávaro-Polonio, C. Z., Pamphile, J. A., & Polonio, J. C. (2019). Effects of textile dyes on health and the environment and bioremediation potential of living organisms. *Biotechnology Research and Innovation*, *3*(2), 275–290.

Li, P., Miao, R., Wang, P., Sun, F., & Li, X. (2021). Bi-metal oxide-modified flat-sheet ceramic membranes for catalytic ozonation of organic pollutants in wastewater treatment. *Chemical Engineering Journal*, *426*, 131263.

Liang, D., Chang, Z., Chen, Y., Chen, J., Zhao, H., Sha, L., & Guo, D. (2023). High mass loading paper-based electrode material with cellulose fibers under coordination of zirconium oxyhydroxide nanoparticles and sulfosalicylic acid. *International Journal of Biological Macromolecules*, 125414.

Liang, J., Xiao, X., Chou, T.-M., & Libera, M. (2021). Analytical cryo-scanning electron microscopy of hydrated polymers and microgels. *Accounts of Chemical Research*, *54*(10), 2386–2396.

Liu, B., Wu, H., & Parkin, I. P. (2019). Gaseous Photocatalytic Oxidation of Formic Acid over TiO2: A Comparison between the Charge Carrier Transfer and Light-Assisted Mars–van Krevelen Pathways. *The Journal of Physical Chemistry C*, *123*(36), 22261–22272.

Liu, B., Zheng, H., Wang, Y., Chen, X., Zhao, C., An, Y., & Tang, X. (2018). A novel carboxylrich chitosan-based polymer and its application for clay flocculation and cationic dye removal. *Science of the Total Environment*, *640*, 107–115.

Liu, Y., Li, C., Bao, J., Wang, X., Yu, W., & Shao, L. (2022a). Degradation of azo dyes with different functional groups in simulated wastewater by electrocoagulation. *Water*, *14*(1), 123.

Liu, Y., Li, C., Bao, J., Wang, X., Yu, W., & Shao, L. (2022b). Degradation of azo dyes with different functional groups in simulated wastewater by electrocoagulation. *Water*, *14*(1), 123.

Ma, J., Wang, R., Wang, X., Zhang, H., Zhu, B., Lian, L., & Lou, D. (2019a). Drinking water treatment by stepwise flocculation using polysilicate aluminum magnesium and cationic polyacrylamide. *Journal of Environmental Chemical Engineering*, *7*(3), 103049.

Ma, J., Wang, R., Wang, X., Zhang, H., Zhu, B., Lian, L., & Lou, D. (2019b). Drinking water treatment by stepwise flocculation using polysilicate aluminum magnesium and cationic polyacrylamide. *Journal of Environmental Chemical Engineering*, *7*(3), 103049.

Ma, Y., Zhai, X., & Liu, J. (2020). Synthesis of hexagonal-phase indium tin oxide nanoparticles by deionized water and glycerol binary solvothermal method and their resistivity. *Journal of Materials Science*, *55*(9), 3860–3870.

Mahmood, R. T., Asad, M. J., Hadri, S. H., El-Shorbagy, M. A., Mousa, A. A. A., Dara, R. N., Awais, M., & Tlili, I. (2022). Bioremediation of textile industrial effluents by Fomitopsis pinicola IEBL-4 for environmental sustainability. *Human and Ecological Risk Assessment: An International Journal*, 1–18.

Mahy, J. G., Kiendrebeogo, M., Farcy, A., & Drogui, P. (2023). Enhanced Decomposition of H2O2 Using Metallic Silver Nanoparticles under UV/Visible Light for the Removal of p-Nitrophenol from Water. *Catalysts*, *13*(5), 842.

Mantzavinos, D., & Psillakis, E. (2004). Enhancement of biodegradability of industrial wastewaters by chemical oxidation pre-treatment. *Journal of Chemical Technology &*

Biotechnology: International Research in Process, Environmental & Clean Technology, *79*(5), 431–454.

Manzoor, J., & Sharma, M. (2020). Impact of textile dyes on human health and environment. In *Impact of textile dyes on public health and the environment* (pp. 162–169). IGI Global.

Marzorati, S., Schievano, A., Idà, A., & Verotta, L. (2020). Carotenoids, chlorophylls and phycocyanin from Spirulina: Supercritical CO 2 and water extraction methods for added value products cascade. *Green Chemistry*, *22*(1), 187–196.

Masarbo, R. S., & Karegoudar, T. B. (2022). Decolourisation of toxic azo dye Fast Red E by three bacterial strains: Process optimisation and toxicity assessment. *International Journal of Environmental Analytical Chemistry*, *102*(11), 2686–2696.

Masomboon, N., Ratanatamskul, C., & Lu, M.-C. (2009). Chemical oxidation of 2, 6dimethylaniline in the Fenton process. *Environmental Science & Technology*, *43*(22), 8629–8634.

Matsukatova, A. N., Emelyanov, A. V., Minnekhanov, A. A., Sakharutov, D. A., Vdovichenko, A. Y., Kamyshinskii, R. A., Demin, V. A., Rylkov, V. V., Forsh, P. A., & Chvalun, S. N. (2020). Memristors based on poly (p-xylylene) with embedded silver nanoparticles. *Technical Physics Letters*, *46*, 73–76.

Mcyotto, F. O., Wei, Q., Chow, C. W., Nadeem, Z., Li, Z., & Liu, J. (2020). Eco-friendly decolorization of cationic dyes by coagulation using natural coagulant Bentonite and biodegradable flocculant Sodium Alginate. *Earth Sci. Environ. Stud*, *5*, 51–60.

Mehra, S., Singh, M., & Chadha, P. (2021). Adverse impact of textile dyes on the aquatic environment as well as on human beings. *Toxicology International*, *28*(2), 165–176.

Mei, M., Du, P., Li, W., Xu, L., Wang, T., Liu, J., Chen, S., & Li, J. (2023). Aminofunctionalization of lignocellulosic biopolymer to be used as a green and sustainable adsorbent for anionic contaminant removal. *International Journal of Biological Macromolecules*, *227*, 1271–1281.

Mella, B., Puchana-Rosero, M. J., Costa, D. E. S., & Gutterres, M. (2017). Utilization of tannery solid waste as an alternative biosorbent for acid dyes in wastewater treatment. *Journal of Molecular Liquids*, *242*, 137–145.

Milaković, M., Vestergaard, G., González-Plaza, J. J., Petrić, I., Kosić-Vukšić, J., Senta, I., Kublik, S., Schloter, M., & Udiković-Kolić, N. (2020). Effects of industrial effluents containing moderate levels of antibiotic mixtures on the abundance of antibiotic resistance genes and bacterial community composition in exposed creek sediments. *Science of The Total Environment*, *706*, 136001.

Milanović, Ž. B., Dimić, D. S., Avdović, E. H., Milenković, D. A., Marković, J. D., Klisurić, O. R., Trifunović, S. R., & Marković, Z. S. (2021). Synthesis and comprehensive spectroscopic (X-ray, NMR, FTIR, UV–Vis), quantum chemical and molecular docking investigation of 3-acetyl-4-hydroxy-2-oxo-2H-chromen-7-yl acetate. *Journal of Molecular Structure*, *1225*, 129256.

Mistry, H., Thakor, R., Patil, C., Trivedi, J., & Bariya, H. (2021). Biogenically proficient synthesis and characterization of silver nanoparticles employing marine procured fungi Aspergillus brunneoviolaceus along with their antibacterial and antioxidative potency. *Biotechnology Letters*, *43*, 307–316.

Mohammadi, L., Mohammadpour, A., Hosseini, M. R., Shahsavani, E., Rayeni, R. A., Golaki, M., Rahdar, A., & Pandey, S. (2023). Optimization of photocatalytic degradation of biochemical oxygen demand from textile industry effluent using copper oxide nanoparticles by response surface methodology. *Environmental Progress & Sustainable Energy*, *42*(1), e13962.

Mohan, K., Ganesan, A. R., Ezhilarasi, P. N., Kondamareddy, K. K., Rajan, D. K., Sathishkumar, P., Rajarajeswaran, J., & Conterno, L. (2022). Green and eco-friendly approaches for the extraction of chitin and chitosan: A review. *Carbohydrate Polymers*, *287*, 119349.

Mohtashim, Q., & Rigout, M. (2021). Surface Chemical Analysis of Ci Leuco Sulphur Black 1 Dyed Cotton Fabric After-Treated with Plant-Derived Tannin-Based Protective Agent. *Cellulose Chemistry and Technology*, *55*(7–8), 883–891.

Morin, J.-F. (2017). Recent advances in the chemistry of vat dyes for organic electronics. *Journal of Materials Chemistry C*, *5*(47), 12298–12307.

Mujumdar, N., de la Peña, A. M., & Campiglia, A. D. (2019). Classification of pre-dyed textile fibers exposed to weathering and photodegradation by non-destructive excitationemission fluorescence spectroscopy paired with discriminant unfolded-partial least squares. *Forensic Chemistry*, *12*, 25–32.

Mumbi, A. W., & Watanabe, T. (2021). Willingness to Pay and Participate in Improved Water Quality by Lay People and Factory Workers: A Case Study of River Sosiani, Eldoret Municipality, Kenya. *Sustainability*, *13*(4), 1934.

Mustroph, H., & Towns, A. (2021). Indophenol and related dyes. *Physical Sciences Reviews*.

Nagia, F. A., & El-Mohamedy, R. S. R. (2007). Dyeing of wool with natural anthraquinone dyes from Fusarium oxysporum. *Dyes and Pigments*, *75*(3), 550–555.

Nardino, V., Guzzi, D., Lastri, C., Palombi, L., Coluccia, G., Magli, E., Labate, D., & Raimondi, V. (2023). Compressive Sensing Imaging Spectrometer for UV-Vis Stellar Spectroscopy: Instrumental Concept and Performance Analysis. *Sensors*, *23*(4), 2269.

Nasrollahi, N., Ghalamchi, L., Vatanpour, V., & Khataee, A. (2021). Photocatalytic-membrane technology: A critical review for membrane fouling mitigation. *Journal of Industrial and Engineering Chemistry*, *93*, 101–116.

Nawabjohn, M. S., Sivaprakasam, P., Anandasadagopan, S. K., Begum, A. A., & Pandurangan, A. K. (2021). Green synthesis and characterisation of silver nanoparticles using Cassia tora seed extract and investigation of antibacterial potential. *Applied Biochemistry and Biotechnology*, 1–15.

Nawarkar, C. J., & Salkar, V. D. (2019). Solar powered electrocoagulation system for municipal wastewater treatment. *Fuel*, *237*, 222–226.

Neves, C. V., Scheufele, F. B., Nardino, A. P., Vieira, M. G. A., da Silva, M. G. C., Módenes, A. N., & Borba, C. E. (2018). Phenomenological modeling of reactive dye adsorption onto fish scales surface in the presence of electrolyte and surfactant mixtures. *Environmental Technology*, *39*(19), 2467–2483.

Nicolaisen, B. (2003). Developments in membrane technology for water treatment. *Desalination*, *153*(1–3), 355–360.

Noël, S., Léger, B., Ponchel, A., Sadjadi, S., & Monflier, E. (2021). Cyclodextrins as multitask agents for metal nano-heterogeneous catalysis: A review. *Environmental Chemistry Letters*, *19*(6), 4327–4348.

Obotey Ezugbe, E., & Rathilal, S. (2020). Membrane technologies in wastewater treatment: A review. *Membranes*, *10*(5), 89.

Okeke, E. S., Ezeorba, T. P. C., Okoye, C. O., Chen, Y., Mao, G., Feng, W., & Wu, X. (2022). Analytical detection methods for azo dyes: A focus on comparative limitations and prospects of bio-sensing and electrochemical nano-detection. *Journal of Food Composition and Analysis*, 104778.

Okur, M. C., Akyol, A., Nayir, T. Y., Kara, S., Ozturk, D., & Civas, A. (2022). Performance of Ti/RuO2-IrO2 electrodes and comparison with BDD electrodes in the treatment of textile wastewater by electro-oxidation process. *Chemical Engineering Research and Design*, *183*, 398–410.

Omrani, N., & Nezamzadeh-Ejhieh, A. (2020). A comprehensive study on the mechanism pathways and scavenging agents in the photocatalytic activity of BiVO4/WO3 nanocomposite. *Journal of Water Process Engineering*, *33*, 101094.

Osemba, M., Muriuki-Hutchins, M., Karenga, S., & Keru, G. (2024). Chitosan Coupled Silver Nanoparticles Electrocatalyst Synthesis and Characterization. *International Journal of Pure and Applied Chemistry*, *2*(1), 1–12.

Osemba, M. O. (2019). *Electrochemical Degradation and Chemical Assessment of Azo Dyes in the Textile Waste Water* [PhD Thesis, Pwani University]. https://elibrary.pu.ac.ke/handle/123456789/826

Osemba, M. O., Muriuki-Hutchins, M., Karenga, S., & Keru, G. (2024). Production of Chitosan from Crab Shells. *International Journal of Advanced Research*, *7*(1), 244–250.

Osemba, M. O., Ojwang, L., & Maghanga, J. (2024). Electrochemical Color Removal of Azo Dyes Using Boron-Doped Diamond Electrodes and Silver Nanoparticles as Electrocatalyst. *International Journal of Advanced Research*, *7*(1), 251–265.

Othmani, B., Gamelas, J. A., Rasteiro, M. G., & Khadhraoui, M. (2020). Characterization of two cactus formulation-based flocculants and investigation on their flocculating ability for cationic and anionic dyes removal. *Polymers*, *12*(9), 1964.

Oyetade, J. A., Machunda, R. L., & Hilonga, A. (2022). Photocatalytic degradation of azo dyes in textile wastewater by Polyaniline composite catalyst-a review. *Scientific African*, e01305.

Ozgun, H., Dereli, R. K., Ersahin, M. E., Kinaci, C., Spanjers, H., & van Lier, J. B. (2013). A review of anaerobic membrane bioreactors for municipal wastewater treatment: Integration options, limitations and expectations. *Separation and Purification Technology*, *118*, 89–104.

Pakizeh, M., Moradi, A., & Ghassemi, T. (2021). Chemical extraction and modification of chitin and chitosan from shrimp shells. *European Polymer Journal*, *159*, 110709.

Panda, M. K., Dhal, N. K., Kumar, M., Mishra, P. M., & Behera, R. K. (2021). Green synthesis of silver nanoparticles and its potential effect on phytopathogens. *Materials Today: Proceedings*, *35*, 233–238.

Pandey, A., Singh, P., & Iyengar, L. (2007). Bacterial decolorization and degradation of azo dyes. *International Biodeterioration & Biodegradation*, *59*(2), 73–84.

Patidar, R., & Srivastava, V. C. (2022). Ultrasound-assisted electrochemical treatment of cosmetic industry wastewater: Mechanistic and detoxification analysis. *Journal of Hazardous Materials*, *422*, 126842.

Peng, W., Fu, Y., Wang, L., Wang, Y., Dong, Y., Huang, Y., & Wang, Z. (2021). Effects of exogenic chloride on oxidative degradation of chlorinated azo dye by UV-activated peroxodisulfate. *Chinese Chemical Letters*, *32*(8), 2544–2550.

Pesaresi, M., Pirani, F., Tagliabracci, A., Valsecchi, M., Procopio, A. D., Busardò, F. P., & Graciotti, L. (2020). SARS-CoV-2 identification in lungs, heart and kidney specimens by transmission and scanning electron microscopy. *European Review for Medical and Pharmacological Sciences*, *24*(9), 5186–5188.

Pinheiro, L. R. S., Gradíssimo, D. G., Xavier, L. P., & Santos, A. V. (2022a). Degradation of azo dyes: Bacterial potential for bioremediation. *Sustainability*, *14*(3), 1510.

Pinheiro, L. R. S., Gradíssimo, D. G., Xavier, L. P., & Santos, A. V. (2022b). Degradation of azo dyes: Bacterial potential for bioremediation. *Sustainability*, *14*(3), 1510.

Qi, H., Rizopoulos, D., & van Rosmalen, J. (2023). Sample size calculation for clinical trials analyzed with the meta-analytic-predictive approach. *Research Synthesis Methods*, *14*(3), 396–413.

Qiao, Z.-A., Wang, Y., Gao, Y., Li, H., Dai, T., Liu, Y., & Huo, Q. (2010). Commercially activated carbon as the source for producing multicolor photoluminescent carbon dots by chemical oxidation. *Chemical Communications*, *46*(46), 8812–8814.

Qumar, U., Hassan, J., Naz, S., Haider, A., Raza, A., Ul-Hamid, A., Haider, J., Shahzadi, I., Ahmad, I., & Ikram, M. (2021). Silver decorated 2D nanosheets of GO and MoS2 serve as nanocatalyst for water treatment and antimicrobial applications as ascertained with molecular docking evaluation. *Nanotechnology*, *32*(25), 255704.

Rachtanapun, P., Klunklin, W., Jantrawut, P., Jantanasakulwong, K., Phimolsiripol, Y., Seesuriyachan, P., Leksawasdi, N., Chaiyaso, T., Ruksiriwanich, W., & Phongthai, S. (2021). Characterization of chitosan film incorporated with curcumin extract. *Polymers*, *13*(6), 963.

Rafaëlly, L., Héron, S., Nowik, W., & Tchapla, A. (2008). Optimisation of ESI-MS detection for the HPLC of anthraquinone dyes. *Dyes and Pigments*, *77*(1), 191–203.

Rahmani, A. R., Gilan, R. A., Asgari, G., Leili, M., & Dargahi, A. (2022). Enhanced degradation of Rhodamine B dye by Fenton/peracetic acid and photo-Fenton/peracetic acid processes. *International Journal of Chemical Reactor Engineering*, *20*(12), 1251–1260.

Rajashekarappa, K. K., Mahadevan, G. D., Neelagund, S. E., Sathynarayana, M., Vijaya, D., & Mulla, S. I. (2022). Decolorization of amaranth RI and fast red E azo dyes by thermophilic Geobacillus thermoleovorans KNG 112. *Journal of Chemical Technology & Biotechnology*, *97*(2), 482–489.

Rakness, K. L. (2011). *Ozone in drinking water treatment: Process design, operation, and optimization*. American Water Works Association.

Ramesh, K., Gnanamangai, B. M., & Mohanraj, R. (2021). Investigating techno-economic feasibility of biologically pretreated textile wastewater treatment by electrochemical oxidation process towards zero sludge concept. *Journal of Environmental Chemical Engineering*, *9*(5), 106289.

Ramzan, U., Shakoori, F. R., Shakoori, A. R., Abbas, S. Z., Wabaidur, S. M., Eldesoky, G. E., Islam, M. A., & Rafatullah, M. (2022). Biodegradation and decolorization of Reactive Red 2 azo dye by Paramecium jenningsi and Paramecium multimicronucleatum in industrial wastewater. *Biomass Conversion and Biorefinery*, 1–9.

Ren, X., Tang, P., Hou, B., Yu, Z., Huang, J., Wang, Q., & Song, K. (2023). Evaluating the degradation of Rhodamine B using a sequential batch three-dimensional electrode reactor. *Journal of Environmental Chemical Engineering*, 109475.

Renuka, R., Renuka Devi, K., Sivakami, M., & Thilagavathi, T. (2021). Solanum torvum mediated synthesis and characterization of silver nanoparticles for antibacterial activities. *Journal of Plant Biochemistry and Biotechnology*, *30*(3), 596–601.

Riaz, N., Hassan, M., Siddique, M., Mahmood, Q., Farooq, U., Sarwar, R., & Khan, M. S. (2020). Photocatalytic degradation and kinetic modeling of azo dye using bimetallic photocatalysts: Effect of synthesis and operational parameters. *Environmental Science and Pollution Research*, *27*(3), 2992–3006.

Rydz, J., Šišková, A., & Andicsová Eckstein, A. (2019). Scanning electron microscopy and atomic force microscopy: Topographic and dynamical surface studies of blends, composites, and hybrid functional materials for sustainable future. *Advances in Materials Science and Engineering*, *2019*.

Sadat, A., & Joye, I. J. (2020). Peak fitting applied to fourier transform infrared and raman spectroscopic analysis of proteins. *Applied Sciences*, *10*(17), 5918.

Safaripour, M., Parandi, E., Aghel, B., Gouran, A., Saidi, M., & Nodeh, H. R. (2023). Optimization of the microreactor-intensified transesterification process using silver titanium oxide nanoparticles decorated magnetic graphene oxide nanocatalyst. *Process Safety and Environmental Protection*, *173*, 495–506.

Saidu, F. K., Joseph, A., Varghese, E. V., & Thomas, G. V. (2020). Silver nanoparticlesembedded poly (1-naphthylamine) nanospheres for low-cost non-enzymatic electrochemical H2O2 sensor. *Polymer Bulletin*, *77*(11), 5825–5846.

Saini, R. D. (2017). Textile organic dyes: Polluting effects and elimination methods from textile waste water. *Int J Chem Eng Res*, *9*(1), 121–136.

Saratale, R. G., Saratale, G. D., Chang, J.-S., & Govindwar, S. P. (2011). Bacterial decolorization and degradation of azo dyes: A review. *Journal of the Taiwan Institute of Chemical Engineers*, *42*(1), 138–157.

Schallemberger, J. B., Libardi, N., Puerari, R. C., Matias, W. G., & Nagel-Hassemer, M. E. (2023). Effect of Spent Mushroom Substrate on Azo Dye Removal and Effluent Treatment. *Brazilian Archives of Biology and Technology*, *66*.

Sevastre, A.-S., & Hodorog, A. D. (2021). RECENT INVESTIGATIONS ON ANTICANCER PROPERTIES OF AZO-DYES. *Medico Oncology*, *2*(2), 11–25.

Shahedi, A., Darban, A. K., Taghipour, F., & Jamshidi-Zanjani, A. (2020). A review on industrial wastewater treatment via electrocoagulation processes. *Current Opinion in Electrochemistry*, *22*, 154–169.

Shahid, M., Wertz, J., Degano, I., Aceto, M., Khan, M. I., & Quye, A. (2019). Analytical methods for determination of anthraquinone dyes in historical textiles: A review. *Analytica Chimica Acta*, *1083*, 58–87.

Shanmugam, L., Ahire, M., & Nikam, T. (2020). Bacopa monnieri (L.) Pennell, a potential plant species for degradation of textile azo dyes. *Environmental Science and Pollution Research*, *27*(9), 9349–9363.

Sharma, J., Sharma, S., & Soni, V. (2021). Classification and impact of synthetic textile dyes on Aquatic Flora: A review. *Regional Studies in Marine Science*, *45*, 101802.

Sharma, N., Das, T., Kumar, S., Bhosale, R., Kabir, M., & Ogale, S. (2019). Photocatalytic activation and reduction of CO2 to CH4 over single phase nano Cu3SnS4: A combined experimental and theoretical study. *ACS Applied Energy Materials*, *2*(8), 5677–5685.

Sharma, P., & Kumar, S. (2021). Bioremediation of heavy metals from industrial effluents by endophytes and their metabolic activity: Recent advances. *Bioresource Technology*, *339*, 125589.

Shen, F., Xu, Y.-J., Wang, Y., Chen, J., & Wang, S. (2022). Rapid and ultra-trace levels analysis of 33 antibiotics in water by on-line solid-phase extraction with ultraperformance liquid chromatography-tandem mass spectrometry. *Journal of Chromatography A*, 463304.

Sher, F., Hanif, K., Iqbal, S. Z., & Imran, M. (2020). Implications of advanced wastewater treatment: Electrocoagulation and electroflocculation of effluent discharged from a wastewater treatment plant. *Journal of Water Process Engineering*, *33*, 101101.

Shi, J., Zang, L., Zhang, L., Wang, J., Xu, Q., Zhang, Y., & Sun, L. (2023). Porous ball-in-ball N-doped carbon loading Co nanoparticles for high-performance asymmetric capacitor. *Diamond and Related Materials*, *133*, 109705.

Shi, Y., Yang, Z., Xing, L., Zhang, X., Li, X., & Zhang, D. (2021). Recent advances in the biodegradation of azo dyes. *World Journal of Microbiology and Biotechnology*, *37*, 1–18.

Shindhal, T., Rakholiya, P., Varjani, S., Pandey, A., Ngo, H. H., Guo, W., Ng, H. Y., & Taherzadeh, M. J. (2021). A critical review on advances in the practices and perspectives for the treatment of dye industry wastewater. *Bioengineered*, *12*(1), 70–87.

Shindy, H. A. (2017). Fundamentals in the chemistry of cyanine dyes: A review. *Dyes and Pigments*, *145*, 505–513.

Shy, S. S., Chen, Y. R., Lin, B.-L., & Maznoy, A. (2021). Ignition enhancement and deterioration by nanosecond repetitively pulsed discharges in a randomly-stirred lean n-butane/air mixture at various inter-electrode gaps. *Combustion and Flame*, *231*, 111506.

Siddique, M. S., Xiong, X., Yang, H., Maqbool, T., Graham, N., & Yu, W. (2022). Dynamic variations in DOM and DBPs formation potential during surface water treatment by ozonation-nanofiltration: Using spectroscopic indices approach. *Chemical Engineering Journal*, *427*, 132010.

Silah, H., Erkmen, C., Demir, E., & Uslu, B. (2021). Modified indium tin oxide electrodes: Electrochemical applications in pharmaceutical, biological, environmental and food analysis. *TrAC Trends in Analytical Chemistry*, *141*, 116289.

Sillanpää, M., Mahvi, A. H., Balarak, D., & Khatibi, A. D. (2023). Adsorption of Acid orange 7 dyes from aqueous solution using Polypyrrole/nanosilica composite: Experimental and modelling. *International Journal of Environmental Analytical Chemistry*, *103*(1), 212–229.

Singh, P. K., & Singh, R. L. (2017). Bio-removal of azo dyes: A review. *International Journal of Applied Sciences and Biotechnology*, *5*(2), 108–126.

Slama, H. B., Chenari Bouket, A., Pourhassan, Z., Alenezi, F. N., Silini, A., Cherif-Silini, H., Oszako, T., Luptakova, L., Golińska, P., & Belbahri, L. (2021). Diversity of synthetic dyes from textile industries, discharge impacts and treatment methods. *Applied Sciences*, *11*(14), 6255.

Sleptsov, V. V., Diteleva, A. O., Kukushkin, D. Y., Tsyrkov, R. A., & Diteleva, E. O. (2022). Vacuum as a continuum medium forming energy inhomogeneities with a high energy density in the liquid phase. *Modern Electronic Materials*, *8*(2), 73–78.

Śmigiel-Kamińska, D., Pośpiech, J., Makowska, J., Stepnowski, P., Wąs-Guba\la, J., & Kumirska, J. (2019). The identification of polyester fibers dyed with disperse dyes for forensic purposes. *Molecules*, *24*(3), 613.

Smith, D., & Starborg, T. (2019). Serial block face scanning electron microscopy in cell biology: Applications and technology. *Tissue and Cell*, *57*, 111–122.

Solís, M., Solís, A., Pérez, H. I., Manjarrez, N., & Flores, M. (2012). Microbial decolouration of azo dyes: A review. *Process Biochemistry*, *47*(12), 1723–1748.

Song, D., Xu, W., & Zhou, Y.-G. (2023). In situ modified electrodes. *Journal of Electroanalytical Chemistry*, *940*, 117504.

Sreedharan, V., Saha, P., & Rao, K. V. B. (2021). Dye degradation potential of Acinetobacter baumannii strain VITVB against commercial azo dyes. *Bioremediation Journal*, *25*(4), 347–368.

Srivastava, R., & Sofi, I. R. (2020). Impact of synthetic dyes on human health and environment. In *Impact of textile dyes on public health and the environment* (pp. 146–161). IGI Global.

Su, K.-Y., & Lee, W.-L. (2020). Fourier transform infrared spectroscopy as a cancer screening and diagnostic tool: A review and prospects. *Cancers*, *12*(1), 115.

Supriyanto, A., Nurosyid, F., & Ahliha, A. H. (2018). Carotenoid pigment as sensitizers for applications of dye-sensitized solar cell (DSSC). *IOP Conference Series: Materials Science and Engineering*, *432*(1), 012060.

Syam Babu, D., Anantha Singh, T. S., Nidheesh, P. V., & Suresh Kumar, M. (2020). Industrial wastewater treatment by electrocoagulation process. *Separation Science and Technology*, *55*(17), 3195–3227.

Tafreshi, S. S., Moshfegh, A. Z., & de Leeuw, N. H. (2019). Mechanism of photocatalytic reduction of CO2 by Ag3PO4 (111)/g-C3N4 nanocomposite: A first-principles study. *The Journal of Physical Chemistry C*, *123*(36), 22191–22201.

Tang, C. Y., Yang, Z., Guo, H., Wen, J. J., Nghiem, L. D., & Cornelissen, E. (2018). *Potable water reuse through advanced membrane technology*. ACS Publications.

Tang, J., Cheng, Z., Li, H., & Xiang, L. (2022). Electro-Chemical Degradation of Norfloxacin Using a PbO2-NF Anode Prepared by the Electrodeposition of PbO2 onto the Substrate of Nickel Foam. *Catalysts*, *12*(11), 1297.

Tanveer, A., Kapoor, S. G., Mujumdar, S., & Curreli, D. (2023). One-Dimensional Plasma Model of Electrical Discharge Machining in Deionized Water for Prediction of Plasma Characteristics Along the Interelectrode Gap. *Journal of Manufacturing Science and Engineering*, *145*(1), 011012.

Tara, N., Iqbal, M., Habib, F., Khan, Q. M., Iqbal, S., Afzal, M., & Brix, H. (2021). Investigating degradation metabolites and underlying pathway of azo dye “Reactive

Black 5" in bioaugmented floating treatment wetlands. *Environmental Science and Pollution Research*, *28*(46), 65229–65242.

Tian, W., Chen, G., Gui, Y., Zhang, G., & Li, Y. (2021). Rapid quantification of total phenolics and ferulic acid in whole wheat using UV–Vis spectrophotometry. *Food Control*, *123*, 107691.

Tibebe, D., Negash, A., Mulugeta, M., Kassa, Y., Moges, Z., & Yenealem, D. (2022). Investigation of selected physico-chemical quality parameters in industrial wastewater by electrocoagulation process, Ethiopia. *BMC Chemistry*, *16*(1), 1–9.

Tkaczyk, A., Mitrowska, K., & Posyniak, A. (2020). Synthetic organic dyes as contaminants of the aquatic environment and their implications for ecosystems: A review. *Science of the Total Environment*, *717*, 137222.

Tucker, H. H. (1971). The coloring of human hair with semipermanent dyes. *J. Soc. Cosmet. Chem*, *22*, 379–398.

Türgay, O., Ersöz, G., Atalay, S., Forss, J., & Welander, U. (2011). The treatment of azo dyes found in textile industry wastewater by anaerobic biological method and chemical oxidation. *Separation and Purification Technology*, *79*(1), 26–33.

Ullah, F., Ahmad, M., Zafar, M., Parveen, B., Ashfaq, S., Bahadur, S., Safdar, Q., Safdar, L. B., Alam, F., & Luqman, M. (2022). Pollen morphology and its taxonomic potential in some selected taxa of Caesalpiniaceae observed under light microscopy and scanning electron microscopy. *Microscopy Research and Technique*, *85*(4), 1410–1420.

Valand, R., Tanna, S., Lawson, G., & Bengtström, L. (2020). A review of Fourier Transform Infrared (FTIR) spectroscopy used in food adulteration and authenticity investigations. *Food Additives & Contaminants: Part A*, *37*(1), 19–38.

van Reis, R., & Zydney, A. (2007). Bioprocess membrane technology. *Journal of Membrane Science*, *297*(1–2), 16–50.

Van Tran, V., Park, D., & Lee, Y.-C. (2018). Hydrogel applications for adsorption of contaminants in water and wastewater treatment. *Environmental Science and Pollution Research*, *25*(25), 24569–24599.

Veerasingam, S., Ranjani, M., Venkatachalapathy, R., Bagaev, A., Mukhanov, V., Litvinyuk, D., Mugilarasan, M., Gurumoorthi, K., Guganathan, L., & Aboobacker, V. M. (2021). Contributions of Fourier transform infrared spectroscopy in microplastic pollution research: A review. *Critical Reviews in Environmental Science and Technology*, *51*(22), 2681–2743.

Velusamy, S., Roy, A., Sundaram, S., & Kumar Mallick, T. (2021a). A review on heavy metal ions and containing dyes removal through graphene oxide-based adsorption strategies for textile wastewater treatment. *The Chemical Record*, *21*(7), 1570–1610.

Velusamy, S., Roy, A., Sundaram, S., & Kumar Mallick, T. (2021b). A review on heavy metal ions and containing dyes removal through graphene oxide-based adsorption strategies for textile wastewater treatment. *The Chemical Record*, *21*(7), 1570–1610.

Venkatadri, R., & Peters, R. W. (1993). Chemical oxidation technologies: Ultraviolet light/hydrogen peroxide, Fenton's reagent, and titanium dioxide-assisted photocatalysis. *Hazardous Waste and Hazardous Materials*, *10*(2), 107–149.

Veréb, G., Gayır, V. E., Santos, E. N., Fazekas, Á., Kertész, S., Hodúr, C., & László, Z. (2019a). Purification of real car wash wastewater with complex coagulation/flocculation methods using polyaluminum chloride, polyelectrolyte, clay mineral and cationic surfactant. *Water Science and Technology*, *80*(10), 1902–1909.

Veréb, G., Gayır, V. E., Santos, E. N., Fazekas, Á., Kertész, S., Hodúr, C., & László, Z. (2019b). Purification of real car wash wastewater with complex coagulation/flocculation methods using polyaluminum chloride, polyelectrolyte, clay mineral and cationic surfactant. *Water Science and Technology*, *80*(10), 1902–1909.

Vikal, S., Gautam, Y. K., Meena, S., Parewa, V., Kumar, A., Kumar, A., Meena, S., Kumar, S., & Singh, B. P. (2023). Surface functionalized silver-doped ZnO nanocatalyst: A sustainable cooperative catalytic, photocatalytic and antibacterial platform for waste treatment. *Nanoscale Advances*, *5*(3), 805–819.

Vilchis-Carmona, J. A., Rodríguez-Luna, I. C., Elufisan, T. O., Sánchez-Varela, A., BibbinsMartínez, M., Rivera, G., Paz-Gonzalez, A. D., Villalobos-López, M. A., & Guo, X. (2021). The decolorization and degradation of azo dyes by two Stenotrophomonas strains isolated from textile effluent (Tepetitla, Mexico). *Brazilian Journal of Microbiology*, *52*, 1755–1767.

Wac\lawek, S., Silvestri, D., Hrabák, P., Padil, V. V., Torres-Mendieta, R., Wac\lawek, M., Černík, M., & Dionysiou, D. D. (2019). Chemical oxidation and reduction of hexachlorocyclohexanes: A review. *Water Research*, *162*, 302–319.

Waffo, L. C. M., Dikdim, J. M. D., Noumi, G. B., Doumbi, R. T., Kaichouh, G., Sieliechi, J. M., Haji, I., Guessous, A., & El Karbane, M. (2022). Electrochemical production of sulfate radicals for degradation of Tenofovir in aqueous solution. *Case Studies in Chemical and Environmental Engineering*, *6*, 100235.

Wakrim, A., Zaroual, Z., El Ghachtouli, S., Jamal Eddine, J., & Azzi, M. (2022). Treatment and Degradation of Azo Dye Waste Industry by Electro-Fenton Process. *Physical Chemistry Research*, *10*(4), 495–504.

Wang, C., Sun, R., Huang, R., & Cao, Y. (2021). A novel strategy for enhancing heterogeneous Fenton degradation of dye wastewater using natural pyrite: Kinetics and mechanism. *Chemosphere*, *272*, 129883.

Wang, C.-C., Juang, L.-C., Hsu, T.-C., Lee, C.-K., Lee, J.-F., & Huang, F.-C. (2004). Adsorption of basic dyes onto montmorillonite. *Journal of Colloid and Interface Science*, *273*(1), 80–86.

Wang, H., Zhang, G., Mia, R., Wang, W., Xie, L., Lü, S., Mahmud, S., & Liu, H. (2022). Bioreduction (Ag+ to Ag0) and stabilization of silver nanocatalyst using hyaluronate biopolymer for azo-contaminated wastewater treatment. *Journal of Alloys and Compounds*, *894*, 162502.

Wasim, M., Sabir, A., Shafiq, M., & Khan, R. U. (2019). Fractionation of direct dyes using modified vapor grown carbon nanofibers and zirconia in cellulose acetate blend membranes. *Science of The Total Environment*, *677*, 194–204.

Wei, Q., Zhang, Y., Zhang, K., Mwasiagi, J. I., Zhao, X., Chow, C. W., & Tang, R. (2022). Removal of direct dyes by coagulation: Adaptability and mechanism related to the molecular structure. *Korean Journal of Chemical Engineering*, *39*(7), 1850–1862.

Willans, M., Szczecinski, E., Roocke, C., Williams, S., Timalsina, S., Vongsvivut, J., McIlwain, J., Naderi, G., Linge, K. L., & Hackett, M. J. (2023). Development of a rapid detection protocol for microplastics using reflectance-FTIR spectroscopic imaging and multivariate classification. *Environmental Science: Advances*, *2*(4), 663–674.

Wilts, E. M., Herzberger, J., & Long, T. E. (2018). Addressing water scarcity: Cationic polyelectrolytes in water treatment and purification. *Polymer International*, *67*(7), 799–814.

Woo, H. C., & Jhung, S. H. (2021). Adsorptive removal of nitro-or sulfonate-containing dyes by a functional metal–organic framework: Quantitative contribution of hydrogen bonding. *Chemical Engineering Journal*, *425*, 130598.

Wooster, C. B., Segool, H. D., & Allan Jr, T. T. (1938). γ, γ, γ-Triphenylpropyl Derivatives. *Journal of the American Chemical Society*, *60*(7), 1666–1667.

Wulandari, P., Handayani, Y. S., Hidayat, R., Wang, P., Ryuzaki, S., Okamoto, K., & Tamada, K. (2018). Surface plasmon resonance effect of silver nanoparticles on the enhanced efficiency of inverted hybrid organic–inorganic solar cell. *Journal of Nonlinear Optical Physics & Materials*, *27*(02), 1850017.

Xiang, W., Zhang, X., Chen, J., Zou, W., He, F., Hu, X., Tsang, D. C., Ok, Y. S., & Gao, B. (2020). Biochar technology in wastewater treatment: A critical review. *Chemosphere*, *252*, 126539.

Xiao, H., Yan, W., Zhao, Z., Tang, Y., Li, Y., Yang, Q., Luo, S., & Jiang, B. (2022). Chlorate induced false reduction in chemical oxygen demand (COD) based on standard dichromate method: Countermeasure and mechanism. *Water Research*, *221*, 118732.

Xu, M., Wang, X., Zhou, B., & Zhou, L. (2021). Pre-coagulation with cationic flocculantcomposited titanium xerogel coagulant for alleviating subsequent ultrafiltration membrane fouling by algae-related pollutants. *Journal of Hazardous Materials*, *407*, 124838.

Xu, Y., Wang, C., Huang, Y., & Fu, J. (2021). Recent advances in electrocatalysts for neutral and large-current-density water electrolysis. *Nano Energy*, *80*, 105545.

Yadav, S., Kamsonlian, S., Gola, D., & Pal, S. (2023). Reduction of Contaminants from Municipal Wastewater of Salori Sewage Treatment Plant Using Electrochemical Membrane Bioreactor and Bioelectricity Generation. *Ecological Engineering & Environmental Technology*, *24*(1), 264–271.

Ye, J., Zheng, M., Ma, H., Xuan, Z., Tian, W., Liu, H., Wang, S., & Zhang, Y. (2022). Development and Validation of an Automated Magneto-Controlled Pretreatment for Chromatography-Free Detection of Aflatoxin B1 in Cereals and Oils through Atomic Absorption Spectroscopy. *Toxins*, *14*(7), 454.

Yehuala, G., Worku, Z., Angassa, K., Nkambule, T. T., & Fito, J. (2022). Electrochemical degradation of chemical oxygen demand in the textile industrial wastewater through the modified electrodes. *Arabian Journal for Science and Engineering*, *47*(5), 5911–5922.

Yin, Y., Xu, G., Xin, Z., Liu, Y., He, X., & Zhang, H. (2022). Synthesis, characterization and photocatalytic degradation of dyestuffs with a composite material, 3-nOCoPc/SnO2. *Journal of Coordination Chemistry*, 1–13.

Younis, S., Usman, M., ul Haq, A., Akram, N., Saeed, M., Raza, S., Siddiq, M., & Bukhtawar, F. (2020). Solubilization of reactive dyes by mixed micellar system: Synergistic effect of nonionic surfactant on solubilizing power of cationic surfactant. *Chemical Physics Letters*, *738*, 136890.

Yusuf, M. (2019a). Synthetic dyes: A threat to the environment and water ecosystem. *Textiles and Clothing*, 11–26.

Yusuf, M. (2019b). Synthetic dyes: A threat to the environment and water ecosystem. *Textiles and Clothing*, 11–26.

Zafar, S., Bukhari, D. A., & Rehman, A. (2022). Azo dyes degradation by microorganisms-An efficient and sustainable approach. *Saudi Journal of Biological Sciences*, 103437.

Zeng, C., Kim, S., Chen, Y., Fu, Y., Bao, J., Xu, Z., & Wang, W. (2023). In Situ Characterization of Kinetics, Mass Transfer, and Active Electrode Surface Area for Vanadium Redox Flow Batteries. *Journal of The Electrochemical Society*, *170*(3), 030507.

Zhang, J., Wang, L., Tan, W., Li, Q., Dong, F., & Guo, Z. (2022). Preparation of chitosanrosmarinic acid derivatives with enhanced antioxidant and anti-inflammatory activities. *Carbohydrate Polymers*, *296*, 119943.

Zhang, Q., Xie, X., Xu, D., Hong, R., Wu, J., Zeng, X., Liu, N., & Liu, J. (2021). Accelerated azo dye biodegradation and detoxification by Pseudomonas aeruginosa DDMZ1-2 via fructose co-metabolism. *Environmental Technology & Innovation*, *24*, 101878.

Zhang, R., Peng, W., Huang, Y., Gautam, S., Wang, J., Mechref, Y., & Tang, H. (2022). A Reciprocal Best-hit Approach to Characterize Isomeric N-Glycans Using Tandem Mass Spectrometry. *Analytical Chemistry*.

Zhang, Y., Wang, Y.-T., Kang, X.-X., Ge, M., Feng, H.-Y., Han, J., Wang, D.-H., & Zhao, D.Z. (2018). Azobenzene disperse dye-based colorimetric probe for naked eye detection of Cu2+ in aqueous media: Spectral properties, theoretical insights, and applications. *Journal of Photochemistry and Photobiology A: Chemistry*, *356*, 652–660.

Zhao, B., Bian, J., Rao, M., She, X., Lou, Y., Cai, J., & Ma, W. (2022). A dilute-and-shoot liquid chromatography–tandem mass spectrometry method for urinary

18hydroxycortisol quantification and its application in establishing reference intervals. *Journal of Clinical Laboratory Analysis*, e24580.

Zhou, Z., Mukherjee, S., Hou, S., Li, W., Elsner, M., & Fischer, R. A. (2021). Porphyrinic MOF film for multifaceted electrochemical sensing. *Angewandte Chemie International Edition*, *60*(37), 20551–20557.

Zhuang, J., Li, M., Pu, Y., Ragauskas, A. J., & Yoo, C. G. (2020). Observation of potential contaminants in processed biomass using fourier transform infrared spectroscopy. *Applied Sciences*, *10*(12), 4345.

Zhuo, Q., Xu, X., Xie, S., Ren, X., Chen, Z., Yang, B., Li, Y., & Niu, J. (2022). Electrooxidation of Ni (II)-citrate complexes at BDD electrode and simultaneous recovery of metallic nickel by electrodeposition. *Journal of Environmental Sciences*, *116*, 103–113.

Zor, E. (2018). Silver nanoparticles-embedded nanopaper as a colorimetric chiral sensing platform. *Talanta*, *184*, 149–155.

APPENDICES

Appendix I: The permit to collect crab shell samples

COUNTY GOVERNMENT OF KILIFI

Department of Agriculture, Livestock Development and Fisheries
Fisheries Directorate

MALINDI SUB COUNTY

FISHERIES OFFICE,
P.O.BOX 12,
-80200
MALINDI.

1st SEPTEMBER 2022

When replying please quote
REF: KCG/MSC/FL/VOL.1/10

TO WHOM IT MAY CONCERN

RE: MARTIN OUMA OSEMBA ID No: 27219014

This office has no objection to the above named having with him one (10) crabs shells to Pwani University, Kilifi for research. The same was purchased from licensed processor in Malindi.

Assist where necessary.

Yours faithfully

NYIRO C. KASIWA
FOR: MALINDI SUB COUNTY FISHERIES OF

Appendix II: Letters of introduction

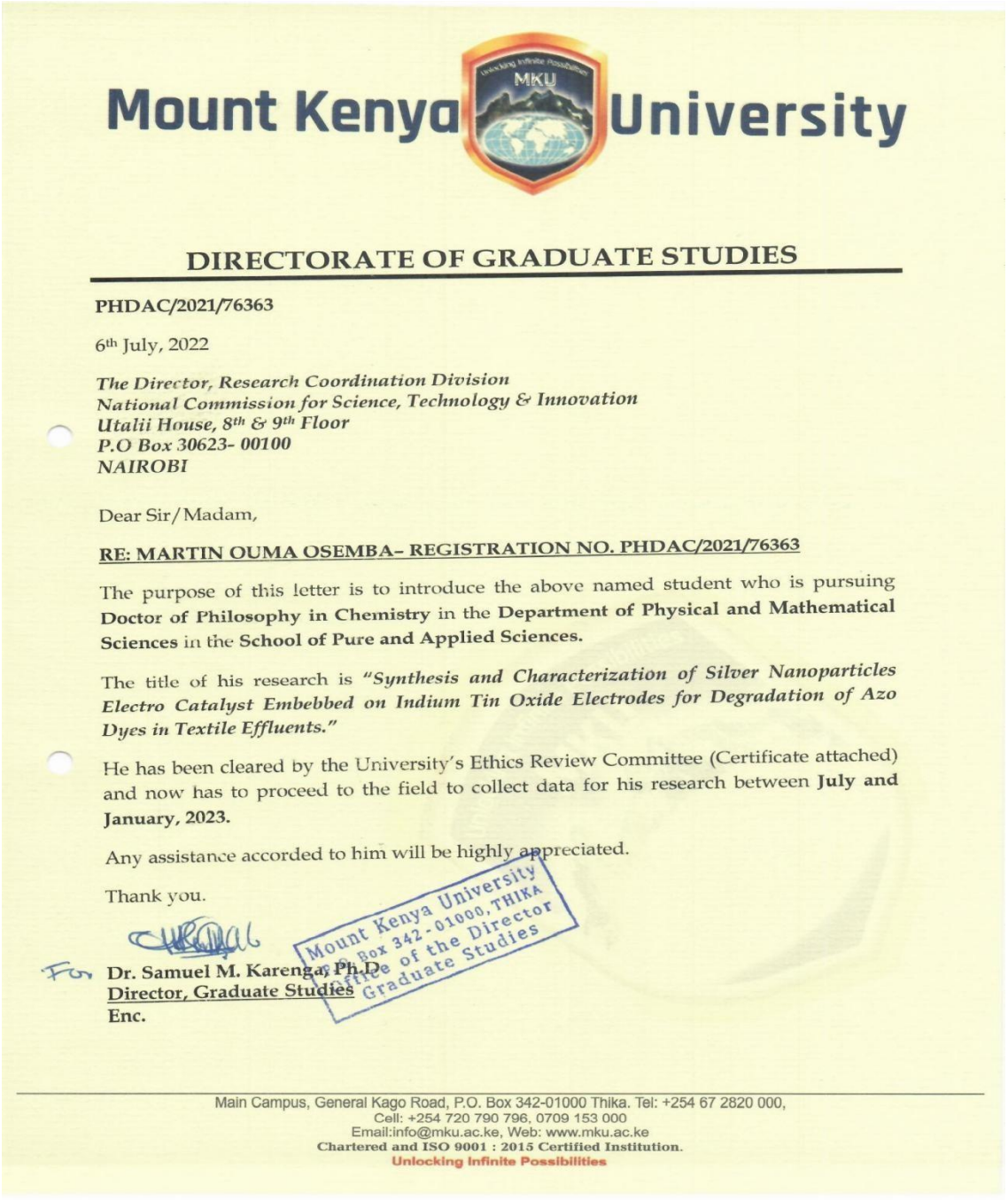

Mount Kenya University

DIRECTORATE OF GRADUATE STUDIES

PHDAC/2021/76363

6th July, 2022

The Director, Research Coordination Division
National Commission for Science, Technology & Innovation
Utalii House, 8th & 9th Floor
P.O Box 30623- 00100
NAIROBI

Dear Sir/Madam,

RE: MARTIN OUMA OSEMBA– REGISTRATION NO. PHDAC/2021/76363

The purpose of this letter is to introduce the above named student who is pursuing **Doctor of Philosophy in Chemistry** in the **Department of Physical and Mathematical Sciences** in the **School of Pure and Applied Sciences.**

The title of his research is ***"Synthesis and Characterization of Silver Nanoparticles Electro Catalyst Embebbed on Indium Tin Oxide Electrodes for Degradation of Azo Dyes in Textile Effluents."***

He has been cleared by the University's Ethics Review Committee (Certificate attached) and now has to proceed to the field to collect data for his research between **July and January, 2023.**

Any assistance accorded to him will be highly appreciated.

Thank you.

Mount Kenya University
P.O Box 342-01000, THIKA
Office of the Director
Graduate Studies

For **Dr. Samuel M. Karenga, Ph.D.**
Director, Graduate Studies
Enc.

Main Campus, General Kago Road, P.O. Box 342-01000 Thika. Tel: +254 67 2820 000,
Cell: +254 720 790 796, 0709 153 000
Email:info@mku.ac.ke, Web: www.mku.ac.ke
Chartered and ISO 9001 : 2015 Certified Institution.
Unlocking Infinite Possibilities

Appendix III: Letters of ethical clearance certificate

Mount Kenya University

REF: **MKU/ERC/2272**
TO. **MARTIN OUMA OSEMBA**

Date: 30 June 2022

REG: **PHDAC/2021/76363**

Dear Sir/Madam,

RE: SYNTHESIS AND CHARACTERIZATION OF SILVER NANOPARTICLES ELECROCATALYST EMBEBBED ON INDIUM TIN OXIDE ELECTRODES FOR DEGRADATION OF AZO DYES IN TEXTILE EFFLUENTS

This is to inform you that **Mount Kenya University** has reviewed and approved your above research proposal. Your application approval number is **1345.** The approval period is **30/06/2022 - 29/06/2023.**

This approval is subject to compliance with the following requirements;

i. Only approved documents including informed consents, study instruments, MTA will be used
ii. All changes including amendments, deviations and violations are submitted for review and approval by **Mount Kenya University**
iii. Death and life threatening problems and serious adverse events or unexpected adverse events whether related or unrelated to the study must be reported to **Mount Kenya University** within 72 hours of notification
iv. Any changes, anticipated or otherwise that may increase the risks or affect the safety or welfare of study participants and others or affect the integrity of the research must be reported to **Mount Kenya University** within 72 hours
v. Clearance for export of biological specimens must be obtained from relevant institutions
vi. Submission of a request for renewal of approval at least 60 days prior to expiry of the approval period. Attach a comprehensive progress report to support the renewal
vii. Submission of an executive summary report within 90 days upon completion of the study to **Mount Kenya University**

Yours sincerely,

The Chairman
Mount Kenya University
Ethics Review Committee
P.O. Box 342 01000, Thika

Dr. Peter G. Kirira
Chairman, Mount Kenya University IERC

Main Campus, General Kago Road, P.O. Box 342-01000 Thika
Tel: 020-2878 000, Cell: +254 709 153 000
Email: info@mku.ac.ke Web: www.mku.ac.ke

Appendix IV: Research permit from NACOSTI

THE SCIENCE, TECHNOLOGY AND INNOVATION ACT, 2013 (Rev. 2014)
Legal Notice No. 108: The Science, Technology and Innovation (Research Licensing) Regulations, 2014

The National Commission for Science, Technology and Innovation, hereafter referred to as the Commission, was the established under the Science, Technology and Innovation Act 2013 (Revised 2014) herein after referred to as the Act. The objective of the Commission shall be to regulate and assure quality in the science, technology and innovation sector and advise the Government in matters related thereto.

CONDITIONS OF THE RESEARCH LICENSE

1. The License is granted subject to provisions of the Constitution of Kenya, the Science, Technology and Innovation Act, and other relevant laws, policies and regulations. Accordingly, the licensee shall adhere to such procedures, standards, code of ethics and guidelines as may be prescribed by regulations made under the Act, or prescribed by provisions of International treaties of which Kenya is a signatory to.
2. The research and its related activities as well as outcomes shall be beneficial to the country and shall not in any way; i. Endanger national security ii. Adversely affect the lives of Kenyans
   iii. Be in contravention of Kenya's international obligations including Biological Weapons Convention (BWC), Comprehensive Nuclear-Test-Ban Treaty Organization (CTBTO), Chemical, Biological, Radiological and Nuclear (CBRN).
   iv. Result in exploitation of intellectual property rights of communities in Kenya v. Adversely affect the environment vi. Adversely affect the rights of communities vii. Endanger public safety and national cohesion viii. Plagiarize someone else's work
3. The License is valid for the proposed research, location and specified period.
4. Neither the license nor any rights thereunder are transferable.
5. The Commission reserves the right to cancel the research at any time during the research period if in the opinion of the Commission the research is not implemented in conformity with the provisions of the Act or any other written law.
6. The Licensee shall inform the relevant County Director of Education, County Commissioner and County Governor before commencement of the research.
7. Excavation, filming, movement, and collection of specimens are subject to further necessary clearance from relevant Government Agencies.
8. The License does not give authority to transfer research materials.
9. The Commission may monitor and evaluate the licensed research project for the purpose of assessing and evaluating compliance with the conditions of the License.
10. The Licensee shall submit one hard copy, and upload a soft copy of their final report (thesis) onto a platform designated by the Commission within one year of completion of the research.
11. The Commission reserves the right to modify the conditions of the License including cancellation without prior notice.
12. Research, findings and information regarding research systems shall be stored or disseminated, utilized or applied in such a manner as may be prescribed by the Commission from time to time.
13. The Licensee shall disclose to the Commission, the relevant Institutional Scientific and Ethical Review Committee, and the relevant national agencies any inventions and discoveries that are of National strategic importance.
14. The Commission shall have powers to acquire from any person the right in, or to, any scientific innovation, invention or patent of strategic importance to the country.
15. Relevant Institutional Scientific and Ethical Review Committee shall monitor and evaluate the research periodically, and make a report of its findings to the Commission for necessary action.

National Commission for Science, Technology and Innovation(NACOSTI),
Off Waiyaki Way, Upper Kabete,
P. O. Box 30623 - 00100 Nairobi, KENYA
Telephone: 020 4007000, 0713788787, 0735404245
E-mail: dg@nacosti.go.ke

Website: www.nacosti.go.ke

Appendix V: Similarity index report

SYNTHESIS AND CHARACTERIZATION OF SILVER NANOPARTICLES ELECROCATALYST EMBEBBED ON INDIUM TIN OXIDE

ELECTRODES FOR

SY THESIS AND CHARACTERIZATION OF SILVER NANOPARTICLES 1 s,yi. D•rlritloo: Heading 1

ELECROCATALVST EMBEBBED ON INDIUM TJN OXIDE ELECTRODES

'OR DEGRADATH)N OFAZO DYES

MARTIN OUMA OSEt\JffiA

PHDAC/!02117636.l

B.Ecl. (Science), M.Sc. (Chemistry)

a

A THESIS SUBl\llTIED FOR

THE FULFILMENT OF

THE REQUIREMENTS

FOR THE A WARD OF

DOCTOR OF

PHILOSOPHY IN

CHEMISTRY OF MOUNT K'ENYA

UNIVERSITY,

KENYA.

SYNTHESIS AND CHARACTERIZATION OF SILVER

NANOPARTICLES ELECROCATALYST EMBEBBED ON INDIUM TIN OXIDE ELECTRODES FOR DEGRADATION OF AZO DYES

ORIGINALITY REPORT

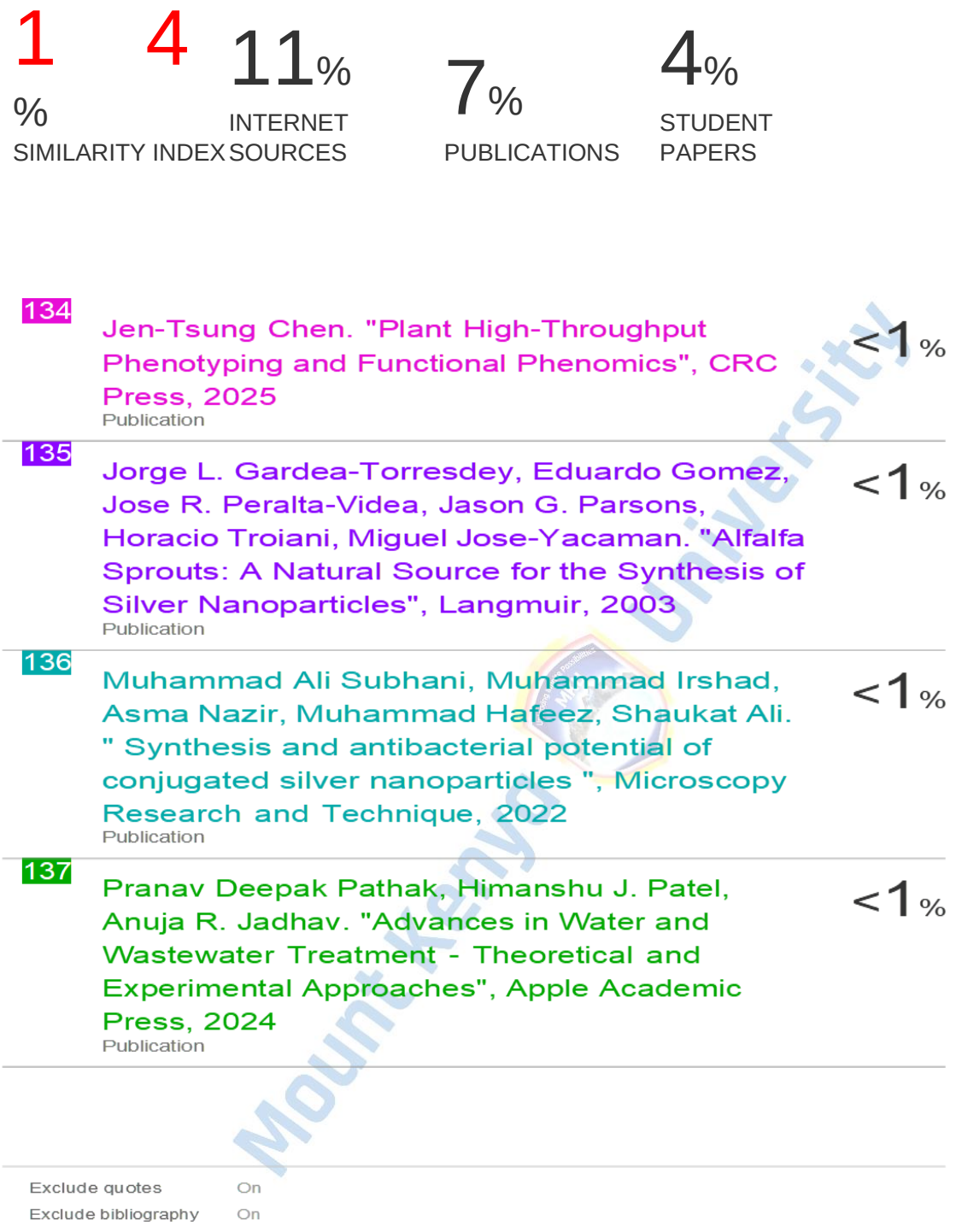

Appendix VI:Results obtained from Two Factor Anova with Replication

(a) Impact of inter- electrode gap on current and power consumption using ITO-AgNPs coupled electrodes

Anova: Two-Fac+L5:S32tor With Replication

SUMMARY	Electrode Gap	Power	Total
ER 1			
Count	4	4	8
Sum	20	13.342	33.342
Average	5	3.3355	4.16775
Variance	6.666667	5.520156	6.014513
EM 1			
Count	4	4	8
Sum	20	11.5598	31.5598
Average	5	2.88995	3.944975
Variance	6.666667	4.016067	5.850403
Total			
Count	8	8	
Sum	40	24.9018	
Average	5	3.112725	
Variance	5.714286	4.143671	

ANOVA

Source of Variation	*SS*	*df*	*MS*	*F*	*P-value*	*F crit*
Sample	0.198515	1	0.198515	0.034721	0.008554	4.747225
Columns	14.24723	1	14.24723	2.491911	0.014047	4.747225
Interaction	0.198515	1	0.198515	0.034721	0.005294	4.747225
Within	68.60867	12	5.717389			
Total	83.25293	15				

(b)Impact of the inter-electrode gap on current and power consumption using ITO electrodes

Anova: Two-Factor With Replication						
SUMMARY	Electrode	Power (w	aTotal			
ER 2						
Count	4	4	8			
Sum	20	20.7111	40.7111			
Average	5	5.177775	5.088888			
Variance	6.666667	23.02808	12.73535			
EM 2						
Count	4	4	8			
Sum	20	35.1252	55.1252			
Average	5	8.7813	6.89065			
Variance	6.666667	97.14349	48.57527			
ER 2						
Count	4	4	8			
Sum	20	21.0882	41.0882			
Average	5	5.27205	5.136025			
Variance	6.666667	23.61819	13.00037			
EM 2						
Count	4	4	8			
Sum	20	36.9069	56.9069			
Average	5	9.226725	7.113363			
Variance	6.666667	103.2355	52.20529			

Total						
Count	16	16				
Sum	80	113.8314				
Average	5	7.114463				
Variance	5.333333	53.24112				
ANOVA						
ce of Varia	*SS*	*df*	*MS*	*F*	*P-value*	*F crit*
Sample	28.77048	3	9.590162	0.28032	0.839051	3.008787
Columns	35.76761	1	35.76761	1.045485	0.316746	4.259677
Interactio	n28.77048	3	9.590162	0.28032	0.839051	3.008787
Within	821.0759	24	34.21149			
Total	914.3844	31				

© *Impact of AgNPs concentration on time, Current and power consumption*

Anova: Two-Factor With Replication						
SUMMARY	AgNPs (pp	Power (w	aTotal			
ER 3						
Count	5	5	10			
Sum	20	5.15616	25.15616			
Average	4	1.031232	2.515616			
Variance	10	0.320996	7.035327			
EM 3						

Count	5	5	10			
Sum	20	7.176	27.176			
Average	4	1.4352	2.7176			
Variance	10	0.179862	6.351661			
Total						
Count	10	10				
Sum	40	12.33216				
Average	4	1.233216				
Variance	8.888889	0.267934				
ANOVA						
ce of Varia	*SS*	*df*	*MS*	*F*	*P-value*	*F crit*
Sample	0.203988	1	0.203988	0.039801	0.002338	4.493998
Columns	38.27547	1	38.27547	7.468072	0.014747	4.493998
Interactio	n0.203988	1	0.203988	0.039801	0.002384	4.493998
Within	82.00343	16	5.125214			
Total	120.6869	19				

(d) A table showing the effect of varying potential difference (Pd) on current (I) generation and specific energy consumption using ITO-AgNPs coupled electrodes

Anova: Two-Factor with Replication

SUMMARY	Potential difference (V)	Power (watt-hour)	Total
ER 4			
Count	4	4	8
Sum	72	10.444	82.444
Average	18	2.611	10.3055
Variance	48	1.553577	88.90048
ER 4			
Count	4	4	8
Sum	72	10.7044	82.7044
Average	18	2.6761	10.33805
Variance	48	1.514961	88.31267
Total			
Count	8	8	
Sum 144 21.1484	Average 18 2.64355		
Variance	41.14286	1.316299	

ANOVA

Source of Variation	*SS*	*df*	*MS*	*F*	*P-value*	*F crit*
Sample	0.004238	1	0.004238	0.000171	0.989778	4.747225
Columns	943.2822	1	943.2822	38.08605	4.79E-05	4.747225
Interaction	0.004238	1	0.004238	0.000171	0.989778	4.747225
Within	297.2056	12	24.76713			
Total	1240.496	15				

(e) A table showing determination of colour removal level of the Azo dyes in the textile effluent before and after treatment using different electrodes

Anova: Two-Factor with Replication

SUMMARY	Pt-Co before	Pt-Co after	Total
ER 8			
Count	4	4	8
Sum	7305	0.264	7305.264
Average	1826.25	0.066	913.158
Variance	324706.3	0.000349	1092002
ER 8			
Count	4	4	8
Sum	7305	699.6	8004.6
Average	1826.25	174.9	1000.575
Variance	324706.3	8102.3	921762.8
Total			
Count	8	8	
Sum	14610	699.864	
Average	1826.25	87.483	
Variance	278319.6	12205.82	

ANOVA

Source of Variation	*SS*	*df*	*MS*	*F*	*P-value*	*F crit*
Sample	30566.93	1	30566.93	0.185954	0.000441	4.747225
Columns	12093243	1	12093243	73.5694	1.83E-06	4.747225
Interaction	30566.93	1	30566.93	0.185954	0.000441	4.747225
Within	1972544	12	164378.7			

Total	14126921	15

(f) A table showing COD of the azo dyes in the textile effluent before and after treatment using different electrodes

Anova: Two-Factor With Replication						
SUMMARY	COD (mg/	LCOD (mg/	LTotal			
ER 10						
Count	4	4	8			
Sum	2912	333.8	3245.8			
Average	728	83.45	405.725			
Variance	11727.33	142.5967	123785.6			
ER 10						
Count	4	4	8			
Sum	2912	616.6	3528.6			
Average	728	154.15	441.075			
Variance	11727.33	108.1167	99159.14			
Total						
Count	8	8				

Sum	5824	950.4				
Average	728	118.8				
Variance	10052	1535.589				
ANOVA						
ce of Varia	*SS*	*df*	*MS*	*F*	*P-value*	*F crit*
Sample	4998.49	1	4998.49	0.843436	0.014206	4.747225
Columns	1484499	1	1484499	250.4914	2.10E-09	4.747225
Interactio	n 4998.49	1	4998.49	0.843436	0.014251	4.747225
Within	71116.14	12	5926.345			
Total	1565612	15				

(g) A table showing COD of the azo dyes in the textile effluent before and after treatment using different electrodes

Anova: Two-Factor With Replication						
SUMMARY	BOD (mg/	LBOD mg/L	Total			
ER 12						
Count	4	4	8			
Sum	709	90	799			

Average	177.25	22.5	99.875			
Variance	152.25	11.66667	6912.411			
ER 12						
Count	4	4	8			
Sum	709	380.8	1089.8			
Average	177.25	95.2	136.225			
Variance	152.25	162.7467	2058.485			
Total						
Count	8	8				
Sum	1418	470.8				
Average	177.25	58.85				
Variance	130.5	1584.831				
ANOVA						
ce of Varia	*SS*	*df*	*MS*	*F*	*P-value*	*F crit*
Sample	5285.29	1	5285.29	44.14402	0.0000238	4.747225
Columns	56074.24	1	56074.24	468.3456	5.54342843	4.747225
Interactio	n 5285.29	1	5285.29	44.14402	0.0000238	4.747225
Within	1436.74	12	119.7283			
Total	68081.56	15				

(h) A table showing impact of pH on power consumption at a pd of 24 V

Anova: Two-Fac+L5:S32tor With Replication

SUMMARY	pH	Power	Total
ER 1			
Count	4	4	8
Sum	20	13.342	33.342
Average	5	3.3355	4.16775
Variance	6.666667	5.520156	6.014513
EM 1			
Count	4	4	8
Sum	20	11.5598	31.55983.94497
Average	5	2.88995	5
Variance	6.666667	4.016067	5.850403
Total			
Count	8	8	
Sum	40	24.9018	
Average	5	3.11272 5	
Variance	5.714286	4.143671	

ANOVA

Source of Variation	*SS*	*df*	*MS*	*F*	*P-value*	*F crit*
Sample	0.198515	1	0.198515	0.034721	0.007854	4.747225
Columns	14.24723	1	14.24723	2.491911	0.013046	4.747225
Interaction	0.198515	1	0.198515	0.034721	0.001292	4.747225
Within	68.60867	12	5.717389			

Total	83.25293	15	

(i) A table showing impact of temperature on the Azo dyes degradation

Anova: Two-Factor with Replication

SUMMARY	Temp before	Temp after	Total
ER 8			
Count	4	4	8
Sum	7305	0.264	7305.264
Average	1826.25	0.066	913.158
Variance	324706.3	0.000349	1092002
ER 8			
Count	4	4	8
Sum	7305	699.6	8004.6
Average	1826.25	174.9	1000.575
Variance	324706.3	8102.3	921762.8
Total			
Count	8	8	
Sum	14610	699.864	
Average	1826.25	87.483	
Variance	278319.6	12205.82	

ANOVA

Source of Variation	*SS*	*df*	*MS*	*F*	*P-value*	*F crit*
Sample	30566.93	1	30566.93	0.185956	0.000879	3.547220
Columns	12093243	1	12093243	73.5697	1.83678	4.747225
Interaction	30566.93	1	30566.93	0.185959	0.0007831	3.547226
Within	1972544	12	164378.7			

Total	14126921	15